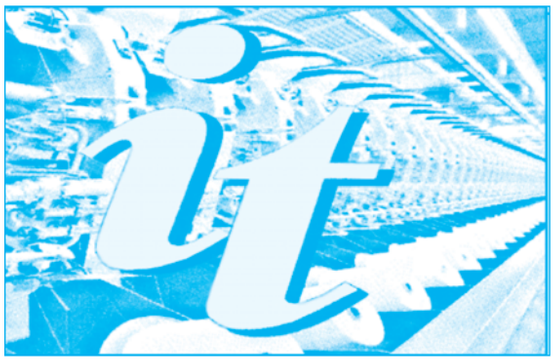


# Industria Textilă

ISSN 1222–5347

1/2024


**Special Issue on Smart and high functional textiles**


*ISI rated journal, included in the **ISI Master Journal List** of the Institute of Science Information, Philadelphia, USA, starting with vol. 58, no. 1/2007, with **impact factor 1.4 and AIS 0.110 in 2022 (Q2 ranked for Materials Science, Textiles category**).*

***The journal is indexed by CrossRef, starting with no. 1/2017 having the title DOI: https://doi.org/10.35530/IT.***

*Edited in 6 issues per year, indexed and abstracted in:*
**Science Citation Index Expanded (SCIE), Materials Science Citation Index®, Journal Citation Reports/Science Edition, World Textile Abstracts, Chemical Abstracts, VINITI, Scopus, Toga FIZ technik, EBSCO, ProQuest Central, Crossref**
**Edited with the Romanian Ministry of Research, Innovation and Digitalization support**

***EDITORIAL STAFF***

***General Manager:*** Dr. Eng. Alexandra-Gabriela Ene
***Editor-in-chief:*** Dr. Eng. Sabina Olaru
***Onorific editor:*** Dr. Eng. Emilia Visileanu
***Graphic designer:*** Florin Prisecaru
***Translator:*** Cătălina Costea
***Site administrator:*** Constantin Dragomir
e-mail: industriatextila@incdtp.ro

INDUSTRIA TEXTILA journal, edited by INCDTP BUCHAREST, implements and respects Regulation 2016/679/EU on the protection of individuals with regard to the processing of personal data and on the free movement of such data ("RGPD"). For information, please visit the Personal Data Processing Protection Policy link or e-mail to DPO rpd@incdtp.ro

Aknowledged in Romania, in the Engineering sciences domain, by the National Council of the Scientific Research from the Higher Education (CNCSIS), in group A
Journal edited in colaboration with **Editura AGIR**, 118 Calea Victoriei, sector 1, Bucharest, tel./fax: 021-316.89.92; 021-316.89.93; e-mail: editura@agir.ro, www.edituraagir.ro

# Implementation method of intelligent emotion-aware clothing system based on nanofibre technology

DOI: 10.35530/IT.075.01.202379

LUO QISHU


## ABSTRACT – REZUMAT

### Implementation method of intelligent emotion-aware clothing system based on nanofibre technology

*The creation of smart clothing technologies now has more options because of the merging of fashion design, and wearable technology with nanofibre technology. This study suggests a means for putting a nanofibre-based, intelligent, emotion-aware clothing system into practice. By recognizing and reacting to the wearer's psychological state, the system seeks to improve user convenience and well-being. In this study, a unique, self-sufficient weight-tuned Kohonen neural network (SW-KNN) method is used to categorize emotional states. To determine the wearer's emotional state, we first collect a dataset of signals from the body, including pulse, body temperature, and perspiration production. The dataset is then added to the preprocessing stage, where the raw data is normalized using the min-max method. The important features from the cleaned data are then extracted using the Fast Fourier Transform (FFT). The smart control unit processes the physiological signals that have been acquired. The proposed approach is utilized to categorize the wearer's emotional state, and the white shark optimization (WSO) approach is used to improve the classification accuracy. The control unit has a microchip and wireless connectivity abilities, enabling it to send the devices' connected devices the classified emotional status. The clothing technology can continuously modify its features based on the identified emotional state to enhance the wearer's comfort. The findings of the study stated that the proposed technique has provided accuracy and precision of 97.8% and 98.1% respectively.*


***Keywords:*** *smart clothing technology, fashion design, wearable technology, nanofibre technology, emotional state classification, self-sufficient weight-tuned Kohonen neural network (SW-KNN)*


### Metodă de implementare a unui sistem inteligent de îmbrăcăminte axat pe inteligenţa emoţională pe baza tehnologiei nanofibrelor

*Crearea tehnologiilor inteligente de îmbrăcăminte are acum mai multe opțiuni datorită îmbinării designului de modă, a tehnologiei purtabile cu tehnologia bazată pe nanofibre. Acest studiu sugerează o modalitate de a pune în practică un sistem de îmbrăcăminte inteligent, bazat pe nanofibre și pe inteligenţa emoţională. Prin recunoașterea și reacționarea la starea psihologică a purtătorului, sistemul urmărește să îmbunătățească confortul și bunăstarea utilizatorului. În acest studiu, este utilizată o metodă unică, pe baza rețelei neuronalale Kohonen (SW-KNN) autosuficiente, reglată în funcție de greutate, pentru a clasifica stările emoționale. Pentru a determina starea emoțională a purtătorului, am colectat mai întâi un set de date de semnale de la corp, inclusiv pulsul, temperatura corpului și producția de transpirație. Setul de date este apoi adăugat la etapa de preprocesare, unde datele brute sunt normalizate folosind metoda min-max. Caracteristicile importante din datele curățate sunt apoi extrase folosind transformata Fourier rapidă (FFT). Unitatea de control inteligentă procesează semnalele fiziologice care au fost colectate. Abordarea propusă este utilizată pentru a clasifica starea emoțională a purtătorului, iar abordarea de optimizare White Shark (WSO) este utilizată pentru a îmbunătăți acuratețea clasificării. Unitatea de control este dotată cu un microcip și abilități de conectivitate wireless, permițându-i să trimită dispozitivelor conectate starea emoțională clasificată. Tehnologia de îmbrăcăminte își poate modifica continuu caracteristicile pe baza stării emoționale identificate pentru a spori confortul purtătorului. Concluziile studiului au afirmat că tehnica propusă a oferit acurateţe și precizie de 97,8% și, respectiv, 98,1%.*


***Cuvinte-cheie****: tehnologie de îmbrăcăminte inteligentă, design de modă, tehnologie purtabilă, tehnologie pe bază de nanofibre, clasificarea stării emoționale, rețea neuronală Kohonen autosuficientă reglată în funcție de greutate (SW-KNN)*

## INTRODUCTION

An idea that blends cutting-edge textile components with artificial intelligence (AI) to produce clothes that can detect and respond to the wearer's emotions is known as an intelligent emotion-aware clothing system based on nanofibre technologies. By giving people new opportunities to express themselves and improve their general health, this cutting-edge technology has the potential to completely transform the fashion business. Based on nanofibre technology, develop a smart emotion-aware apparel system [1]. Nanofibre manufacturing includes creating fibres with nanometre-sized diameters, usually fewer than 100 nanometres. These nanofibres have distinctive qualities such as great strength, adaptability, and excellent surface area-to-volume ratios. They may be manufactured from many materials, such as polymers, metallic ones, or ceramics. Nanofibres are perfect for

the creation of smart clothing since they can be manufactured to have certain features, such as detecting capacities [2]. The intelligent emotion-aware clothing system makes use of sensors built right into the fabric to identify emotional-related physiological rhythms and impulses. These sensors can be of numerous kinds, such as electrodermal activity (EDA) sensors to measure sweat gland activity, electrocardiography (ECG) sensors for tracking the rhythm of the heart, and even sensors that can recognise fluctuations in the temperature of the body or expressions on the face [3].

An AI algorithm or machine learning model processes the data gathered by these sensors to evaluate the signals and ascertain the wearer's emotional state. This approach takes into consideration variables like conductance of the skin, cardiac variation, and other physiological responses that connect with certain emotions [4, 5]. To effectively identify and understand the wearer's state of mind, the AI model is trained on a sizable collection of physiological data associated with emotions. Different responses from the clothing system are possible depending on the identified emotions. For instance, it may alter its colour, pattern, or texture to visibly reflect the wearer's feelings. A major benefit of smart garment technology is improved comfort and convenience. Imagine clothing that adjusts temperature depending on body heat, weather, and activities. Intelligent sensors and microprocessors manage heat and moisture in these adaptable fabrics to give wearers a personalized experience. Smart clothing may also include responsive lighting, letting customers alter its colour or pattern with a touch or smartphone app.

Additionally, it might produce haptic feedback to produce a soothing or exciting experience, such as soft pressure or vibrations. The system may also communicate with other hardware or software to offer tailored suggestions or interventions based on the emotional state of the user, such as recommending relaxation methods or playing uplifting music [6, 7]. Smart clothing technologies will revolutionize fashion and self-expression beyond comfort. Flexible screens and programmable textiles allow clothes to show dynamic patterns, colours, and pictures. This allows users to change their look and dress for different situations without buying several garments, allowing for infinite creative expression and inventiveness. An intelligent, emotion-aware apparel system has several advantages. It can encourage mental health, facilitate self-expression, and aid people in better understanding and controlling their emotions. It has the potential to improve human relationships and experiences in a variety of fields, including healthcare, sports performance, entertainment, and style. Smart clothing aims to reinvent fashion beyond health. Clothing is a dynamic canvas for self-expression since it may change colours, patterns, and styles. Advanced algorithms and machine learning can assess human preferences and environmental circumstances to recommend outfits that match tastes and the occasion. This blend of aesthetics and technology ushers in a new age of individualized fashion that blurs virtual and real barriers. To generate an all-encompassing emotional experience, the garment system may communicate with outside objects and settings [8, 9]. The wearer's psychological health can be enhanced by immersive settings and coordinated reactions made possible by its connection to smartphones, smart homes, and virtual reality devices. For instance, the garment can produce visual or haptic feedback to amplify good feelings if the user gets a message indicating delight. Security and privacy are top priorities while developing this system. The security of the wearer's private information is a top priority for the intelligent emotion-aware clothing system. It upholds stringent privacy rules, uses encryption to protect private data, and gives the wearer complete discretion over how their emotional information is distributed [10].

### Key contribution

The following are the main contributions of this research on the development of smart clothing technologies by combining wearable technology and nanofibre technology.

- The paper presents a nanofibre-based, emotion-aware clothing system. This device detects and responds to the wearer's mental state to increase comfort and well-being. Smart fabrics with sensors and control units can adjust to the wearer's emotional condition.
- The study categorizes emotional states using a self-sufficient weight-tuned Kohonen neural network (SW-KNN). This method analyses the wearer's pulse, body temperature, and perspiration. The SW-KNN analyses and classifies the wearer's emotional state based on data.
- WSO Improves Classification Accuracy: White shark optimization (WSO) improves emotional state classification in the study. White sharks influenced the metaheuristic optimisation algorithm WSO. This method improves emotional state detection and clothing system reactions. The WSO algorithm refines classification, improving the emotion-aware clothing system.

## RELATED WORKS

The related works summary is presented in table 1.

## MATERIALS AND METHOD

The combination of wearable technology and nanofibre technology has increased the choices for developing smart clothing technologies. This paper makes recommendations for how to implement a nanofibre-based, intelligent, emotion-aware clothing system. Figure 1 depicts the overall methodology.

### Dataset

ECG signals are frequently employed for emotion recognition and evaluation because they precisely convey human emotion. To allow real-time user emotion forecasting, the user's emotional representations

Table 1

| RELATED WORKS | | |
|---|---|---|
| **Reference** | **Objectives** | **Findings** |
| Hassabo et al. [11] | To improve the performance, functionality, and comfort of sportswear and associated products, the study investigated the developments in nanotechnology and its prospective applications. | Textile nanotechnology technologies like nanomaterials and sensors have increased physicochemical qualities. NPs in textiles improve self-cleaning, UV protection, flame resistance, and antibacterial properties. |
| Deng and Liu [12] | The research developed a multi-task Using a deep convolutional neural network, customers may participate in design via transferable learning. Learn deep image attributes for picture recovery utilizing client-clicking information. Parameterized programming and neural networks were used to generate garment designs and build wearer-cantered smart outdoor sportswear automatically. | The research produced a new garment design method that lets individuals engage and develop distinctive designs. Visitor-clicking information allows reliable retrieval of images using multi-task deep convolutional neural network learning. Genetic algorithms generate several clothing styles for people. Sensor technology in outdoor sportswear monitors heart rate and microclimate warmth. |
| Yang et al. [13] | The study created an emotion-aware system using artificial intelligence as well as graphs. The system provides personal emotion identification, smart suggestions, and relationship identification. The research analyses various scenarios to improve the suggested system's efficacy and usability. | The findings indicated that a private machine, smart clothes, cloud terminal, and algorithms might successfully recognize and communicate human feelings, giving significant advantages to consumers. |
| Moreira et al. [14] | The paper aimed to enhance emotion-aware intelligent algorithms to detect depression following childbirth in pregnant hypertension women. The program analysed biological and socioeconomic information to identify people at risk and create a childbirth health issues reaction strategy. | Mixture predictors predict pregnancy-related psychological illnesses well. The article shows that the method can predict depression after childbirth in pregnant hypertension women. The snippet does not include findings or measurements of performance. |
| Hu et al. [15] | The work proposed and validated the MULTI-EASE structure to improve user interaction in emotion identification tasks while minimizing end-to-end delay and energy usage. The paper also investigated the MULTI-EASE structure flexible scheduling of tasks. | The study validated the MULTI-EASE structure with a working system. Research findings showed that MULTI-EASE was an effective and durable evaluation of emotions tool. The proposed architecture saves edge computing energy and increases emotional interaction. The study's findings illuminate MULTI-EASE structure flexible planning. |
| Chen et al. [16] | The paper looked at the network architecture, energy consumption optimization mode, and body area network node design of smart clothing for physiological monitoring. A general review of the requirements and key technologies for body area network transmission of smart apparel is also provided. | The results show that the researchers' internal network-optimized structure for smart clothing satisfies the requirements for safety, dependability, low power consumption, and portability, especially in the area of physiological monitoring. It is also simple to use, portable, and practical. |
| McDuff et al. [17] | The article described how the platform's audio, visual, and application processing components store and share data for other programs. A tool that encourages creative interfaces between humans and computers was enhancing emotional computing. | The paper's findings described the multisensory emotion and contextual sensor platform's visual, auditory, and computational processor elements. It described how every part helps the overall system record and transmit real-time emotional information. The document explains data storage and communication, allowing other programs to use emotional information for research or API interaction. |
| Shanmugam and Singh [18] | The purpose of the study was to provide a system that recognizes emotions and includes a personal robot, smart clothing, and a cloud interface. An innovative 'people-centred' method of emotional engagement has been developed. | The data perception and emotion-cognition engines analyse user interactions and environments. The suggested system uses communication, computing, and storage integrated by the artificial intelligence algorithm in the personal robot, smart clothing, and cloud terminal to respond to customer demands. |

Table 1 (continuation)

| Reference | Objectives | Findings |
|---|---|---|
| Peng et al. [19] | The purpose of the study is to contribute to this subject by examining the relevant literature. They suggested a three-tiered structure that encompasses the fundamentals of emotion analysis, various technologies and models, concerns about privacy, and implementation settings. | They examine the significance of integrating emotional intelligence into urban design and emphasize the potential of various technologies to contribute to an increase in the well-being of the populace. In general, this framework offers a complete method for examining feelings and their interactions with new technology in an urban setting. |
| Miao et al. [20] | The article investigates a technique for the automated development of clothing styles and designs parameterized code for use with the said approach. Compared to image feature representation based on image recognition training on artificially labelled datasets, the image and text feature representations developed in this study better reflect genuine user demands. | The research uses parametric binary coding to develop suit-style pieces using interactive genetic algorithms automated design approach. The interactive genetic algorithm based on the usual style optimizes garment inheritance and benignly evolves suit design depending on user assessment. |
| Chen et al. [21] | The article suggested a small portion of that market was smart apparel. Companies may maximize smart clothing's capability by engaging both device owners for personal data insights and big data analysis for commercial use, unlike personal wearable gadgets. | In these platforms collect large amounts of data from corporate systems and external sources, use powerful machine learning algorithms for rigorous, predictive, and continuous analysis, and provide actionable insights for mission-critical business imperatives. |
| Dang and Zhao [22] | This article introduced smart fibres and smart textiles and described their functionality and main categories. The article also covered smart fibre and textile usage across industries. It also emphasizes these new textile techniques' infinite growth and potential for profit. | This article covered smart fabrics and materials. It discusses form memory, colour-changing, intelligent heat leadership, impermeable and moisture-permeable, cleans themselves, and digitally stored smart fabrics. It also explores intelligent fibres and textiles' use in medical care, military protection, entertainment, sports, and clothing. These novel textile innovations have great potential for sale, as the paper underlines. |
| Hu et al. [23] | The research creates sensor-based smart apparel for home and ambulatory health monitoring during menopause. Initially, a survey analyses biological data to identify menopausal transition symptoms and target body locations for sensor placement on clothes. | The results show that this smart clothing monitoring system can accurately measure skin temperature and relative humidity and calculate the frequency, duration, and intensity of hot flashes in different body areas, as reported by subjects. |
| Krishna et al. [24] | The research polled people to discover smart clothing adoption barriers. Thus, perceived hazards and unavailability of smart garments, new items, have raised innovation resistance. | As a consequence of this, it has been proven that the fashion-forwardness of customers plays a role in boosting innovation resistance to inexpensive smart apparel. It is possible to conclude that customers who place a higher priority on maintaining their image face the additional pressure of having to make frequent purchases of somewhat pricey trendy clothing to stay on trend. |
| Ahsan et al.[25] | The structure provided requirements for design, detectors, and textile materials for smart apparel, particularly pants. The goal also involved seamlessly incorporating detectors into garments and developing a system for gathering data, manufacturing, and making choices approach to medical diagnosis and prediction. | The framework's specs for design, detector connection methods, and smart garment components are shown. Examples show how to apply the structure. Addressed were the problems of promoting smart clothing and its promise for medical athletics, sports, and style. |

based on a previous ECG dataset are created in the cloud, and their accessibility is tested on a testbed. In addition, 20 volunteers – 8 men and 12 women, ranging in age from 22 to 29 – were enlisted for the study's conduct and assessment, and their ECG signals were labelled with five emotional states: normal, joyful, furious, fearful, and sad. For independent feature extraction, the entire set of ECG data is split into a training set (60 percent) and a testing set (40 percent).

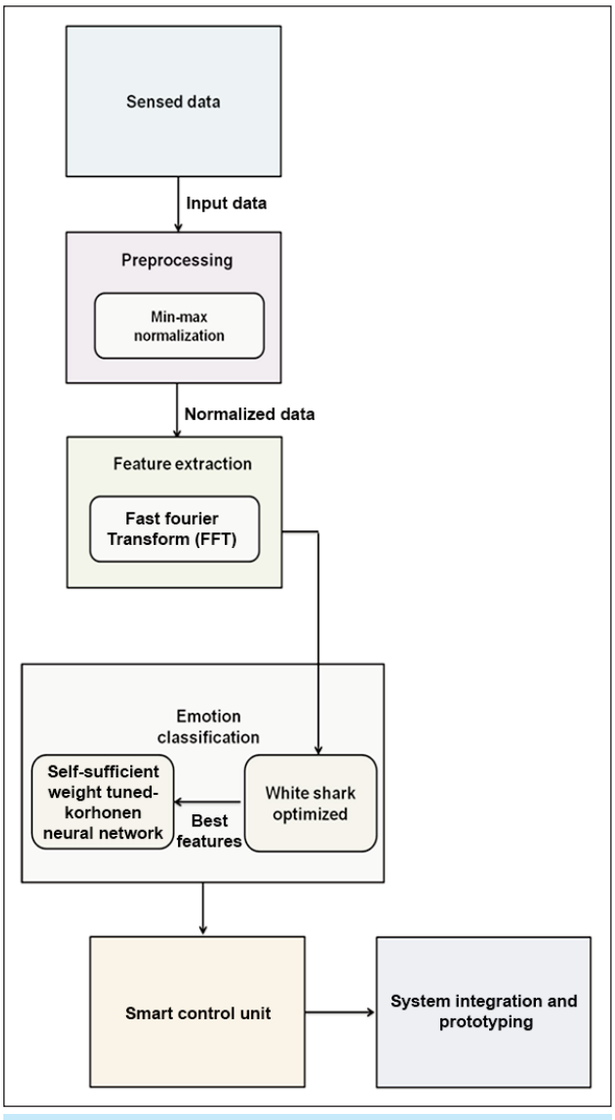


Fig. 1. Proposed model

## Data preprocessing

*Min-max normalization*

A common tool for data preprocessing, used by the majority of data mining systems, is normalization. To normalize a dataset, scale each attribute's values such that they all lie inside a small specified range, say, 0.0 to 1.0. Preprocess data from children to estimate the risk of malnutrition using the min-max normalization strategy. With this technique, the features or outputs are scaled from one set of values to another. The characteristics are often rescaled to fall between [0, 1] and [–1, 1] or anywhere in between. A formula for linear interpretation is often used to do the rescaling in (equation 1), such as:

$$y' = \frac{y - min_E}{max_E - min_E}(new\_max_E - new\_min_E) + \\ + new\_min_E \quad (1)$$

where $max_E$ is the attribute's highest value, $min_E$ – its lowest value, and ($new\_max_E$ – $new\_min_E$) = 0. When $max_E$ – $min_E$ = 0, it means that the value for that feature in the data is always the same. When the min-max normalization is used, each feature will stay the same as long as it is in the new range of values.

## Feature extraction

*Fast Fourier transform*

The Discrete Fourier Transform (DFT) of a sequence can be calculated effectively using the FFT technique. Using the discrete Fourier transform (DFT), an impulse in the time domain can be computationally converted into a comparable signal in the domain of frequencies. The FFT approach makes the DFT substantially faster for large input sizes by reducing the complexity of computation from $O(n^2)$ to $O(n \log n)$.

The following is the equation for the DFT of a sequence of length $N$, $x[n]$:

$$X[k] = \sum n = 0 \text{ to } N - 1\, x[n] * exp\left(\frac{-j2pink}{N}\right) \quad (2)$$

where $X[k]$ stands for the frequency element at index $k$ in the frequency domain, $j$ is the imaginary unit $\sqrt{-1}$, pi is the number pi, or roughly 3.14159, and $exp()$ stands for the exponential function.

The input sequence is broken down into smaller subproblems by the FFT method, which then combines the answers to get the final DFT. One of the most used FFT algorithms, the Cooley-Tukey algorithm, is described in general terms as follows:

***Step 1***: The DFT is simply the value of the input sequence if the length of the input sequence $N$ is 1; thus, return it.

***Step 2***: Divide the input sequence into two smaller sequences, each of length $N/2$, if $N$ is more than 1. Let's give them the names $X_{even}$ and $X_{odd}$ to stand for the original sequence's even- and odd-indexed components, accordingly.

***Step 3***: Apply the FFT procedure to each and then recursively compute the DFT of $X_{even}$ and $X_{odd}$.

$$X_{even} = FFT(x_{even}) \quad (3)$$

$$X_{odd} = FFT(x_{odd}) \quad (4)$$

***Step 4***: To get the final DFT of the initial sequence, combine the findings from the DFT of $X_{even}$ and $X_{odd}$. In this phase, the DFT of $X_{odd}$ is multiplied by the necessary twiddle factors and added to the DFT of $X_{even}$.

For $k$ = 0 to $N/2-1$:

$$X[k] = X_{even}[k] + W_N{}^k * X_{odd}[k] \quad (5)$$

$$X\left[k + \frac{N}{2}\right] = X_{even}[k] - W_N{}^k * X_{odd}[k] \quad (6)$$

where $W_N{}^k = exp\left(\frac{-j2pink}{N}\right)$ is the twiddle factor.

***Step 5***: The resulting DFT sequence is returned as $X[k]$.

## Kohonen neural network (SW-KNN)

An artificial neural network design that was modelled after the way neurons are arranged in the visual cortex of the human brain is called a Kohonen neural network. This architecture is also known as a self-organizing map (SOM). It has widespread use in the

fields of high-dimensional data clustering, visualization, and dimensionality reduction. The most important job of the network is to convert the high-dimensional input data into a lower-dimensional grid while maintaining the topological connections between the data points. This makes it possible for the network to discover hidden patterns and structures within the complicated information. Competitive learning characterizes the Kohonen neural network. The input layer accepts data, while the output layer is frequently grid-arranged. Each output layer neuron matches a grid node. The network changes its weights (synaptic strengths) to fit input data during training. The general architecture of KNN is shown in figure 2.

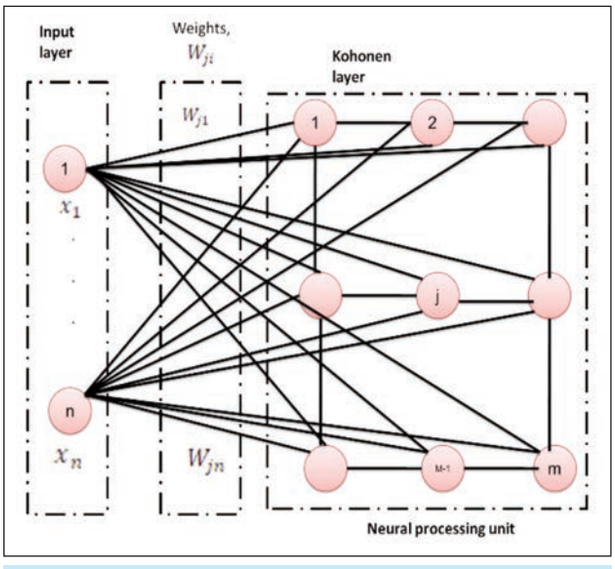


Fig. 2. General architecture of KNN

**KNN training algorithm:**

***Step 1***: Give the first input ($x$), a weight matrix ($w$) with random initialization, and a learning rate ($\alpha$).

***Step 2***: Euclidean distances should be calculated for each output layer.

$$c(i) = \sum_{j\neq1}^{M} (w_j - x_{old})^2 \quad (7)$$

***Step 3***: the neuron ($j$) with the least distance value should be located.

***Step 4***: Specifically alter the winner neuron's weights.

$$x_{ji}(new) = x_{ji}(old) + [w_j - x_{ji}(old)] \quad (8)$$

***Step 5***: Steps 2 through 4 should be repeated with the new set of weights.

***Step 6***: The process should be repeated 100–200 times for each iteration.

*Modified Self-sufficient Weight-tunedKohonen neural network (SW-KNN) I*

Since the SW-KNN is an unsupervised network, it has a lower accuracy level than the BPN. The training algorithm has undergone several changes to improve Accuracy. New weight values in SW-KNNs heavily rely on activation. Therefore, new weight values in this upgraded SW-KNN won't rely on old weight values. The proposed architecture of KNN is shown in figure 3.

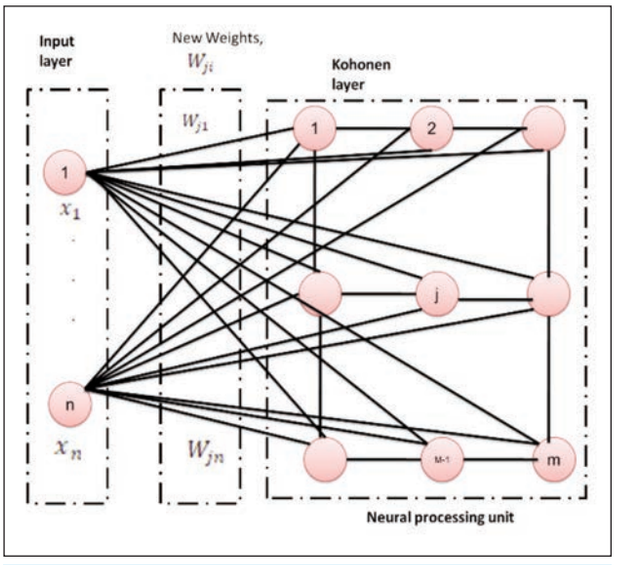


Fig. 3. Proposed architecture of KNN

**Training algorithm of Modified SW-KNN I:**

***Step 1***: First input ($x$), a weight matrix ($w$) with starting values chosen at random, and a learning rate ($\alpha$) should be provided.

***Step 2***: Each output layer's Euclidean distance should be known.

$$c(i) = \sum_{j\neq1}^{M} (w_j - x_{old})^2 \quad (9)$$

***Step 3***: It is important to identify the neuron ($j$) whose distance value is the smallest.

***Step 4***: Specifically alter the winner neuron's weights

$$\Delta x_{ji} = 2 \propto w_j + \propto \quad (10)$$

***Step 5***: With the new set of weights, repeat steps 2 through 4 again.

***Step 6***: Repeat the algorithm a certain number of times. (150).

This work uses an alpha value of 0.6. The procedure of weight correction is distinct from the traditional system. The distinction between the inputs and the old weights has no bearing on the weight modification procedure in the suggested method. The efficiency of the typical system is subpar since this gap can never be zero. The suggested way gets around this.

*Modified Self-sufficient Weight-tunedKohonen neural network (SW-KNN) II*

A few further adjustments are made to the modified SW-KNN II to improve Accuracy compared to the original SW-KNN. This network's accuracy level is greater than that of the standard Kohonen and lower than that of the modified SW-KNN II.

**Application algorithm of Improved SW-KNN II:**

***Step 1***: The weight matrix ($w$) with a randomly initialized first input ($x$), and learning rate ($\alpha$) should be provided.

***Step 2***: Each output layer's Euclidean distance should be known.

$$c(i) = \sum_{j\neq1}^{M} (w_j - x_{old})^2 \quad (11)$$

***Step 3***: It is important to identify the neuron (*j*) whose distance value is smallest.

***Step 4***: Specifically alter the winner neuron's weights.

$$\Delta x_{ji} = 2 \propto w_j - \propto^2 \quad (12)$$

***Step 5***: Repeat the process using the updated weights.

***Step 6***: For a set number of repetitions, repeat the process. (150)

This work uses an alpha value of 0.6.

*White Shark Optimization (WSO)*

This section provides a full explanation of the mathematical equations that were created to describe the behaviours of hunting with white sharks to solve the OPF problem. This entails hunting down and killing prey.

*WSO's initialization*

In the accompanying two-dimensional matrix, which displays a populace of *n* where shark optimization in an area with *d* examine domain dimensions, the position of each pole suggests a possible answer to the difficulties that have been identified:

$$x = \begin{bmatrix} x_1^1 & x_2^1 & \cdots & x_c^1 \\ x_1^2 & x_2^2 & \cdots & x_c^2 \\ \cdots & \cdots & \cdots & \cdots \\ x_1^m & x_2^m & \cdots & x_c^m \end{bmatrix} \quad (13)$$

where *d* indicates the quantity of choice varying for a particular assignment, and *w* shows the precise position of every shark in the search region.

*Movement Speed Toward Prey*

Equation 14 shows how a white shark can locate its target by detecting a pause in the movement of the waves.

$$v_{l+1}^j = \mu[v_l^j + o1(x_{h\,best_l} - x_l^j) \times d_1 + o2(x_{best}^{u_l^j} - x_l^j) \times d_2 \quad (14)$$

The new speed vector of the $i^{th}$ shark is indicated by $u_{l+1}^j$ and the integers $i = 1, 2, \ldots, n$ = index of sizes. Equation 15 indicates that $u^i$ is the $i^{th}$ index vector of sharks reaching the ideal position:

$$u = [m \times rand\,(1,m)] + 1 \quad (15)$$

where *rand* (1,*m*) is a collection of randomly generated numbers with a range of [0, 1]:

$$o_1 = o_{max} + (o_{max} - o_{min}) \times f^{-(4k/k)^2} \quad (16)$$

$$o_2 = o_{min} + (o_{max} - o_{min}) \times f^{-(4k/k)^2} \quad (17)$$

where $o_{min}$ and $o_{max}$ stand for the beginning and ending speeds for white shark motion, and = *current,* and *K* = *maximum* repetitions. The values of $o_{min}$ and $o_{max}$ were determined to be 0.5 and 1.5, accordingly, after a careful study.

$$\alpha = \frac{2}{\left|2 - \tau - \sqrt{\tau^2 - 4\tau}\right|} \quad (18)$$

$\tau$ denotes the acceleration factor, which was determined through thorough research to be 4.125.

*Generally moving in the direction of the best opportunity*

In this context, the conduct of white sharks as they approach prey was described using the position update mechanism provided in equation 19.

$$x_{l+1}^j = \begin{cases} x_l^j, \rightarrow \oplus x_0 + v.b + k.a; rand < nu \\ x_l^j + \frac{v_l^j}{f}; rand \geq nu \end{cases} \quad (19)$$

*b* and *a* are defined as binary vectors, accordingly, in equations (20) and (21):

$$b = thm(x_l^j - v) > 0 \quad (20)$$

$$a = thm(x_l^j - v) < 0 \quad (21)$$

$$x_0 = \oplus(b, a) \quad (22)$$

where $\oplus$ equation (22), the result of a bitwise xor, is used to represent the result. Equations 22 and 23, respectively, describe the white shark's propensity for wavy motion and how often it strikes prey.

$$e = e_{min} + \frac{e_{max} - e_{min}}{e_{max} + e_{min}} \quad (23)$$

$$nu = \frac{1}{a_0 + f^{(1/2-l)/b_1}} \quad (24)$$

where the control exploration and exploitation locations are determined by the constants $a_0$ and $b_1$.

*Aiming to go towards the path of the shark*

Sharks may hold their ground in front of the nearest target, the most beneficial competitor. Equation 25 illustrates the expression for these phenomena.

$$x_{l=1}^{\prime j} = x_{h\,best_l} + q_1 \vec{C}_x thm(q_2 - 0.5)\, q_3 < T_t \quad (25)$$

To change the searching path, $thm(q_2 - 0.5)$ yields 1 or –1, and $q_1$, $q_2$, and $q_3$ are all rand values. $x_{l=1}^{\prime j}$ = the position of the improved shark. No, in the range [0, 1], equation 26 states that *Dw* = length for both the target and the shark. Equation 27 calls for the parameter $T_t$ to represent the strength of white sharks:

$$\vec{C}_x = \left|rand \times (x_{hbest} - x_l^j)\right| \quad (26)$$

$$T_t = \left|1 - f^{(-b_2 \times l/l)}\right| \quad (27)$$

where the location factor $b_2$ controls the amount of exploitation and exploration.

*Behaviour in Fish Schools*

White shark fish school behaviour was defined using the equation shown below:

$$x_{l=1}^j = \frac{x_l^j + x_{l+1}^{\prime j}}{2 \times rand} \quad (28)$$

where and stands for a [0, 1]-dimensional random number with a uniform distribution equation 27, which shows that the sharks can alter based on the best shark that has arrived at the optimal place, which is extremely close to the goal, to determine its position, shows that the sharks can. Sharks' last resting place is typically near their prey in the search area. Fish behaviour, shark motion to the largest shark, and

enhanced global and local search skills are indicators of WSO interaction.

*WSO execution and evaluation*

White sharks constantly work to get closer to the overall ideal solution when evaluating functions. White sharks are more likely to discover the best solution by leveraging and investigating the study area around the space, which explains why. This ability is achieved by using the location of the superior sharks and their victims. Sharks may, therefore, constantly scout out possible prey-rich areas and contribute to them. The main operations of Algorithm 1's algorithm can be utilized to summarize WSO's pseudo code.

Algorithm 1: WSO's pseudo code

1. Initialize the Parameter of the Problem,
2. Initialize the parameter of WSO
3. Randomly generate the initial positions of WSO
4. Initialize the velocity of the initial population
5. Evaluate the position of the initial population
6. While($l$<$L$)do
7. Update the parameters $u$, $o_1$, $o_2$, m, $b$, $a$, $x_0$, $e$, $x_u$, and $T_t$ using equations 15–18, 20–24 and 27, respectively
8. For $j = q$ to $m$ do
9. $v_{l+1}^{j} = \mu[v_l^j + o1\left(x_{h\,best_l} - x_l^j\right) \times d_1 + + o2\left(x_{best}^{u_l^j} - x_l^j\right) \times d_2$
10. End for
11. For $j$ = 1 to $m$ do
12. If $rand < nu$ then
13. $x_l^j, \rightarrow \oplus x_0 + v.b + k.a$; $rand < nu$
14. Else
15. $x_{l+1}^{j} = x_l^j + \frac{v_l^j}{f}$
16. Endif
17. End for
18. For $j$ = 1 to $m$ do
19. If rand $\leq T_t$
20. $|rand \times (x_{hbest} - x_l^j)|$
21. If $j$ = 1 then
22. $x_{l=1}^{j} = x_{h\,best_l} + q_1 \vec{C}_x thm(q_2 - 0.5)$
23. Else
24. $x'^{j}_{l=1} = x_{h\,best_l} + q_1 \vec{C}_x thm(q_2 - 0.5)$
25. $x_{l=1}^{j} = \frac{x_l^j + x'^{j}_{l+1}}{2 \times rand}$
26. End if
27. Endif
28. End for
29. Make the necessary adjustments to the positions of the white sharks that go over the barrier.
30. Examine and bring the new positions up to date.
31. $l = l + 1$
32. end while
33. Return the best outcome you've so far found

## RESULT AND DISCUSSION

In this section, we analyse the following metrics: Accuracy (%), Precision (%), Recall (%), and F1-score (%), Root Mean Square Error (RMSE), and Mean Absolute Error (MAE). Existing approaches include such as and Deep Convolutional Neural Networks (D-CNN) [15], Convolutional Neural Networks–Long Short-Term Memory (CNN-LSTM) [20].

The performance of a classification model can be evaluated using various statistical metrics, one of which is Accuracy. A comparison of the Accuracy of the recommended method with the Accuracy of the traditional method is presented in figure 4 and table 2, respectively. D-CNN and CNN-LSTM had values of 89.6 percent and 90.5 percent, respectively, when tested against the existing methods; however, the technique that was recommended (SW-KNN) has a value of 97.9 percent. The performance of the method that we have proposed as a direct consequence of this factor is significantly improved.

$$Accuracy = \frac{TP + TN}{TP + TN + FP + FN} \quad (29)$$

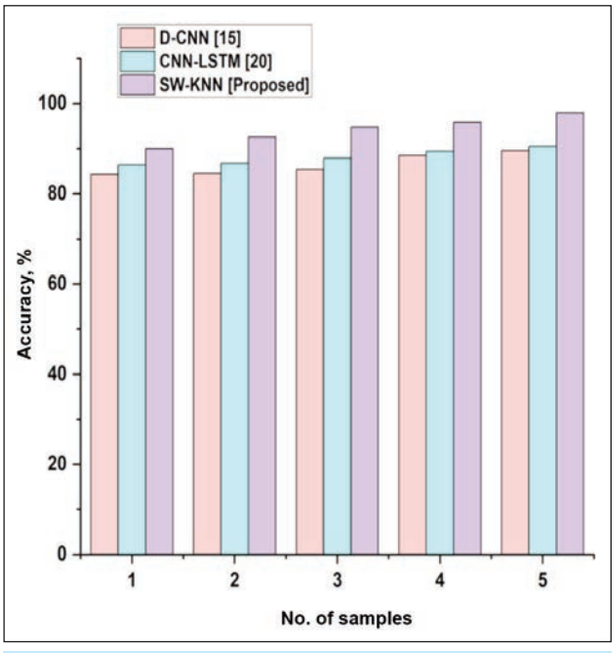


Fig. 4. Result of accuracy

Table 2

RESULT OF ACCURACY

| No. of samples | Accuracy (%) | | |
|---|---|---|---|
| | D-CNN [15] | CNN-LSTM [20] | SW-KNN [Proposed] |
| 1 | 84.3 | 86.4 | 90 |
| 2 | 84.5 | 86.8 | 92.6 |
| 3 | 85.4 | 87.9 | 94.8 |
| 4 | 88.5 | 89.4 | 95.9 |
| 5 | 89.6 | 90.5 | 97.9 |

A statistical parameter called precision is used to assess a classification model's performance, particularly in binary classification problems. Out of all occurrences projected as positive, including both true positives and false positives, it calculates the percentage of accurately predicted positive instances (true positives). Figure 5 and table 3 show a contrast between the precision of the recommended method and the precision of the conventional method. When compared to the well-known approaches, D-CNN and CNN-LSTM scored 89.4% and 92.6 percent, respectively; however, the strategy that was suggested (SW-KNN) scored 98.1 percent. As a direct result of this factor, the solution we have suggested performs substantially better.

$$Precision = \frac{TP}{TP + FP} \quad (30)$$

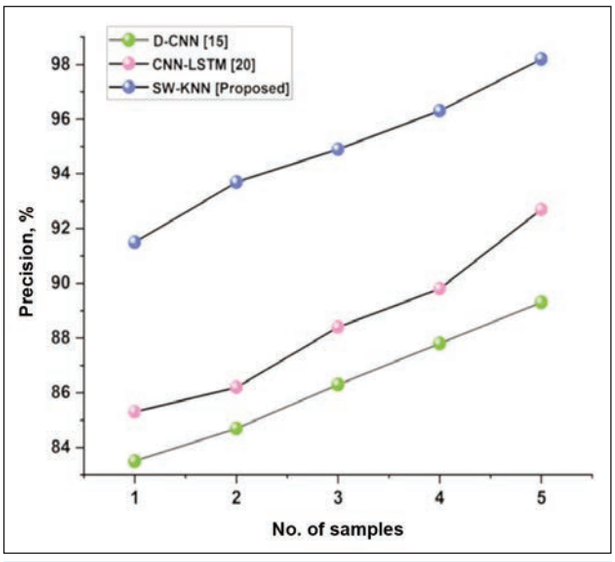


Fig. 5. Result of precision

Table 3

RESULT OF PRECISION

| No. of samples | Precision (%) | | |
|---|---|---|---|
| | D-CNN [15] | CNN-LSTM [20] | SW-KNN [Proposed] |
| 1 | 83.6 | 85.2 | 91.4 |
| 2 | 84.8 | 86.2 | 93.6 |
| 3 | 86.2 | 88.3 | 94.8 |
| 4 | 87.9 | 89.9 | 96.2 |
| 5 | 89.4 | 92.6 | 98.1 |

A statistical parameter called recall, often referred to as sensitivity or true positive rate, is used to assess a classification model's performance, particularly in binary classification problems. Out of all actual positive instances, it calculates the percentage of accurately anticipated positive instances (true positives). The recall of the recommended approach and the recall of the conventional way are contrasted in figure 6 and table 4. D-CNN and CNN-LSTM scored 88.4% and 90.1 percent in comparison to the existing methods; however, the proposed method (SW-KNN) scored 97.1 percent. This factor directly contributes to the significantly superior performance of the approach we have proposed.

$$Recall = \frac{TP}{TP + FP} \quad (31)$$

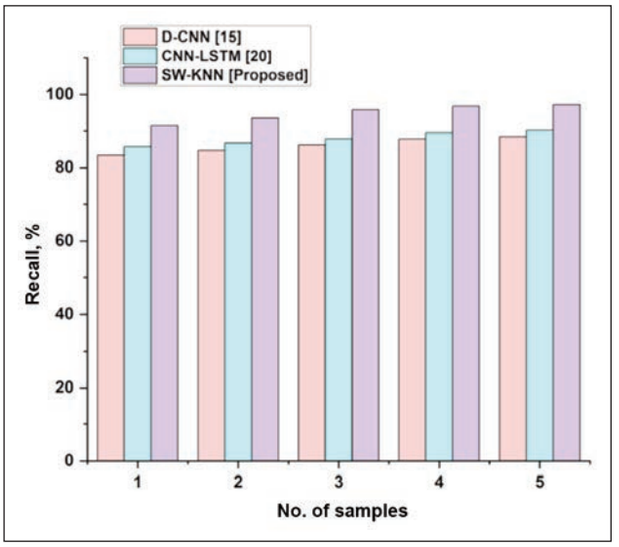


Fig. 6. Result of recall

Table 4

RESULT OF RECALL

| No. of samples | Recall (%) | | |
|---|---|---|---|
| | D-CNN [15] | CNN-LSTM [20] | SW-KNN [Proposed] |
| 1 | 83.3 | 85.9 | 91.4 |
| 2 | 84.8 | 86.9 | 93.4 |
| 3 | 86.3 | 87.8 | 95.9 |
| 4 | 87.8 | 89.4 | 96.9 |
| 5 | 88.4 | 90.1 | 97.1 |

A statistical metric used to assess a classification model's performance, particularly in binary classification problems, is the F1 score. It provides a fair evaluation of the model's efficacy by combining precision and recall into a single measure. Figure 7 and table 5 compare the F1-Score of the suggested method with the F1-Score of the traditional method.

Comparatively to the well-known approaches, D-CNN and CNN-LSTM scored 88.9% and 89.8%, respectively; however, the proposed method (SW-KNN) scored 98.5 percent. This component directly contributes to our suggested method performing much better.

$$F1 - Score = 2 \times \frac{Precision * recall}{Precision + recall} \quad (32)$$

Root Mean Square Error is referred to as RMSE. The average difference between a model's predicted values and the actual values is a frequently used metric

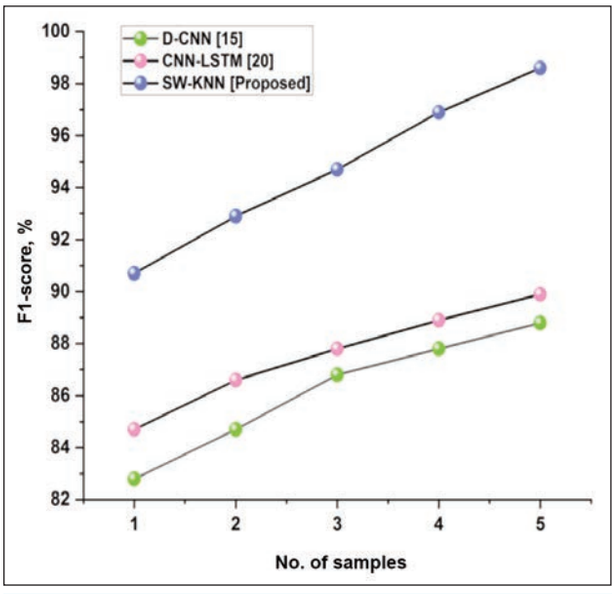


Fig. 7. Result of F1-Score

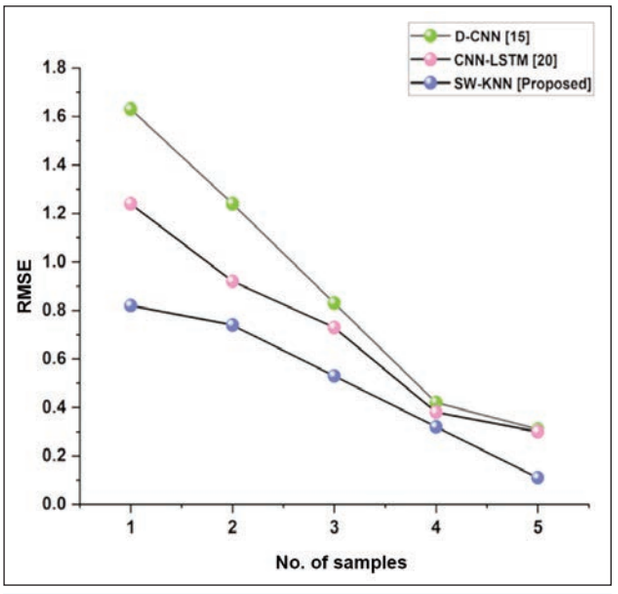


Fig. 8. Result of RMSE

Table 5

| RESULT OF F1-SCORE | | | |
|---|---|---|---|
| No. of samples | F1-Score (%) | | |
| | D-CNN [15] | CNN-LSTM [20] | SW-KNN [Proposed] |
| 1 | 82.9 | 84.8 | 90.6 |
| 2 | 84.8 | 86.8 | 92.8 |
| 3 | 86.8 | 87.9 | 94.6 |
| 4 | 87.9 | 88.9 | 96.8 |
| 5 | 88.9 | 89.8 | 98.5 |

Table 6

| RESULT OF RMSE | | | |
|---|---|---|---|
| No. of samples | RMSE (%) | | |
| | D-CNN [15] | CNN-LSTM [20] | SW-KNN [Proposed] |
| 1 | 1.63 | 1.24 | 0.82 |
| 2 | 1.24 | 0.92 | 0.74 |
| 3 | 0.83 | 0.73 | 0.53 |
| 4 | 0.42 | 0.38 | 0.32 |
| 5 | 0.31 | 0.3 | 0.11 |

in regression tasks. The performance of models that predict continuous numerical values can be assessed with the use of RMSE. Figure 8 and table 6 show a comparison of the RMSE between the recommended and conventional approaches. In contrast, the suggested methods SW-KNN, D-CNN and CNN-LSTM all achieve RMSE values of 0.31, 0.3, and 0.11, respectively. The SW-KNN algorithms that have been suggested have a lower RMSE value than the existing methods. It demonstrates that the suggested approach is more successful.

$$RMSE = \sqrt{1/n * sum(predicted_i - actual_i)^2} \quad (33)$$

Mean Absolute Error is referred to as MAE. The average absolute deviation between a model's predicted values and the actual values is a regularly used metric in regression tasks. MAE is especially helpful for assessing how well models work when they predict continuous numerical values. A comparison of the MAE between the suggested and traditional procedures is shown in figure 9 and table 7. SW-KNN, D-CNN and CNN-LSTM, on the other hand, all produce MAE values of 0.2, 0.31, and 0.3, respectively, when used as indicated techniques. The recommended SW-KNN algorithms have a lower MAE value than the current techniques. It proves that the suggested strategy is more effective.

$$MAE = \left(\frac{1}{n}\right) * sum(|predicted_i - actual_i|) \quad (34)$$

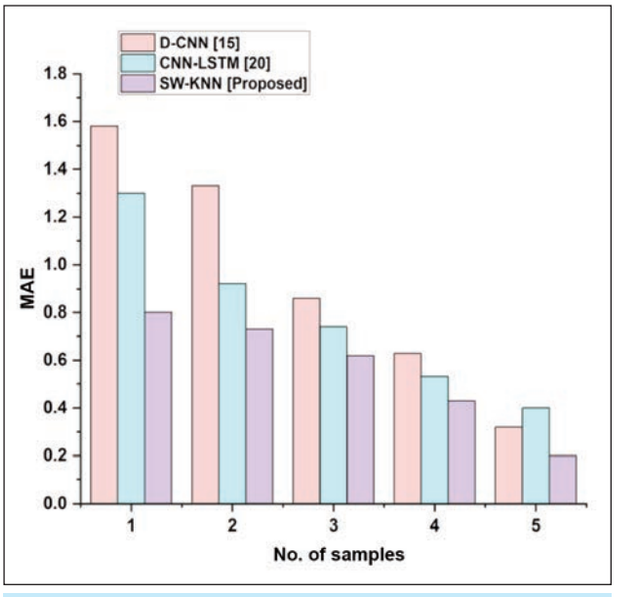


Fig. 9. Result of MAE

Table 7

| RESULT OF MAE | | | |
|---|---|---|---|
| No. of samples | MAE (%) | | |
| | D-CNN [15] | CNN-LSTM [20] | SW-KNN [Proposed] |
| 1 | 1.59 | 1.29 | 0.9 |
| 2 | 1.32 | 0.91 | 0.72 |
| 3 | 0.85 | 0.73 | 0.61 |
| 4 | 0.62 | 0.52 | 0.42 |
| 5 | 0.31 | 0.3 | 0.2 |

## CONCLUSION

Emotional states are categorized using a novel, self-sufficient weight-tuned Kohonen neural network (SW-KNN) technique. We first gather a dataset of bodily signals, such as pulse, body temperature, and sweat production, to ascertain the wearer's emotional state. The dataset is subsequently included in the preparation stage, where the min-max approach is used to normalize the raw data. The Fast Fourier Transform (FFT) is then used to extract the significant features from the cleaned data. For the proposed method's performance, we were able to obtain values for Accuracy (97.8%), Precision (98.1%), Recall (97.1%), F1-Score (98.5%), RMSE (0.12), and MAE (0.20). The proposed method was compared to the one that is currently being used, and the results of the experiments showed that the proposed strategy was more effective. Using physiological information to classify emotions limits the study's sophisticated emotion-aware clothing system. Physiological signs like pulse, body temperature, and perspiration can reveal a person's emotional state, but they may not convey its complete complexity and nuances. Incorporating multi-modal data fusion techniques into the intelligent emotion-aware clothing system to increase emotion recognition is one of the potential future applications for this technology.

## REFERENCES


[1] Muhammad, G., Alshehri, F., Karray, F., El Saddik, A., Alsulaiman, M., Falk, T.H., *A comprehensive survey on multi-modal medical signals fusion for smart healthcare systems*, In: Information Fusion, 2021, 76, 355–375

[2] Chen, M., Qian, Y., Hao, Y., Li, Y., Song, J., *Data-driven computing and caching in 5G networks: Architecture and delay analysis*, In: IEEE Wireless Communications, 2018, 25, 1, 70–75

[3] Zheng, J., Zhang, Q., Xu, S., Peng, H., Wu, Q., *Cognition-based context-aware cloud computing for intelligent robotic systems in mobile education*, In: IEEE Access, 2018, 6, 49103–49111

[4] Qian, Y., Lu, J., Miao, Y., Ji, W., Jin, R., Song, E., *AIEM: AI-enabled affective experience management*, In: Future Generation Computer Systems, 2018, 89, 438–445

[5] Song, J., Liu, M., Wu, G., Lu, W., Li, Y., Song, E., *Emotion Communications Driven by Big Data Cloud, Smart Clothing, and Robotics,* In: 12th EAI International Conference on Testbeds and Research Infrastructures for the Development of Networks & Communities, 2018, 34–41

[6] Saranya, P., Asha, P., *Survey on big data analytics in health care,* In: 2019 International Conference on Smart Systems and Inventive Technology (ICSSIT), IEEE, 2019, 46–51

[7] Chen, M., Yang, J., Hao, Y., Mao, S., Hwang, K., *A 5G cognitive system for healthcare,* In: Big Data and Cognitive Computing, 2017, 1, 1, 2

[8] Zhou, P., Hossain, M.S., Zong, X., Muhammad, G., Amin, S.U., Humar, I., *Multi-task emotion communication system with dynamic resource allocations*, In: Information Fusion, 2019, 52, 167–174

[9] Mbunge, E., Muchemwa, B., *Towards emotive sensory Web in virtual health care: Trends, technologies, challenges, and ethical issues*, In: Sensors International, 2022, 3, 100134

[10] Rumiantcev, M., Khriyenko, O., *Emotion-based music recommendation system,* In: Proceedings of Conference of Open Innovations Association FRUCT. Fruct Oy, 2020

[11] Hassabo, A.G., Zayed, M., Bakr, M., Abd-Elaziz, E., Othman, H.A., *Applications of Supercritical Carbon Dioxide in Textile Finishing: A Review*, In: Journal of Textiles, Coloration, and Polymer Science, 2022, 19, 2, 179–187

[12] Deng, H., Liu, M., *Personalized smart clothing design based on multi-modal visual data detection*. Computational intelligence and neuroscience, 2022

[13] Yang, J., Wang, R., Guan, X., Hassan, M.M., Almogren, A., Alsanad, A., *AI-enabled emotion-aware robot: The fusion of smart clothing, edge clouds, and robotics*, In: Future Generation Computer Systems, 2020, 102, 701–709

[14] Moreira, M.W., Rodrigues, J.J., Kumar, N., Saleem, K., Illin, I.V., *Postpartum depression prediction through pregnancy data analysis for emotion-aware smart systems*, In: Information Fusion, 2019, 47, 23–31

[15] Hu, L., Li, W., Yang, J., Fortino, G., Chen, M., *A sustainable multi-modal multi-layer emotion-aware service at the edge*, In: IEEE Transactions on Sustainable Computing, 2019, 7, 2, 324–333

[16] Chen, M., Yang, J., Zhu, X., Wang, X., Liu, M., Song, J., *Smart home 2.0: Innovative smart home system powered by botanical IoT and emotion detection*, In: Mobile Networks and Applications, 2017, 22, 1159–1169

[17] McDuff, D., Rowan, K., Choudhury, P., Wolk, J., Pham, T., Czerwinski, M., *A multi-modal emotion-sensing platform for building emotion-aware applications*, 2019, arXiv preprint arXiv:1903.12133

[18] Shanmugam, M., Singh, M., *Analysis of emotion-aware healthcare and Google Cloud messaging*, In: 2017 International Conference on Innovative Mechanisms for Industry Applications (ICIMIA), IEEE, 2017, 667–670

[19] Peng, Y., Peng, L., Zhou, P., Yang, J., Rahman, S.M.M., Almogren, A., *Exploiting energy-efficient emotion-aware mobile computing*, In: Mobile Networks and Applications, 2017, 22, 1192–1203
[20] Miao, Y., Wu, G., Liu, C., Hossain, M.S., Muhammad, G., *Green cognitive body sensor network: architecture, energy harvesting, and smart clothing-based applications,* In: IEEE Sensors Journal, 2018, 19, 19, 8371–8378
[21] Chen, M., Ma, Y., Li, Y., Wu, D., Zhang, Y., Youn, C.H., *Wearable 2.0: Enabling human-cloud integration in next-generation healthcare systems*, In: IEEE Communications Magazine, 2017, 55, 1, 54–61
[22] Dang, T., Zhao, M., *The application of smart fibres and smart textiles*, In: Journal of Physics: Conference Series, IOP Publishing, 2021, 1790, 1, 012084
[23] Hu, L., Yang, J., Chen, M., Qian, Y., Rodrigues, J.J., *SCAI-SVSC: Smart clothing for effective interaction with a sustainable vital sign collection*, In: Future Generation Computer Systems, 2018, 86, 329–338
[24] Krishna, K.V., Rao, M.V., Murthy, G.V., *Secured System Design for Big Data Application in Emotion-Aware Healthcare*, 2017
[25] Ahsan, M., Teay, S.H., Sayem, A.S.M., Albarbar, A., *Smart clothing framework for health monitoring applications*, In: Signals, 2022, 3, 1, 113–145

**Author:**

LUO QISHU

Guangdong Industry Polytechnic, Guangzhou, Guangdong-510000, China

**Corresponding author:**

LUO QISHU
e-mail: luoqishu2023@163.com, QishuLuo202306@outlook.com

# Investigations for the development of smart trousers for paraplegic wheelchair users. Part 1 – Design recommendations for smart trousers to improve the thermal comfort of the legs of paraplegics

DOI: 10.35530/IT.075.01.202320

ANDREJA RUDOLF
VANJA KOLANOVIČ
MONIKA HUDOURNIK
JASNA ŠTAMPFER
JAKOB NOVAK
MATEJ BOROVEC
ROK BELŠAK

**ABSTRACT – REZUMAT**

**Investigations for the development of smart trousers for paraplegic wheelchair users. Part 1 – Design recommendations for smart trousers to improve the thermal comfort of the legs of paraplegics**

*In this article, a study was conducted on the design of smart trousers to improve the thermal comfort of the legs of paraplegics. It was based on the survey of paraplegics about the thermoregulation of their legs in cold environments, the warming of the legs during and after outdoor activities, the type of clothing for outdoor activities and the need for smart heating clothing for the lower extremities. The skin surface temperatures on the legs of fully mobile people and paraplegics were measured in a neutral state to find out to which temperature the microclimate inside the trousers can be warmed and the smart trousers can be used safely. The survey of paraplegics was conducted nationwide and included sixty-one adult male and female subjects. Skin surface temperatures were measured at eight measurement points on the right and left leg and performed on eighteen participants. After evaluating all the results of this study, recommendations for the design of smart heating trousers were proposed. The results of this part of the research can provide designers with important information about the specific requirements for smart heating trousers and enable them to design and develop products that meet real needs and are safe for paraplegic wheelchair users. Furthermore, this work aims to raise awareness of the needs of wheelchair users that enable them to integrate into the social environment on an equal footing.*

***Keywords:*** *paraplegics, cold protection, thermal comfort, legs skin surface temperature, smart heating trousers design*

**Investigații pentru dezvoltarea pantalonilor inteligenți pentru utilizatorii cu paraplegie în scaune cu rotile. Partea 1 – Recomandări de proiectare pentru pantaloni inteligenți pentru a îmbunătăți confortul termic al picioarelor persoanelor cu paraplegie**

*În acest articol, a fost realizat un studiu despre designul pantalonilor inteligenți pentru a îmbunătăți confortul termic al picioarelor persoanelor cu paraplegie. Studiul s-a bazat pe sondajul efectuat persoanelor cu paraplegie despre termoreglarea picioarelor în medii reci, încălzirea picioarelor în timpul și după activitățile în aer liber, tipul de îmbrăcăminte pentru activități în aer liber și necesitatea îmbrăcămintei inteligente cu încălzire pentru extremitățile inferioare. Temperaturile suprafeței pielii picioarelor persoanelor complet mobile și ale persoanelor cu paraplegie au fost măsurate în stare neutră pentru a afla până la ce temperatură poate fi încălzit microclimatul din interiorul pantalonilor, iar pantalonii inteligenţi să poată fi utilizaţi în siguranță. Sondajul pentru persoanele cu paraplegie a fost realizat la nivel național și a inclus 61 de subiecți adulți, bărbați și femei. Temperaturile suprafeței pielii au fost măsurate în opt puncte de măsurare pe piciorul drept și stâng și efectuate pe optsprezece participanți. După evaluarea tuturor rezultatelor acestui studiu, au fost propuse recomandări pentru proiectarea pantalonilor inteligenţi cu încălzire. Rezultatele acestei părți a studiului pot oferi designerilor informații importante despre cerințele specifice pentru pantalonii inteligenţi cu încălzire și le permit să proiecteze și să dezvolte produse care răspund nevoilor reale și sunt sigure pentru utilizatorii cu paraplegie ai scaunelor cu rotile. În plus, această activitate urmărește să crească gradul de conștientizare cu privire la nevoile utilizatorilor de scaune cu rotile care să le permită să se integreze în mediul social în mod egal.*

***Cuvinte-cheie****: persoane cu paraplegie, protecție împotriva frigului, confort termic, temperatura suprafeței pielii picioarelor, design inteligent al pantalonilor cu încălzire*

## INTRODUCTION

Human thermal comfort has been defined as a state of mind that illustrates satisfaction with the thermal environment. Thermal comfort is related to the thermal balance between the human body and the thermal comfort of its environment [1, 2]. Exposure to cold can lead to cold injuries, which are divided into freezing and non-freezing injuries. Freezing cold injuries occur because the temperature is lowered by cooling to such an extent that the tissue fluid freezes. Non-freezing cold injuries occur when blood flow is reduced after cooling and the low temperature causes nerve damage. Less severe injuries include cracked

skin and frostbite or itchy swellings on the skin, typically on the hand or foot, nose or ears, caused by poor blood flow to the skin when exposed to cold [3–5].

With smart garments, it is possible to protect people from cold stress and put them in a thermally neutral or comfortable state. Three basic types of heating garments are known: electric heating garments with embedded heating elements, heating garments with phase change materials (PCM) that store and release large amounts of energy by changing the solid-liquid state, and chemical heating garments that use a reaction of chemical substances to generate heat [5].

This paper focuses on the design of smart trousers for a paraplegic wheelchair user. They are restricted in the movement of their lower limbs due to spinal cord injuries and often face other health problems such as incontinence, chronic urinary tract infections, skin irritation and inflammation, pressure ulcers, cardiovascular complications, frequent colds, poor blood circulation to the lower limbs and hence body temperature regulation and hypothermia of the lower limbs [6–8]. Previous research has shown that paraplegics are extremely careful to avoid hypothermia in their lower limbs. They try to regulate the temperature of the lower limbs when it is cold by choosing warm clothing, covering the legs with a blanket and keeping an eye on the duration of outdoor activities [8, 9]. Feng and Hui [10] conducted a systematic literature review on the clothing needs of wheelchair users. They found eight main characteristics related to the clothing needs of wheelchair users: functional needs, appropriate textile materials, safety aspects of clothing patterns, aesthetic and expressive needs, quality of life and extrinsic attributes, reflecting two general groups, the physical and psychological needs of wheelchair users. None of the research addresses smart clothing to protect the health and prevent additional injuries of wheelchair users.

The body temperature of a healthy person is very stable under normal conditions. It is usually measured orally and reflects the temperature of the blood [11–13]. The normal oral temperature measured in a large population ranges from 36.5°C to 36.9°C [12, 13], and the range of this interval is quite similar in many other studies. People with spinal cord injuries may have impaired regulation of body temperature or a poorer response to environmental changes. People with high-level spinal cord injuries may be particularly insensitive to changes in heat or cold, most likely due to loss of hypothalamic control, poor vasomotor responses, or other unknown factors [13]. Basically, in a hot environment, the body normally sends an overheating signal from the brain to the spinal cord. Then overheating is prevented by instructing the body to cool itself by sweating. In a cold environment, the brain sends the signal for the blood vessels to constrict to prevent hypothermia and signals us to dress warmer. Paraplegics have no sensation in the lower limbs (below the lesion) and cannot send these signals properly, so the body experiences hyperthermia (heat) or hypothermia (cold) [14]. In a study by Khan S. et al. [13], subnormal body temperature (35°C) was found to be very common in people with chronic spinal cord injury (66%), and a critically low temperature in the hypothermic range (<35°C) requiring therapeutic intervention was found in 3% of measurements.

When the skin temperatures of ten body segments of fully mobile subjects (forehead, upper arm, forearm, back of the hand, chest, thigh, anterior calf, posterior calf, instep of the foot) were examined at an air temperature of 20°C to 30°C at a rate of 1°C, the skin temperatures for the thigh were 32.0°C, the anterior calf 31.1°C, the posterior calf 30.2°C and the instep of the foot 30.3°C at an air temperature of about 25°C [15]. A study by Kingma et al. [16] analysed combinations of core body temperature (Tc), skin temperature (Ts), and ambient temperature (Ta) that correspond to the biophysical requirements of the thermoneutral zone (TNZ) in humans. The TNZ is defined as the range of ambient temperature in which the body can maintain its core temperature alone and in which heat production and heat loss are balanced [16]. It has been found that the TNZ for a clothed person is in the Ta range of 14.8°C – 24.5°C when the Ts range is between 28.8°C and 36.4°C and the Tc range is between 36°C and 38° [16]. Trbovich [17] investigated that the mean skin temperature at rest at neutral ambient temperature (20°C) in healthy (31.7°C) and spinal cord injured participants (31.4°C) and in participants with paraplegia (29.5°C) and tetraplegia (30.6°C) were similar, while in paraplegic individuals the skin temperatures at the thigh (30.3°C) and calf (29.0°C) were lower than in healthy individuals (thigh – 31.6°C; calf – 31.7°C).

Maintaining physical condition is the main activity of a paraplegic wheelchair user, using outdoor activities [18]. In windy, damp and cold weather, their integration into the social environment is hampered. To reduce the risk of cold injuries, wearing smart heating clothing can increase the time wheelchair users spend in a cold environment.

There are no special smart heating trousers on the world market that are suitable and safe for wheelchair users. The reasons for this are: (a) paraplegic wheelchair users have no feeling of warmth in their legs, (b) the design of the trousers must be adapted to the sitting posture [19] and (c) the constant contact of the buttocks, hips and thighs (back) with the wheelchair. The heating trousers on the market can cause additional health problems for paraplegic wheelchair users. Heating pads in the area of the buttocks or hips in contact with the wheelchair can in fact cause sweating and inflammation of the skin as well as pressure sores, as we can see from the examples [20, 21]. The electric heating pads available on the market can be easily integrated into clothing. They are washable, produce a maximum temperature of 65°C and should not be used by people who are not sensitive enough to heat [22]. What all the heating garments presented here have in common is that we can choose the temperature of the

heating elements ourselves, which is not without danger for paraplegics.

The main objective of this research was to: (1) identify the problems of paraplegic wheelchair users with thermoregulation of their legs and their needs in terms of developing smart heating trousers to maintain the thermoneutral status of paraplegics in cold outdoor conditions by surveying paraplegics, (2) investigate the skin surface temperature of the legs of fully mobile persons and wheelchair users to find out temperature to which the microclimate within the trousers can be heated so that the smart heating trousers can be used safely; and (3) present design recommendations for smart heating trousers that will enable paraplegics to use them safely on a controlled temperature basis within the trouser microclimate.

## METHODOLOGY

### Survey

A survey was conducted among the members of the Slovenian Paraplegic Association. The questionnaire was divided into three groups in addition to the basic questions: (1) thermoregulation of the lower extremities and garments commonly used to warm the legs outdoors, (2) need for smart heating garments and specific desires to control them, and (3) other functional characteristics of smart heating garments. The questionnaire was answered anonymously and contained different types of questions: demographic questions, dichotomous questions, multiple choice questions and open questions to get the best possible opinion on smart heating garment design. The questionnaire was analysed using descriptive statistics, as the main purpose was to get a clear need and idea about smart heating garment design.

### Measurements of the skin surface temperatures on the legs

To assess the ability of the lower extremities to thermoregulate, measurements of the surface skin temperatures on the legs of the two groups, healthy fully mobile individuals and paraplegic individuals, in continuation Fully Mobile Individuals (FMI) and Immobile Individuals (IMI), were made using a FLIR thermal camera. The locations of the measurements were based on the results of the questionnaire.

*Participants and measurements*

Measurements were taken on 18 volunteer participants, 10 FMI and 8 IMI. A total of fourteen men (7 FMI, 7 IMI) and four women (3 FMI, 1 IMI) participated in both groups. The basic data of the measured individuals are listed in table 1.

Skin surface temperatures were measured at eight measurement points on both the right leg (RL) and the left leg (LL): T1 – middle of the anterior midline of the thigh; T2 – lateral lower thigh above the knee; T3 – middle of the front of the knee; T4 – middle of the anterior midline of the tibia; T5 – middle of the lateral line of the tibia; T6 – ankle lateral; T7 – middle part of the instep; T8 – thumb. The subjects' measurements were taken at rest, sitting in a wheelchair or chair, at a daytime temperature of 24°C ± 1°C and relative humidity of 50% ± 2.5%, wearing shorts and a T-shirt. This daytime temperature provided a thermoneutral environment [16] during the measurements. All participants were informed in advance about the research purposes and the requirements for the measurements and had the opportunity to discuss these before giving their consent to participate.

*Data Analysis*

Average values ($\bar{x}$), standard deviations (SD) and coefficients of variation (CV) of the skin surface temperatures measured at eight points on the legs were calculated. The differences between the average values of the skin surface temperatures of RL and LL were calculated for FMI and IMI and between FMI and IMI for both legs.

### Design recommendations for smart heating trousers

After reviewing all the data collected in this study as well as literature studies, recommendations for the design of smart heating trousers were proposed. The requirements for smart heating trousers for paraplegic wheelchair users were divided into four different groups, summarised by source [23]: (a) fit and comfort, (b) textile materials, (c) safety and (d) special requests.

## RESULTS AND DISCUSSION

### Results of the survey

Sixty-one paraplegics, both men (70%) and women (28%), who using a wheelchair for an average of 19.6 years, answered the questionnaire (no response 1%). The survey was mainly attended by paraplegics over 41 years of age: age group 18–20 years (3%), 21–30 years (5%), 31–40 years (13%), 41–50 years (25%), 51–60 years (28%) and over 60 years (26%).

Table 1

BASIC DATA OF THE INDIVIDUALS MEASURED

| IMI | | | | FMI | | | |
|---|---|---|---|---|---|---|---|
| **Age (years)** | **Height (cm)** | **Weight (kg)** | **BMI** | **Age (years)** | **Height (cm)** | **Weight (kg)** | **BMI** |
| Male (mean ± SD) | | | | Male (mean ± SD) | | | |
| 51.71 ± 10.32 | 174.86 ± 3.44 | 84.14 ± 7.95 | 27.48 ± 1.88 | 25.50 ± 10.76 | 181.20 ± 12.48 | 78.80 ± 16.67 | 23.67 ± 3.39 |
| Female (mean ± SD) | | | | Female (mean ± SD) | | | |
| 54.00 ± 0.00 | 170.00 ± 0.00 | 50.00 ± 0.00 | 17.30 ± 0.00 | 21.33 ± 2.08 | 164.33 ± 5.13 | 65.67 ± 13.43 | 25.65 ± 5.25 |

*Lower limb thermoregulation and garments to warm the legs outdoors*

The paraplegic wheelchair users predominantly estimate the warmth of their legs as chilly – fairly cold (39%) and cool – slightly cold (31%). Some of them estimate that their legs are usually icy – very cold (11%) and some that they are warm (13%), while of the 5% of respondents, their legs are icy in winter and the feeling of their legs depends on the temperature and their legs cool down very quickly. Problems with hypothermia were already experienced by 25% of the paraplegic respondents.

When asked what kind of leg protection they use, most respondents answered with a blanket (41%) and only 8% with a heating leg bag. A surprisingly high percentage of paraplegics do not use leg protection (34%). This is consistent with the responses to the open-ended questions that some of them prefer to wear two pairs of trousers or warm functional ski underwear under their trousers. They also prefer warm functional socks (36%) and gaiters (25%).

The answers clearly show that paraplegic wheelchair users want to warm their feet (72%), knees (64%), ankles (64%), shins (52%), and thighs (26%). The open response on the parts of the body that should not be warmed revealed that these are the buttocks, abdomen, crotch and the parts of the hips and thighs that come into contact with the wheelchair.

*Needs for smart heating garment and particular desires for its control*

Of the sixty-one paraplegic wheelchair users, almost all respondents (98%) expressed a desire for a smart garment that warms their legs. They would feel safer if the smart heating garment measured the temperature of their legs and displayed it on their smartphone (89%), as well as the outside temperature (69%). They would like to control the smart heating garment with their smartphone (66%), with buttons integrated into the garment (23%), with a touch screen attached to the wheelchair (10%), and with a wristband on their hand (1%).

The results show how strong the desire for outdoor social contact is among wheelchair users. With smart heating garments, they would like to go for a long walk (84%), participate in social (62%) and sporting events (56%) and have a chat over a coffee outside (61%). 46% of respondents would like to do their outdoor activities between 1 and 3 hours and 38% between 3 and 5 hours.

*The desire for a specific smart heating garment and its' functional properties*

Respondents were asked what type of smart heating garment they would prefer to wear. 41% of the respondents answered that they would like smart heating trousers in the classic trousers pattern design, while 25% of the paraplegics prefer sports trousers, only 7% skinny trousers and 5% others (jeans, custom-made). The paraplegics expressed that the smart heating garment should above all be easy to put on (90%), windproof (82%), waterproof (70%) and have an aesthetic appearance (46%). Under the trousers, they wear ski underwear (36%), stockings (33%), and leggings (18%) in a cold environment. They want the trousers to close with a zip (57%), Velcro (15%), buttons (13%), snaps (2%) and others (11% – elastic band). They predominantly (90%) want trousers in neutral colours and less in bright colours.

From the results of the survey, it can be concluded that paraplegic wheelchair users would like to have smart heating trousers that only warm the front of the thighs and the entire knee, shin and ankle area for a period of 1 to 5 hours during outdoor activities. They would feel safer if the smart heating trousers measured and displayed the temperature of their legs and the outside temperature. They would like the smart heating trousers to be controllable via a smartphone. In addition, the trousers should have a classic pattern design, be made of windproof and waterproof textile material in neutral colours, have a zip, be easy to put on and look aesthetically pleasing.

**Skin surface temperatures on the legs**

The results of the measured skin surface temperatures of the legs under thermoneutral environmental conditions at the eight temperature measurement points (T1 – T8) on the right leg (RL) and left leg (LL) for FMI and IMI are summarised in table 2.

The average skin surface temperatures at the measured points on the legs vary between 28.31°C (T8-LL) and 32.70°C (T5-LL) for FMI and between 26.31°C (T8-RL) and 29.00°C (T6-LL) for IMI. The lowest skin surface temperature is measured at the thumb (T8) for both FMI and IMI. For both FMI and IMI, there are large differences between T8 for the individuals measured, as the CV for FMI is 18.25% (RL) and 16.57% (LL) and for IMI the CV is 12.76% (RL) and 14.86% (LL). The comparison of skin surface temperatures between the right and left legs in figure 1 shows that the temperatures between the right and left legs are not as different for FMI as they are for IMI. The average difference in skin surface temperature between the left and right leg is 0.02°C for FMI and 0.5°C on average for IMI and is higher for the left leg, table 3.

The comparison of skin surface temperatures between FMI and IMI for the right and left leg shows a clear difference in the measured temperatures, which are higher for FMI, but their trend at the measurement points is similar, figure 2. The difference in skin surface temperature of the right leg between FMI and IMI ranges from 1.96°C (T6) to 4.40°C (T5) and for the left leg from 0.81°C (T8) to 3.84°C (T5), table 3. The average skin surface temperature of the right leg is 3.31°C higher for FMI compared to IMI and for the left leg, it is 2.79°C higher for FMI compared to IMI, table 3.

The measured skin surface temperatures on the legs and the results of this study are in agreement with the results of the studies [15, 17]. In the study of [24], skin surface temperature (SST) was measured on the 12 body regions (from the head to the sole of the foot) of 30 healthy individuals at a constant temperature and humidity of 24.4°C ± 1.1°C and

Table 2

| MEASUREMENTS OF SKIN SURFACE TEMPERATURES ON THE LEGS OF FMI AND IMI | | | | | | | | | | | | |
|---|---|---|---|---|---|---|---|---|---|---|---|---|
| **Measurement location on RL and LL** | **Measurements of the leg's skin surface temperatures** | | | | | | | | | | | |
| | **RL_FMI** | | | **LL_FMI** | | | **RL_IMI** | | | **LL_IMI** | | |
| | (°C) | SD(°C) | CV(%) | (°C) | SD(°C) | CV(%) | (°C) | SD(°C) | CV(%) | (°C) | SD(°C) | CV(%) |
| T1 – Middle of the anterior midline of the thigh | 31.76 | 1.15 | 3.61 | 32.24 | 1.40 | 4.38 | 28.50 | 1.87 | 6.56 | 28.99 | 1.51 | 5.21 |
| T2 – Lateral lower thigh above the knee | 32.32 | 1.38 | 4.26 | 32.24 | 1.36 | 4.21 | 28.63 | 2.34 | 8.18 | 28.70 | 1.91 | 6.64 |
| T3 – Middle of the front of the knee | 30.30 | 2.51 | 8.3 | 30.70 | 2.42 | 7.88 | 26.71 | 2.52 | 9.43 | 27.17 | 2.96 | 10.90 |
| T4 – Middle of the anterior midline of the tibia | 32.60 | 0.87 | 2.66 | 32.57 | 0.87 | 2.66 | 28.74 | 1.94 | 6.76 | 28.77 | 2.15 | 7.46 |
| T5 – Middle of the lateral line of the tibia | 32.63 | 0.90 | 2.76 | 32.70 | 0.89 | 2.73 | 28.23 | 2.04 | 7.22 | 28.86 | 2.08 | 7.22 |
| T6 – Ankle lateral | 30.06 | 2.64 | 8.79 | 30.08 | 2.9 | 9.63 | 28.10 | 2.79 | 9.94 | 29.00 | 2.33 | 8.05 |
| T7 – Middle part of the instep | 31.67 | 1.96 | 6.20 | 31.32 | 1.61 | 5.15 | 28.37 | 2.76 | 9.73 | 28.67 | 3.20 | 11.18 |
| T8 – Thumb | 28.73 | 5.24 | 18.25 | 28.31 | 4.69 | 16.57 | 26.31 | 3.36 | 12.76 | 27.50 | 4.09 | 14.86 |

Table 3

| DIFFERENCES (D) BETWEEN THE MEAN VALUES OF RL AND LL SKIN SURFACE TEMPERATURES AND BETWEEN FMI AND IMI | | | | |
|---|---|---|---|---|
| **Measurement location on RL and LL** | **Differences in the leg's skin surface temperatures (°C)** | | | |
| | $D_{RL-LL}FMI$* | $D_{RL-LL}IMI$* | $DRL_{FMI-IMI}$ | $DLL_{FMI-IMI}$ |
| T1 – Middle of the anterior midline of the thigh | – 0.29 | – 0.49 | 3.26 | 3.06 |
| T2 – Lateral lower thigh | 0.08 | – 0.07 | 3.69 | 3.54 |
| T3 – Middle of the front of the knee | – 0.40 | – 0.46 | 3.59 | 3.53 |
| T4 – Middle of the anterior midline of the tibia | – 0.20 | 0.03 | 3.86 | 3.80 |
| T5 – Middle of the lateral line of the tibia | – 0.07 | – 0.63 | 4.40 | 3.84 |
| T6 – Ankle lateral | – 0.02 | – 0.90 | 1.96 | 1.08 |
| T7 – Middle part of the instep | 0.34 | – 0.30 | 3.30 | 2.65 |
| T8 – Thumb | 0.42 | – 1.19 | 2.42 | 0.81 |
| Average difference | – 0.02 | – 0.50 | 3.31 | 2.79 |

Note: *A negative value means higher skin temperature of the left leg compared to the right leg.

46.3% ± 6.5%. This study found the highest SST of 35.0°C ± 0.5°C for the front of the neck, the thigh of 31.9°C ± 0.7°C and the lowest SST of 29.8°C ± 1.6°C for the sole of the left foot. The measurement conditions and results of this study for the SST of the legs agree quite well with our results for the FMI.

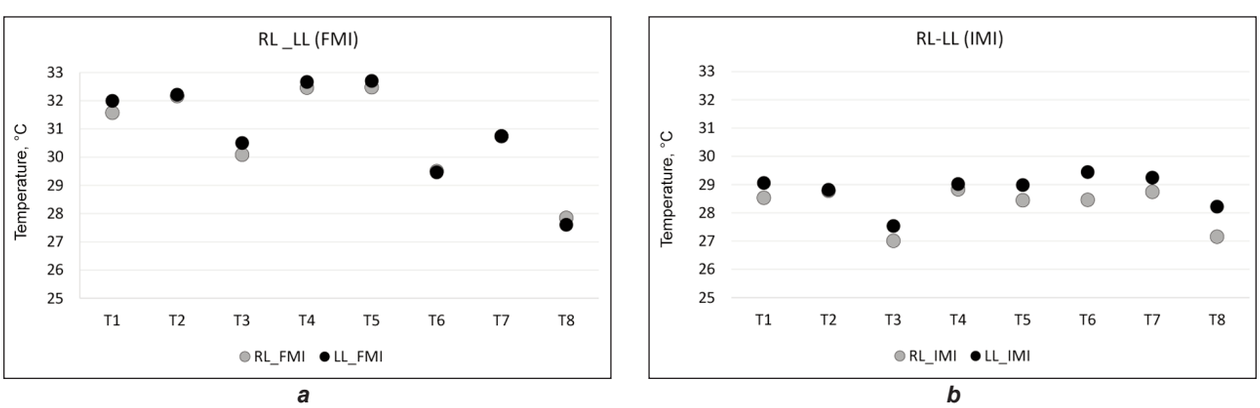


*a* *b*

Fig. 1. Comparison of skin temperatures between the right and left leg for: *a* – FMI; *b* – IMI

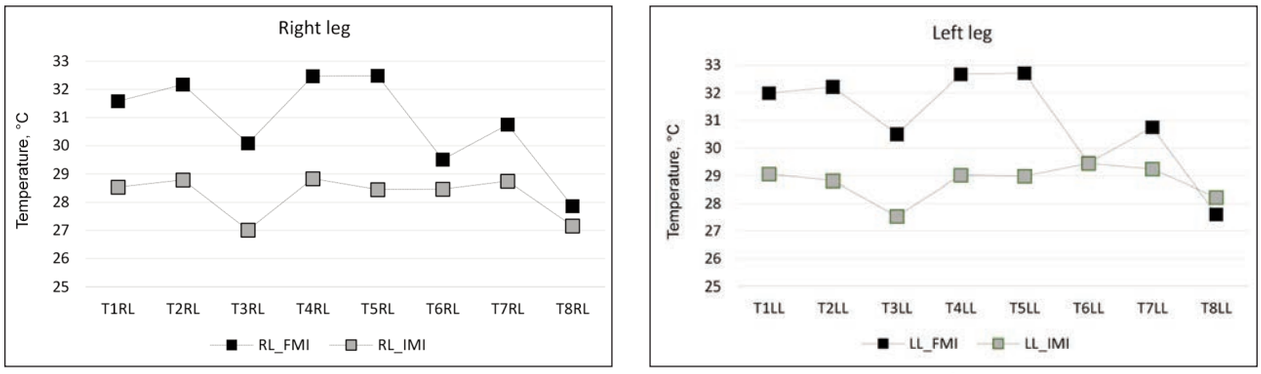


*a* *b*

Fig. 2. Comparison of skin surface temperatures between FMI and IMI for: *a* – the right leg; *b* – the left leg

The results obtained indicate that it is necessary to bring the skin temperature of paraplegics closer to that of a fully mobile person by regulating the microclimate of the garment.

Garments create a specific microclimate around the body that depends on the thermal state of the person, the environmental conditions and the characteristics of the garment. The temperature of the microclimate in clothing refers to the layer of air closest to the skin when people wear garments [25] and depends on many factors, such as the humidity and temperature under the clothing and the carbon dioxide under the clothing [26]. Under environmental conditions within the comfort range, it has been studied that the temperature of the innermost layer of the garment could have a greater impact on the comfort of wearing a particular garment than the temperature of the microclimate [25]. In this study, the temperature of the innermost layer of the garment was found to be slightly lower than the skin temperature.

The average skin surface temperature on the legs (T1-T6) without measurements on the foot (T7-T8) is 31.61°C for the right leg and 31.72°C for the left leg of FMI, i.e. 3.46°C higher for the right leg and 3.14°C higher for the left leg compared to IMI. Based on the results of this part of the study and the review of other studies, we can assume that the legs of paraplegics can be safely warmed to a skin surface temperature of 31.7°C. In the future, further research is needed on the relationship between the temperature of the inner layer of the smart heating garment, the skin surface temperature, and the thermal comfort of paraplegics to ensure the highest level of safety when wearing the smart heating garment.

## Design recommendations for smart heating trousers

The design of well-fitting, comfortable and functional garments should take into account the interaction between garment design and the characteristics of the human body, i.e. anatomical, physiological and psychological needs and desires.

Based on the results, the proposed design recommendations related to the different problems, needs and desires of paraplegics were classified into four groups, which are briefly explained in table 4. The design of the smart heating trousers is shown in figure 3, after which the prototype was developed and tested, the results of which will be presented in Part 2 of this article.

*Fit and comfort*

Adaptation of trousers to a sitting posture

Due to the sitting posture of paraplegics in wheelchairs, the smart heating trousers must be ergonomically adapted to the sitting posture and body measurements of the person. This is the only way to achieve a perfect fit and comfort in the trousers and to prevent possible additional health problems for paraplegics [19, 27].

(1) The trousers must be constructed according to the body measurements of the paraplegic in a sitting posture.

(2) To prevent the trousers from wrinkling below the waist and being uncomfortable and unaesthetic when sitting, the trousers should be designed lower at the front and higher at the back in the lumbar region to increase comfort and reduce possible health problems caused by an open lumbar region.

(3) Shifting the knee line to a seated posture prevents the trousers from putting pressure on the thighs.

(4) Lengthening the trouser legs is necessary because of the seated posture.

(5) Trousers should not be too tight and exert excessive pressure on the body, hindering blood circulation. On the other hand, they should not be too wide either, as this can cause skin irritation on the buttocks and hips due to wrinkling.

(6) Classic pockets on the front and back of the trousers can put excessive pressure on the body.

(7) All seams of the trousers, especially those in contact with the body, must be sewn as flat as possible to avoid friction and irritation of the skin of the paraplegic.

Easy dressing

The results of this and previous surveys have shown that one of the biggest functional requirements for trousers is to be easy to dress.

(1) The type of trouser fastening used by paraplegics is a zip, which can be slightly longer than in normal

Table 4

| RECOMMENDATIONS FOR THE DESIGN OF SMART HEATING TROUSERS FOR PARAPLEGICS | |
|---|---|
| **Problems and needs of paraplegics** | **Recommendations for the design of smart heating trousers** |
| Fit and Comfort | |
| Adaptation of trousers to a sitting posture | 1 – Body measurements<br>2 – Adjustment of trouser waistline to a sitting posture<br>3 – Shifting of knee line to a sitting posture<br>4 – Lengthening of trouser legs<br>5 – Adjustment of trousers width<br>6 – Without pockets<br>7 – Seams |
| Easy dressing | 1 – Zip fastening<br>2 – Elastic waistband<br>3 – Aids for dressing |
| Other | 1 – Easy handling of the urine bag<br>2 – Thermal insulation |
| Textile materials | |
| Functional textile materials | 1 – Durable and soft textiles<br>2 – Good thermal insulation<br>3 – Waterproof and windproof<br>4 – Highly breathable |
| Safety | |
| Trousers heating areas | 1 – The permitted areas of heating |
| Controlled regulation of the temperature of the microclimate in the trouser | 1 – Maximum microclimate temperature<br>2 – Microclimate temperature sensors<br>3 – Automatic shutdown of heating<br>4 – Turning on the heating<br>5 – Application for temperature regulation<br>6 – Position of switch, microcontroller, and battery |
| Special desires | |
| Trousers appearance | 1 – Classic pattern design<br>2 – Neutral colours<br>3 – Aesthetic appearance |
| Use | 1 – Outdoor activities<br>2 – Care |

trousers to create more volume and make the trousers easier to pull onto the body.

(2) The use of an elastic band at the waist helps to easier dressing and improves the fit and comfort of the trousers.

(3) Dressing aids in the form of sewn-in longer inner loops at the back of the trousers at the waist can assist paraplegics in pulling the trousers onto the body.

Other

(1) Due to urinary incontinence, some paraplegics need to use a urine bag, which is usually worn on the calf. It is therefore necessary to adjust the width of the trouser leg on the side of the urine bag and discreetly insert a hidden zip in the seam to facilitate changing the urine bag.

(2) To ensure good thermal insulation and prevent heat from escaping along the length of the trousers, the inner edge of the trouser legs can be fitted with an elastic cuff.

*Textile materials*

The desire for outdoor activities and social contact, even in a cold environment, is very strong among wheelchair users. Therefore, when developing smart heating trousers, we must always choose textiles with good thermal insulation as well as water and wind-resistant textiles. Sweating and wetness on the skin, especially at the contact areas between the body and the wheelchair, require the selection of highly breathable and soft textiles to avoid skin irritation or inflammation. Paraplegics pull their trousers on their body and the trousers rub when sitting in a wheelchair, which requires the selection of a durable textile material for smart heating trousers.

*Safety*

Trousers heating areas

The permitted areas for heating in smart trousers are ankles, calves, knees and thighs. Heating of the buttocks, abdomen, crotch and areas of the hips and thighs that are in constant contact with the wheelchair is not permitted for health reasons for paraplegics.

Controlled regulation of the temperature of the microclimate in the trousers

(1) The maximum allowable temperature of the microclimate of the smart heating trousers must be

automatically controlled and regulated to ensure maximum safety from overheating of the body. In this study, the highest average skin surface temperature on the leg in a healthy person was found to be 31.7°C, measured in the thermally neutral zone and at rest. Research [26] shows that the optimal skin surface temperature at rest is 32.1°C – 34.3°C. If this temperature deviates between 1.5°C – 3.0°C, the person feels slightly cold or hot, and if it deviates by more than 4.5°C, they feel uncomfortable. Based on this data, the prototype of the smart heating trousers should be tested in the next phase of the research under different weather conditions and depending on the activity of the paraplegic.

(2) Based on the results of this study, the temperature of the microclimate inside the trousers should be measured on the inside of each trouser leg so that we have control over both legs and the possibility of regulating them, figure 3.

(3) The algorithm should automatically switch off the heating when the maximum allowable temperature of the trouser microclimate is reached so that the body does not overheat and the paraplegic is not injured.

(4–6) Based on this research, it is recommended that the heating of the trousers also be switched on and off via the application on the mobile phone.

(5) The application for regulating the temperature of the trouser microclimate should display both the real temperature of the environment and the temperature of the microclimate of both trouser legs on the phone.

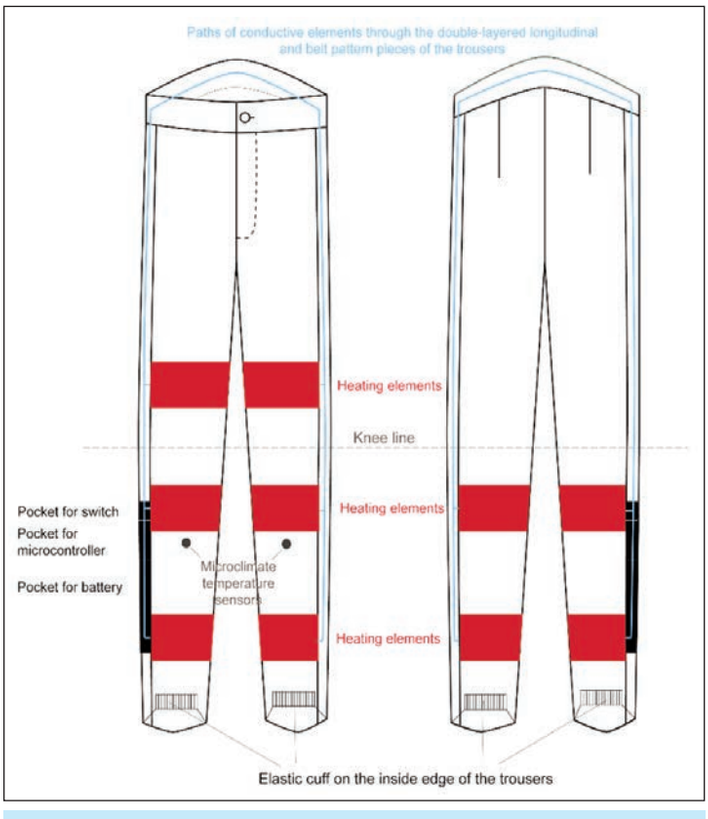


Fig. 3. A design of smart heating trousers

(6) The switch, the microcontroller and the battery should be located on the longitudinal side part of the trousers below the knee so that they do not come into contact with the wheelchair.

*Special desires*

Trousers appearance

(1–3) The smart heating trousers should have a classic pattern design, be made of functional textile material in neutral colours and look aesthetically pleasing.

Use

(1) Smart heating trousers shall allow wheelchair users to move outdoors for 1 to 5 hours (data needed to power the trousers with the battery).

(2) The battery must be removed from the trousers before washing, the microcontroller and switch are sealed inside the trousers to be waterproof.

## CONCLUSIONS

The thermoregulatory centre of paraplegics is disturbed due to damage to the spinal cord, and the perception and regulation of lower limb temperature are impaired. The first part of this article deals with the design of a smart heating garment to protect the lower limbs of wheelchair users, while the developed prototype and the results of its tests are presented in Part 2 of this article.

Based on the findings from the survey of wheelchair users and measurements of skin surface temperatures of FMI and IMI, the design of smart heating trousers was developed to improve the thermal comfort of paraplegics. It covers the full range of parameters divided into four basic groups about the different problems, needs and desires of paraplegics. The proposed smart heating system in trousers informs the user of the ambient temperature and the temperature of the microclimate in each trouser leg and enables automatic temperature regulation, switching off when the required temperature is reached and providing heat for up to five hours.

The application potential is broader as the wheelchair user group also includes other groups of people with spinal cord injuries who have impaired thermoregulation of the lower extremities, as well as elderly people.

## ACKNOWLEDGEMENTS

The authors would like to express their deepest gratitude to all those who participated in the research.

## FUNDING

The research was partially supported financially by the European Union through the European Social Fund and Slovenian Ministry of Education, Contract number: 11081-24/2018, as well as by the Slovenian Research Agency (Research Programme P2-0123: Clothing Science, Comfort and Textile Materials).

## REFERENCES


[1] Wang, X.L, Peterson, F.K., *Estimating thermal transient comfort.* In: ASHRAE Transactions, 1992, 98, Part 1 (paper number 3561), 182–188

[2] ASHRAE Standard 55: 2010, *Thermal environmental conditions for human occupancy*. Atlanta: American Society of Heating, Refrigerating, and Airconditioning, Inc.

[3] Parsons, K., *Human thermal environments – the effect of hot, moderate and cold environments on human health, comfort and performance,* (2nd ed.), London, UK: Taylor & Francis, 2003

[4] Edholm, O.G, Weiner, J.S., *The principles and practice of human physiology,* (1st ed.), London, UK: Academic Press, 1981

[5] Wang, F., Gao, C., Kuklane, K., Holmér, I., *A Review of Technology of Personal Heating Garments*. In: International Journal of Occupational Safety and Ergonomics (JOSE), 2010, 16, 3, 387–404

[6] Chang, W.M., Zhao, Y.X., Guo, R.P., Wang, Q., Gu, X.D., *Design and Study of Clothing Structure for People with Limb Disabilities*. In: Journal of Fiber Bioengineering and Informatics, 2009, 2, 2, 61–66

[7] Šavrin, R., *Patient with chronic spinal cord lesion*, In: Šavrin R (ed) Pozni zapleti pri bolnikih z okvaro hrbtenjače (in Slovene) (Late complications of patients with spinal cord impairment), Ljubljana: University Rehabilitation Institute Republic of Slovenia – Soča, 2015

[8] Rudolf, A., Stjepanović, Z., *Protective garments for wheelchair users*, In: Proceedings book, 1st International Conference "Engineering and Entrepreneurship", ICEE 2017, November 17–18, 2017, Tiranë, Alb. Tiranë: Promo print sh.p.k. (promo publishing).

[9] Rudolf, A., Drstvenšek, I., Šauperl, O., Brajlih, T., Strnad, M., Ermenc, H., Bačun, U., Berkovič, L., Selimović, I., Görlichová, L., Kožuh, A., Lemut, M., Jevšnik, M., Salobir, A., Zadravec, M., *Research and development of functional garments for paraplegics,* (In Slovene): Public call for co-financing of projects Following the creative path to practical knowledge: contract number 11047-23/2014, University of Maribor, Faculty of Mechanical Engineering, 2015

[10] Feng, Q., Hui, C., *Clothing Needs for Wheelchair Users: A Systematic Literature Review*, In: Advances in Aging Research, 2021, 10, 1, 1–30

[11] McCullough, L., Arora, S., *Diagnosis and treatment of hypothermia*, In: American Family Physician, 2004, 70, 12, 2325–2332

[12] Ivy, A.C., *What is normal or normality?,* In: Q Bull Northwestern Univ Med School, 1944, 18, 1, 22–32

[13] Khan, S., Plummer, M., Martinez-Arizala, A., Banovac, K., *Hypothermia in Patients With Chronic Spinal Cord Injur*, In: The Journal of Spinal Cord Medicine, 2007, 30, 1, 27–30

[14] Shirley Ryan, *AbilityLab. Spinal Cord Injury Complications: Temperature Regulation*, Available at: https://www.sralab.org/lifecenter/resources/spinal-cord-injury-complications-temperature-regulation [Accessed on August 29, 2022]

[15] Choi, J.H., Loftness, V., *Investigation of human body skin temperatures as a bio-signal to indicate overall thermal sensations*, In: Building and Environment, 2012, 58, 258–269

[16] Kingma, B.R., Frijns, A.J., Schellen, L., van Marken Lichtenbelt, W.D., *Beyond the classic thermoneutral zone, Including thermal comfort*, In: Temperature (Austin), 2014, 1, 2, 142–149

[17] Price, M.J., Trbovich, M., *Thermoregulation following spinal cord injury,* In: Romanovsky, A.A. (Ed.). Handbook of Clinical Nurology: Thermoregulation: From Basic Neuroscience to Clinical Neurology, 2018, Part II, 157, 799–820

[18] Musil, B., Čuš Babič, N., Šenk, P., Rudolf, A., Kregar, L., Štampfer, J., Kuharič, M., Jerič, J., Rudolf, T., Žnidaršič, L., Mernik, P., Fašmon, M., Lubej, A., Vrečko, V., *Paraplegics and the social environment,* (In Slovene): Public call "Project work with the non-economic and non-profit sector – student innovative project for social benefit 2016–2018": contract number: 11083-25/2017, University of Maribor, Faculty of Mechanical Engineering, 2018

[19] Rudolf, A., Cupar, A., Kozar, T., Stjepanović, Z., *Study regarding the virtual prototyping of garments for paraplegics*, In: Fibers and Polymers, 2015, 16, 5, 1177–1192

[20] *ActionHeat 5V Base Layer Battery Heated Pants for Men – Electric Heating Pants with Tri-Zone Heating Panels – Heated Trouser for Cold Weather Outdoor Camping, Hiking, Motorcycling*, Available at: https://www.amazon.com/ActionHeat-Layer-Battery-Heated-Pants/dp/B07Z6HX2BC [Accessed on February 23, 2023]

[21] *Gerbing Heated Pant Liner – 12V Motorcycle*, Available at: https://www.thewarmingstore.com/gerbing-gyde-12v-heated-pant-liner.html [Accessed on February 23, 2023]

[22] *5pcs 65°C Electric Heating Pad 3 Gear Adjusted DIY Thermal Vest Heated Clothes*, Available at: https://www.banggood.com/5pcs-65-Electric-Heating-Pad-3-Gear-Adjusted-DIY-Thermal-Vest-Heated-Clothes-p-1255073.html?rmmds=detail-top-buytogether-auto&cur_warehouse=CN [Accessed on February 23, 2023]

[23] Bragança, S., Castellucci, I., Gill, S., Matthias, P., Carvalho, M., Arezes, P., *Insights on the apparel needs and limitations for athletes with disabilities: The design of wheelchair rugby sports-wea*r, In: Applied Ergonomics, 2018, 67, 9–25

[24] Lee, C.M., Jin, S.P., Doh, E.J., Lee, D.H., Chung, J.H., *Regional Variation of Human Skin Surface Temperature*, In: Annals of Dermatology, 2019, 31, 3, 349–352

[25] Kwon, J., Choi, J., *Clothing insulation and temperature, layer and mass of clothing under comfortable environmental conditions*, In: Journal of Physiological Anthropology, 2013, 32, 11, 1–8

[26] Parkova, I., Vilumsone, A., *Microclimate of Smart Garment*, In: Scientific Journal of Riga Technical University, Material Science. Textile and Clothing Technology, 2011, 6, 99–104

[27] Rudolf, A., Görlichová, L., Kirbiš, J., Repnik, J., Salobir, A., Selimović, I., Drstvenšek, I., *New technologies in the development of ergonomic garments for wheelchair users in a virtual environment*, In: Industria Textila, 2017, 68, 2, 83–94, https://doi.org/10.35530/IT.068.02.1371

**Authors:**

ANDREJA RUDOLF[1], VANJA KOLANOVIČ[2], MONIKA HUDOURNIK[3], JASNA ŠTAMPFER[4], JAKOB NOVAK[5], MATEJ BOROVEC[6], ROK BELŠAK[7]

[1]University of Maribor, Faculty of Mechanical Engineering, Institute of Engineering Materials and Design, 2000 Maribor, Slovenia

[2]University of Maribor, Faculty of Medicine, 2000 Maribor, Slovenia
e-mail: vanja.kolanovic@student.um.si

[3]3fs Nordic SI, d. o. o., 2000 Maribor, Slovenia
e-mail: hudournik.mony@gmail.com

[4]Žiher d.o.o., 2272 Gorišnica, Slovenia
e-mail: jasna.stampfer@gmail.com

[5]Inel d.o.o., 3000 Celje, Slovenia
e-mail: jakob.novak@inel.com

[6]AVL, Battery engineering, Hans-List-Platz 1, 8020 Graz, Austria
e-mail: matejbrvc105@gmail.com

[7]University of Maribor, Faculty of Mechanical Engineering, Mechanical Engineering Research Institute, 2000 Maribor, Slovenia
e-mail: rok.belsak@um.si

**Corresponding author:**

ANDREJA RUDOLF
e-mail: andreja.rudolf@um.si

# Investigations for the development of smart trousers for paraplegic wheelchair users. Part 2 – Development of a test prototype of smart heating trousers

DOI: 10.35530/IT.075.01.202325

ANDREJA RUDOLF
VANJA KOLANOVIČ
MONIKA HUDOURNIK
JASNA ŠTAMPFER
JAKOB NOVAK
MATEJ BOROVEC
ROK BELŠAK

**ABSTRACT – REZUMAT**

**Investigations for the development of smart trousers for paraplegic wheelchair users. Part 2 – Development of a test prototype of smart heating trousers**

*The main objective of this research was to develop smart trousers for paraplegic wheelchair users to improve the thermal comfort of their lower extremities when exposed to cold environments. In this part of the research, a test prototype of smart heating trousers was developed and tested on the thermal manikin. The development of the test prototype of the smart heating trousers is based on the design recommendations explored in the first part of this paper. The design recommendations relate both to the development of a trousers pattern design for the sitting posture of wheelchair users and the possibility of integrating electrical components into the trouser design, as well as the development of a smart heating system that provides safety for the wearer of the trousers. The results of this part of the research show that the developed smart heating trousers can improve the thermal insulation of the legs and the thermal comfort of the wearer. This is ensured by a carefully planned and safe algorithm that automatically regulates the temperature of the microclimate inside the trousers.*

***Keywords:*** *paraplegics, cold protection, thermal comfort, smart heating trousers, thermal insulation*

**Investigații pentru dezvoltarea pantalonilor inteligenți pentru utilizatorii cu paraplegie în scaune cu rotile. Partea 2 – Dezvoltarea unui prototip de testare ai pantalonilor inteligenţi cu încălzire**

*Obiectivul principal al acestui studiu a fost de a dezvolta pantaloni inteligenți pentru utilizatorii cu paraplegie în scaune cu rotile, pentru a îmbunătăți confortul termic al extremităților inferioare atunci când sunt expuse la medii reci. În această parte a studiului, a fost dezvoltat și testat un prototip de testare ai pantalonilor inteligenţi cu încălzire pe manechinul termic. Dezvoltarea prototipului de testare al pantalonilor inteligenţi cu încălzire se bazează pe recomandările de proiectare explorate în prima parte a acestui studiu. Recomandările de proiectare se referă atât la dezvoltarea unui model de pantaloni pentru postura de șezut a utilizatorilor în scaune cu rotile, la posibilitatea de a integra componente electrice în designul pantalonilor, cât și la dezvoltarea unui sistem inteligent de încălzire care oferă siguranță purtătorului de pantaloni. Rezultatele acestei părți a studiului arată că pantalonii inteligenţi cu încălzire dezvoltați pot îmbunătăți izolarea termică a picioarelor și confortul termic al purtătorului. Acest lucru este asigurat de un algoritm atent planificat și sigur care reglează automat temperatura microclimatului din interiorul pantalonilor.*

***Cuvinte-cheie****: persoane cu paraplegie, protecţie la frig, confort termic, pantaloni inteligenţi cu încălzire, izolaţie termică*

## INTRODUCTION

Health is wealth, and we can support it with appropriate garments, especially when there is heat or cold stress on a person. With smart garments, we can protect people from cold stress by putting them in a thermally neutral or comfortable state. Paraplegics are particularly exposed to cold stress due to poor blood circulation in the lower limbs and the associated regulation of body temperature and hypothermia of the lower limbs. Therefore, we need to provide them with functional textile materials and clothing systems that can prevent cold stress.

The realisation that multi-layer clothing systems compress the inner layer of air, reducing its thickness and significantly decreasing the insulation of the garment, is likely to encourage the development of functional textile materials for cold protection that are thinner and provide better thermal insulation than the multi-layer clothing systems we used to wear. Multi-layered clothing systems are also usually stiffer and restrict the user's freedom of movement. Today, people are striving for ever greater comfort and clothing is becoming thinner and thinner while still providing the same level of warmth as thicker clothing [1] or multi-layer clothing systems. Smart heating clothing can meet these requirements very well and its concept was developed a long time ago [2].

Based on the advantages and disadvantages of personal heating garments described in the article by Wang et al. [3], it was found that electric heating

garments have a promising feature. At the same time, they pointed out that the battery power does not meet the demands placed on electric heating clothing for long stays in cold environments. Today, functional textile materials and miniaturised electronic components enable the realisation of smart garments that improve or extend the functionality of ordinary garments. Together with mobile phones, they include applications that have an easy-to-use interface and use Bluetooth as a wireless communication method [4]. To avoid the risk of disease and physical harm and to increase thermal comfort, various personal heating systems have been developed to provide thermal comfort to the body through integrated heating units, e.g. heated garments, heated socks and gloves, heated insoles [5]. In this article, four types of personal heating systems (electrically heated seat, electrically heated garment, electrically heated garment with an aerogel layer and chemically heated insole) were studied in different cold environments. The results showed that the ambient temperature had no significant effect on the insulation of the garment, while increased air velocity significantly reduced the insulation of the garment. Electric heaters were also used in the construction of sleeping bags to improve thermal comfort for the feet and allow eight hours of comfortable sleep in the cold environment studied [6]. Wu et al. [7] have developed a smart heating garment for elderly women that uses a carbon heating film and can automatically adjust the microclimate to different thermal conditions. Older people's ability to regulate their body temperature decreases with age and they are more prone to thermal discomfort in a cold environment. The difference between them and paraplegics is that older people still perceive the warmth of the lower extremities, whereas paraplegics do not. A study conducted by Feng Q. and Hui [8] on the clothing needs of wheelchair users has shown that there is no developed smart garment to improve the thermal comfort of the lower extremities of paraplegics.

The thermal insulation of garments can be determined with the help of the thermal manikin. The early thermal manikins are static and standing, which provides only limited information. Therefore, they were developed with joints that allow the manikin to move. The dry manikin can measure the thermal insulation of clothing, while a sweating manikin can provide more valuable information about heat transfer through evaporation [9–11]. Research into the thermal insulation of clothing with thermal manikins is particularly important for protective clothing to ensure adequate protection against hazards [10, 12, 13], as well as for testing different types of everyday clothing for cold environments in different environmental conditions, such as down jackets, motorbike jackets [14, 15], or also for clothing systems designed for work in office [16].

The main objective of this part of the research was to develop a test prototype of smart heating trousers, to test the developed smart heating system and the thermal insulation of the prototype smart heating trousers using the thermal manikin.

## METHODOLOGY

The development of the test prototype of smart heating trousers is based on the research presented in the first part of this article. It provides insights into the thermoregulation of the lower limbs of paraplegics and proposes the design of smart heating trousers based on the results of an extensive survey of paraplegics and a literature review of the clothing requirements and needs of paraplegics.

### Development of the test prototype of smart heating trousers

The design of the smart heating system in the trousers is based on detecting the temperature of the microclimate in the left and right trouser leg and automatically regulating the temperature in the left and right trouser leg to the maximum allowable temperature for the safety of the user. It is integrated into the design of the paraplegic trousers and manages the smart heating system via a Bluetooth application.

The pattern design of the prototype of the smart heating trousers was developed based on the four categories of requirements studied (fit and comfort, textile materials, safety, and special requirements) and presented in the first part of this article. In addition, the size of the smart heating trousers was adapted to the dimensions of the male thermal manikin to be able to carry out tests on the thermal insulation of the trousers.

The softshell fabric used to make a test prototype of the smart heating trousers has a surface weight of 346.37 $gm^{-2}$ and a thickness of 1.826 mm. This textile material itself provides good thermal insulation. It is waterproof, windproof, highly breathable, soft, and high-performing.

### Testing the prototype of smart heating trousers

To measure the temperature and heat flow for the nineteen segments under constant test conditions, a thermal manikin was used, keeping the temperature of all nineteen segments of the manikin constant according to the standard ISO 15831 [17–19].

This thermal manikin heats all nineteen segments from standard environmental temperature to a fixed temperature of 36 °C. Therefore, for testing the designed smart heating system, the maximum allowable microclimate temperature of the smart heating trousers was set at 36.5 °C. The temperature and heat flow were then measured. The thermal resistance of an individual segment of the manikin was calculated using the known area of the individual segments. The thermal insulation of the garment for a manikin segment in Clo (1 Clo = 0.155 $K \cdot m^2 \cdot W^{-1}$) is automatically calculated for each of the nineteen segments individually. The thermal insulation results are given for the smart heating trousers (a) without heating and (b) with heating for eight leg segments between the nineteen segments of the manikin (right

and left thigh on the front and back, right and left calf on the front and back). During the tests, the thermal manikin was dressed in a T-shirt and a jumper to prevent heat loss. Jeans and trousers are normally worn by paraplegic men. Therefore, a comparison of the thermal insulation of jeans trousers and smart heating trousers was carried out.

The thermal properties of the fabrics for the tested trousers were evaluated using a KES-FB Thermo Labo II. The warm-cool feeling (qmax), the constant thermal conductivity (λ), and the constant thermal resistance (R) were determined.

## RESULTS AND DISCUSSION

### Test prototype of smart heating trousers

The design of the smart heating trousers was recommended in the first part of the article, figure 1, *a*. The development of the pattern design of the test prototype of smart heating trousers was based on design recommendations and a schematic diagram of the connection of heating elements with electrical components and communication via a Bluetooth connection with a mobile phone, figure 1, *b*, as well as on the dimensions of the heating elements and electrical components. Electric heating pads are one of the most practical and advanced technologies today and can significantly improve thermal comfort. However, their usefulness must be adapted to the specifics of the user to avoid heat damage and burns from the heat. The textile structure of the heating pad is a general form of multi-layer structure in which a conductive material (carbon fibre wire) is sewn inside the two base layers of cotton fabric. When an electric current is applied, the resistivity of the conductive material causes the heating pad to heat up. On the outside of the heating pad is an insulating layer that prevents excessive temperature loss.

The developed trousers have a classic pattern design without pockets and have an extended zip fastening and a waistline adapted to the sitting posture of paraplegics.

During the development process of the trousers pattern, attention was paid to the correct position and insertion of the heating elements in the permissible body areas of the heating, as these must not be located in the areas where the body comes into contact with the wheelchair. At the same time, attention was also paid to the connections of the heating elements and temperature sensors with the microcontroller. Thus, the pattern pieces of the trousers are constructed in such a way that they allow the placement of conductive paths for the connection of the electronic functional blocks.

The heating elements are inserted inside the trousers in two-layer pockets on the thighs above the knees, below the knees and slightly above the ankles, as shown in figure 2, *a*. Temperature sensors are placed below the knee heating elements to measure the microclimate temperature in both trouser legs. The trousers have longitudinal narrow double-layered pattern pieces on the sides of the trouser legs, figure 2, *b*. They are used to route signals to/from the heating elements and temperature sensors through the belt at the back of the trousers to the microcontroller, figure 2, *c*, which detects and processes the signals and automatically regulates the microclimate temperature of the trousers (right trouser leg below the knee). This area also contains a switch to turn the heating on and off and a battery. In this test prototype of the smart heating trousers, the microcontroller, the switch and the battery are placed in pockets on the two-layer pattern pieces on the side of the right trouser leg so that they do not come into contact with the wheelchair, figure 2, *b*. An elastic cuff on the lower inner edges of the trouser legs encloses the ankles and prevents heat from escaping from the trousers.

The development of the smart heating system is based on the application for regulating the temperature of

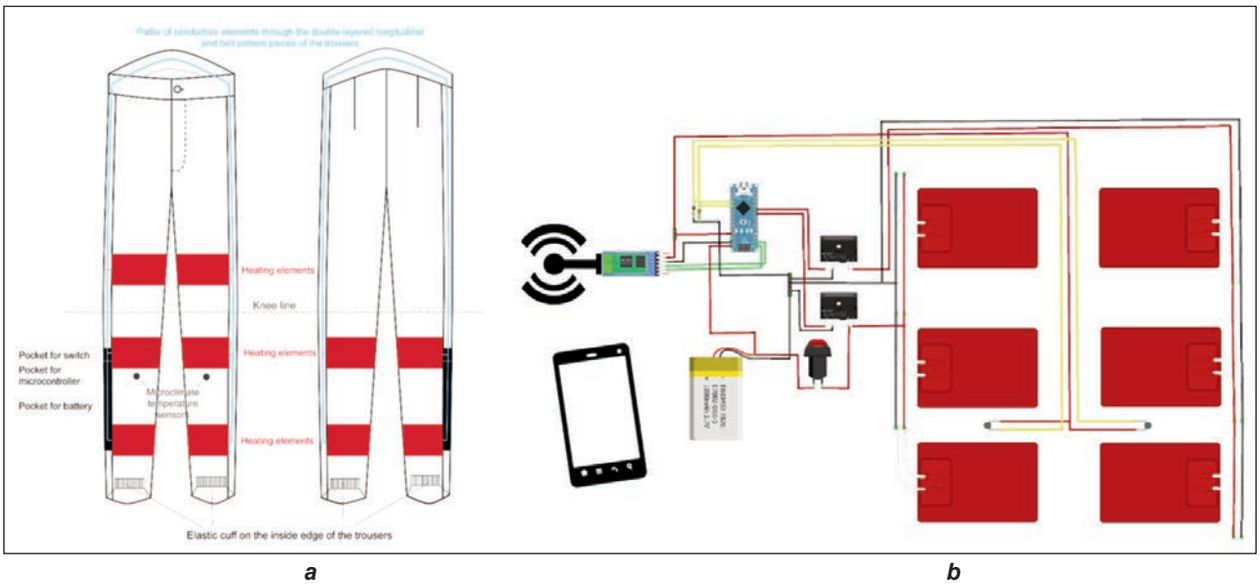


*a* *b*

Fig. 1. Design of: *a* – smart heating trousers; *b* – schematic representation of the connection of heating elements with electrical components and communication via a Bluetooth connection with a mobile phone

*a* *b* *c*

Fig. 2. Details of smart pants: *a* – double-layered pockets inside the trousers on the thighs above the knees, below the knees and above the ankles; *b* and *c* – longitudinal narrow double-layered pattern pieces on the sides of the trousers (right trouser leg – front view and left trouser leg – inside view of double-layered pattern piece)

the microclimate of the trousers, which displays both the real temperature of the environment and the temperature of the microclimate in both trouser legs on the mobile phone. The temperature of the trouser's microclimate is monitored by the microcontroller using NTC (Negative Temperature Coefficient) resistance thermistors. The controller has stored in its memory a program algorithm for processing the input values of the NTC thermistors and regulating the temperature in the trouser legs. The regulation algorithm is performed by comparing the input set temperature and the actual temperature of the heating element in the trousers. We have chosen a PI controller as the control algorithm, as we believe that more accurate algorithms are not necessarily due to the slow temperature response, as shown in figure 3. By setting the PI control constants (Kp – proportional and Ki – integral) the amount of heating power, through voltage, changes depending on the error (the larger the error, the more heating power is supplied to the heating element, the smaller the temperature error, the less heating power is supplied), as shown in equation 1:

$$u(t) = K_p \cdot e(t) + K_i \int_0^t e(\tau)\,d\tau \qquad (1)$$

where $u(t)$ is the controlled variable, which is converted into an electrical variable and indirectly into heating energy, and $e(\tau)$ is the error value as the difference between the desired setpoint $r(t)$ and the measured process variable (from the heating process). $K_p$ and $K_i$ are non-negative coefficients for the proportional and integral terms. In equation 1 we see that the equation depends on time, where the variables $t$ is time or instantaneous time (the present) and $t$ is the integration variable (takes values from time 0 to the present).

The desired maximum temperature of the microclimate in the trousers is set by the software and cannot be changed for safety reasons.

If the error is equal to 0°C, no power is used for heating. Likewise, if the current temperature is greater than or equal to the upper allowable temperature limit, which is checked outside the control loops, heating will not take place. In the first part of this article, it was stated that the highest average skin surface temperature on the leg for a healthy person is 31.7°C, measured in the thermally neutral zone and at rest. Therefore, it can be assumed that the legs of paraplegics can be safely warmed to this skin surface temperature.

At the same time, the temperature measurements are taken separately in both trouser legs, i.e. we implement two regulation loops for the automatic heating of the trousers. Bluetooth communication

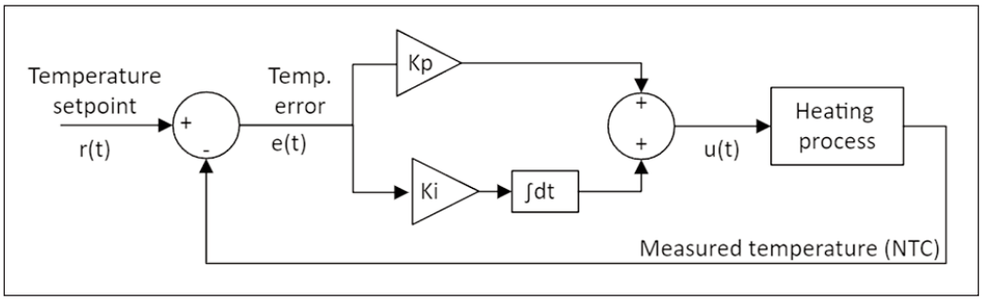


Fig. 3. PI controller for one trouser leg heater

takes place between the mobile phone and the microcontroller built into the trousers to switch the heating of the trousers on or off and to display the current and desired temperature. The complete flow chart of the control algorithm is shown in figure 4.

A test prototype of smart heating trousers with controlled temperature within the trousers microclimate is shown in figure 5. The smart heating system is robust and is used to test the temperature regulation algorithm on the microcontroller, which is connected to the app on the mobile phone via Bluetooth communication, figure 5. The following research activities focus on the development of a textile heating element and the incorporation of miniature electrical components into the trousers, including a battery that enables the smart heating trousers to be worn for up to 5 hours in a cold environment. In addition, a new test prototype of the smart heating trousers will be developed according to the body measurements of the paraplegic. The virtual 3D prototyping process based on a 3D body model of the paraplegic enables precise positioning of the heating elements in the allowed heating areas. An example of a 3D virtual prototyping process of personalised smart heating trousers has been included in the Erasmus+ e-learning materials of the project *OptimTex – Software tools for textile creatives* (2020–2022). The project aimed to improve the knowledge and skills of university students in the field of software applications and increase their employability in textile companies by providing them with adequate training for their profession. Therefore, five e-learning materials were produced as part of this project: Design and Modelling of Woven Structures, Design and Modelling of Knitted Structures, Design and Modelling of Garments through 3D Scanning Software and CAD/PDS Software, Design and Modelling of Embroidered Structures and Software for Experimental Design [20]. The realisation that 3D technologies are becoming increasingly important in the fashion world has led to the new Erasmus+ project *DigitalFashion – Collaborative Online International Learning (COIL) in Digital Fashion* (2022–2025) [21]. It aims to build an educational platform for fashion design through personalised 3D virtual garment customisation and to design curricula for COIL digitally based on the new methodology for a common framework on COIL and a knowledge library (the three databases) for virtual fashion design and technology [22, 23]. The DigitalFashion project is already the

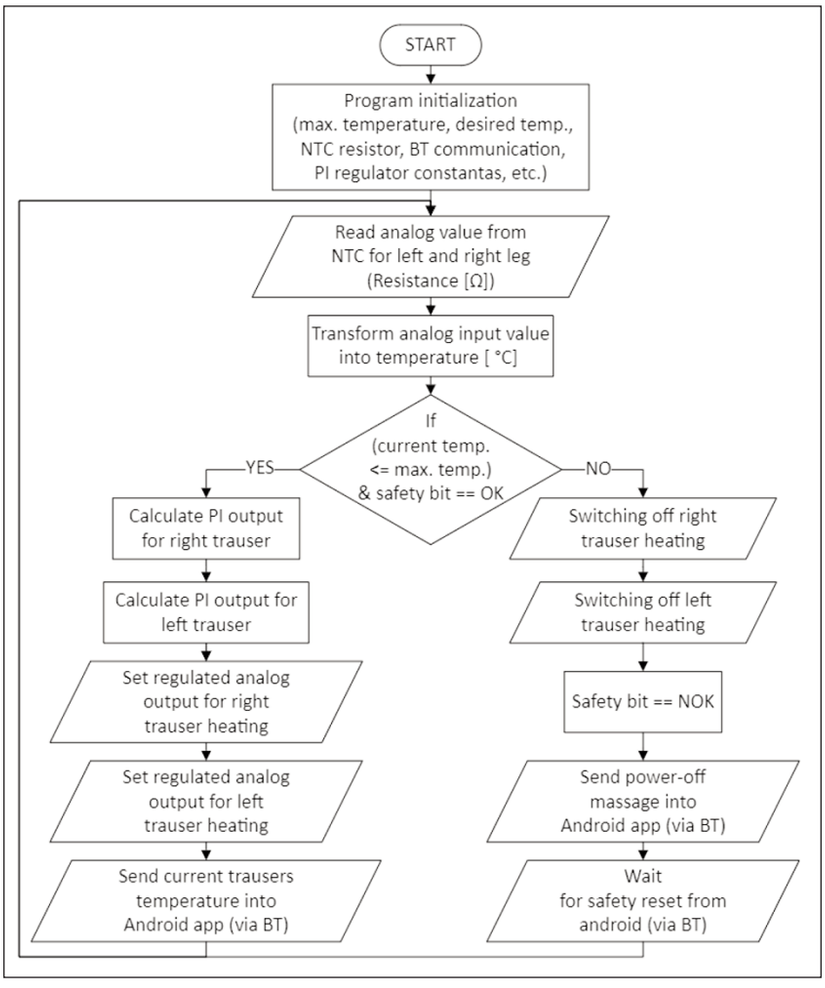


Fig. 4. Control algorithm flow diagram

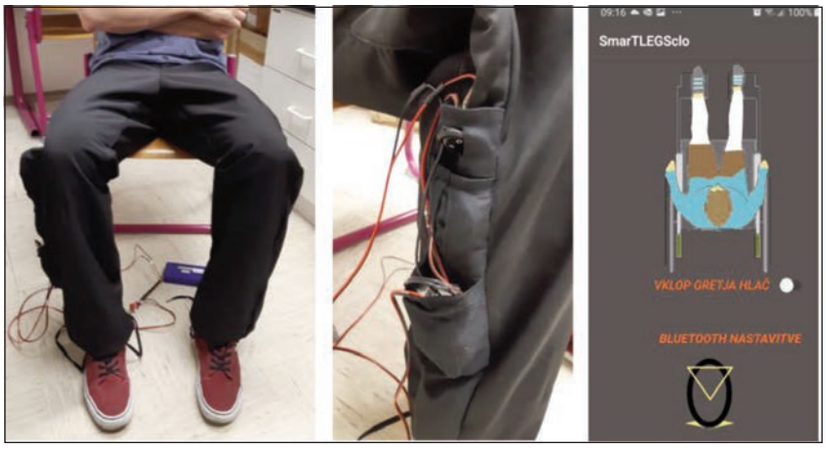


Fig. 5. A test prototype of smart heating trousers and an app on the mobile phone

next and fifth successful project dedicated to e-learning in the wider textile sector (Advan2Tex, TexMatrix, Skills4Smartex, OptimTex). The projects were carried out by a consortium of universities and institutes from European countries, coordinated by the National Research and Development Institute for Textiles and Leather, INCDTP – Romania.

### Results on the thermal insulation of smart heating trousers prototype

The results of the measurement of the thermal properties of trousers fabrics obtained with the Thermo Labo II measuring system show better thermal insulation of the softshell fabric compared to the jeans fabric, based on the measured warm-cool feeling, constant thermal conductivity and constant thermal resistance.

The softshell fabric used for the smart heating trousers has a warm-cool feeling of 0.203 W/cm$^2$, a constant thermal conductivity of 0.045 W/mK and a constant thermal resistance of 0.040 m$^2$K/W. The jeans fabric has a warm-cool feeling of 0.176 W/cm$^2$, a constant thermal conductivity of 0.073 W/mK and a constant thermal resistance of 0.0138 m$^2$K/W.

The results of the thermal insulation in Clo for the smart heating trousers, measured with and without heating, and for the jeans trousers are shown in figure 6 for the eight leg segments of the thermal manikin (right and left thigh on the front and back, right and left calf on the front and back). As we expected, the thermal insulation of jeans trousers is lower than that of trousers made of softshell fabric. By setting up a smart heating system in the trousers, the thermal insulation was increased and the heating system was set up in both trouser legs.

Future research with the thermal manikin will focus on the controlled regulation of the lower extremity skin surface temperature of the thermal manikin set to the average lower extremity skin surface temperatures studied in the first part of this research. In this way, we will be able to accurately monitor the effectiveness of the trousers' thermal insulation and predict the thermal comfort of wheelchair users' legs under different environmental conditions (temperature, air velocity) with the developed smart heating trousers.

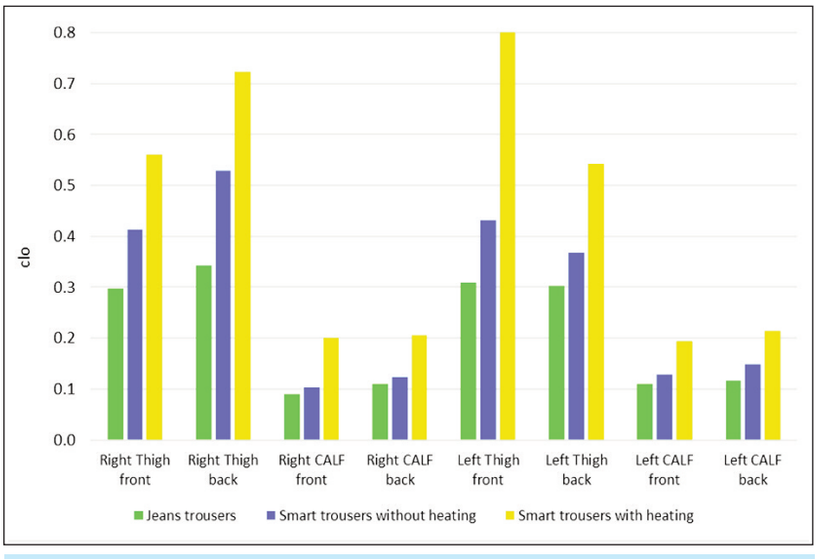


Fig. 6. Clo values of the trousers on the segments of the thermal manikin

## CONCLUSIONS

Clothing is important to protect the human body from exposure to cold. This is especially important for paraplegics who cannot feel the temperature of their legs. Wearing smart heating clothing can increase the time wheelchair users spend in a cold environment and therefore reduce the risk of cold injuries. The research presented has shown that the use of smart heating trousers can improve the thermal insulation of the legs. The smart technology in the trousers provides heating of the microclimate in the leg area when the paraplegic is exposed to a cold environment for a prolonged period, which is ensured by a carefully planned and safe algorithm. The proposed smart heating system allows automatic regulation of the temperature of the trousers' microclimate, which switches off when the maximum allowable temperature is reached. The next step in our research is to test the dependency between the different environmental conditions and the temperature of the trousers microclimate, as well as the heating time interval of the developed smart trousers on the thermal manikin.


## ACKNOWLEDGEMENTS

The authors would like to express their deepest gratitude to all those who participated in the research.

We thank the Laboratory for Intelligent Manufacturing Systems at the Mechanical Engineering Research Institute, Faculty of Mechanical Engineering, University of Maribor, for performing the measurements on the thermal manikin.

## FUNDING

The research was partially supported financially by the European Union through the European Social Fund and Slovenian Ministry of Education, Contract number: 11081-24/2018, the Slovenian Research Agency (Research Programme P2-0123: Clothing Science, Comfort and Textile Materials), the EC Programme Erasmus+, project OptimTex, project No. 2020-1-RO01-KA203-079823 and the project of EC Programme Erasmus+, project DigitalFashion, project No. 2021-1-RO01-KA220-HED-000031150.

## REFERENCES


[1] Sora, S., Hae-Hyun, C., Yung, B., Byung-Hee, H., Young, L.J., *Evaluation of body heating protocols with graphene heated clothing in a cold environment*, In: International Journal of Clothing Science and Technology, 2017, 29, 6, 830–844

[2] Kukkonen, K., Vuorela, T., Rantanen, J., Ryyndnen, O., Siffi, A., Vanhala, J., *The design and implementation of electrically heated clothing*, In: Proceedings Fifth International Symposium on Wearable Computers, Zurich, Switzerland, 2001, 180–181

[3] Wang, F., Gao, C., Kuklane, K., Holmér, I., *A Review of Technology of Personal Heating Garments*, In: International Journal of Occupational Safety and Ergonomics (JOSE), 2010, 16, 3, 387–404

[4] Fan, X., Lin, H., Ye, C., Guo, Y., Huang, L., *Smart Heating Clothes Based on Bluetooth*, 2019 14th International Conference on Computer Science & Education (ICCSE), Toronto, ON, Canada, 2019, 200–203

[5] Li, S., Deng, Y., Cao, B., *Study on the Performance of Personal Heating in Extremely Cold Environments Using a Thermal Manikin,* In: Buildings, 2023, 13, 2, 362

[6] Zhang, C., Ren, C., Li, Y., Song, W., Xu, P., Wang, F., *Designing a smart electrically heated sleeping bag to improve wearers' feet thermal comfort while sleeping in a cold ambient environment,* In: Textile Research Journal, 2017, 87, 10, 1251–1260

[7] Wu, Y., Wang, Z., Xiao, P., Zhang, J., He, R., Zhang, G. H., Chu, A., *Development of smart heating clothing for the elderly*, In: The Journal of The Textile Institute, 2022, 113, 11, 2358–2368

[8] Feng, Q., Hui, C., *Clothing Needs for Wheelchair Users: A Systematic Literature Review*, In: Advances in Aging Research, 2021, 10, 1, 1–30

[9] Lei, Z., *Review of application of thermal manikin in evaluation on thermal and moisture comfort of clothing*, In: Journal of Engineered Fibers and Fabrics, 2019,14, 1–10

[10] Frydrych, I., Cichocka, A., Gilewicz, P., Dominiak, J., *Thermal Manikin Measurements of Protective Clothing Assemblies*, In: Fibres & Textiles in Eastern Europe, 2018, 26, 1, 127, 126–133

[11] Virgílio, A., Oliveira, M., Gaspar, A.R., Francisco, S.C., Quintela, D.A., *Analysis of natural and forced convection heat losses from a thermal manikin: Comparative assessment of the static and dynamic postures*, In: Journal of Wind Engineering and Industrial Aerodynamics, 2014, 132, 66–76

[12] Frydrych, I., Cichocka, A., Gilewicz, P., Dominiak, J., *Comparative analysis of thermal insulation of traditional and new designed protective clothing for foundry workers*. In: Polymers 2016, 8, 10, 348.

[13] Gilewicz, P., Cichocka, A., Frydrych, I., *Underwear for Protective Clothing used for Foundry Worker,* In: Fibres & Textiles in Eastern Europe, 2016, 24, 5, 119, 96–99

[14] Wang, F., *Comparisons of Thermal and Evaporative Resistances of Kapok Coats and Traditional Down Coats*, In: Fibres & Textiles in Eastern Europe, 2010, 18, 1, 78, 75–78

[15] Zwolińska, M., *Case Study of the Impact of Motorcycle Clothing on the Human Body and its Thermal Insulation*, In: Fibres & Textiles in Eastern Europe, 2013, 21, 5, 101, 124–130

[16] Atasağun, H.G., Okur, A., Psikuta, A., Rossi, R.M., Annaheim, S., *The effect of garment combinations on thermal comfort of office clothing*, In: Textile Research Journal, 2019, 89, 21–22, 4425–4437

[17] Pahole, I., Valentan, B., Zavec Pavlinič, D., Ficko, M., Balič, J., *Initial study of immersion thermal manikin development and its manufacture from solid blocks*, In: Tehnički vjesnik, 2015, 22, 6,1623–1631

[18] Vujica-Herzog, N., Zavec Pavlinič, D., Kuzmanović, B., Buchmeister, B., *Thermal manikin and its stability for accurate and repeatable measurements,* In: International Journal of Simulation Modelling, 2016,15, 4, 676–687

[19] ISO 15831:2004, *Clothing – Physiological effects – Measurement of thermal insulation by means of a thermal manikin*

[20] Radulescu, I.R., Scarlat, R., Grosu, C., Dias, A., Malengier, B., Stjepanović, Z., Blaga, M., Polansky, R., *E-learning instrument and glossary of terms for design and modelling of textiles*, In Proceedings ELSE 2022 – 18th International Scientific Conference eLearning and Software for Education, May 12–13, 2022, Bucharest, Romania

[21] Grosu, M.C., Radulescu, I.R., Visileanu, E., Ionescu, I., Avadanei, M., Olaru, S., Zeng, X., Odhiambo, S., Cardoso, A., Rudolf, A., *Analysis of the Learning Requirements of Less Advantaged Groups on the Romanian Level*, In: Proceedings ICAMS 2022 – 9th International Conference on Advanced Materials and Systems, October 26th – 28th, 2022, Bucharest, Romania

[22] Penko, T., Stjepanović, Z., Rudolf, A., *Digital fashion & digital skills*, In: Proceedings V International Conference Contemporary Trends and Innovations in the Textile Industry, 2022, 15–16 September 2022, Beograd, Serbia

[23] Rudolf, A., Penko, T., Stjepanović, Z., Radulescu, I.R., De Raeve, A., Zeng, X., Ionescu, I., Avadanei, M., Cardoso, A., *Research on digital skills needed for the fashion and clothing companies in European countries*, In: Proceedings 13th International Scientific-Professional Conference Textile Science and Economy, 2022, 21st October, Zrenjanin: Technical Faculty "Mihajlo Pupin", 2022

**Authors:**

ANDREJA RUDOLF[1], VANJA KOLANOVIČ[2], MONIKA HUDOURNIK[3], JASNA ŠTAMPFER[4], JAKOB NOVAK[5], MATEJ BOROVEC[6], ROK BELŠAK[7]

[1]University of Maribor, Faculty of Mechanical Engineering, Institute of Engineering Materials and Design, 2000 Maribor, Slovenia

[2]University of Maribor, Faculty of Medicine, 2000 Maribor, Slovenia
e-mail: vanja.kolanovic@student.um.si

[3]3fs Nordic SI, d. o. o., 2000 Maribor, Slovenia
e-mail: hudournik.mony@gmail.com

[4]Žiher d.o.o., 2272 Gorišnica, Slovenia
e-mail: jasna.stampfer@gmail.com

[5]Inel d.o.o., 3000 Celje, Slovenia
e-mail: jakob.novak@inel.com

[6]AVL, Battery engineering, Hans-List-Platz 1, 8020 Graz, Austria
e-mail: matejbrvc105@gmail.com

[7]University of Maribor, Faculty of Mechanical Engineering, Mechanical Engineering Research Institute, 2000 Maribor, Slovenia
e-mail: rok.belsak@um.si

**Corresponding author:**

ANDREJA RUDOLF
e-mail: andreja.rudolf@um.si

# Influence of PEDOT:PSS coating on screen-printed textile

DOI: 10.35530/IT.075.01.202376

SAŠA PETROVIĆ
SANDRA DEDIJER
NEMANJA KAŠIKOVIĆ
ŽELJKO ZELJKOVIĆ
VESNA GVOIĆ
IVANA JURIČ
MLADEN STANČIĆ

**ABSTRACT – REZUMAT**

**Influence of PEDOT:PSS coating on screen-printed textile**

*This paper reports the impact of screen-printed PEDOT:PSS conductive ink on the optical properties of polyester fabric and colourimetric properties of yellow screen printing ink printed in a different number of layers. Yellow was chosen as one of four process colours which should theoretically suffer the most prominent changes from PEDOT:PSS overprinting. The study found that PEDOT:PSS ink significantly impacts the optical properties of the fabric and yellow ink, especially regarding the lightness and b-coordinate of the yellow ink. The acid treatment of samples, to increase PEDOT:PSS conductivity, also affected the optical characteristics through partial neutralization of the changes in the b-coordinate, especially when the sample was printed with a larger number of layers of the yellow ink and a smaller number of layers of PEDOT:PSS ink. Samples with two layers of yellow and one layer of PEDOT:PSS ink showed good conductivity results even without acid treatment, while the base colour appeared slightly darker. This change in the lightness can be compensated to some extent, proving that the aforementioned combination of PEDOT:PSS and base ink layers are the best when aspects, such as optical characteristics, conductivity, the complexity of production, production time, and limitations of the use of substrate materials are taken into account. This study provides useful insights for optimizing the printing process of PEDOT:PSS conductive inks over screen printed fabrics for various applications, including wearable electronics and smart textiles.*

***Keywords:*** *colourimetric properties, conductive ink, conductivity, acid treatment, smart textile*

**Influența stratului PEDOT:PSS asupra textilelor imprimate prin serigrafie**

*Acest studiu raportează impactul cernelii conductoare PEDOT:PSS pentru imprimarea prin serigrafie asupra proprietăților optice ale țesăturii din poliester și proprietăților colorimetrice ale cernelii galbene pentru imprimarea prin serigrafie în număr diferit de straturi. Culoarea galben a fost aleasă drept una dintre cele patru culori de proces care ar trebui, teoretic, să sufere cele mai importante modificări de la supraimprimarea PEDOT:PSS. Studiul a constatat că cerneala PEDOT:PSS are un impact semnificativ asupra proprietăților optice atât ale țesăturii, cât și ale cernelii galbene, în special în ceea ce privește luminozitatea și coordonata b a cernelii galbene. Tratamentul cu acid al probelor, cu scopul de a crește conductivitatea PEDOT:PSS, a afectat și caracteristicile optice prin neutralizarea parțială a modificărilor coordonatei b, mai ales când proba a fost imprimată cu un număr mai mare de straturi de cerneală galbenă și un număr mai mic de straturi de cerneală PEDOT:PSS. Probele cu două straturi de galben și un strat de cerneală PEDOT:PSS au prezentat rezultate bune de conductivitate chiar și fără tratament cu acid, în timp ce culoarea de bază a apărut puțin mai închisă. Această modificare a luminozității poate fi compensată într-o oarecare măsură, demonstrând că această combinație de PEDOT:PSS și straturi de cerneală de bază este cea mai eficientă atunci când anumite caracteristici, cum ar fi cele optice, conductivitatea, complexitatea producției, timpul de producție și limitările de utilizare ale materialelor suport sunt luate în considerare. Acest studiu oferă informații utile pentru optimizarea procesului de imprimare a cernelurilor conductoare PEDOT:PSS peste țesături imprimate prin serigrafie pentru diverse aplicații, inclusiv electronice portabile și textile inteligente.*

***Cuvinte-cheie****: proprietăți colorimetrice, cerneală conductoare, conductivitate, tratament cu acid, material textil inteligent*

## INTRODUCTION

Screen printing is a versatile printing method that can be widely applied. This technique involves pushing ink through a screen and onto a substrate, which can be textiles, paper, ceramics, plastics, and more. In addition to printing on various materials, screen printing can also be used to print on objects of different shapes and sizes, such as tennis balls, mugs, and printed electronics [1].

Screen printing is a popular method for manufacturing electronics, mainly because it allows for printing a thick layer of ink in a single pass while applying lower printing pressure, which is especially important for delicate and softer surfaces, unlike gravure printing [2]. The ink layer thickness in screen printing typically ranges from 20 to 100 μm. Various types of conductive inks, including those containing particles of silver, gold, or copper, are used for functional screen printing

of electronics, circuits, and antennas for RFID tags. Some inks utilize other conductive materials, and the most commonly used opaque inks are silver- and graphene-based. However, for achieving high transparency, ITO (Indium Tin Oxide) is frequently used, but it is typically produced in the form of thin films. ITO is fragile and shows weak adhesion to polymeric materials, and in addition, the cost of indium is increasing [3].

For products where transparency is crucial, an alternative to ITO films is available in the form of conductive inks based on PEDOT:PSS polymers. These inks contain a mixture of poly(3,4-ethylene dioxythiophene) (PEDOT) and polystyrene sulfonate (PSS), which produce films that are highly transparent in the visible part of the spectrum, mechanically stable, and thermally and flexibly outstanding. However, the conductivity of these films is very low, below 1 S/cm [4], due to the presence of a thin layer of PSS chains surrounding the short, conductive PEDOT chains.

One significant advantage of PEDOT:PSS inks over ITO is that they can be printed using various techniques, commonly screen or inkjet printing. Although PEDOT:PSS ink layers may have a slightly bluish tint, they are suitable for areas requiring touchscreen capabilities, flexibility, and resistance to surface wear. Due to its conductivity and flexibility, there is a possibility that PEDOT:PSS could be used in the production of RFID antennas.

PEDOT:PSS is known for its exceptional ability to form films, high transparency, excellent thermal stability, and adjustable conductivity through the addition of secondary dopants [5, 6]. Furthermore, its conductivity can be improved by various methods such as thermal or light treatments, organic solvents, ionic liquids, surfactants, salts, dipolar ions, and acids. The mechanism behind this conductivity enhancement is based on the dissolution of the PSS component of the ink, which acts as an insulator and forms a layer around the conductive PEDOT components. This layer prevents their proper orientation and contact, which significantly limits conductivity.

Acid treatment is commonly used to enhance conductivity, with HCl and $H_2SO_4$ being the most frequently used strong acids for additional deposition on films. Yun et al. [7] concluded that the $H_2SO_4$ treatment results in conformational changes between PEDOT and PSS molecules while concurrently forming PEDOT-rich crystalline nanofibres with a drop in PSS composition, and that such transitions increase electrical conductivity and catalytic activity. Ouyang [8] investigated the use of medium, strong, and weak organic acids to improve PEDOT:PSS conductivity, with an 8M methanesulfonic acid treatment resulting in a conductivity increase to 3300 S/cm. Formic acid treatment by McCarthy et al. [9] and Mengistie et al. [10] led to a conductivity of approximately 2000 S/cm in PEDOT:PSS films.

In a study on the effect of coating on the colourimetric properties of prints conducted by Simonot and Elias [11], it was concluded that the coating layer does not significantly affect the hue but rather has more of an effect on the gloss and saturation of the samples.

Galić et al. [12] concluded in their research that UV coating not only improves the appearance of the final product and increases its mechanical resistance but also affects the colourimetric values of spot colours. In addition to the type of printing substrate and changes in gloss, changes in colourimetric values also occur due to the physical and chemical properties and interactions of spot colours and UV coating.

In the domain of integrating PEDOT:PSS with textile materials, previous studies have mainly focused on researching the electrical conductivity properties of PEDOT:PSS and the techniques used for its application on knitted and non-woven fabrics. The approaches used for textile treatment with PEDOT:PSS vary in complexity and can be categorized as conductive fibre spinning [13, 14], polymerization of PEDOT:PSS on the textile substrate [15, 16], coating/dyeing of textiles with PEDOT:PSS [17, 18], and application of PEDOT:PSS to textiles by ink-jet [19, 20] or screen printing [21, 22]. Among these methods, printing stands out as the only one that allows precise application to pre-made textiles and allows the creation of specific patterns. Screen printing is also recognized for its cost-effectiveness and practicality on an industrial scale. Previous research that applied PEDOT:PSS directly to textiles encountered difficulties in highlighting the property of transparency, which is a key differentiator from other conductive materials, due to the absorbent nature of textiles.

While some transparency analysis was conducted in research related to solar cell production using the Spin Coating method, screen printing was rendered infeasible due to the hydrophobic nature of the printing surfaces [23]. It is noteworthy that the researchers who investigated the use of PEDOT:PSS in solar cells did not measure or draw conclusions about the effects of the material on the spectral and colourimetric properties of the underlying substrates, despite considering transparency. In the textile sector, there is a lack of measurements and analyses on the influence of PEDOT:PSS on the colourimetric and spectrophotometric properties of the target samples, as this particular property of the material is impaired when applied directly to textiles.

Given the basis of previous research and the growing demand for the subsequent application of transparent electrodes, antennas, and conductive layers in the manufacture of smart textiles, there is a pronounced need for further investigation into the effects of these materials on the visual aspects of screen-printed textile designs. Therefore, the objective of this research is to establish a simple, fast, and industry-ready process for screen printing PEDOT:PSS onto pre-printed textiles. Particular attention will be paid to maximising the transparency of PEDOT:PSS while minimising any interference with the visual aesthetics of the printed textile design and reducing the visibility

of printed electrodes, antennas, and conductive layers.

The scientific contribution and novelty of this study include a comprehensive evaluation of the influence of several screen-printed PEDOT:PSS layers, base yellow ink layers, and subsequent sulfuric acid treatment on changes in a variety of parameters belonging to different groups. The first group includes optical, spectrophotometric, and colourimetric parameters, while the second one is limited to the electrical conductivity properties of the samples. Furthermore, this research is expected to yield insights into the optimal production process and the ideal combination of process ink and PEDOT:PSS ink layers, encompassing all the parameters mentioned above, in contrast to earlier research that exclusively focused on conductivity properties.

## MATERIALS AND METHODS

The white 100% polyester fabric with a weight of 166 g/m$^2$ was the chosen printing substrate.

The base ink was yellow process screen printing ink – phthalate-free Tiflex Everest (table 1). For the conductive ink, Heareus PEDOT:PSS Clevios SV4 screen printing ready ink (table 2) was chosen.

Table 1

| TIFLEX EVEREST INK SPECIFICATIONS | |
|---|---|
| **Property** | **Value** |
| Appearance | Satin, yellow |
| Average density | 1.25 g/cm$^3$ |
| Rheology | Thixotropic ink |
| Polymerisation | 2 minutes at 150–160°C |
| Coverage rate | 25 m$^2$/l with 62 threads/cm mesh |

Table 2

| HEAREUS CLEVIOS SV4 INK SPECIFICATIONS | |
|---|---|
| **Property** | **Value** |
| Appearance | Semi-transparent, dark blue |
| Average density | 1.06 g/cm$^3$ |
| Viscosity | 3.7 Pa/s |
| Boiling point | 112°C |
| Sheet resistance | 244 Ohm/sq |
| Solubility | Water soluble |

### Sample generation

The test chart consists of 120×40 mm solid colour fields to be printed using yellow screen printing ink and PEDOT:PSS conductive ink.

*Screen development*

The silk screens employed for printing featured aluminium frames and a weaving density of 68 threads/cm. The silk net was attached to the measuring aluminium frame size of 580×840 mm. After screen mesh tightening, the tensile force was 18 N/cm$^2$. To create the stencil, Amex Screen-Sol QT BLU emulsion was applied in two layers, measuring 40 µm in total, and exposed to UV light through a positive film with a test chart image.

*Printing*

During printing, the squeegee angle was maintained at 60°, and the printing speed was 150 mm/s. The distance between the stencil and the substrate was 3 mm. The thickness of the ink layer printed in one pass was limited by the stencil thickness and was approximately 40 µm. Samples were printed with varying combinations of process yellow and conductive ink layers, ranging from 0 to 3 layers.

Firstly, the yellow ink was applied to all of the samples in 1–3 layers. The ink was dried in a drying oven for 2 minutes at 150°C after applying each layer. After measuring colourimetric, spectrophotometric and surface roughness parameters, we proceeded to overprint the samples with 1–3 layers of PEDOT:PSS. To prevent mechanical deformation of the polyester printing substrate, the PEDOT:PSS ink was dried for 1.5 minutes in a hot air oven at 150 °C after each applied layer. After printing, all of the previously measured parameters were measured again to characterize the influence of PEDOT:PSS on the colourimetric and spectrophotometric properties of the samples. In addition, measurements were taken to investigate the effect of several base ink and PEDOT:PSS ink layers on conductivity.

*Acid treatment*

After measuring all of the parameters, the samples with PEDOT:PSS were immersed in a 1M solution of $H_2SO_4$ in order to increase ink conductivity. The samples were kept in acid for 10 seconds and dried in a drying oven for 2 minutes at 160°C. Afterwards, all of the measurements were repeated to see the influence of acid treatment on conductivity, colourimetric, and spectrophotometric properties.

*Labelling of the samples*

The samples were labelled to indicate the number of yellow ink layers as 1y, 2y, and 3y for 1, 2 and 3 layers of yellow ink respectively, and 0p, 1p, 2p, and 3p for samples printed with different numbers of PEDOT:PSS ink layers. Samples with overprinting were labelled according to the number of yellow ink layers and the number of PEDOT:PSS layers (e.g. 2y1p for samples with two layers of process yellow ink and one layer of conductive PEDOT:PSS ink). Samples that were treated with acid are marked with an asterisk (*) added to the label of the number of layers of conductive ink (e.g. 2y1p*).

*Testing devices and standards*

The testing and analysis of the samples involved the use of various devices and adherence to specific standards to ensure accuracy and reliability.

*Substrate characterization*

Substrate characterization was conducted according to ISO 1833 standards for material composition and ISO 3801 for fabric weight.

*Printing equipment*

The printing process was executed using the TIC ST6HB carousel screen printing machine. The squeegee used had a thickness of 5 mm and was 200 mm in length with a hardness rating of 75 Shore A. The samples were dried in the laboratory drying oven COLO DRYS53A.

*Colorimetric and spectrophotometric measurements*

Colourimetric and spectrophotometric measurements of the samples were conducted using the Techkon Spectrodens device with directional geometry. Colourimetric values (CIE Lab) and colour differences were measured by the settings and measurement method prescribed by EN-ISO 105-J01 and 105-F10 standards. Three layers of the same material on which the printing was done were used as a base for the measurements. Before the measurement, the device was calibrated on an absolute white plate. Measurements were performed for a 10° standard observer under D65 standard light source conditions to achieve a maximum approximation of values to how the human eye perceives colours.

Measurements were taken at 3 different locations on the surface of each sample, and the average values of the L, a, and b parameters were calculated. Based on the average values of the parameters, absolute colour differences CIE 2000 ($\Delta E_{00}$) were calculated:

$$\Delta E_{00} = \sqrt{\frac{\Delta L'}{k_L S_L} + \frac{\Delta C'}{k_C S_C} + \frac{\Delta H'}{k_H S_H} + R_T \frac{\Delta C' \Delta H'}{S_C S_H}} \quad (1)$$

where $\Delta L' = L'_1 - L'_2$ is a difference in lightness value, $\Delta C' = C'_1 - C'_2$ is a difference in chromatic value, $\Delta H = 2\sqrt{C'_1 C'_2} \sin\frac{\Delta H'}{2}$ is a difference in hue value, and parametric weighting factors $k_L = k_C = k_H = 1$.

In addition to absolute differences, discrete values of L, a, and b were compared to determine the direction of the changes and the influence of the different numbers of yellow and PEDOT:PSS ink layers on the CIE Lab colourimetric coordinates of the colour.

Spectral reflectance curves were generated at 10 nm intervals, covering wavelengths from 400 to 700 nm, which correspond to the visible spectrum, also under standard D65 illumination and a 10° standard observer.

*Surface roughness and electrical resistance measurements*

Measurements of the Ra surface roughness parameter were conducted using the Mahr M1 perthometer, following the ISO 4288-1996 standard. Gaussian filtering was applied during results processing, and average values of the Ra surface roughness parameter were calculated from 3 measurements taken longitudinal and 3 measurements taken cross-direction.

Electrical resistance measurements of the samples were carried out using a VC9208N multimeter. Measurements were taken by positioning the measuring probes 3 cm apart in the middle of the samples. Three measurements were taken and the average value was calculated.

## RESULTS AND DISCUSSION

### Spectral reflectance

The spectral reflectance curves corresponding to yellow printed using one, two, and three layers (as depicted in figure 1, *b–d*, respectively) reveal that an increase in the number of ink layers has an insignificant impact on the alteration in reflectance. Moreover, this increment in ink layers does not result in a substantial darkening of the colour. This observation aligns with the inherent characteristics of yellow, which is renowned for its lightness and lower density in comparison to other process colours.

The spectral reflectance curve for the unprinted textile (figure 1, *a*) demonstrates the textile's pristine white nature, characterized by a notably high whiteness index. The application of PEDOT:PSS ink elicits a notable alteration in the spectral reflectance curve (figure 1, *a*). When applied to non-absorbent materials, PEDOT:PSS ink imparts a transparent print with a slight bluish hue [24]. However, the polyester textile is absorbant [25], meaning that PEDOT:PSS cannot preserve its transparency characteristics, leading to the pronounced dying of the textile in a blueish hue. An increase in the number of PEDOT:PSS layers leads to increased ink absorption, making the textile grey, similar to dyed samples in research by Ding, Invernale and Sotzing [26].

The most substantial alterations in the spectral reflectance curve of a single layer of yellow ink manifest when one layer of PEDOT:PSS is applied. This change is most pronounced within the spectral range corresponding to wavelengths spanning from 500 to 700 nm, as illustrated in figure 1, *b*. Notably, the hue remains relatively stable, while an augmented absorption at longer wavelengths contributes to an overall darkening of the colour. This absorption occurs because one layer of yellow ink does not sufficiently prevent polyester from absorbing PEDOT:PSS. This is happening due to the porosity and high ink uptake of the fabric, similar to the findings of Figueira et al. [27].

With the progressive addition of PEDOT:PSS layers, both the transparency of PEDOT:PSS and the saturation of yellow undergo a discernible reduction. Concurrently, the presence of a blue hue becomes more conspicuous. This is notably reflected in a pronounced decline in reflectance within the wavelength range of 600 nm to 700 nm. As a consequence of these spectral changes, it can be inferred that the fundamental yellow hue experiences a perceptible shift towards a greener appearance.

The inclusion of a second layer of yellow ink demonstrates a substantial reduction in the alterations induced by the PEDOT:PSS coating (figure 1, *c*). The most prominent decline in reflectance occurs following the application of a solitary layer of PEDOT:PSS. Nevertheless, when compared to samples featuring only one layer of yellow ink, the curve's configuration more closely approximates that of pure yellow, particularly noticeable within the spectral range spanning from 510 nm to 700 nm. This phenomenon can

be attributed to the substantial reduction in the likelihood of PEDOT:PSS absorption by the textile when multiple layers of base ink are applied, thereby preserving the conductive ink transparency characteristics.

The transparency of PEDOT:PSS becomes less pronounced as its number of layers increases [23], leading to a somewhat greater reduction in reflectance within the wavelength range of 620 nm to 700 nm. The disparities in reflectance between samples with one and two layers of PEDOT:PSS are more substantial compared to the distinctions between samples with two and three layers.

The application of a PEDOT:PSS coating atop three layers of yellow ink (figure 1, *d*), does not yield any substantial disparities when contrasted with samples featuring two layers of yellow ink. This is because the chance of PEDOT:PSS being absorbed by the textile, or filling the pores of the fabric is minimized already after application of the second layer of yellow ink. It can be concluded that no more than two layers of base ink are needed to ensure that PEDOT:PSS will retain its transparency characteristics.

Treating samples bearing PEDOT:PSS directly printed onto the textile with a 20% $H_2SO_4$ acid solution does not lead to a substantial shift in spectral reflectance, similar to the treatment of textile fibres in the experiment by Zhang et al. [14].

Upon subjecting samples with one (figure 1, *b*), two (figure 1, *c*), or three layers (figure 1, *d*) of yellow ink, each overlaid with varying numbers of PEDOT:PSS layers, to a 20% $H_2SO_4$ treatment, a marginal increase in reflectance becomes apparent. Similar observations were made in the research by McCarthy et al. [9] where formic acid was used for the treatment of PEDOT:PSS ink films. This increase in transparency of PEDOT:PSS is marginal because $H_2SO_4$ mostly removes already transparent PSS components. Furthermore, acid treatment leads to a slight reduction of conductive ink layer thickness and reorganization of the PEDOT component [9]. This allows for more light to pass through the conductive ink layer, reducing the dominance of the blue hue and allowing the yellow ink to be more prominent. As more layers of PEDOT:PSS are introduced, the observed changes become less pronounced, similar to the observations made by McCarthy et al. [9].

## Lab coordinates

The introduction of PEDOT:PSS consistently results in a reduction in the lightness of the samples, attributed to incomplete transparency and the inherent bluish tint of the conductive ink. The magnitude of this reduction in lightness is less pronounced when a greater number of yellow ink layers are employed, as illustrated in figure 2, *a*. Along the "a" coordinate, a discernible shift towards a less red or more green colouration is observed, as demonstrated in figure 2, *b*. Conversely, alterations along the "b" coordinate are notably more substantial, primarily due to the presence of a blue hue within PEDOT:PSS, which significantly alters the "b" coordinate of the yellow ink (figure 2, *c*).

These changes are most prominent immediately following the application of the first layer of PEDOT:PSS. The least pronounced alterations in coordinates are observed when two layers of yellow ink are used, preventing direct contact between

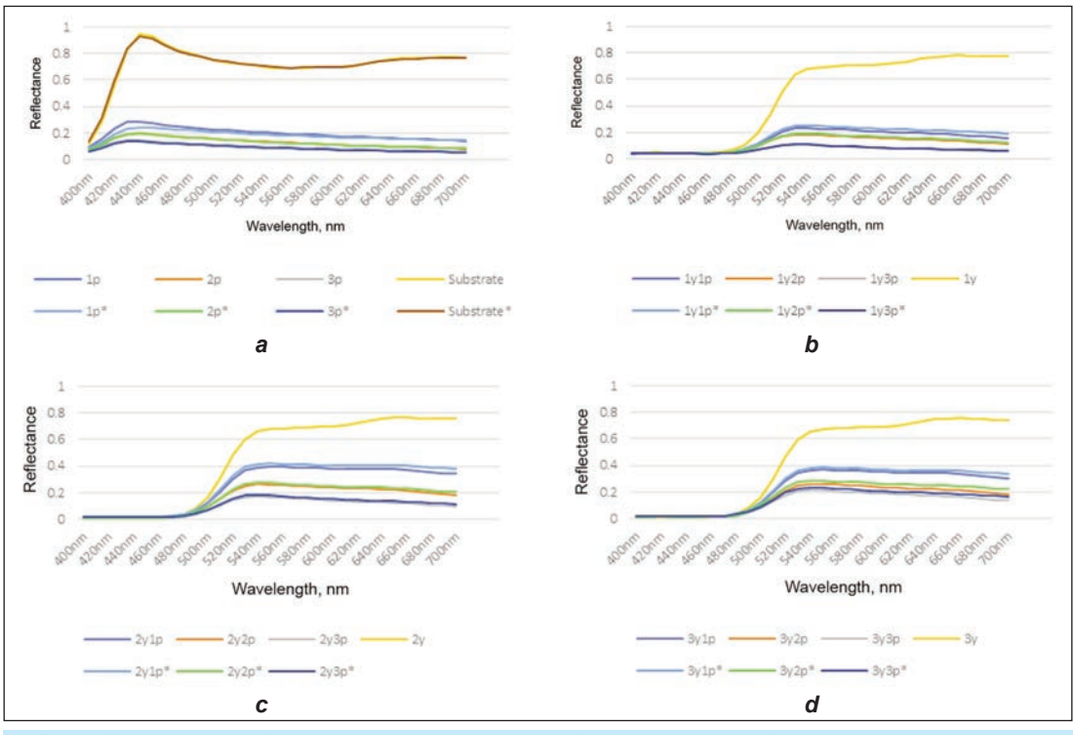


Fig. 1. The spectral reflectance curves before and after acid treatment for: *a* – substrate; *b* – one layer of yellow; *c* – two layers of yellow; *d* – three layers of yellow overprinted with one, two and three layers of PEDOT:PSS

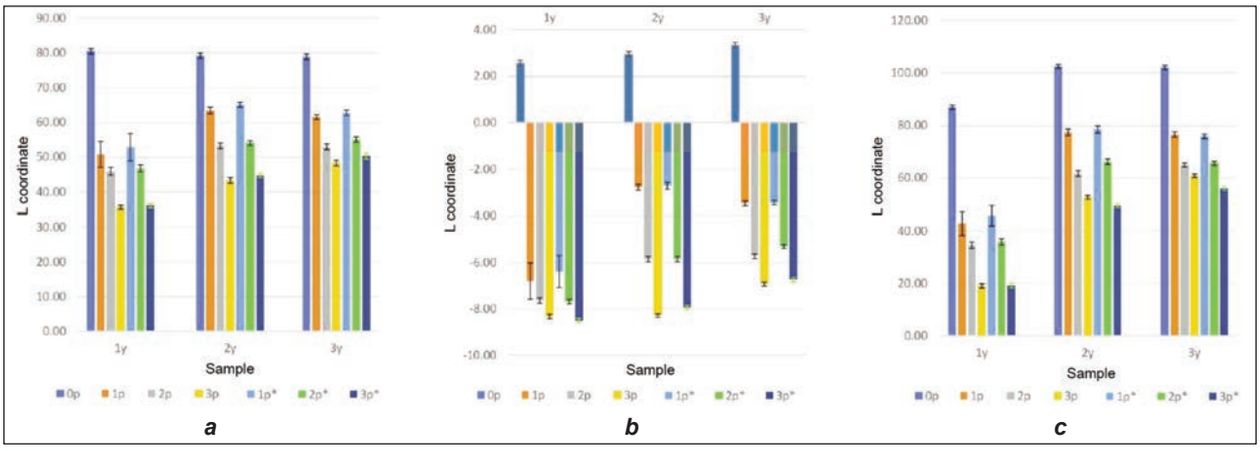


Fig. 2. Values of: *a* – lightness; *b* – a chromatic coordinate; *c* – b chromatic coordinate for all of the sample combinations before and after acid treatment

PEDOT:PSS and the textile. Conversely, the most significant changes occur with a sole layer of yellow ink, attributed to the interaction between PEDOT:PSS and the textile, as witnessed in research by Ding, Invernale and Sotzing [26].

The alteration in lightness after acid treatment is nearly imperceptible (figure 2, *a*). Changes along the "a" coordinate tend to approach neutral values in most instances, albeit with minimal shifts (figure 2, *b*). These shifts can be attributed to the reduction of the blueish hue introduced with the application of PEDOT:PSS. This reduction diminishes the green component obtained through the blending of blue and yellow.

In contrast, changes along the "b" coordinate are more pronounced, and post-acid treatment demonstrates a trend of reduction in the dominance of the blue hue (figure 2, *c*). This reduction occurs due to the PSS component being dissolved, thus allowing for PEDOT component reorganization. Notably, the number of layers of yellow ink does not appear to significantly impact the degree of change in the "b" coordinate.

### Colour difference ΔE

When manipulating the number of layers of both the yellow and PEDOT:PSS inks, a discernible and reasonably consistent pattern emerges in the variation of colour difference. The most substantial change occurs following the initial application of PEDOT:PSS, particularly when applied on a single layer of the base yellow ink. In this scenario, the conductive ink partially dyes the textile, leading to more pronounced alterations, as demonstrated in figure 3, *a*. As additional layers of the conductive ink are applied, discrepancies in colour differences mainly stem from the profound impact of its dominant bluish hue on the "b" coordinate of the yellow.

The colour difference exhibits a decline in correspondence with an increase in the number of yellow ink layers (figure 3, *a*). This phenomenon arises from the inability of the PEDOT:PSS ink to get in contact with the textile. When employing more than one layer of yellow ink, the colour difference between samples featuring one and two layers of conductive ink is somewhat more pronounced. This effect can be attributed to the fact that the initial application of PEDOT:PSS minimally impacts the base ink, as it remains transparent due to its inability to get in contact with the textile. This leaves more space for the second layer of PEDOT:PSS to make changes, as in the case of applying several layers of transparent coating in the study by Dailliez et al. [28]. The introduction of the second layer of PEDOT:PSS leads to a more pronounced colour difference. This is due to the intensification of properties within the ink, manifesting

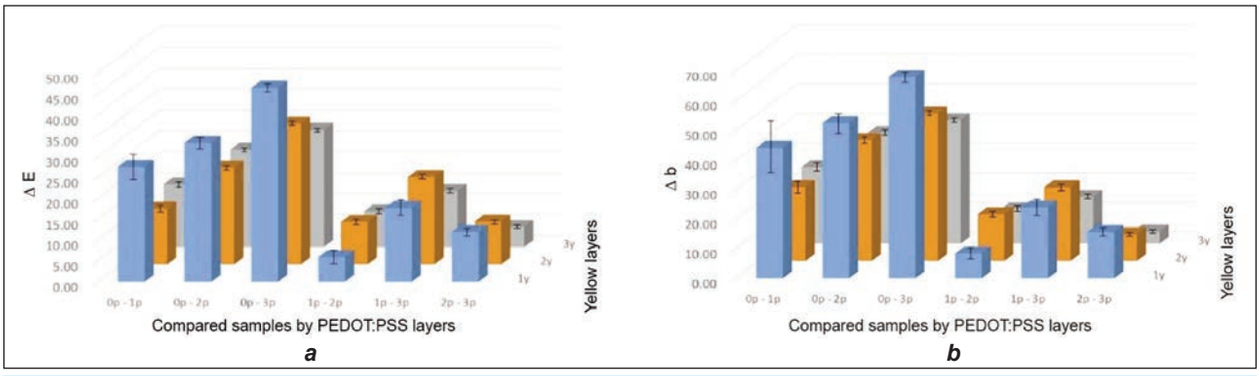


Fig. 3. Values of: *a* – Δ*E* absolute colour difference; *b* – Δ*b* b chromatic coordinate difference measured between all of the samples before acid treatment

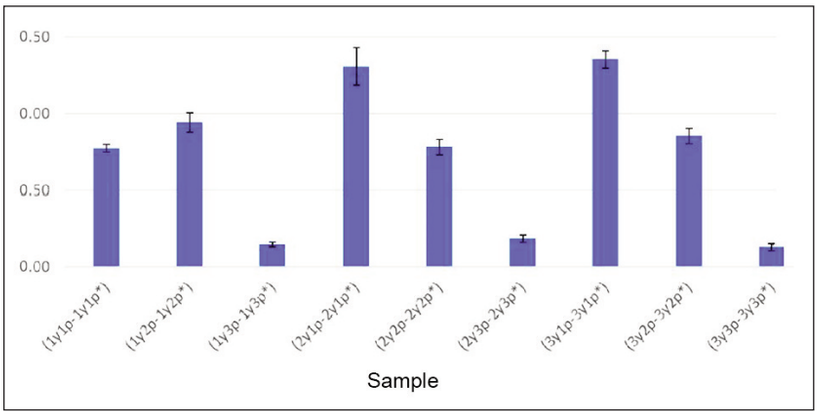


Fig. 4. Values of ΔE absolute colour difference measured between samples before and after acid treatment

as darkening and an increasingly dominant bluish hue that leads to modifications in lightness and chromatic coordinates, particularly along the "b" coordinate, as illustrated in figure 3, *b*. Subsequent applications of PEDOT:PSS ink result in relatively uniform and slightly lower changes. This happens because the ink approaches a layer thickness beyond which further alterations in transparency, and thus lightness and saturation are negligible [9, 23, 29].

The colour difference before and after the treatment of samples with 20% $H_2SO_4$ was calculated for each pair of samples individually (figure 4). Differences are generally greatest when using one or two layers of PEDOT:PSS because PSS decomposition and PEDOT reorganization allow the yellow ink to become more pronounced, especially in samples with 2 layers of yellow. Changes in the samples with 3 layers of PEDOT:PSS are least pronounced and can only be noticed by a trained eye, especially if printed over 3 layers of yellow ink.

## Conductivity

Before analysing and discussing the results of electrical conductivity (resistance) (figure 5), it is important to note that as the resistance (measured quantity) decreases, the conductivity increases because they are inversely proportional. In addition, the average values of Ra surface roughness parameter are 34.21 µm for pure textile, 19.13 µm for 1 layer of yellow, 7.68 µm for 2 layers of yellow, and 5.04 µm for three layers of yellow.

In terms of conductivity, the best results are obtained for the following samples, and in the following order:

1. 1 layer of yellow and 3 layers of PEDOT:PSS ink after acid treatment
2. 1 layer of yellow and 2 layers of PEDOT:PSS ink after acid treatment
3. 1 layer of yellow and 2 layers of PEDOT:PSS ink before acid treatment
4. 2 layers of yellow and 2 layers of PEDOT:PSS ink before acid treatment
5. 1 layer of yellow and 1 layer of PEDOT:PSS ink after acid treatment (increases conductivity up to 4 times compared to the sample before acid treatment).

The results are similar, so the sample with two layers of yellow and two layers of PEDOT:PSS ink (considering the optical characteristics, conductivity, and financial aspects) has a clear advantage because no acid treatment is required, which significantly simplifies and speeds up the process and avoids damage to the textile material caused by acid. This allows printing on cotton and other materials that would otherwise be substantially damaged by $H_2SO_4$ [30]. The only negative aspect is a slightly higher cost due to the application of two layers of PEDOT:PSS, as well as an additional drying time of 3 minutes after the first layer of PEDOT:PSS is applied.

## Qualitative analysis of the samples

A comprehensive qualitative analysis of the samples (figure 6) reveals pronounced alterations resulting from the application of PEDOT:PSS and acid treatment. Notably, the visual impact of PEDOT:PSS on the textile is evident in the images of samples 1p and 1y1p, where the dyeing effect is apparent.

Furthermore, the images of samples 2y1p, 2y2p, and 3y1p demonstrate that two layers of base yellow ink suffice to hinder PEDOT:PSS from permeating the textile and significantly modifying the sample's colour.

Additionally, the image of sample 2y2p underscores that an increase in the number of PEDOT:PSS layers intensifies the bluish hue. Lastly, observations from the images of samples 2y1p*, 2y2p*, and 3y1p* indicate that acid treatment results in the reduction of the blue hue and an enhancement in the uniformity, especially when only one layer of PEDOT:PSS is applied.

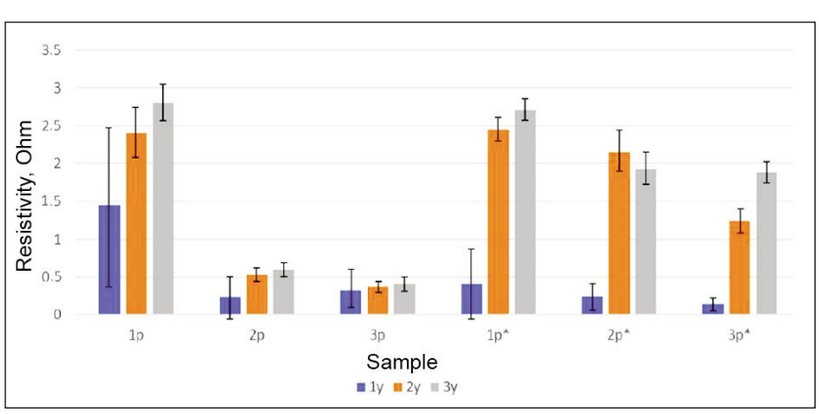


Fig. 5. Electrical resistance of all of the sample combinations before and after acid treatment

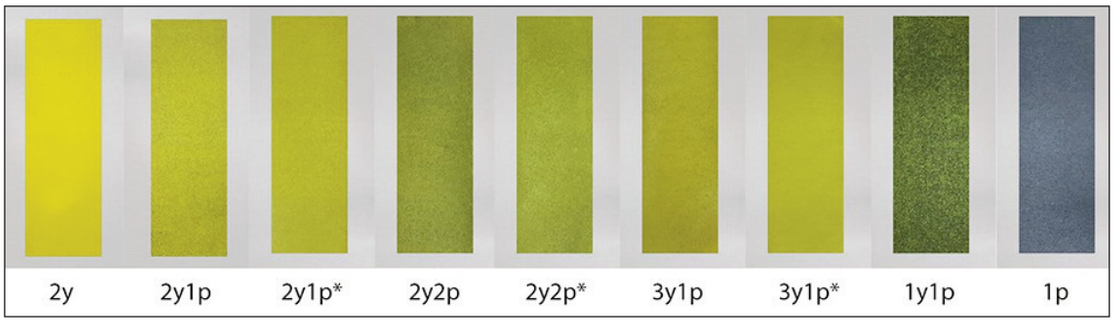


Fig. 6. Images of the samples

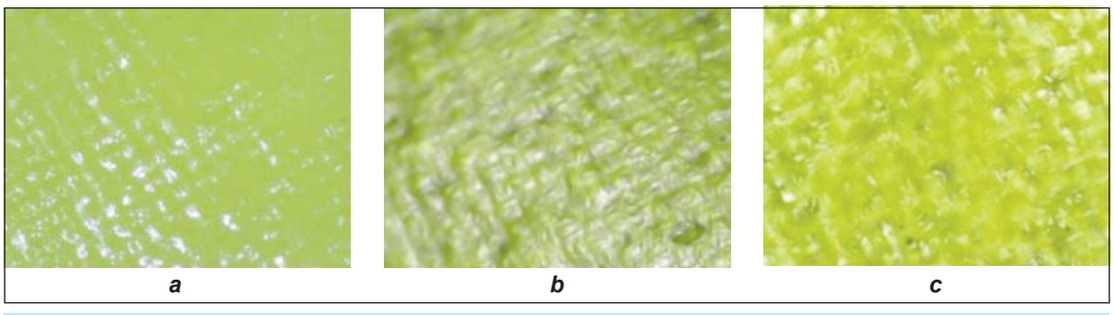


Fig. 7. Microscopic image of 400x magnified: *a* – 2y; *b* – 2y2p; *c* – 2y2p* sample

Similar observations can be made from analysis of the microscopic images of the sample with two layers of yellow ink (figure 7, *a*). The introduction of two layers of PEDOT:PSS ink (figure 7, *b*) distinctly illustrates the influence of PEDOT:PSS on the hue and lightness of the sample, rendering it bluer and darker. The subsequent acid treatment elicits a shift in the sample's characteristics, reducing its bluish tint and promoting uniformity (figure 7, *c*).

## CONCLUSIONS

The influence of the PEDOT:PSS ink on the optical properties is such that the lightness of the base yellow ink changes the most, of course in addition to the b-coordinate as it is opposite to the b coordinate of the PEDOT:PSS ink. The a-coordinate of the base yellow ink also changes in correlation with the change in the b-coordinate caused by the application of PEDOT:PSS.

Samples with a combination of two layers of yellow and one layer of PEDOT:PSS ink give the best optical results. This is due to the inability of PEDOT:PSS to make contact with the fabric and dye it. In addition, the lightness and saturation of two layers of yellow are higher than those of the samples with three layers of yellow, making it more able to compensate for the changes caused by PEDOT:PSS. The acid treatment of samples, which aims to increase conductivity, affects the optical characteristics through partial neutralization of the changes in the b-coordinate. This is especially apparent when the sample is printed with a larger number of layers of the base yellow ink and a smaller number of layers of the conductive ink.

As for conductivity, the discovery that the number of layers of both PEDOT:PSS and the base yellow ink affects it opens up the possibility of finding the "golden middle", which represents the best combination of the number of layers of the base yellow and conductive PEDOT:PSS inks, while providing good conductivity results. When choosing the best combination, it is also important to pay attention to the optical and financial aspects, as well as the complexity of production, limitations on the use of substrate materials, and production time.

Samples with a combination of two layers of the base yellow and two layers of PEDOT:PSS ink give good conductivity results even without acid treatment. In contrast, the surface of the samples is uniform and without a grainy structure. However, the yellow in this case appears darker, which can be compensated to some extent, so this combination could be chosen as the best if all of the previous aspects are taken into account. All of the previous findings can be applied to other base colours, as most of them are less prone to the changes by the PEDOT:PSS blueish hue than yellow. Future research on this topic could go in the direction of printing and analysing the impact of other transparent conductive inks, such as silver nanowire inks, or even a combination of several types of transparent inks.

## ACKNOWLEDGEMENTS

This research (paper) has been supported by The Ministry of Science, Technological Development and Innovation through project no. 451-03-47/2023-01/200156 “Innovative scientific and artistic research from the FTS (activity) domain”.

## REFERENCES


[1] Novaković, D., Kašiković, N., *Propusna štampa*, FTN Izdavaštvo, Novi Sad, 2013

[2] Suganuma, K., *Introduction to Printed Electronics*, Springer, New York, 2014, 129, https://doi.org/10.1007/978-1-4614-9625-0

[3] Tao, C.S., Jiang, J., Tao, M., *Natural resource limitations to terawatt-scale solar cells*, In: Solar Energy Materials and Solar Cells, 2011, 95, 12, 3176–3180, https://doi.org/10.1016/j.solmat.2011.06.013

[4] Wei, H.Y., Huang, J.H., Hsu, C.Y., Chang, F.C., Ho, K.C., Chu, C.W., *Organic solar cells featuring nanobowl structures*, In: Energy & Environmental Science, 2013, 6, 4, 1192–1198, https://doi.org/10.1039/C3EE24128A

[5] Pillai, A.S., Chandran, A., Peethambharan, S.K., *MWCNT Ink with PEDOT:PSS as a multifunctional additive for energy efficient flexible heating applications*, In: Applied Materials Today, 2021, 23, https://doi.org/10.1016/j.apmt.2021.100987

[6] Nguyen, V.A., Kuss, C., *Review – Conducting Polymer-Based Binders for Lithium-Ion Batteries and Beyond*, In: Journal of The Electrochemical Society, 2020, 167, 6, https://doi.org/10.1149/1945-7111/ab856b

[7] Yun, D.J., Ra, H., Kim, J.M., Lee, J.H., Park, S.H., Hwang, J., Chung, J.G., Kim, S.H., Kim, Y.S., Jeong, Y.J., Lee, S.H., *A study on distinctive transition mechanism of sulfuric acid treatment on performance enhancement of poly(3,4-ethylenedioxythiophene): Polystyrene based electrodes depending on multiwall carbon nanotube dose*, In: Applied Surface Science, 2019, 487, 480–487, https://doi.org/10.1016/j.apsusc.2019.05.125

[8] Ouyang, J., *Solution-Processed PEDOT:PSS Films with Conductivities as Indium Tin Oxide through a Treatment with Mild and Weak Organic Acids*, In: ACS Applied Materials & Interfaces, 2013, 5, 24, 13082–13088, https://doi.org/10.1021/am404113n

[9] McCarthy, J.E., Hanley, C.A., Brennan, L.J., Lambertini, V.G., Gun'ko, Y.K., *Fabrication of highly transparent and conducting PEDOT:PSS films using a formic acid treatment*, In: Journal of Materials Chemistry C, 2014, 2, 4, 764–770, https://doi.org/10.1039/C3TC31951B

[10] Mengistie, D.A., Ibrahem, M.A., Wang, P.C., Chu, C.W., *Highly Conductive PEDOT:PSS Treated with Formic Acid for ITO-Free Polymer Solar Cells*, In: ACS Applied Materials & Interfaces, 2014, 6, 4, 2292–2299, https://doi.org/10.1021/am405024d

[11] Simonot, L., Elias, M., *Colour change due to a varnish layer*, In: Colour Research & Application, 2004, 29, 3, 196–204, https://doi.org/10.1002/col.20008

[12] Galić, E., Ljevak, I., Zjakić, I., *The Influence of UV Varnish on Colorimetric Properties of Spot Colours*, In: Procedia Engineering, 2015, 100, 1532–1538, https://doi.org/10.1016/j.proeng.2015.01.525

[13] Zhou, J., Li, E.Q., Li, R., Xu, X., Ventura, I.A., Moussawi, A., Anjum, D.H., Hedhili, M.N., Smilgies, D.-M., Lubineau, G., Thoroddsen, S.T., *Semi-metallic, strong and stretchable wet-spun conjugated polymer microfibres*, In: Journal of Materials Chemistry C, 2015, 3, 11, 2528–2538, https://doi.org/10.1039/C4TC02354D

[14] Zhang, J., Seyedin, S., Qin, S., Lynch, P.A., Wang, Z., Yang, W., Wang, X., Razal, J.M., *Fast and scalable wet-spinning of highly conductive PEDOT:PSS fibres enables versatile applications*, In: Journal of Materials Chemistry A, 2019, 7, 11, 6401–6410, https://doi.org/10.1039/C9TA00022D

[15] Allison, L., Hoxie, S., Andrew, T.L., *Towards seamlessly-integrated textile electronics: methods to coat fabrics and fibres with conducting polymers for electronic applications*, In: Chemical Communications, 2017, 53, 7182–7193, https://doi.org/10.1039/C7CC02592K

[16] Bashir, T., Skrifvars, M., Persson, N.-K., *High-strength electrically conductive fibres: Functionalization of polyamide, aramid, and polyester fibres with PEDOT polymer*, In: Polymers for Advanced Technologies, 2017, 29, 1, 310–318, https://doi.org/10.1002/pat.4116

[17] Lund, A., Darabi, S., Hultmark, S., Ryan, J.D., Andersson, B., Ström, A., Müller, C., *Roll-to-Roll Dyed Conducting Silk Yarns: A Versatile Material for E-Textile Devices*, In: Advanced Materials Technologies, 2018, 3, 12, https://doi.org/10.1002/admt.201800251

[18] Tadesse, M.G., Mengistie, D.A., Chen, Y., Wang, L., Loghin, C., Nierstrasz, V., *Electrically conductive highly elastic polyamide/lycra fabric treated with PEDOT:PSS and polyurethane*, In: Journal of Materials Science, 2019, 54, 9591–9602, https://doi.org/10.1007/s10853-019-03519-3

[19] Guo, Y., Otley, M.T., Li, M., Zhang, X., Sinha, S.K., Treich, G.M., Sotzing, G.A., *PEDOT:PSS "Wires" Printed on Textile for Wearable Electronics*, In: ACS Applied Materials & Interfaces, 2016, 8, 40, 26998–27005, https://doi.org/10.1021/acsami.6b08036

[20] Kye, M.J., Cho, J., Yu, J. C., Chang, Y.-W., Han, J., Lee, E., Lim, H.S., Lim, J.A., *"Drop-on-textile" patternable aqueous PEDOT composite ink providing highly stretchable and wash-resistant electrodes for electronic textiles*, 2018, 155, 150–158, https://doi.org/10.1016/j.dyepig.2018.03.024

[21] Sinha, S.K., Noh, Y., Reljin, N., Treich, G.M., Hajeb-Mohammadalipour, S., Guo, Y., Chon, KH., Sotzing, G. A., *Screen-Printed PEDOT:PSS Electrodes on Commercial Finished Textiles for Electrocardiography*, In: ACS Applied Materials & Interfaces, 2017, 9, 43, 37524–37528, https://doi.org/10.1021/acsami.7b09954

[22] Tseghai, G.B., Malengier, B., Fante, K.A., Nigusse, A.B., Van Langenhove, L., *Development of a Flex and Stretchy Conductive Cotton Fabric Via Flat Screen Printing of PEDOT:PSS/PDMS Conductive Polymer Composite*, In: Sensors, 2020, 20, 6, https://doi.org/10.3390/s20061742

[23] Pali, L.S., Jindal, R., Garg, A., *Screen printed PEDOT:PSS films as transparent electrode and its application in organic solar cells on opaque substrates*, In: Journal of Materials Science: Materials in Electronics, 2018, 29, 11030–11038, https://doi.org/10.1007/s10854-018-9185-y

[24] Kawahara, J., Andersson Ersman, P., Engqist, I., Berggren, M., *Improving the colour switch contrast in PEDOT:PSS-based electrochromic displays*, In: Organic Electronics, 2012, 13, 3, 469–474, https://doi.org/10.1016/j.orgel.2011.12.007

[25] Yousef, M., Othman, H., Hassabo, A.G., *A Recent Study for Printing Polyester Fabric with Different Techniques*, In: Journal of Textiles, Colouration and Polymer Science, 2021, 18, 2, 247–252, https://doi.org/10.21608/jtcps.2021.84754.1072

[26] Ding, Y., Invernale, M.A., Sotzing, G.A., *Conductivity Trends of PEDOT-PSS Impregnated Fabric and the Effect of Conductivity on Electrochromic Textile*, In: ACS Applied Materials & Interfaces, 2010, 2, 6, 1588–1593, https://doi.org/10.1021/am100036n

[27] Figueira, J., Bonito, R. M., Caravlho, J.T., Vieira, E.M.F., Gaspar, C., Loureiro, J., Correia, J.H., Fortunato, E., Martins, R., Pereira, L., *Screen-printed, flexible, and eco-friendly thermoelectric touch sensors based on ethyl cellulose and graphite flakes inks*, In: Flexible and Printed Electronics, 2023, 8, 2, https://doi.org/10.1088/2058-8585/acc114

[28] Dailliez, F., Hébert, M., Blayo, A., Chagas, L., Fournel, T., *Impact of a Transparent Coating on the Reflectance of a Line Halftone Pattern*, In: Coatings, 2021, 11, 12, https://doi.org/10.3390/coatings11121465

[29] Pang, Y.C., Li, Z.J., Shi, L.L., *Study on Relationship of Ink Thickness and Colour Saturation*, In: Applied Mechanics and Materials, 2015, 731, 295–299, https://doi.org/10.4028/www.scientific.net/AMM.731.295

[30] Paul Dauglas Vincent, B.A., *The effect of treatment with sulphuric acid on the breaking load of cotton*, In: Journal of the Textile Institute Transactions, 1924, 15, 5, T281–T290, https://doi.org/10.1080/19447022408661302

**Authors:**

SAŠA PETROVIĆ[1], SANDRA DEDIJER[1], NEMANJA KAŠIKOVIĆ[1], ŽELJKO ZELJKOVIĆ[1], VESNA GVOIĆ[1], IVANA JURIČ[1], MLADEN STANČIĆ[2]

[1]University of Novi Sad, Faculty of Technical Sciences, Department of Graphic Engineering and Design, Trg Dositeja Obradovića 6, 21000, Novi Sad, Serbia
e-mail: petrovic.sasa@uns.ac.rs, dedijer@uns.ac.rs, knemanja@uns.ac.rs, kecic@uns.ac.rs, rilovska@uns.ac.rs

[2]University of Banja Luka, Faculty of Technology, Department of Graphic Engineering and Design, Bulevar Vojvode Stepe Stepanovića 73, 78000, Banja Luka, Bosnia & Herzegovina
e-mail: mladen.stancic@tf.unibl.org

**Corresponding author:**

ŽELJKO ZELJKOVIĆ
e-mail: zeljkoz@uns.ac.rs

# Experimental design using the Taguchi method for the development of conductive textiles used in flexible thermoelectric generators

DOI: 10.35530/IT.075.01.202360

RALUCA MARIA AILENI CRISTINA STROE


## ABSTRACT – REZUMAT

### Experimental design using the Taguchi method for the development of conductive textiles used in flexible thermoelectric generators

*This paper presents several aspects of the robust experimental design methodology using the Taguchi method to develop electrically conductive textiles. These conductive textiles will be used to make thermoelectric generators based on the Seebeck effect. Since the experimental development involves the use of the magnetron sputtering method with more than three variables, the Taguchi method was selected to observe how different parameters (5 independent variables such as argon flow, power, pressure, deposition surface area and metal type used for solid targets) influence the mean and variance of the process performance defined by the thickness of the metal film deposited (dependent variable). In the experimental design framework, the analysis using the Taguchi method, followed by optimisation, helped select the optimal experiments from the set of possible experiments. This methodology reduced the number of experiments by 21–42% and minimised resource consumption (e.g., metal targets, argon, energy).*


***Keywords:*** *conductive, electrical resistance, experimental plan, Taguchi method, textile, thermoelectric generator*


### Design experimental pe baza metodei Taguchi pentru dezvoltarea materialelor textile conductive pentru generatoare termoelectrice flexibile

*Această lucrare prezintă câteva aspecte ale metodologiei designului experimental robust utilizând metoda Taguchi, pentru a dezvolta textile electroconductive. Aceste textile conductive vor fi folosite pentru realizarea generatoarelor termoelectrice bazate pe efectul Seebeck. Deoarece dezvoltarea experimentală implică utilizarea metodei de pulverizare magnetron cu mai mult de trei variabile, a fost selectată metoda Taguchi pentru a observa modul în care diferiți parametri (5 variabile independente, cum ar fi debitul de argon, puterea, presiunea, suprafața de depunere și tipul de metal pentru ţintele solide) influențează media și varianța performanței procesului definit de grosimea stratului metalic depus (variabilă dependentă). În cadrul designului experimental, analiza folosind metoda Taguchi, urmată de optimizare, a ajutat la selectarea experimentelor optime din setul de experimente posibile. Această metodologie a redus numărul de experimente cu 21–42% și a minimizat consumul de resurse (de exemplu, ţinte metalice, argon, energie).*


***Cuvinte-cheie***: *conductiv, rezistenţă electrică, plan experimental, metoda Taguchi, textil, generator termoelectric*

## INTRODUCTION

The transformation of the textile into an electrical thermoelectric generator (TEG) is a challenge for researchers. Scientific literature presents numerous methods for creating flexible thermoelectric generators integrated into garments by conducting polymers such as polyelectrolyte complex poly(3,4-ethylene dioxythiophene): poly(styrene sulfonate) (PEDOT: PSS) as the p-type material and sewing conductive yarns [1, 2], vertically aligned p-type PEDOT: PSS and carbon nanotubes [3-5] or PEDOT: PSS thin film (as p-type) and aluminium wire (as n-type) integrated [3] by the 3D printing method in TEG using the Seebeck effect. In addition, PEDOT: PSS, MWCNTs, and Bi2Te3 were reported to coat polyester yarns (P-type thermoelectric legs) connected by copper wires [6]. A scientific approach is to use the Taguchi method for designing TEG-based cubic-shaped P-type (Bi0.5Sb1.5Te3) and N-type (Bi2Se0.5Te2.5) thermoelectric leg-based Seebeck effects [7]. The materials used for P-type and N-type thermoelectric legs influence the performance of the final TEG (inner resistance, output voltage and power) [8].

## EXPERIMENTAL PART

Based on the Seebeck effect, an experimental plan using the Taguchi method has been designed to develop conductive materials for thermoelectric generators. The specific parameters for the deposition of conductive layers using the magnetron sputtering method are:

– the specific thickness (100 nm, 150 nm, 200 nm);
– textile surface with area A (100 $mm^2$, 150 $mm^2$, 200 $mm^2$);
– argon flow (40 sccm, 50 sccm, 60 sccm);
– pressure ($3\times10^{-5}$ mbar, $4\times10^{-5}$ mbar, $5\times10^{-5}$ mbar);
– RF generator power (80 W, 100 W, 150 W);
– metal targets (silver, copper and nickel).

To create the experimental plan, 5 variable influence factors (table 1) and three levels (distinct values)

were used for each factor, as follows: metal (copper, nickel, silver), pressure ($3\times10^{-5}$ mbar, $4\times10^{-5}$ mbar, $5\times10^{-5}$ mbar), generator power (80 W, 100 W, 150 W), argon flow (40 sccm, 50 sccm, 60 sccm) and the response variable the thickness of the deposited metal thin layer (100 nm, 150 nm and 200 nm) by the magnetron sputtering method.

To obtain conductive materials to generate electricity through the thermocouple effect, the minimum electrical resistance (Rs = $10^3$) associated with the maximum value for the thickness of the metal layer [9] deposited (200 nm) by the magnetron sputtering method was considered.

## ANALYSING THE EXPERIMENTAL DATA

The signal-to-noise ratios (S/N) and the thickness response variable were used depending on the independent variables (metal, metal deposition surface, pressure and argon flow) to analyse the Taguchi experimental plan. The signal-to-noise ratio (S/N) is a measure of robustness and can be used to identify the appropriate settings for factors to reduce the effect of noise on the response. The signal-to-noise ratio (S/N) was calculated separately for each combination of control factor levels in the experimental design. For the S/N ratio (equation 1), the static model 'larger is better' was chosen to maximise the response (thickness).

$$\frac{S}{N} = -10 \log\left[\sum(1/y^2)/n\right] \quad (1)$$

where $y$ represents the responses given at the factor level and $n$ is the number of factor-level responses.

For the influencing factors, the signal-to-noise responses are presented in table 2. The main effects plot (figures 1 and 2) shows how each factor influences the response characteristic (S/N ratio or mean values). A main effect exists when different factor levels (e.g., metal deposition surface) affect the S/N ratio differently. For a factor 'metal' with three levels, it is observed that there are increases and a reduction for three levels (200 $mm^2$, 150 $mm^2$ and 100 $mm^2$) compared to the average value of the S/N ratio. This aspect indicates that the deposition surface cannot precisely influence the thickness of the deposited layer because the distribution of the metal deposition

Table 1

EXPERIMENTAL PLAN FOR THE DEPOSITION OF CONDUCTIVE MATERIALS BY THE MAGNETRON SPUTTERING METHOD

| No. | Metal | Surface area ($mm^2$) | Pressure (mbar) | Argon flow (sccm) | Power (W) | Thickness (nm) |
|---|---|---|---|---|---|---|
| 1 | Copper | 100 | $3x10^{-5}$ | 40 | 80 | 100 |
| 2 | Copper | 100 | $3x10^{-5}$ | 40 | 100 | 100 |
| 3 | Copper | 100 | $3x10^{-5}$ | 40 | 150 | 100 |
| 4 | Copper | 150 | $4x10^{-5}$ | 50 | 80 | 150 |
| 5 | Copper | 150 | $4x10^{-5}$ | 50 | 100 | 150 |
| 6 | Copper | 150 | $4x10^{-5}$ | 50 | 150 | 150 |
| 7 | Copper | 200 | $5x10^{-5}$ | 60 | 80 | 200 |
| 8 | Copper | 200 | $5x10^{-5}$ | 60 | 100 | 200 |
| 9 | Copper | 200 | $5x10^{-5}$ | 60 | 150 | 200 |
| 10 | Nickel | 100 | $4x10^{-5}$ | 60 | 80 | 100 |
| 11 | Nickel | 100 | $4x10^{-5}$ | 60 | 100 | 100 |
| 12 | Nickel | 100 | $4x10^{-5}$ | 60 | 150 | 100 |
| 13 | Nickel | 150 | $5x10^{-5}$ | 40 | 80 | 150 |
| 14 | Nickel | 150 | $5x10^{-5}$ | 40 | 100 | 150 |
| 15 | Nickel | 150 | $5x10^{-5}$ | 40 | 150 | 150 |
| 16 | Nickel | 200 | $3x10^{-5}$ | 50 | 80 | 200 |
| 17 | Nickel | 200 | $3x10^{-5}$ | 50 | 100 | 200 |
| 18 | Nickel | 200 | $3x10^{-5}$ | 50 | 150 | 200 |
| 19 | Silver | 100 | $5x10^{-5}$ | 50 | 80 | 100 |
| 20 | Silver | 100 | $5x10^{-5}$ | 50 | 100 | 100 |
| 21 | Silver | 100 | $5x10^{-5}$ | 50 | 150 | 100 |
| 22 | Silver | 150 | $3x10^{-5}$ | 60 | 80 | 150 |
| 23 | Silver | 150 | $3x10^{-5}$ | 60 | 100 | 150 |
| 24 | Silver | 150 | $3x10^{-5}$ | 60 | 150 | 150 |
| 25 | Silver | 200 | $4x10^{-5}$ | 40 | 80 | 200 |
| 26 | Silver | 200 | $4x10^{-5}$ | 40 | 100 | 200 |
| 27 | Silver | 200 | $4x10^{-5}$ | 40 | 150 | 200 |

Table 2

| SIGNAL-NOISE RATIOS (S/N) | | | | | |
|---|---|---|---|---|---|
| **Level** | **Metal** | **Surface area** | **Pressure** | **Argon flow** | **Power** |
| 1 | 43.18 | 40 | 43.18 | 43.18 | 43.18 |
| 2 | 43.18 | 43.52 | 43.18 | 43.18 | 43.18 |
| 3 | 43.18 | 46.02 | 43.18 | 43.18 | 43.18 |
| Delta | 0 | 6.02 | 0 | 0 | 0 |
| Rank | 3.5 | 1 | 3.5 | 3.5 | 3.5 |

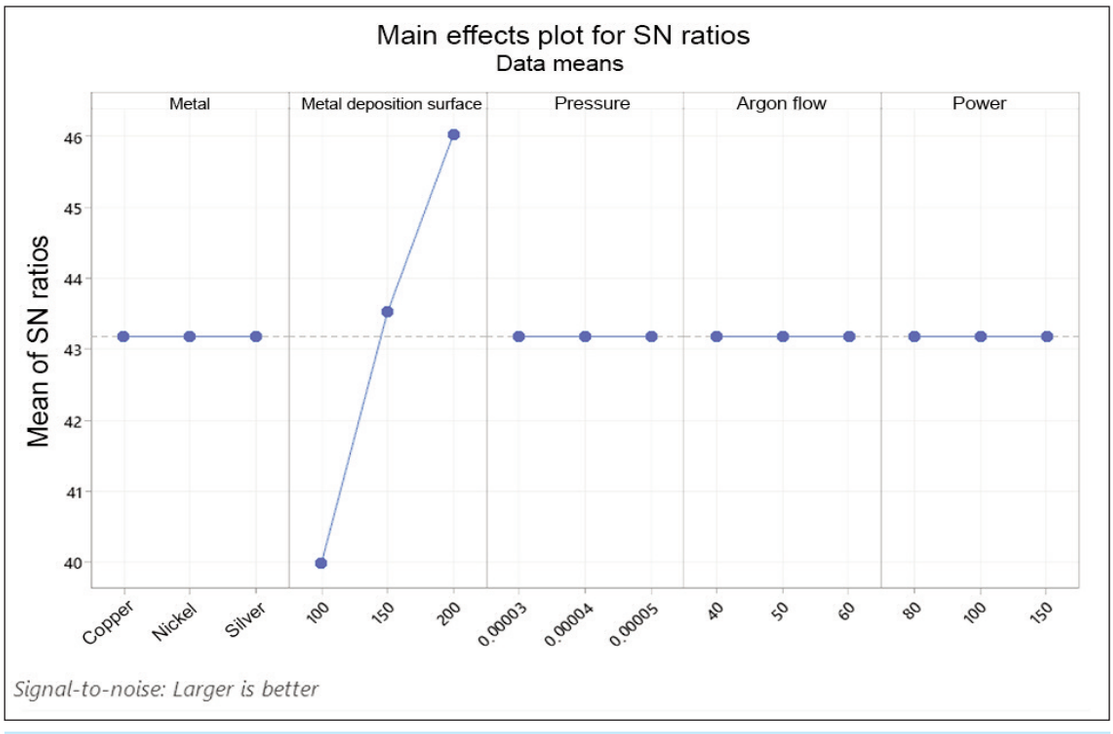


Fig. 1. Main effects plot for *S/N* ratios

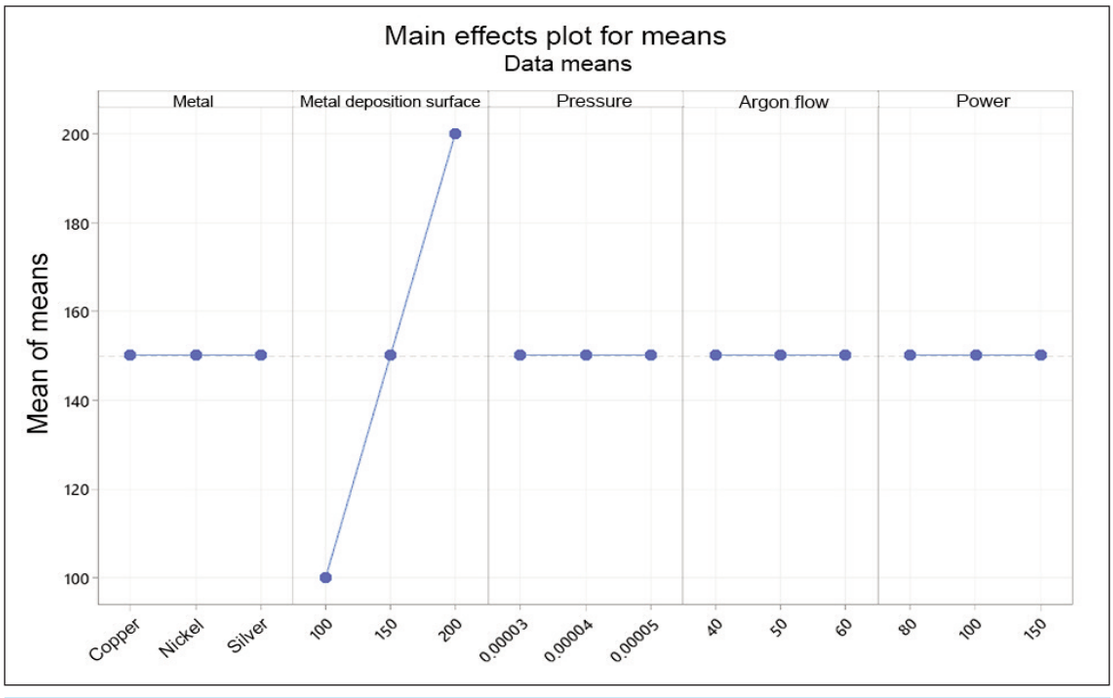


Fig. 2. Main effects plot for means

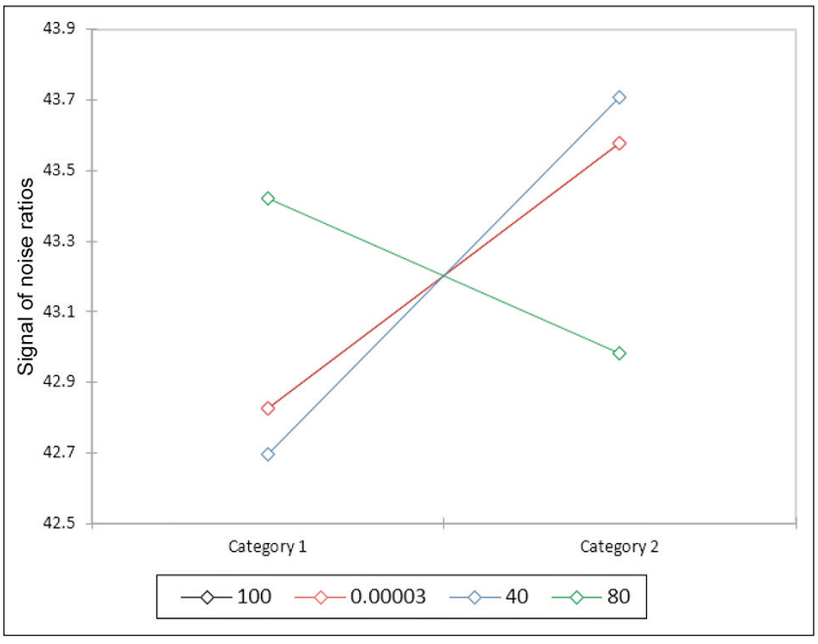


Fig. 3. LS means (Signal to Noise ratios)

Figure 3 shows the S/N ratio for the factor (independent variable) levels represented by categories 1 and 2 (table 3) of the independent variables pressure, argon flow and power. Table 4 presents the variance analysis for the signal-to-noise ratio.

Equation 2 for the signal-to-noise ratio (Rsz) model is shown below:

$$R_{sz} = 44.2387516318562 - 0.752574989159954*x_1 - 150 - 0.752574989159939*x_2 - 0.00004 - 1.00833760139685*x_3 - 50 + 0.440228147639218*x_4 - 100 \quad (2)$$

The model that considers the average values of the influence factors (*Rm*) is presented in mathematical expression 3 below:

$$R_m = 165.625 - 12.5*x_1 - 150 - 12.5*x_2 - 0.00004 - 12.5*x_3 - 50 + 6.25*x_4 - 100 \quad (3)$$

where $x_1$ is the surface of the metal deposit, $x_2$ – the pressure, $x_3$ – the argon flow, $x_4$ – the power.

In the experimental plan design by the Taguchi method, the robustness of the method is evaluated by identifying the control factors that reduce the variability of a product or process by minimising the effects of uncontrolled factors (noise factors). Control factors are those design and process parameters that can be controlled. Noise factors cannot be controlled during the production or use of the product, but they can be controlled during experiments. Tables 4 and 5 present the analysis of variance for the signal-to-noise ratio and the mean values.

Table 3

| INFORMATION ABOUT CATEGORY 1 AND CATEGORY 2 FOR INDEPENDENT VARIABLES | | | |
|---|---|---|---|
| **Variables** | **Categories number** | **Category 1** | **Category 2** |
| Surface Area | 2 | 150 | 200 |
| Pressure | 2 | $4\times10^{-5}$ | $5\times10^{-5}$ |
| Argon Flow | 2 | 50 | 60 |
| Power | 2 | 100 | 150 |

shows nonuniformity. In table 2, the Delta is the difference between each factor's highest and lowest mean response values. Ranks are assigned based on Delta values. Rank 1 corresponds to the highest Delta value.

Table 4

| ANALYSIS OF VARIANCE (SIGNAL-TO-NOISE RATIOS) | | | | | |
|---|---|---|---|---|---|
| **Source** | **DF** | **Sum of squares** | **Mean squares** | **F** | **Pr>F** |
| Model | 4 | 18.746 | 4.687 | 0.769 | 0.555 |
| Error | 27 | 164.454 | 6.091 | | |
| Corrected Total | 31 | 183.201 | | | |

Table 5

| ANALYSIS OF VARIANCE (MEANS) | | | | | |
|---|---|---|---|---|---|
| **Source** | **DF** | **Sum of squares** | **Mean squares** | **F** | **Pr>F** |
| Model | 4 | 4062.500 | 1015.625 | 0.597 | 0.668 |
| Error | 27 | 45937.500 | 1701.389 | | |
| Corrected Total | 31 | 50000.000 | | | |

Table 6

| MODEL (1) PARAMETERS (SIGNAL TO NOISE RATIOS) | | | | | | |
|---|---|---|---|---|---|---|
| **Source** | **Value** | **Standard Error (SE)*** | **t** | **Pr>\|t\|** | **Lower bound (95%)** | **Upper bound (95%)** |
| Intercept | 44.239 | 0.976 | 45.347 | **<0.0001** | 42.237 | 46.240 |
| 100–150 | –0.753 | 0.873 | –0.862 | 0.396 | –2.543 | 1.038 |
| 100–200 | 0.000 | 0.000 | | | | |
| 0.00003–0.00004 | –0.753 | 0.873 | –0.862 | 0.396 | –2.543 | 1.038 |
| 0.00003–0.00005 | 0.000 | 0.000 | | | | |
| 40–50 | –1.008 | 0.873 | –1.156 | 0.258 | –2.799 | 0.782 |
| 40–60 | 0.000 | 0.000 | | | | |
| 80–100 | 0.440 | 0.873 | 0.505 | 0.618 | –1.350 | 2.231 |
| 80–150 | 0.000 | 0.000 | | | | |

Table 7

| MODEL (2) PARAMETERS (MEANS) | | | | | | |
|---|---|---|---|---|---|---|
| **Source** | **Value** | **Standard Error (SE)*** | **t** | **Pr>\|t\|** | **Lower bound (95%)** | **Upper bound (95%)** |
| Intercept | 165.625 | 16.305 | 10.158 | **<0.0001** | 132.171 | 199.079 |
| 100–150 | –12.500 | 14.583 | –0.857 | 0.399 | –42.423 | 17.423 |
| 100–200 | 0.000 | 0.000 | | | | |
| 0.00003–0.00004 | –12.500 | 14.583 | –0.857 | 0.399 | –42.423 | 17.423 |
| 0.00003–0.00005 | 0.000 | 0.000 | | | | |
| 40–50 | –12.500 | 14.583 | –0.857 | 0.399 | –42.423 | 17.423 |
| 40–60 | 0.000 | 0.000 | | | | |
| 80–100 | 6.250 | 14.583 | 0.429 | 0.672 | –23.673 | 36.173 |
| 80–150 | 0.000 | 0.000 | | | | |

Tables 6 and 7 present the parameters of the models that take into account the S/N ratio and the average values of the influencing factors on 2 levels.
Standard Error is calculated with the following equation:

$$*SE = \sigma / \sqrt{n} \quad (4)$$

where $\sigma$ is the standard deviation and $n$ – the number of samples.

## RESULTS AND DISCUSSION

Using the Taguchi plan with the response variable, the thickness of the deposited layer ($\delta$, the dependent variable) and applying the optimisation to maximise the value of the metal layer deposited by the magnetron sputtering method at 200 nm, with the help of the maximisation function $F(x) = y$ ($y$ = 200 nm), a deposited metal layer with a maximum thickness of 200 nm can be obtained using experimental parameters such as pressure $1\times10^{-5}$ mbar, argon flow 60 sccm, deposition surface 200 mm$^2$ and power 150 W (figure 4). The optimal parameters for the experiment (argon flow = 60 sccm, pressure $1\times10^{-5}$ mbar, power = 150 W, deposition surface = 200 mm$^2$) lead to obtaining a surface with a metal layer 200 nm thick (figure 4).

## CONCLUSIONS

In conclusion, the analysis by the Taguchi method and the realisation of experimental plans, followed by optimisation by maximisation, is essential because it can help to select the optimal experiment from the set of possible experiments. Thus, the number of experiments is reduced, implying the reduction of resource consumption (metal targets, argon, energy) to a few experiments (e.g., from 24 experiments to 5–10 experiments) to obtain conductive textile surfaces to develop electric thermoelectric generators.


## ACKNOWLEDGEMENTS

This work was carried out through the Core Programme within the National Research Development and Innovation Plan 2022–2027, carried out with the support of MCID, project no. 6N/2023, PN 23 26 01 03, project title "Materiale electroconductive pe baza de metalizari multistrat pentru sisteme termoelectrice, ecranare electromagnetica si senzori biomedicali integrati in sisteme IoT (3D-WearIoT)".

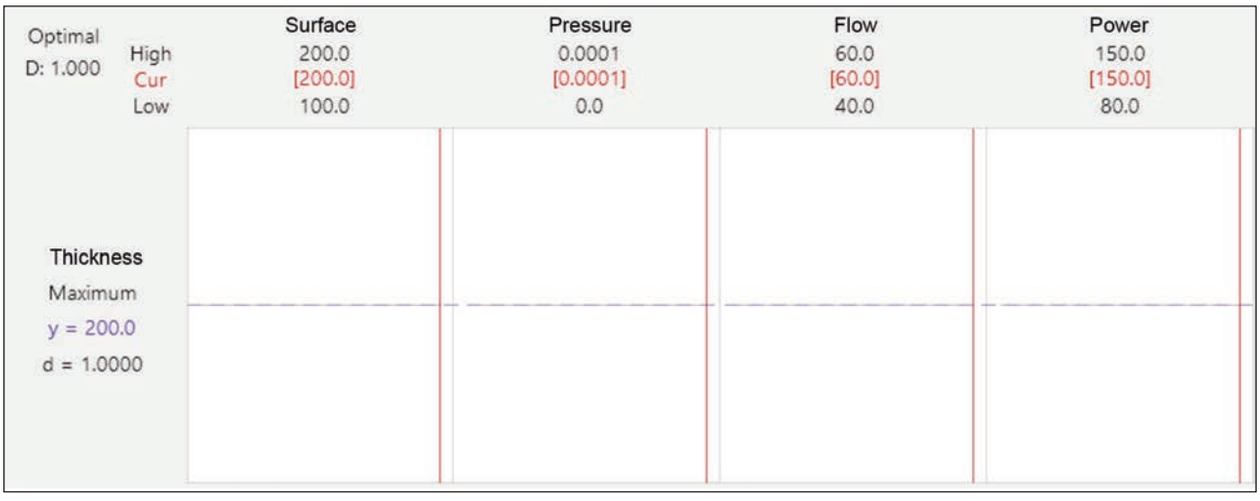


Fig. 4. Optimisation graph of experiments for the realisation of conductive materials for thermoelectric generators

## REFERENCES


[1] Lund, A., Tian, Y., Darabi, S., Müller, C., *A polymer-based textile thermoelectric generator for wearable energy harvesting*, In: Journal of Power Sources, 2020, 480, 228836

[2] Wen, N., Fan, Z., Yang, S., Zhao, Y., Cong, T., Xu, S., Zhang, H., Wang, J., Huang, H., Li, C., Pan, L., *Highly conductive, ultra-flexible and continuously processable PEDOT: PSS fibers with high thermoelectric properties for wearable energy harvesting*, In: Nano Energy, 2020, 78, 105361

[3] Hasan, M.N., Ahmad Asri, M.I., Saleh, T., Muthalif, A.G., Mohamed Ali, M.S., *Wearable thermoelectric generator with vertically aligned PEDOT: PSS and carbon nanotubes thermoelements for energy harvesting*, In: International Journal of Energy Research, 2022, 46, 11, 15824–15836

[4] Xu, C., Yang, S., Li, P., Wang, H., Li, H., Liu, Z., *Wet-spun PEDOT: PSS/CNT composite fibers for wearable thermoelectric energy harvesting*, In: Composites Communications, 2022, 32, 101179

[5] Hasan, M.N., Nayan, N., Nafea, M., Muthalif, A.G., Ali, M.S.M., *Novel structural design of wearable thermoelectric generator with vertically oriented thermoelements*, In: Energy, 2022, 259, 125032

[6] Ding, D., Wu, Q., Gao, Y., Wang, J., Chen, Y., Li, Q., *PEDOT/CNT/Bi2Te3 coated porous thermoelectric yarns for textile based wearable thermoelectric generator*, In: Smart Materials and Structures, 2023, 32, 3, 035036

[7] Li, Y., Wang, X., Luo, D., Shi, Y., Ren, Y., Yan, Y., *Recent development in structural designs and thermal enhancement technologies of thermoelectric generator with different types of heat sources: A review,* In: e-Prime-Advances in Electrical Engineering, Electronics and Energy, 2023, 100180

[8] Wang, Y., Shi, Y., Mei, D., Chen, Z., *Wearable thermoelectric generator to harvest body heat for powering a miniaturized accelerometer*, In: Applied Energy, 2018, 215, 690–698

[9] *Sensing Performance – an overview | ScienceDirect Topics*, Available at: www.sciencedirect.com/topics/engineering/sensing-performance [Accessed on May 2023]



**Authors:**

RALUCA MARIA AILENI, CRISTINA STROE

National Research & Development Institute for Textiles and Leather,
Lucretiu Patrascanu 16, 030508 Bucharest, Romania

**Corresponding author:**

RALUCA MARIA AILENI
e-mail: raluca.aileni@incdtp.ro

# Flexural and impact performance of Kevlar/basalt fabric interlayer hybrid curved composites

DOI: 10.35530/IT.075.01.202313

FANGTAO RUAN
HAO WANG
CHENGLONG XIA
QINGYONG YANG
LIHUA ZOU
ZHENZHEN XU

**ABSTRACT – REZUMAT**

**Flexural and impact performance of Kevlar/basalt fabric interlayer hybrid curved composites**

*FRP composite has become one of the most preferred materials in lightweight applications. Design freedom is a key benefit which is reflected in the choice of fibres, stacking sequence and others. Hybridisation of hard inorganic fibre and organic ductile fibres can lead to synergetic effects. In this paper, an interlayer hybrid curved laminated composite reinforced with woven Kevlar and basalt fabrics and manufactured by a hand lay-up process with epoxy resin was prepared. Experimental investigation on the flexural and impact properties of composite laminates has been performed. The results of the investigation showed that the placement of Kevlar fibres on the impact side can increase the impact and flexural strengths, sample H3 (K3B2K3B2) has the highest impact strength and absorbed energy among seven hybrid laminates, valued at 92.89 KJ/m$^2$ and 2.48 KJ. Compared with H5(B4K6) improved 41.6% and 40.9%, respectively. However, H5 has the highest flexural strength, reaching 231.7 MPa. In addition, the use of basalt fabric on the impact reverse side or multi-layer hybrid structuring further improves the impact properties of the materials. A sandwich-structure composite with basalt layers in the middle and Kevlar layers on both sides shows further improvement in the flexural properties.*

***Keywords:*** *composites, woven fabrics, basalt fabrics, stacking sequence, stacking sequence, three-point flexural, impact*

**Performanța la încovoiere și la impact a compozitelor hibride curbate interstrat din țesătură Kevlar/bazalt**

*Compozitul FRP a devenit unul dintre materialele preferate utilizate în aplicațiile cu greutate redusă. Libertatea de proiectare este un beneficiu cheie care s-a reflectat în alegerea fibrelor, secvența de stivuire și altele. Hibridizarea fibrelor anorganice dure și a fibrelor organice ductile poate duce la efecte sinergetice. În acest studiu, a fost pregătit un compozit laminat hibrid curbat interstrat, consolidat cu țesături Kevlar și bazalt și fabricat printr-un proces manual de întindere cu rășină epoxidică. Au fost efectuate investigații experimentale asupra proprietăților de încovoiere și de impact ale laminatelor compozite. Rezultatele investigației au arătat că plasarea fibrelor de Kevlar pe partea de impact poate crește rezistența la impact și la încovoiere, proba H3 (K3B2K3B2) având cea mai mare rezistență la impact și energie absorbită dintre cele șapte laminate hibride, cu valori de 92,89 KJ/m$^2$ și 2,48 KJ. Comparativ cu H5(B4K6), a existat o îmbunătățire cu 41,6% și, respectiv, cu 40,9%. Cu toate acestea, H5 are cea mai mare rezistență la încovoiere, ajungând la o valoare de 231,7 MPa. În plus, utilizarea țesăturii de bazalt pe partea inversă a impactului sau structurarea hibridă cu mai multe straturi îmbunătățește și mai mult proprietățile de impact ale materialelor. Un compozit cu structură tip sandwich cu straturi de bazalt în mijloc și straturi de Kevlar pe ambele părți arată o îmbunătățire suplimentară a proprietăților de încovoiere.*

***Cuvinte-cheie:*** *compozite, ţesături, țesături de bazalt, secvență de stivuire, încovoiere în trei puncte, impact*

## INTRODUCTION

Fibre-reinforced polymer composite materials (FRP) consist of fibres of high strength and modulus embedded in a polymer matrix. In this form, both the fibres and the polymer matrix retain their physical and chemical identities, yet they act separately [1]. The earliest FRP materials used were glass fibres embedded in polymeric resins made available by the petrochemical industry [2]. The fibre arrangement structure in the composite typically follows that of two-dimensional fabrics, including unidirectional, plain, and twill weaves. The multilayer stacking method must be adapted to meet the requirements for the structure thickness of composite materials, owing to the decrease in fibre cost and improvements in the preparation technology. Recently, interest has grown in the use of FRP in structural applications because they have the characteristics of low weight, high strength, high chemical resistance, and design flexibility, making manufacturing of large integral structures feasible [3]. The application of high-performance fibres in civil fields has recently expanded. FRP is increasingly in demand for protective equipment applications in the sports and labour field, giving rise to new economic growth.

The strength and modulus of elasticity of basalt fibre-reinforced composites (BFRP) are 30% higher than that of glass fibre-reinforced composites (GFRP), the thermal expansion coefficient is $6–8 \times 10^{-6}$/°C, the creep fracture stress is 0.54, and the price is close to GFRP. Compared with aramid fibre fibre-and carbon fibre-reinforced composites, BFRP has the highest performance-to-price ratio [4]. However, BFRP has low resistance under impact loading because of the lower elongation at the break of the basalt fibres [5]. For the optimal design of head protection equipment, it is important to improve the impact resistance of the composite material [6].

Hybrid fabric is an effective means of composite design, such fabric comprises two or more different types of fibres composited with a resin matrix to match the optimised performance requirements [7]. Fibres with different strengths, toughness, and elongations at break are mixed to obtain the advantages of all fibre types in terms of the different properties of the composites [8]. Kevlar fibres show excellent impact resistance owing to their high strength, ductility, and elongation at fracture, although they are considerably more expensive than basalt fibres. The primary limitation of Kevlar fibre-reinforced composites is their weakness in flexural and compression [9]. Notably, composite structures with curved shapes are common and easily experience delamination under loads owing to localised transverse stresses [10]. However, few investigations and little research have been conducted on this. Dong [11] discussed the flexural characteristics of hybrid composites fabricated using glass/carbon fibres and epoxy. Positive hybrid effects were observed when the glass laminae were placed on the compressive side. Similarly, Hung et al. [12] used glass/carbon to form a hybrid composite and found that the flexural strength was controlled by the strength of the bottom layers. Wu et al. [13] studied the flexural properties of a carbon/glass interlayer hybrid composite by theoretical analysis and experimental three-point flexural tests; their results agreed with the previous reports, and they found that the hybrid fibre content has no obvious influence. Subagia et al. [14] studied the effect of stacking order on the flexural properties of carbon/basalt inter-ply hybrid composites. The experimental results showed that the major failure mechanism was compressive failure. In addition, when carbon fibre plies were placed at the compressive side, higher flexural strengths and moduli could be obtained. Amuthakkannan et al. [15] found that sandwich-structured composites, in which the top and bottom layers contain the same fibres, have better impact strength than other interlayer structures for basalt/glass fibre-reinforced composites.

In addition to the use of hybrid fabrics of inorganic fibres, several studies have been conducted on hybrid composites utilising basalt and organic ductile fibres. Such hybrid composites combine the good mechanical properties of the brittle basalt fibre with the excellent impact resistance of the ductile organic fibre. Dehkordi et al. [16] studied the impact performance of basalt/nylon inter-ply hybrid composites. The results showed that the toughening mechanism of pure basalt fibre-reinforced composites under impact was fibre fracture, whereas those of the hybrid composites were debonding of nylon fibre and resin, basalt fibre fracture, and resin shear failure. The impact performance was dependent on the hybridisation and proportion of basalt/nylon fibres at high-impact energies. Sarasini et al. [17] analysed the low-velocity impact response of two different hybrid configurations and concluded that the Kevlar skin/basalt-core type exhibited better energy absorption capability than the lay-up type. Bozkurt et al. [18] investigated the effect of Kevlar/basalt inter-ply hybridisation and revealed that the introduction of basalt fibre on the compressive side provides greater improvement for the flexural resistance; in addition, the flexural properties of the composite are affected by the fibre stacking sequence.

In this study, epoxy-based woven basalt/Kevlar fabrics hybrid composites with hemispherical shapes were prepared using a hand lay-up process.

Specimens with different configurations varying from 100% Kevlar to 100% basalt lamination and several types of inter-ply hybrid composites were designed. The impact and flexural properties of curved inter-ply hybrid composites with different hybrid structures were measured using cantilever impact and three-point flexural testers. The effects of different stacking sequences on the impact, flexural strength, and failure modes of the interlayer hybrid curved composites were discussed.

## EXPERIMENTAL

### Materials

Kevlar fibre (Kevlar1414, plain woven, 200 g/m$^2$) was purchased from China Tongxiang Xuanlei Composite Materials Co., Ltd. Basalt fibre (twill woven, 20013 g/m$^2$) was purchased from China Zhejiang Shijin Basalt Fiber Co., Ltd. Pictures of fabric used for curved laminates are shown in figure 1. Epoxy resin (JL-235) and Hardener (JH-242) were provided by Changshu Jiafa Chemical Co., Ltd, China. The mixture

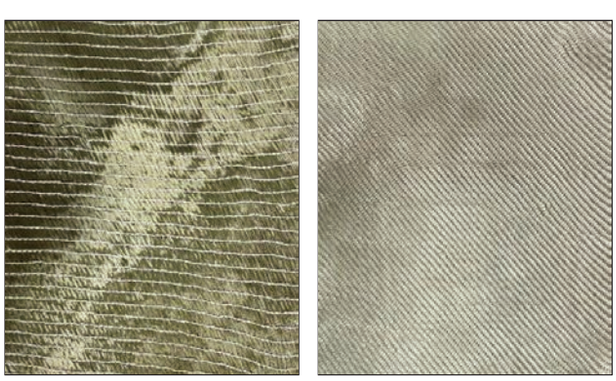

*a* *b*

Fig. 1. Fabric used for curved laminates: *a* – Basalt twill fabric; *b* – Kevlar plain woven fabric

ratio of epoxy resin (1.12–1.16 g/cm$^3$ intensity, 0.54–0.57 eq/100 g in Epoxy value, 175–185 in Epoxy equivalent, 2500 MPa/s in viscosity) and curing agent (0.92–0.96 g/cm$^3$ in density, 450–510 mg KOH/g in amine value, 55–60 g/eq in active hydrogen equivalent, 40–80 MPa/s in viscosity) was 100:30 at ambient temperature (figure 1).

### Preparation of hybrid composite samples and experimental design

The hybrid composite laminates were fabricated by using the hand lay-up and moulding process. The hand lay-up method was relatively simple to operate. There were several steps to accomplish all processes, which include: (a) resin and fabric preparation; (b) resin impregnation; (c) moulding by the self-made mould; and (d) curing of fabricated curved composites. The schematic diagram of the hand lay-up process is shown in figure 2. The hemispherical mould had a diameter of 8 cm and a depth of 5 cm, the radius of curvature was 50 mm. Basalt and Kevlar woven fabrics were cut to a size of 100×100mm, then arranged with different stacking orders in ten plies, among them, there were 4 plies of basalt fibre fabrics and 6 plies of Kevlar fabrics. Sketch maps of various stacking orders of Kevlar and basalt fabric and specimens are shown in figures 3 and 4. The relationships between laminate codes and the stacking sequence of the specimen are presented in table 1. The fibre weight portion of both Kevlar and basalt fibres was 50–55 wt.% in all of the hybrid composite laminate. The Kevlar and basalt fabric were immersed in the matrix with the epoxy resin with an amine curing agent. Then the immersed fabrics were put into the special mould and cured for 24 hours at room temperature.

Table 1

| NUMBERED HYBRID LAMINATE WITH DIFFERENT STACKING SEQUENCE | |
|---|---|
| **Stacking sequence of specimen** | **Laminate codes** |
| K10 | KFRP |
| K3B4K3 | H1 |
| K6B4 | H2 |
| K3B2K3B2 | H3 |
| K2B2K2B2K2 | H4 |
| B4K6 | H5 |
| B2K3B2K3 | H6 |
| B2K6B2 | H7 |
| B10 | BFRP |

### Experiments

*Impact test*

The impact tests were carried out using a digital display simple cantilever impact tester. The absorbed energy during fracture in the impact test is used as a

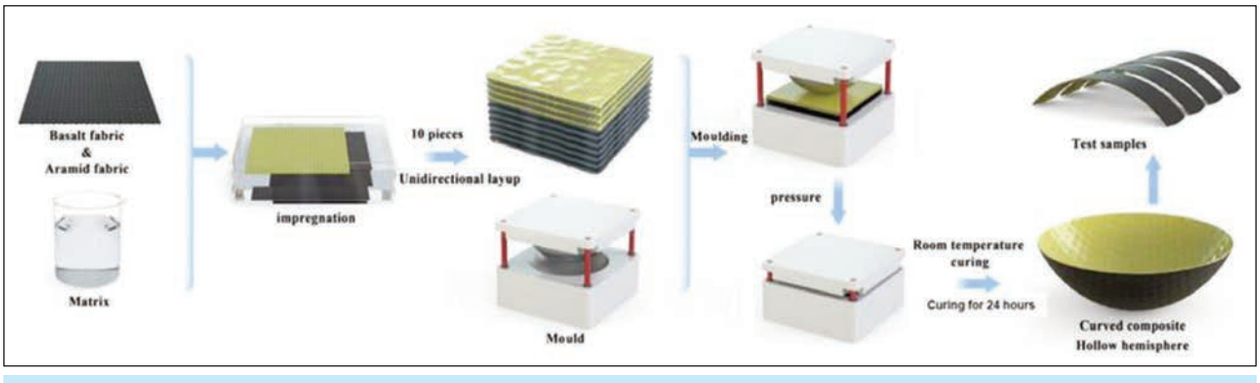


Fig. 2. Schematic diagram of a process for curve composite preparation

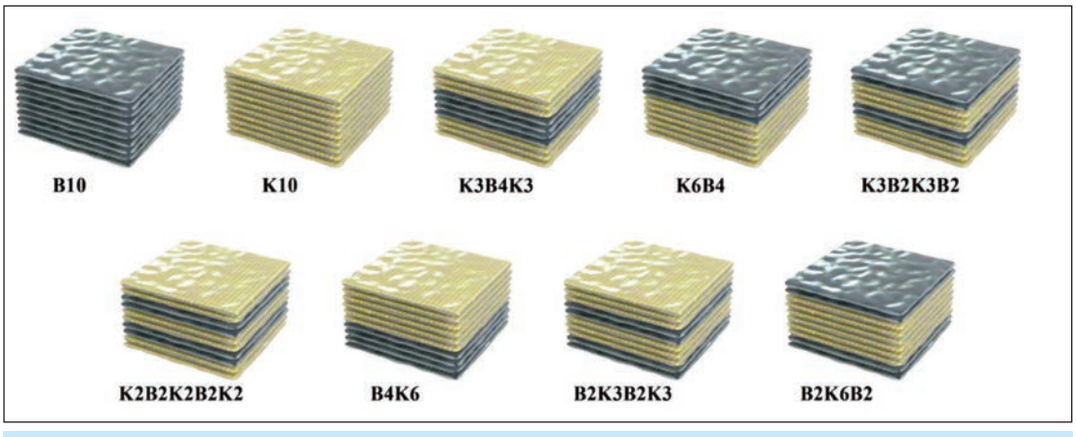


Fig. 3. Stacking sequence of Kevlar (K) and basalt (B) fibre woven

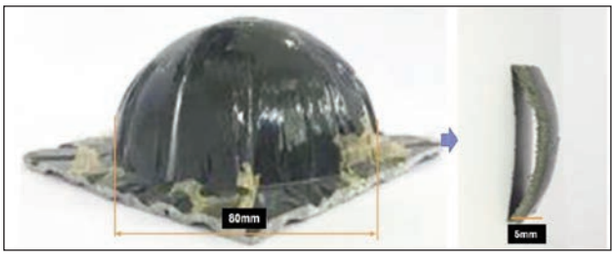


Fig. 4. Pictures of curve shape composite and specimen

measure of impact strength by GB/T1043-1993 [19]. Impact energy in an impactor was transmitted into a structure deformed or damaged, this geometry change for all specimens would absorb part of the energy. The distance between the support lines was 40 mm and the impact speed was 3.8 m/s. The dimensions of impact test specimens were about 5010 mm (length and width). The convex was the impact surface for all specimens, at least five specimens for each laminate. The impact strengths of the specimen were calculated by the formula which references formula 1:

$$a = \frac{P_{max}}{w \cdot h} \times 10^3 \quad (1)$$

where $P_{max}$ is impact strength, which available directly from the digital display. $w$ and $h$ are the width of the specimen, the thickness of the specimen, and the absorbed energy of the specimen, respectively.

*Flexural test*

A flexural performance test was carried out using a universal mechanical testing instrument (WDW-20) by GB/T3356-2014 [20]. The span-to-depth ratio was 16, the test was performed at a constant crossed speed of 5 mm/min. The length of the specimen was about 60 mm, and the width was 10 mm. The convex was the compressive surface for all specimens. The cross-section at the point where the load is applied is consistent with the original stress situation because there is no axial force. Other cross-sections where the damage has changed must be the location where the strength limit occurs. Since the modulus and hardness of this material are high, not much plastic deformation occurs, and the damage to the midpoint of the upper section is completely dominated by bending, we believe that the flexural strength of the specimen can be obtained by formula 2:

$$\sigma_f = \frac{3 P_{max} L}{2 w h^2} \quad (2)$$

where $P_{max}$, $L$, $w$ and $h$ represent the maximum load on the specimen, the span, thickness, and width of the specimen. The pictures of the mechanical properties test in this study are shown in figure 5.

*Fracture surface observation*

Fracture surface analysis was performed to observe the microstructure of the specimen after testing using an electronic magnifying camera (Gaoping, GP-300C) and to understand the failure mechanism.

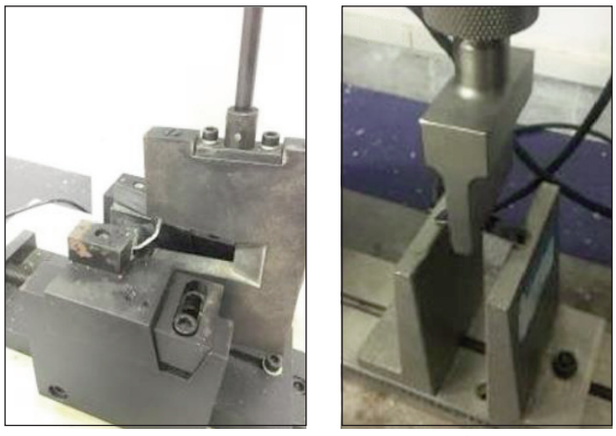

***a*** ***b***

Fig. 5. Photo of: *a* – impact test; *b* – three-point flexural test

## RESULTS AND DISCUSSION

### Impact properties

The impact strength and absorbed energy of hybrid composites are shown in table 1. It was obvious that the KFRP showed the highest strength and absorbed energy because of the high strength of Kevlar fibre. This appears to be contrary to the Bozkurt [18] findings who reported that BFRP has higher impact strength and energy absorption than KFRP. It may be attributed to the fabric structure and curved structure for impact specimens. On the contrary, the BFRP shows the lowest impact strength and absorbed energy due to the basalt fibre being brittle. The KFRP showed impact strength which was 169% greater than that of BFRP. Figure 6 shows the morphology of the impacted and back surfaces for BFRP and KFRP composite. It can be seen from figures 6, *a* and *b*, that many cracks and fibre fractures for BFRP, show a typical failure of crack propagation attributed to the brittle failure of basalt fibres. it can be observed that the damage on the impacted side was relatively large and uncircular, compared with the back side.

While Kevlar fibres were not broken figure 6, *c* and *d*, impact failure was the loss of adhesion between fibre and resin, low-speed impact only causes some impact marks on the surface of the material, and some folds can be observed on the impact surface. It signifies that the material has a stronger impact toughness for KFRP. The deformation of Kevlar fibres is believed to be the key factor that improves the impact resistance of the composite [21]. In addition, it is found that almost no delamination phenomenon for neat basalt and Kevlar reinforced composite may be related to the curved structure.

From table 1, the hybrid composites of basalt and Kevlar fabrics (H1–H7, with different stacking sequences) showed average values between the values of KFRP and BFRP. The impact strength was proportional to the absorbed energy for all hybrid composite specimens. From the impact test results, it was found that the impact strength was higher when the Kevlar fabric was put on the surface. For

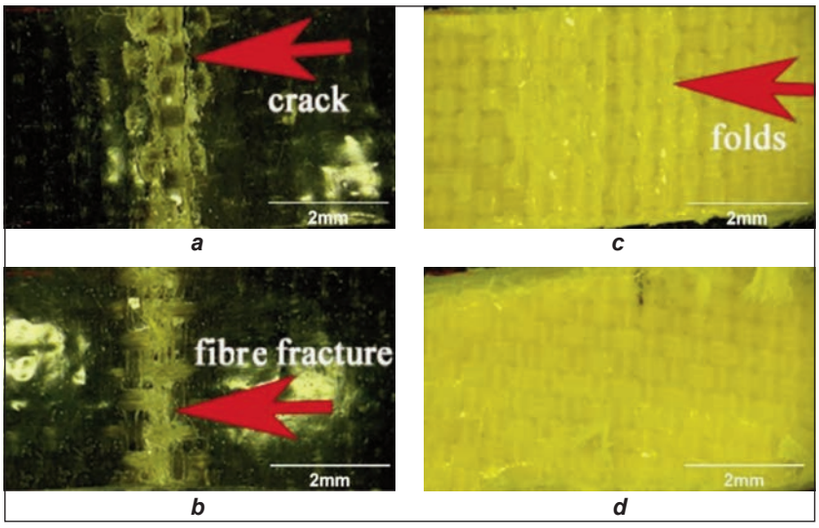


Fig. 6. Failure surfaces of samples after impact test: *a* and *b* – BFRP; *c* and *d* – KFRP; *a* and *c* – at the impacted side; *b* and *d* – at the back side, respectively

instance, the impact strength of H2 hybrid composite laminate was 92.43 kJ/m$^2$, compared with H5 increased by 41%. The impact strength of sample H3 increased by 14.4% compared with H6. The impact surface of the samples H2 and H4 were both Kevlar fabrics, due to the impact surface bearing more impact load, the placement of Kevlar fibres on the impact side should be the cause of increased impact strength. Bozkurt et al. got similar research results, changing the impact side showed differences in the impact absorbed energy of composite, aramid layer at the impacted side will improve impact absorbed energy.

Besides, the type of fabric on the impact reverse side also influenced the impact strength and absorbed energy, compare H1 with H3, the impact side was both Kevlar fibres, yet the impact reverse side of H3 was basalt fibres, its impact strength and absorbed energy were increased by 25.54% and 28.5%, respectively. In addition, the impact performance of H3 was also better than that of H4. In brief, the impact strength and absorbed energy are higher when the impact reverse side is basalt fabrics.

By further analysis, the multi-layer hybrid structure will improve the impact properties, the structures of H5 and H6 were similar, the impact side and reverse side were basalt fibre and Kevlar fibre respectively, and the two types of reinforced fabrics in H6 were arranged alternately, this resulted in a 23.83% increase in impact strength. While the impact side was Kevlar fibre and the reverse side was basalt fibre for both H2 and H3, the difference was that the core of the sandwich structure. There are no significant differences in impact strength and absorbed energy of H2 and H3. This further proves that the placement of Kevlar fibres on the impact side is the main reason for improving impact performance.

It can be seen from figure 6 that the main impact failure forms for hybrid composites were basalt fibre fractures, Kevlar fibre debonding and buckling as well as delamination. In general, the fracture of basalt fibre and the debonding of Kevlar fibre play a great role in absorbing impact energy.

Table 2

IMPACT PROPERTIES OF BFRP, KFRP AND HYBRID COMPOSITE LAMINATES

| Stacking sequence of specimen | Laminate codes | Impact strength (KJ/m$^2$) | Absorbed energy (KJ) |
|---|---|---|---|
| K10 | KFRP | 115.62 | 3.09 |
| K3B4K3 | H1 | 73.99 | 1.93 |
| K6B4 | H2 | 92.43 | 2.47 |
| K3B2K3B2 | H3 | 92.89 | 2.48 |
| K3B2K2B2K2 | H4 | 82.45 | 2.21 |
| B4K6 | H5 | 65.57 | 1.76 |
| B2K3B2K3 | H6 | 81.20 | 2.20 |
| B2K6B2 | H7 | 78.45 | 2.10 |
| B10 | BFRP | 42.98 | 1.14 |

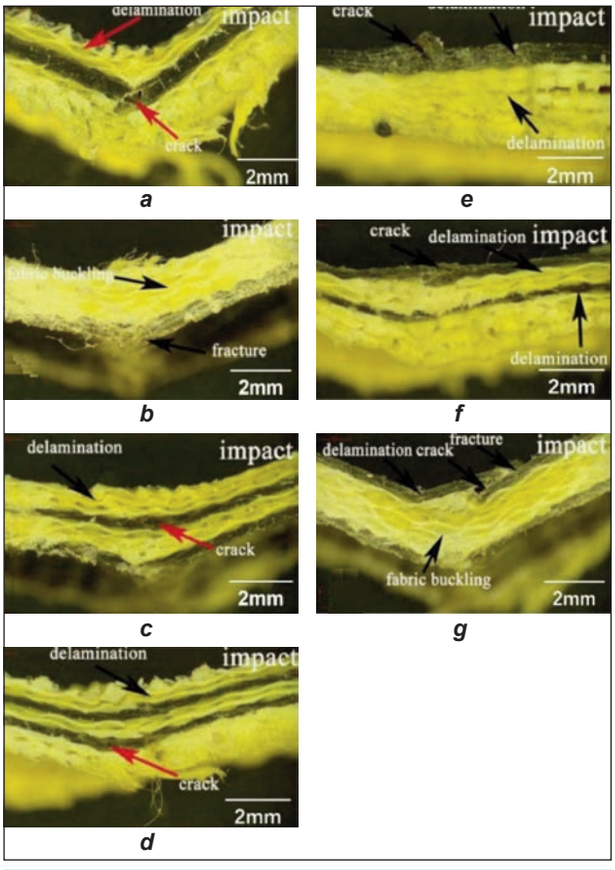


Fig. 7. Side images of failed samples after impact testing: *a* – H1; *b* – H2; *c* – H3; *d* – H4; *e* – H5; *f* – H6; *g* – H7

From the picture of failed sample H5–H7, the degree of deformation showed a reduction with an increase in the layers of basalt fibre at the impacted surface [22]. H1 is a sandwich structure, the basalt fibre in the middle has an obvious penetrating fracture after impact. Since basalt fibres are on the tensile side, the impact deformation of H3 decreases and the crack of basalt fibre becomes more inapparent. Both of them have obvious delamination of Kevlar fibre. H4 is more prone to delamination than H3. From the impact data in table 1, it seems that the fracture of basalt fibre plays a major role in improving the impact performance of the sandwich structure. For non-sandwich structures H2 and H5, the basalt on the impact surface can reduce its deformation but cause more cracks and delamination.

**Flexural properties**

Typical load-displacement curves of specimens (H5 as a representative of inter-layer hybrid composites) are shown in figure 8. BFRP has a typical "hard and weak" material, these curves implied that BFRP had higher flexural modulus but lower flexural strength. On the contrary, the flexural strength of KFRP was relatively high, and the slope of the curve was relatively low, which means that the flexural modulus was low. Like impact properties, the interlayer hybrid composites (H5) had average values between values of KFRP and BFRP. Due to the delamination phenomenon during the flexural test for interlayer hybrid composites, there were 2–3 peaks on each curve until it failed. The highest peak value was taken as the basis for the calculation of flexural strength. The calculation results are shown in table 3.

The three-point flexural experimental results show that flexural strength and modulus are related to the fabric type of compressive side and the tensile side (reverse side for specimens). It is known that the maximum values of the compressive and tensile stresses occur on the external layers. When Kevlar fabric was placed on the tensile side, the flexural strength was higher than that of basalt fabric on the tensile side. Moreover, basalt fibre on the compression side will help to improve flexural strength. In the case of H5, which has the highest flexural strength in interlayer hybrid composite specimens since there are 4 pieces of basalt fabric on the compressive side. Due to 2 pieces of basalt on their compressive side, specimens H6 and H7 also have relatively high flexural strength. Besides, it observed that the flexural strength also depended on what material was placed at the tension side. When the tensile side is Kevlar fabric, its flexural strength increases, and the value of H6 is 15.93% higher than that of H7.

Table 3

FLEXURAL PROPERTIES OF BFRP, KFRP AND HYBRID COMPOSITE LAMINATES

| Stacking sequence of specimen | Laminate codes | Flexural strength (Mpa) | Flexural modulus (GPa) |
|---|---|---|---|
| K10 | KFRP | 133.6 | 0.167 |
| K3B4K3 | H1 | 217.1 | 0.135 |
| K6B4 | H2 | 137.1 | 0.161 |
| K3B2K3B2 | H3 | 153.6 | 0.133 |
| K3B2K2B2K2 | H4 | 180.6 | 0.116 |
| B4K6 | H5 | 231.7 | 0.109 |
| B2K3B2K3 | H6 | 198.0 | 0.132 |
| B2K6B2 | H7 | 170.8 | 0.095 |
| B10 | BFRP | 301.4 | 0.083 |

For specimens H2, H3 and H4, the compressive sides of these specimens are all Kevlar fabric. However, the tensile side of H4 is Kevlar fabric, while the tensile side of H2 and H3 were basalt fabric. The flexural strength of H4 is 31.73% and 27% higher than that of H2 and H3, respectively, This suggests that Kevlar fibre on the tensile side can make the hybrid composites have higher flexural strength. It seems that the selection of tensile side material has a greater impact on the improvement of flexural strength. Sample H1 has a sandwich structure, both tensile and compressive sides are Kevlar fabric, and the interlayer is basalt, this kind of laminated structure also has better flexural strength. Due to the high modulus of Kevlar fabric reinforced composites, the more layers of Kevlar fabric in the compression surface, the higher the flexural modulus for interply hybrid composite.

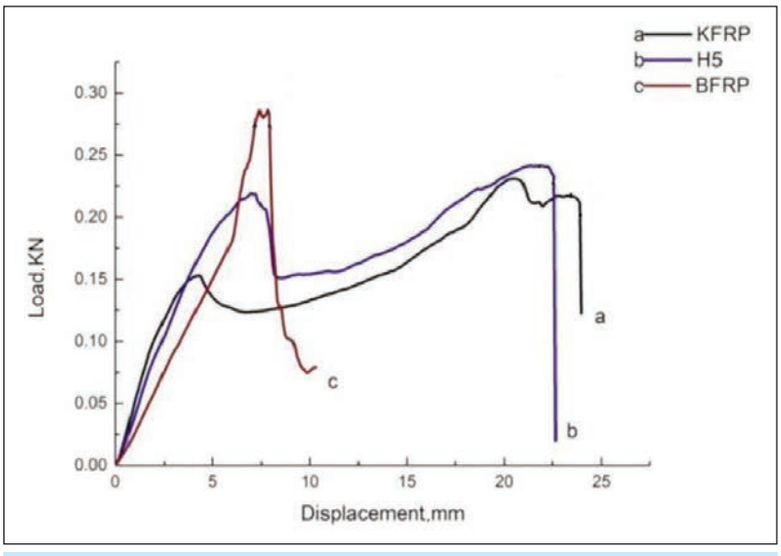


Fig. 8. Load-displacement curves for typical specimens

Figure 9 illustrates photographs of the fractured region for FRP after a three-point flexural test, which is along the sample's thickness. The damage is divided into three parts. Interlayer delamination, fibre fracture by compression and tensile debonding by tension. The cracks formed between

different components begin to start to cause fibre/matrix interface debonding.

The three-point flexural test can be regarded as an impact test with ultra-low speed. There is sufficient time to transfer the force. With the change of flexural strain, the compression layer is destroyed first [23]. The fracture of basalt fibre on the compression side plays a major role in improving flexural performance. The Kevlar fibre on the tension side shows a delamination phenomenon that can be seen in pictures of failed samples after flexural testing.

## CONCLUSIONS

The effects of the interlayer hybrid of Kevlar and basalt fabric on the impact, flexural, and damage appearance of interlayer hybrid curve composites have been experimentally investigated. The hybrid composite laminates were fabricated into a curved shape with the aid of a hemispherical mould. Seven different hybrid laminate configurations and two neat Kevlar and basalt-reinforced epoxy composites were prepared. Each type of interlayer hybrid composite laminate contained 4-layer Kevlar fabric and 6-layer basalt fabric. The main conclusions that can be drawn are the following:

- BFRP showed a relatively lower impact strength and flexural strength compared to KFRP, but this was enhanced by the interlayer hybrid with Kevlar layers. The KFRP showed impact strength which was 169% greater than that of BFRP.
- The type of fabric on the impact reverse side also influenced the impact strength and absorb energy, the placement of Kevlar fibres on the impact side should be the cause of increased impact strength. Besides, if the basalt fabric is on the impact reverse side or multi-layer hybrid structure, that will further improve the impact properties of the material. Sample H3 (K3B2K3B2) has the highest impact strength and absorbed energy among seven hybrid laminates, valued at 92.89 KJ/m$^2$ and 2.48 KJ. Compared with H5(B4K6) improved 41.6% and 40.9%, respectively.
- Sample H5 has the highest flexural strength, reaching 231.7 MPa. The placement of Kevlar fabric was placed on the compressive side, the flexural strength was higher than that of basalt fabric on the compressive side. If it is made into a sandwich structure with basalt layers in the middle and Kevlar layers on both sides, the flexural properties of the material will be further improved.

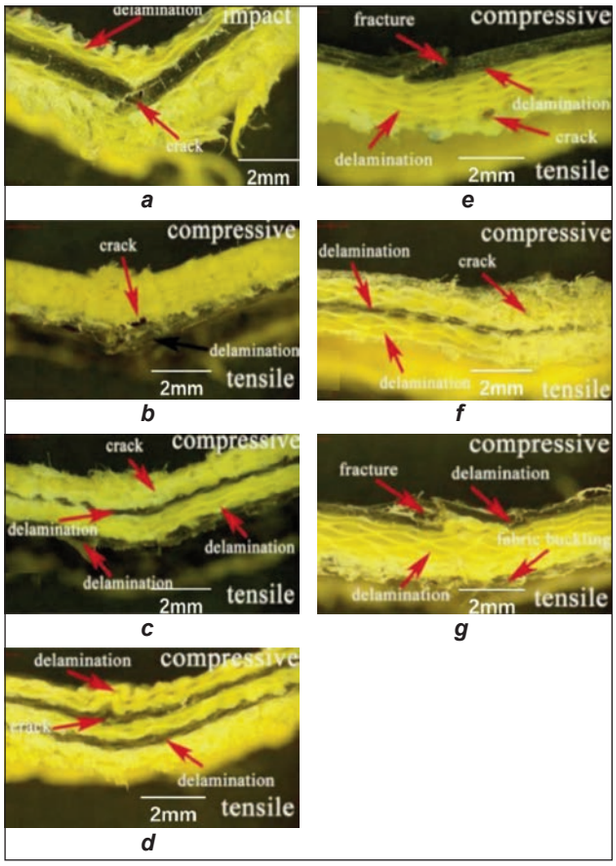


Fig. 9. Side images of failed samples after flexural testing: *a* – H1; *b* – H2; *c* – H3; *d* – H4; *e* – H5; *f* – H6; *g* – H7


## ACKNOWLEDGEMENTS

This work was supported by the Natural Science Foundation of China (No.51903001), Anhui Province University Excellent Talent Cultivation Project (gxgnfx2021133), as well as Scientific research projects to promote undergraduate talent training (FFBK202322).


## REFERENCES


[1] Waghmare, S., Shelare, S., Aglawe, K., et al., *A mini review on fibre-reinforced polymer composites*, In: Materials Today: Proceedings, 2022, 54, 682–689

[2] Laghaei, R., Hejazi, S.M., Fashandi, H., et al., *Improvement in fracture toughness and impact resistance of E-glass/epoxy composites using layers composed of hollow poly (ethylene terephthalate) fibers*, In: Journal of Industrial Textiles, 2022, 51, 4860–4879

[3] Ravishankar, B., Nayak, S.K., Kader M.A., *Hybrid composites for automotive applications A review,* In: Journal of Reinforced Plastics and Composites, 2019,38, 835–845

[4] Zhou, J., Chen, C., Zhang, S., et al., *Enhancing the interfacial adhesion between continuous basalt fibers and epoxy resin by depositing silicon dioxide nanonparticles,* In: Journal of Industrial Textiles, 2022, 51, 3309–3329

[5] Bozkurt, O.Y., Erkli, A., Bulut, M., *Hybridization effects on charpy impact behavior of basalt/aramid fiber reinforced hybrid composite laminates,* In: Polym Composite, 2018, 39, 467–475

[6] Meliande, N.M., Oliveira, M.S., Silveira, PHP.Md., et al., *Curaua Aramid Hybrid Laminated Composites for Impact Applications: Flexural, Charpy Impact and Elastic Properties.* In: Polymers, 2022,14

[7] Swolfs, Y., Verpoest, I., Gorbatikh, L., *Recent advances in fibre-hybrid composites: materials selection, opportunities and applications,* In: International Materials Reviews, 2019, 64,181–215
[8] Ravishankar, B., Nayak, S.K., Kader, M.A., *Hybrid composites for automotive applications A review.* In: Journal of Reinforced Plastics and Composites, 2019, 38, 835–845
[9] Valena, S.L., Griza, S., De, Oliveira, V.G., et al., *Evaluation of the mechanical behavior of epoxy composite reinforced with Kevlar plain fabric and glass/Kevlar hybrid fabric.* In: Composites Part B: Engineering, 2015, 70, 1–8
[10] Chen, Z., Yue, C., Zhang, Y., et al., *Mechanical response and failure mechanism of three-dimensional braided composites under various strain-rate loadings by experimental and simulation research: a review,* In: Textile Research Journal, 2022, 92, 296–314
[11] Chen, D., Sun, G., Meng, M., et al., *Flexural performance and cost efficiency of carbon/basalt/glass hybrid FRP composite laminates,* In: Thin-Walled Structures, 2019, 142, 516–531
[12] Hung, P., Lau, K., Cheng, L., et al., *Impact response of hybrid carbon/glass fibre reinforced polymer composites designed for engineering applications,* In: Composites Part B: Engineering, 2018, 133, 86–90
[13] Wu, W., Wang, Q., Ichenihi, A., et al., *The effects of hybridization on the flexural performances of Carbon/Glass interlayer and intralayer composites,* In: Polymers, 2018, 10
[14] Ary Subagia, I.D.G., Kim, Y., Tijing, L.D., et al., *Effect of stacking sequence on the flexural properties of hybrid composites reinforced with carbon and basalt fibers,* In: Composites Part B: Engineering, 2014, 58, 251–258
[15] Amuthakkannan, P., Manikandan, V., Uthayakumar, M., *Mechanical properties of basalt and glass fiber reinforced polymer hybrid composites,* In: Journal of Advanced Microscopy Research, 2014, 9, 44–49
[16] Tehrani Dehkordi, M., Nosraty, H., Shokrieh, M.M., et al., *The influence of hybridization on impact damage behavior and residual compression strength of intraply basalt/nylon hybrid composites,* In: Materials and Design, 2013, 43, 283–290
[17] Valena, S.L., Griza, S., De Oliveira, V.G., et al., *Evaluation of the mechanical behavior of epoxy composite reinforced with Kevlar plain fabric and glass/Kevlar hybrid fabric,* In: Composites Part B: Engineering, 2015, 70, 1–8
[18] Bozkurt, O.Y., Erkli, A., Bulut, M., *Hybridization effects on charpy impact behavior of basalt/aramid fiber reinforced hybrid composite laminates,* In: Polymer Composite, 2018, 39, 467–475
[19] GB/T3356-2014, *Test method for flexural properties of orientational fibre reinforced polymer matrix composite materials*, In: National Standard of the People's Republic of China
[20] GB/T1043-1993, *Plastics: Determination of Charpy impact strength of rigid materials*, In: National Standard of the People's Republic of China
[21] Siddique, A., Abid, S., Shafiq, F., et al., *Mode I fracture toughness of fiber-reinforced polymer composites: A review,* In: Journal of Industrial Textiles, 2021, 50, 1165–1192
[22] Paramasivam, C., Venugopal, R., *Design and development of glass/basalt fiber reinforced composite material for automobile applications,* In: Journal of Industrial Textiles, 2022, 51, 1668–1681
[23] Ma, Z., Zhang, P., Zhu, J., *Influence of fabric structure on the tensile and flexural properties of three-dimensional angle-interlock woven composites,* In: Journal of Industrial Textiles, 2022, 51, 1641–1657

**Authors:**

FANGTAO RUAN[1], HAO WANG[2], CHENGLONG XIA[1], QINGYONG YANG[1], LIHUA ZOU[1], ZHENZHEN XU[1]

[1]Anhui Polytechnic University, School of Textile and Garment, 241000, Wuhu, China

[2]Shinshu University, Faculty of Textile Science and Technology, 386-8567, Ueda, Japan

**Corresponding authors:**

FANGTAO RUAN
e-mail: ruanfangtao@ahpu.edu.cn
ZHENZHEN XU
e-mail: xuzhenzhen@ahpu.edu.cn

# A study on multi-layered surgical masks performance: permeability, filtration efficiency and breathability

DOI: 10.35530/IT.075.01.202356

ŞEVKAN MACİT AYŞE


## ABSTRACT – REZUMAT

### A study on multi-layered surgical masks performance: permeability, filtration efficiency and breathability

*Surgical masks have been widely used in the past for protection purposes against infection as a hygiene product. Masks, which are often used by healthcare professionals, are also widely used by the general public during pandemic periods. Surgical masks were designed in various ways according to colour, nose strip, earloop, grams per square meter and several layers. Some performance features are expected from these masks according to certain standards. In this study, it has been studied on multi-layered surgical masks. Thickness, air permeability, bacterial filtration efficiency and differential pressure properties of these masks consisting of polypropylene spun bond and melt-blown layers were investigated. The effects of an increase in grams per square meter, the number of layers and the melt-blown layer on the mentioned properties were determined. As a result; it has been observed that the optimal mask is one of the 4-ply masks. Also, it has been concluded that increasing the number of layers does not always provide an increase in performance; instead, an increase in grams per square meter can meet the expectation. Therefore, it can be said that it is necessary to determine the appropriate weight in grams and the appropriate number of layers with suitable raw materials to provide the expected features from the surgical masks.*


***Keywords:*** *surgical mask, air permeability, bacterial filtration efficiency, breathability, spun bond, melt-blown*


### Un studiu asupra performanței măștilor chirurgicale multistratificate: permeabilitate, eficiență de filtrare și respirabilitate

*Măștile chirurgicale au fost utilizate pe scară largă încă din trecut în scopul protecției împotriva infecțiilor, ca produs de igienă. Măștile, care sunt adesea folosite de profesioniștii din domeniul sănătății, sunt, de asemenea, utilizate pe scară largă de către populație, în perioadele de pandemie. Măștile chirurgicale au fost proiectate în diferite moduri în funcție de culoare, bandă pentru nas, buclă pentru ureche, grame per metru pătrat și numărul de straturi. Unele caracteristici de performanță sunt necesare pentru ca aceste măști să respecte anumite standarde. În acest studiu, au fost studiate măştile chirurgicale multistratificate. Au fost investigate grosimea, permeabilitatea la aer, eficiența filtrării bacteriene și proprietățile de presiune diferențială ale acestor măști, constând din straturi de polipropilenă consolidată la filare și filată din topitură. S-a determinat influența creșterii în grame per metru pătrat, a numărului de straturi și a stratului filat din topitură asupra proprietăților menționate. Prin urmare, s-a observat că masca optimă este una dintre măștile cu 4 straturi. De asemenea, s-a ajuns la concluzia că mărirea numărului de straturi nu asigură întotdeauna o creștere a performanței; în schimb, o creștere a gramelor per metru pătrat poate satisface cerinţele. Prin urmare, se poate spune că este necesar să se determine greutatea adecvată în grame și numărul corespunzător de straturi cu materii prime adecvate pentru a oferi caracteristicile așteptate de la măștile chirurgicale.*


***Cuvinte-cheie****: mască chirurgicală, permeabilitate la aer, eficiență de filtrare bacteriană, respirabilitate, consolidare la filare, filat din topitură*

## INTRODUCTION

Hygiene products such as masks, gloves, colognes and disinfectants have an important place in human life. Especially masks have been used frequently by people from the past to the present for protection against infection. Products such as masks, which are widely used by healthcare workers, have also been used general public during the pandemic.

Consumption amounts of preventive health and hygiene products have changed during the pandemic (COVID-19) which affects the whole world [1]. The use of masks to prevent transmission of the pandemic-19 has increased considerably with the start of the pandemic. Masks both prevent infected persons from exposing others and also masks protect uninfected wearers [2]. Wearing a mask prevents respiratory virus transmission [3] and also mask use reduces community transmission [4]. Respiratory particles can be classified as droplets or aerosols based on particle size [5] and different types of face masks can filter particles that have various sizes.

Face masks are categorized generally into four groups: elastomeric respirators, N95 masks, surgical masks and cloth masks [6]. First and above all, surgical masks have a general production method: they have layers made of generally nonwoven polypropylene (PP) [7]. Polypropylene is the most widely used polymer for melt-blown surfaces due to its cheapness and versatility [8]. Surgical mask layers are produced with spun bonding and melt blowing methods. Spun

bond and melt-blown structures come together and SMS structures are formed. SMS nonwoven structures are produced generally with 3 layers as the inner-middle-outer layer [9]. The inner and outer layers are spun bonds and the middle layer is melt-blown as a filter layer. The spun bond layer is preferred for its hydrophobic property while melt-blown is preferred for its filtration property and high fibre density [10]. Different masks have been designed to improve some properties like filtration performance. In addition to 3-ply masks, 4-ply and 5-ply masks that have different weight in grams are produced.
The requirements for surgical masks according to EN 14683:2019 + AC:2019 [11] in terms of bacterial filtration efficiency, differential pressure, splash resistance and microbial cleanliness are shown in table 1.

Table 1

CLASSIFICATION OF SURGICAL MASKS ACCORDING TO RELEVANT STANDARD [10]

| Test | Type I | Type II | Type IIR |
|---|---|---|---|
| Bacterial filtration efficiency | ≥95 | ≥98 | ≥98 |
| Differential pressure (Pa/cm$^2$) | <40 | <40 | <60 |
| Splash resistance (kPa) | - | - | ≥16.0 |
| Microbial cleanliness (cfu/g) | ≤30 | ≤30 | ≤30 |

Type I masks are intended for patients and the general public [12–14]. Type II and Type IIR masks are improved for healthcare workers [13]. Type IIR masks must have splash resistance in comparison to Type II. Many studies have examined the masks. Seid searched air permeability, particle filtration efficiency and bacterial filtration efficiency of spun bond and melt-blown layers [15]. Lordelo et al. studied about microbiological effectiveness of decontamination methods and they examined the effects of these methods on filtration, air permeability and phsycochemical properties [16]. Li et al. compared N95 respirators and surgical masks in terms of filtration efficiency, air permeability and water vapour permeability [17]. Teo et al. and Bagheri et al. analysed filtration efficiency, breathability, and reusability of face masks [18] and mask materials [19]. There are also other studies examining bacterial filtration efficiency [20–23] and breathability [24–25] in the literature. Celep et al. searched some physical and tensile properties of surgical masks and they examined the effects of weight per unit area and melt-blown layer on the properties of masks [26]. Boz and Küçük investigated the effects of the changes in weight in grams and production methods of the selected textile surfaces consisting of spun bond and melt-blown layers on air permeability, water resistance and bursting strength properties of the seam area after the ultrasonic welding process [27].
Lee et al. investigated reusable face masks as an alternative to disposable masks and they examined the factors that affect their comfort [28]. Ullah et al. compared melt-blown filters and nano-fibre filters to evaluate their reusability [29]. There are several studies examining the reusability of various masks [30–34] and these studies also investigated the effect of the washing process on different properties such as bacterial filtration efficiency, and breathability.
Surgical masks have been widely used in the past and they were designed in various ways according to colour, nose strip, earloop, grams per square meter and several layers. Masks with different numbers of layers designed in different grams per square meter were produced and these masks, which were generally designed as 3 layers, were produced in 4 layers or even 5 layers. Increasing in number of layers of a mask has been commercially presented to users with expressions such as high protection, double protection and double mask protection. A perception has emerged that the protection increases with the increase in the number of layers of the mask.
This study aims to comparatively evaluate 2, 3, 4 and 5-ply masks of different grams per square meter (GSM), consisting of spun bond and melt-blown layers, in terms of thickness, air permeability, bacterial filtration efficiency and differential pressure properties. It was desired to examine especially whether a 5-ply mask always has an extra performance and whether increasing in number of layers provides the expected features. This study focuses on the performance of the 4-ply and 5-ply masks as an original aspect of this study.

## MATERIAL AND METHOD

### Material

Polypropylene nonwoven spun bonds and melt-blown layers are used to design the surgical masks in this study. The properties of the layers can be seen in table 2.

Table 2

LAYERS USED IN THE STUDY

| Layer code | Layer | Raw material | Grams per square meter (g/m$^2$) |
|---|---|---|---|
| S1 | S20 (Spun bond 20) | Polypropylene | 20 |
| S2 | S40 (Spun bond 40) | Polypropylene | 40 |
| M1 | M20 (Melt-blown 20) | Polypropylene | 20 |
| M2 | M40 (Melt-blown 40) | Polypropylene | 40 |

Properties of the surgical masks obtained by combining these layers with different layouts also can be seen in table 3 and these masks with different numbers of layers are given visually in figure 1.

Table 3

| IDENTIFICATION OF MASKS USED IN THE STUDY | | | | |
|---|---|---|---|---|
| **Mask code** | **Number of layers** | **Layers** | **Grams per square meter (g/m$^2$)** | **Total grams per square meter (g/m$^2$)** |
| SS-1 | 2 | S20-S20 | 20+20 | 40 |
| SS-2 | 2 | S40-S40 | 40+40 | 80 |
| SSS-1 | 3 | S20-S20-S20 | 20+20+20 | 60 |
| SSS-2 | 3 | S20-S40-S20 | 20+40+20 | 80 |
| SSS-3 | 3 | S40-S20-S40 | 40+20+40 | 100 |
| SMS-1 | 3 | S20-M20-S20 | 20+20+20 | 60 |
| SMS-2 | 3 | S20-M40-S20 | 20+40+20 | 80 |
| SMS-3 | 3 | S40-M20-S40 | 40+20+40 | 100 |
| SMS-4 | 3 | S40-M40-S40 | 40+40+40 | 120 |
| SMMS-1 | 4 | S20-M20-M20-S20 | 20+20+20+20 | 80 |
| SMMS-2 | 4 | S40-M20-M20-S40 | 40+20+20+40 | 120 |
| SMSMS-1 | 5 | S20-M20-S40-M20-S20 | 20+20+40+20+20 | 120 |

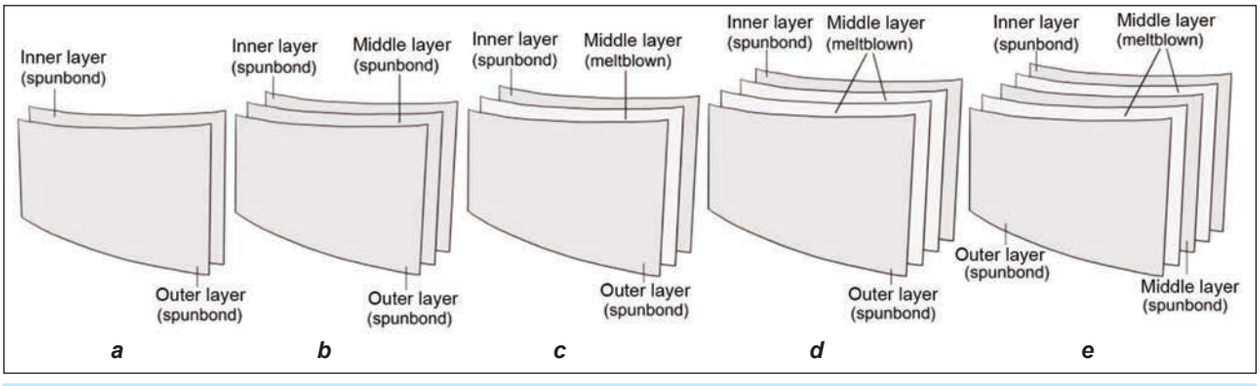


Fig. 1. Masks with different number of layers: *a* – SS; *b* – SSS; *c* – SMS; *d* – SMMS; *e* – SMSMS

## Method

*Thickness test*

The samples were conditioned for 24 hours at a temperature of 20±2°C and relative humidity of 65±4% before the test procedure. Thickness values were measured according to TS 7128 EN ISO 5084:1998 test standard [35] with Schroder/ DM 100 test equipment at a loading pressure of 0.5 kPa. The test process was repeated 20 times.

*Air permeability test*

Before the test procedure, the samples were conditioned as in the thickness test. Air permeability values were measured according to TS 391 EN ISO 9237: 1999 test standard [36] with Textest FX 3300 test equipment with a 20 cm$^2$ test area at a loading pressure of 100 Pa. The test process was repeated 10 times.

*Bacterial filtration efficiency test*

Before the test procedure, the samples were conditioned for a minimum of 4 hours at a temperature of 21±5 °C and relative humidity of 85±5%. The test was performed with a 49 cm$^2$ test area at a flow rate of 28.3 l/min. The mean particle size was 2.7 µm. The values were measured according to EN 14683: 2019 + AC: 2019 [11]. The test process was repeated 5 times.

*Differential pressure test*

Before the test procedure, the samples were conditioned as in the bacterial filtration efficiency test and the values were measured according to the same standard of this test [11]. The test was performed at a flow rate of 8 l/min. The test process was repeated 5 times.

*Statistical analysis*

After the test procedures, the findings were statistically evaluated at a 95% confidence level by using a one-way analysis of variance (One-way ANOVA) via the SPSS 23 package program ($\alpha = 0.05$).

## RESULTS AND DISCUSSION

Firstly, air permeability and thickness values of 4 layers and 12 masks were acquired. Secondly, bacterial filtration efficiency tests were applied to 7 masks that can be compared in terms of the number of layers and GSM. Finally, differential pressure tests were implemented on 5 masks that have bacterial filtration efficiency values exceeding 95% of the relevant standard.

### Air permeability and thickness results

Air permeability and thickness values of layers and masks can be seen in tables 4 and 5, respectively. As can be seen, by the values, the thickness increases in direct proportion to GSM and several layers. On the contrary, air permeability values are generally inversely proportional to GSM and number of layers. Hence, air permeability and thickness values are also inversely proportional to each other as seen in figures 2 and 3, graphically.

Melt-blown is a layer that affects the air permeability of the mask. That's to say; the mask SMS-2 (with a lower total GSM and more melt-blown weight) in comparison to the mask SMS-3 (with a higher total GSM and less melt-blown weight) has lower air permeability values. This result emphasizes the decreasing effect of the melt-blown layer on air permeability. It is an expected result due to the high fibre density of the melt-blown layer. When statistical analysis for thickness and air permeability values are examined separately, it was observed that there is a statistically significant difference for each of these values. Moreover, GSM and several layers have statistically significant effects on these properties (table 8).

Table 4

| THICKNESS AND AIR PERMEABILITY RESULTS OF THE LAYERS | | | | |
|---|---|---|---|---|
| **Layer code** | **Layer** | **Grams per square meter (g/m$^2$)** | **Thickness ±SD** | **Air permeability ±SD** |
| S1 | S20 (Spun bond 20) | 20 | 0.227±0.014 | 3307.00±377.13 |
| S2 | S40 (Spun bond 40) | 40 | 0.393±0.022 | 1706.00±198.34 |
| M1 | M20 (Melt-blown 20) | 20 | 0.213±0.009 | 453.00±19.11 |
| M2 | M40 (Melt-blown 40) | 40 | 0.416±0.012 | 240.20±6.53 |

Table 5

| THICKNESS AND AIR PERMEABILITY RESULTS OF THE MASKS | | | | | |
|---|---|---|---|---|---|
| **Mask code** | **Number of layers** | **Layers** | **Total grams per square meter (g/m$^2$)** | **Thickness ±SD** | **Air permeability ±SD** |
| SS-1 | 2 | S20-S20 | 40 | 0.407±0.017 | 1819.00±116.38 |
| SS-2 | 2 | S40-S40 | 80 | 0.732±0.025 | 1011.30±100.56 |
| SSS-1 | 3 | S20-S20-S20 | 60 | 0.597±0.024 | 1215.00±59.49 |
| SSS-2 | 3 | S20-S40-S20 | 80 | 0.749±0.014 | 992.10±35.46 |
| SSS-3 | 3 | S40-S20-S40 | 100 | 0.974±0.031 | 776.50±27.39 |
| SMS-1 | 3 | S20-M20-S20 | 60 | 0.616±0.020 | 341.00±25.65 |
| SMS-2 | 3 | S20-M40-S20 | 80 | 0.803±0.022 | 211.80±6.39 |
| SMS-3 | 3 | S40-M20-S40 | 100 | 0.942±0.024 | 318.80±11.20 |
| SMS-4 | 3 | S40-M40-S40 | 120 | 1.166±0.026 | 190.40±5.42 |
| SMMS-1 | 4 | S20-M20-M20-S20 | 80 | 0.839±0.012 | 178.50±6.10 |
| SMMS-2 | 4 | S40-M20-M20-S40 | 120 | 1.159±0.017 | 178.50±10.38 |
| SMSMS-1 | 5 | S20-M20-S40-M20-S20 | 120 | 1.214±0.030 | 162.80±3.55 |

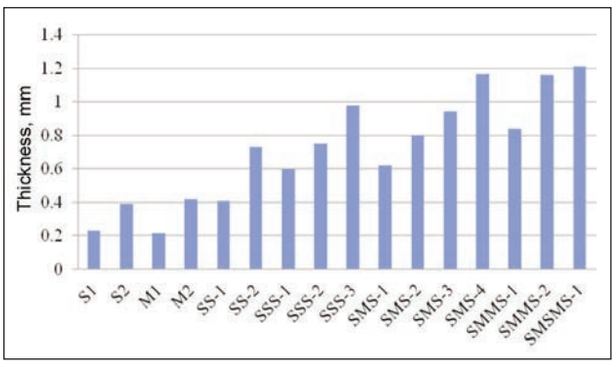


Fig. 2. Thickness results of the layers and masks

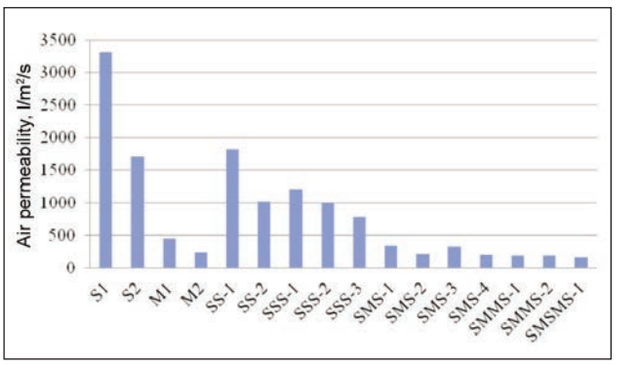


Fig. 3. Air permeability results of the layers and masks

### Bacterial filtration efficiency results

The results can be evaluated in terms of containing of melt-blown layer, number of layers and grams per square meter and the bacterial filtration efficiency (BFE) values are given in table 6.

When the masks SSS-1 and SMS-1 with 60 g/m$^2$ are examined, it can be seen that SMS-1 in comparison to SSS-1 has higher bacterial filtration efficiency. The positive effect of a melt-blown layer on filtration properties has already been pointed out.

As far as three masks with 80 g/m$^2$ are evaluated, it can be concluded that 2-ply mask SS-2 without melt-blown layer has lower BFE values. In addition to that, the masks containing equivalent weight melt-blown, 4-ply SMMS-1 have higher BFE values than the mask 3-ply SMS-2. It can be understood that the number of layers has an increasing effect on filtration. On the other hand, these two masks meet the requirements for Type I in terms of BFE according to 14683:2019 + AC:2019.

As can be seen in table 6, 4-ply, 120 g/m$^2$ SMMS-2 has greater BFE values in comparison to 5-ply, 120 g/m$^2$ SMSMS-1. If their structural differences are evaluated, both masks have 2 “M20” layers and they have equivalent weight spun bonds but the number of spun bond layers they contain is different. On the other hand, inner and outer spun bond layers have lower GSM of 5-ply SMSMS-1. It can be seen that this 5-ply mask designed for high performance has lower BFE values than that of the 4-ply mask. This means that increasing the number of layers doesn’t always work for higher filtration performance. In addition, the 4-ply mask SMMS-2 is the only mask that meets the requirements of Type I, Type II and Type IIR among all masks used in the study.

The only difference between SMMS-1 and SMSMS-1 is that the S40 layer is placed between melt-blown layers. It may have been thought that the 5-ply mask SMSMS-1 would perform higher but it can be seen that the 4-ply mask SMMS-1 has higher BFE values with a slight difference. The “S40” layer, which entered between the melt-blown layers has slightly reduced the filtration efficiency. In essence, both of these masks meet the requirements of Type I according to relevant standards in terms of BFE. In other words, a 4-ply SMMS-1 mask provides the same feature at a lower cost with a lower GSM.

The masks that have different GSM but the same number of layers were investigated to evaluate them in terms of grams per square meter. 3-ply SMS-1 with 60 g/m$^2$ and 3-ply SMS-2 80 g/m$^2$ were compared in terms of BFE values. According to the results, increasing the GSM of the mask provides improved filtration performance as expected. A similar result was also observed in comparison to 4-ply SMMS-1 with 80 g/m$^2$ and 4-ply SMMS-2 with 120 g/m$^2$. From a commercial point of view; three of the masks mentioned SMS-1, SMS-2 and SMMS-1 meet the requirements for the same type: Type I. That’s to say; if Type I is enough for performance requirements, it would be logical for SMS-1 with lower GSM and, a lower number of layers in terms of cost. No doubt increasing GSM unnecessarily will create an increase in cost. Besides, statistical analysis results show that the difference between the bacterial filtration efficiency values is statistically significant. Additionally, GSM and several layers have statistically significant effects on these values (table 8).

### Differential pressure results

Differential pressure value is an indication of breathability [15, 37, 38] and lower DP values mean that the mask is more breathable [15, 37]. On the other hand, air permeability is a fabric property that can be used to evaluate breathability [15]. In addition, lower air permeability signifies higher filtration efficiency due to capturing particles more effectively [39].

The masks with a minimum 95% bacterial filtration efficiency value were subjected to a differential pressure test and the results can be seen in table 7. When the values seen in table 7 are considered in terms of the number of layers; 3-ply SMS-2 with 80 g/m$^2$ and 4-ply SMMS-1 with 80 g/m$^2$ are compared. Differential pressure values of the 4-ply mask were higher than those of the 3-ply mask, meeting requirements Type I, Type II and Type IIR. It can be seen that 4-ply SMMS-2 with 120 g/m$^2$ has higher DP values than that of 5-ply SMSMS-1 with the same GSM.

As far as the differential pressure values are evaluated in terms of grams per square meter; 3-ply SMS-1

Table 6

BACTERIAL FILTRATION EFFICIENCY RESULTS OF THE MASKS (%)

| Mask code | Layers | Total grams per square meter (g/m$^2$) | Bacterial filtration efficiency (BFE) ±SD |
|---|---|---|---|
| SS-2 | S40-S40 | 80 | 83.50±0.27 |
| SSS-1 | S20-S20-S20 | 60 | 79.78±0.13 |
| SMS-1 | S20-M20-S20 | 60 | 95.92±0.08 |
| SMS-2 | S20-M40-S20 | 80 | 97.22±0.18 |
| SMMS-1 | S20-M20-M20-S20 | 80 | 97.64±0.15 |
| SMMS-2 | S40-M20-M20-S40 | 120 | 98.34±0.21 |
| SMSMS-1 | S20-M20-S40-M20-S20 | 120 | 97.44±0.18 |

with 60 g/m$^2$ has higher DP values than that of 3-ply SMS-2 with 80 g/m$^2$ as expected. As seen by the values, the increasing effect of grams per square meter on DP values has been observed for also 4-ply SMMS-1 with 80 g/m$^2$ and 4-ply SMMS-2 with 120 g/m$^2$.

As seen by the values in terms of breathability property, there is an increase in DP values with increasing GSM of the masks. It can be understood that increasing the GSM of the masks has a negative effect on their breathability. In terms of statistical evaluation, a statistically significant difference was observed between differential pressure values and GSM and several layers have statistically significant effects on differential pressure as can be seen in table 8.

Statistical analysis results are given in table 8.

All masks in table 7 meet the requirements of 3 classes according to EN 14683:2019 + AC:2019 in terms of DP. Therefore, it is necessary to investigate BFE and DP values together to determine the mask performance from table 9. Table 9 shows the classification of the masks used in the study according to the relevant standard.

When bacterial filtration efficiency and differential pressure values are evaluated together in terms of meeting the requirements of classes, SMMS-2 is determined as the optimal mask among all masks. In light of this information, it is clear that the 4-ply SMMS-2 mask showed superior properties compared to the 5-ply SMSMS-1 mask. On the other hand, the mask SMMS-2 meets the requirements of

Table 7

DIFFERENTIAL PRESSURE RESULTS OF THE MASKS

| Mask code | Layers | Total grams per square meter (g/m$^2$) | Differential pressure (DP) ±SD |
|---|---|---|---|
| SMS-1 | S20-M20-S20 | 60 | 20.28±1.43 |
| SMS-2 | S20-M40-S20 | 80 | 29.12±1.96 |
| SMMS-1 | S20-M20-M20-S20 | 80 | 35.75±2.72 |
| SMMS-2 | S40-M20-M20-S40 | 120 | 39.58±0.84 |
| SMSMS-1 | S20-M20-S40-M20-S20 | 120 | 37.80±2.68 |

Table 8

THE ANALYSIS OF VARIANCE TABLE FOR THE RESULTS

| Property | Factor | F | p-values |
|---|---|---|---|
| Thickness | Number of layers | 60.864 | 0.000* |
| | Grams per square meter | 2577.958 | 0.000* |
| Air permeability | Number of layers | 171.709 | 0.000* |
| | Grams per square meter | 51.501 | 0.000* |
| Bacterial filtration efficiency | Number of layers | 2118.307 | 0.000* |
| | Grams per square meter | 6.197 | 0.005* |
| Differential pressure | Number of layers | 35.319 | 0.000* |
| | Grams per square meter | 61.260 | 0.000* |

Note: * Statistically significant for $\alpha = 0.05$.

Table 9

CLASSIFICATION OF THE MASKS ACCORDING TO RELEVANT STANDARD

| Mask code | Layers | Total grams per square meter (g/m$^2$) | BFE (%) ±SD | DP (Pa/cm$^2$) ±SD | Type according to EN 14683:2019 + AC:2019 |
|---|---|---|---|---|---|
| SMS-1 | S20-M20-S20 | 60 | 95.92±0.08 | 20.28±1.43 | Type I |
| SMS-2 | S20-M40-S20 | 80 | 97.22±0.18 | 29.12±1.96 | Type I |
| SMMS-1 | S20-M20-M20-S20 | 80 | 97.64±0.15 | 35.75±2.72 | Type I |
| SMMS-2 | S40-M20-M20-S40 | 120 | 98.34±0.21 | 39.58±0.84 | Type I, Type II, Type IIR (DP-at compliance limit for Type I-Type II) |
| SMSMS-1 | S20-M20-S40-M20-S20 | 120 | 97.44±0.18 | 37.80±2.68 | Type I |

all Type I, Type II and Type IIR in terms of bacterial filtration efficiency and differential pressure.

## CONCLUSION

In the study, masks with different grams per square meter and different numbers of layers were designed by using nonwoven spun bond and melt-blown layers and the thickness, air permeability, bacterial filtration efficiency and differential pressure properties of these masks were evaluated comparatively. Based on the findings of these properties, the following general conclusions were reached:

- The increase in GSM and number of layers generally resulted in the thickness, bacterial filtration efficiency and differential pressure values increasing and the air permeability values decreasing. In addition to that, the types of masks change according to EN 14683:2019 + AC:2019 standard, in other words, the user group of masks changes to the general public or healthcare workers. Moreover, it can be said that increasing in grams per square meter gave better results in comparison to increasing the number of layers.
- Surgical masks are usually made of 3 layers as mentioned before. During the pandemic, 4-ply and 5-ply masks were also produced and these masks can also have some advantages in terms of bacterial filtration efficiency depending on weight in grams over 3-ply masks. But presenting 5-ply masks as more protective, double protective than the 3-ply and 4-ply masks should be reviewed. The result may not be like this when the appropriate GSM is not determined. It's necessary here to clarify exactly what is meant by this comparison; in this study, although there is a 5-ply mask, the 4-ply mask SMMS-2 was determined as the optimal mask according to EN 14683:2019 + AC:2019. Only this mask provided the necessary limits for Type I, Type II and Type IIR in terms of bacterial filtration efficiency and differential pressure. It is an obvious fact that the desired performance increase can be observed when the appropriate GSM is determined without any changes in the number of layers.
- Melt-blown layer has resulted great increase in the bacterial filtration efficiency as expected, while having a decreased effect on air permeability and breathability. If changing mask type (Type I, Type II, Type IIR) is important, using a melt-blown layer is important. On the other hand, for the same mask type, masks consisting of only a spun bond layer with a higher GSM compared to the mask containing melt-blown can also provide the expected performance, the same effect can be achieved at a low cost.
- If increasing the number of layers in the mask does not change the mask type depending on the relevant standard, the performance increase does not matter, on the contrary, unnecessary cost occurs. Awareness of this issue is required. Instead of implementation for an extra layer, a slight increase in GSM in existing layers can provide expected mask performance and change mask type.
- Increasing the GSM or the number of layers to increase bacterial filtration efficiency can be considered a solution, but this objective demands greater attention because, on the other hand, the differential pressure may increase too much and exceed the limit value for this feature so it may adversely affect the mask type.
- Given these points, it is apparent that while increasing the number of layers, great attention should be paid to GSM. Equally important, 4-ply masks can have higher performance than 5-ply masks if the appropriate GSM is selected.
- In the study, mask types were expressed according to EN 14683:2019 + AC:2019 standard considering bacterial filtration efficiency and differential pressure. When the splash resistance and microbial cleanliness tests, which are the other requirements in the classification according to relevant standards, are also performed, the type of masks is completely determined.

## ACKNOWLEDGEMENT

The author thanks Mogul Tekstil San. Tic. A. Ş. for supplying spun bond and melt-blown nonwovens

## REFERENCES

[1] Akyüz, H.Ö., Aytekin, İ., *Covid-19 Sürecinde Koruyucu Sağlık ve Hijyen Ürünlerinin Satışı ve Tüketimi Üzerine Bir İnceleme,* In: Medical Research Reports, 2022, 5, 1, 29–41

[2] Brooks, J.T., Butler, J.C., *Effectiveness of mask-wearing to control community spread of SARS-CoV-2,* In: Jama, 2021, 325, 10, 998–999

[3] Li, Y., Liang, M., Gao, L., Ahmed, M.A., Uy, J.P., Cheng, C., Sun, C., *Face masks to prevent transmission of COVID-19: A systematic review and meta-analysis,* In: American journal of infection control, 2021, 49, 7, 900–906

[4] Howard, J., Huang, A., Li, Z., Tufekci, Z., Zdimal, V., Van Der Westhuizen, H.M., Rimoin, A.W., *An evidence review of face masks against COVID-19,* In: Proceedings of the National Academy of Sciences, 2021, 118, 4, e2014564118

[5] Shiu, E.Y., Leung, N.H., Cowling, B.J., *Controversy around airborne versus droplet transmission of respiratory viruses: implication for infection prevention,* In: Current Opinion in Infectious Diseases, 2019, 32, 4, 372–379

[6] Ju, J.T., Boisvert, L.N., Zuo, Y.Y., *Face masks against COVID-19: Standards, efficacy, testing and decontamination methods,* In: Advances in Colloid and Interface Science, 2021, 292, 102435

[7] Zhang, R., Xu, Q., Bai, S., Hai, J., Cheng, L., Xu, G., Qin, Y., *Enhancing the filtration efficiency and wearing time of disposable surgical masks using TENG technology,* In: Nano Energy, 2021, 79, 105434

[8] Duran, K., Duran, D., Oymak, G., Kilic, K., Öncü, E., Kara, M., *Investigation of the physical properties of melt-blown nonwovens for air filtration,* In: Textile and Apparel, 2013, 23, 2, 136–142

[9] Pamuk, O., Öndoğan, Z., *A survey on assesment of surgical gowns based on the opinions of surgical team members,* In: Textile and Apparel, 2008, 18, 2, 142–148

[10] Kırman, C., *Yüz Maskeleri, TMMOB Tekstil Mühendislieri Odası, Covid-19 Krizi Dönemi Genel Bilgilendirme*, 2020, Available at: https://www.tmo.org.tr/images/editorimages/Y%C3%9CZ%20MASKELER%C4%B0%20GENEL%20B%C4%B0LG%C4%B0LEND%C4%B0RME.pdf [Accessed on January 15, 2023]

[11] TS EN 14683+AC, 2019, *Medical face masks – Requirements and test methods*

[12] Avrupa Komisyonu Sağlık ve Gıda Güvenliği Genel Müdürlüğü, , *Tıbbi yüz maskeleri için düzenleyici gerekliliklere dair rehber*, 2020, Available at: https://titck.gov.tr/storage/Archive/2021/contentFile/20.%20T%C4%B1bbi%20y%C3%BCz%20maskeleri%20i%C3%A7in%20d%C3%BCzenleyici%20gerekliliklere%20dair%20rehber_tr_6b942b34-5155-4bfc-afd1-a012b8d86614.pdf [Accessed on January 10, 2023]

[13] Violante, T., Violante, F.S., *Surgical masks vs filtering facepiece respirators for the protection against coronavirus infection: current state of the art,* In: La Medicina del lavoro, 2020, 111, 5, 365

[14] Bahadır Ünal, Z., Gökçen, Ö., *Cerrahi Maskelerin Araştırılması ve Çocuklarda Maske Kullanımı,* In: Turkish Journal of Fashion Design and Management, 2021, 3, 1, 11–24

[15] Seid, Z.M., *Dokusuz Yüzey Kumaşların Fiziksel Özelliklerini ve Tasarımını Analiz Ederek Cerrahi Maske Verimliliğinin Arttırılması,* Master's thesis, Pamukkale Üniversitesi Fen Bilimleri Enstitüsü, 2022

[16] Lordelo, R., Botelho, J.R.S., Morais, P.V., De Sousa, H.C., Branco, R., Dias, A.M., Reis, M.S., *Evaluation of the Microbiological Effectiveness of Three Accessible Mask Decontamination Methods and Their Impact on Filtration, Air Permeability and Physicochemical Properties,* In: International Journal of Environmental Research and Public Health, 2022, 19, 11, 6567

[17] Li, Y., Wong, T., Chung, A.J., Guo, Y.P., Hu, J.Y., Guan, Y.T., Newton, E., *In vivo protective performance of N95 respirator and surgical facemask,* In: American Journal of Industrial Medicine, 2006, 49, 12, 1056–1065

[18] Teo, J.Y., Kng, J., Periaswamy, B., Liu, S., Lim, P.C., Lee, C.E., Yang, Y.Y., *Exploring Reusability of Disposable Face Masks: Effects of Disinfection Methods on Filtration Efficiency, Breathability, and Fluid Resistance,* In: Global Challenges, 2021, 5, 11, 2100030

[19] Bagheri, M.H., Khalaji, I., Azizi, A., Loibl, R.T., Basualdo, N., Manzo, S., Schiffres, S.N., *Filtration efficiency, breathability, and reusability of improvised materials for face masks,* In: Aerosol Science and Technology, 2021, 55, 7, 817–827

[20] Shashina, E.A., Belova, E.V., Gruzdeva, O.A., Skopin, A.Y., Andreev, S.V., Zhernov, Y.V., Mitrokhin, O.V., *Assessment of bacterial filtration and air permeability of face masks used by people during the COVID-19 pandemic,* In: Health, 2022, 1, 86

[21] Wang, D., You, Y., Zhou, X., Zong, Z., Huang, H., Zhang, H., Du, L., *Selection of homemade mask materials for preventing transmission of COVID-19: A laboratory study,* In: PloS one, 2020, 15, 10, e0240285

[22] Pragadheeswari, R., Arunkumar, K., Rajakumar, R., Sangeetha, K., *Nano membrane fibrous on lyocell non-woven fabric for bacterial filtration efficiency in surgical face mask,* In: J. Nanosci. Nanotechnol, 2014, 2, 598–599

[23] Whyte, H.E., Montigaud, Y., Audoux, E., Verhoeven, P., Prier, A., Leclerc, L., Pourchez, J., *Comparison of bacterial filtration efficiency vs. particle filtration efficiency to assess the performance of non-medical face masks,* In: Scientific Reports, 2022, 12, 1, 1188

[24] Pei, C., Ou, Q., Kim, S.C., Chen, S.C., Pui, D.Y., *Alternative face masks made of common materials for general public: fractional filtration efficiency and breathability perspective,* In: Aerosol and Air Quality Research, 2020, 20, 12, 2581–2591

[25] Taborri, J., Stocchi, B., Calabrò, G., Rossi, S., *On the breathability measurement of surgical masks: Uncertainty, repeatability, and reproducibility analysis,* In: IEEE Transactions on Instrumentation and Measurement, 2022, 71, 1–9

[26] Celep, G., Yılmaz, F., Tetik, G.D., *Evaluation of some physical and tensile properties of commercial surgical masks,* In: Indian Journal of Fibre & Textile Research (IJFTR), 2022, 47, 1, 125–130

[27] Boz, S., Küçük, M., *The analysis of the ultrasonic welding performance for the medical protective clothing,* In: Textile and Apparel, 2021, 31, 1, 53–62

[28] Lee, K.P., Yip, J., Kan, C.W., Chiou, J.C., Yung, K.F., *Reusable face masks as alternative for disposable medical masks: factors that affect their wear-comfort,* In: International Journal of Environmental Research and Public Health, 2020, 17, 18, 6623

[29] Ullah, S., Ullah, A., Lee, J., Jeong, Y., Hashmi, M., Zhu, C., Kim, I.S., *Reusability comparison of melt-blown vs nanofiber face mask filters for use in the coronavirus pandemic,* In: ACS Applied nano materials, 2020, 3, 7, 7231–7241

[30] Whyte, H.E., Joubert, A., Leclerc, L., Sarry, G., Verhoeven, P., Le Coq, L., Pourchez, J., *Reusability of face masks: Influence of washing and comparison of performance between medical face masks and community face masks,* In: Environmental Technology & Innovation, 2022, 28, 102710

[31] Sankhyan, S., Heinselman, K. N., Ciesielski, P.N., Barnes, T., Himmel, M.E., Teed, H., Vance, M.E., *Filtration performance of layering masks and face coverings and the reusability of cotton masks after repeated washing and drying,* In: Aerosol and Air Quality Research, 2021, 21, 11, 210117

[32] Hassani, S., Henni, L., Sidali, A., Naitbouda, A., Khereddine, A., Dergham, D., Lekoui, F., *Effect of washing on quality, breathability performance and reusability of disposable face masks,* In: Journal of Medical Engineering & Technology, 2022, 46, 5, 345–353

[33] Üreyen, M.E., Zarif, N., Uraz, E.K., R*eusable fabric masks against COVID-19*, In: Eskişehir Technical University Journal of Science and Technology A-Applied Sciences and Engineering, 2021, 22, 8th ULPAS-Special Issue 2021, 10–18

[34] Whyte, H.E., Joubert, A., Leclerc, L., Sarry, G., Verhoeven, P., Le Coq, L., Pourchez, J., *Impact of washing parameters on bacterial filtration efficiency and breathability of community and medical facemasks,* In: Scientific Reports, 2022, 12, 1, 15853

[35] TS 7128 EN ISO 5084, 1998, *Textiles, Determination of thickness of textiles and textile materials*

[36] TS 391 EN ISO 9237, 1999, *Textiles, Determination of permeability of fabrics to air*

[37] Forouzandeh, P., O'Dowd, K., Pillai, S.C., *Face masks and respirators in the fight against the COVID-19 coc: An overview of the standards and testing methods,* In: Safety Science, 2021, 133, 104995

[38] Kwong, L.H., Wilson, R., Kumar, S., Crider, Y.S., Reyes Sanchez, Y., Rempel, D., Pillarisetti, A., *Review of the breathability and filtration efficiency of common household materials for face masks,* In: ACS nano, 2021, 15, 4, 5904–5924

[39] Yeşil, Y., *Effect of air quenching on characteristics of thermoplastic polyurethane melt-blown nonwoven,* In: Textile and Apparel, 2015, 25, 3, 236–245

**Author:**

ŞEVKAN MACİT AYŞE

Uşak University, Faculty of Engineering and Natural Sciences, Textile Engineering Department,
Ankara İzmir Yolu 8.Km Bir Eylül Kampüsü, 64200, Uşak, Türkiye

**Corresponding author:**

ŞEVKAN MACİT AYŞE
e-mail: ayse.sevkan@usak.edu.tr

# Solutions to reduce the environmental pressure exerted by technical textiles: a review

DOI: 10.35530/IT.075.01.202367

SIMONA TRIPA
LILIANA INDRIE
PABLO DÍAZ GARCÍA
DAIVA MIKUCIONIENE

**ABSTRACT – REZUMAT**

**Solutions to reduce the environmental pressure exerted by technical textiles: a review**

*This paper highlights the fact that the technical textile industry plays a significant role in the textile and apparel industry and the technical textile subsector is one of the most dynamic, accounting for an increasing share of EU textile output. In recent years, there has been a significant increase in the production of technical textiles in the EU, which in turn leads to an increase in the environmental impact generated by the production and consumption of these products. The entire process of producing technical textile items creates several forms of pollution in the air, water, and soil, as well as noise and visual pollution and contributes significantly to global warming. At the same time, considerable volumes of textile waste are created. The reduction of the environmental impact of technical textiles should be considered throughout their life cycle and after their exit from use. In specialized literature, numerous solutions are presented that as viable for clothing but are only partially transferable to technical textiles. This paper provides a review of these solutions, highlighting the successfully applied ones in the case of technical textiles.*

***Keywords:*** *technical textiles, sustainable, environment, waste, recycling*

**O analiză a soluțiilor pentru reducerea presiunii exercitate de textilele tehnice asupra mediului**

*Această lucrare evidențiază rolul semnificativ pe care industria textilelor tehnice îl joacă în industria textilă și de îmbrăcăminte, subsectorul textilelor tehnice fiind unul dintre cele mai dinamice, cu o pondere din ce în ce mai mare în producția de textile din UE. În ultimii ani, s-a înregistrat o creștere semnificativă a producției de textile tehnice în UE, ceea ce duce, la rândul său, la o creștere a impactului asupra mediului, generată de producția și consumul acestor produse. Întregul proces de realizare a textilelor tehnice generează mai multe forme de poluare a aerului, apei și solului, poluare fonică și vizuală și contribuie în mod semnificativ la încălzirea globală. În același timp, se creează volume considerabile de deșeuri textile. Reducerea impactului textilelor tehnice asupra mediului ar trebui luată în considerare pe tot parcursul ciclului lor de viață, cât și după ieșirea lor din uz. În literatura de specialitate sunt prezentate numeroase soluții care sunt viabile pentru îmbrăcăminte, dar care sunt doar parțial transferabile textilelor tehnice. Această lucrare oferă o trecere în revistă a acestor soluții, evidențiindu-le pe cele aplicate cu succes în cazul textilelor tehnice.*

***Cuvinte-cheie:*** *textile tehnice, durabil, mediu, deșeuri, reciclare*

## INTRODUCTION

The textile and apparel industry is a significant component of the European manufacturing sector and it is vital to the social and economic health of many European areas. The industry has 143,000 enterprises, employs 1.3 million people, and has a turnover of €147 billion, according to data from 2021 [1]. The sector in the EU is based on micro and small businesses. More than 90% of workers are employed by companies with fewer than 50 employees, which also generate over 60% of value-added [2]. Technical textiles play a significant role in this industry. Technical textiles have been trending upwards in the world in recent years due to the improvement in economic conditions. Technical textiles are referred to as "*textiles, fibres, materials and support materials meeting technical rather than aesthetic criteria*" [3]. They provide input for other industries such as automotive, construction, healthcare and agro-food. Advances in technology, increased end-use applications, profitability, sustainability, user-friendliness and eco-friendliness of technical textiles have increased demand in the global marketplace. The technical textile industry has one of the greatest growth rates in the world [4]. Compared to traditional textiles, this sector adds more value and serves a wider range of end markets thanks to its high level of innovation and adaptability [5]. These attributes have caused several countries to convert their textile industry from conventional to technical.

**This paper aims** to present various solutions for reducing the environmental impact, that can be successfully applied in the case of technical textiles.

**Methods of scientific research**, that have been used in the paper, are data collection, analysis and interpretation, and summarizing of literature review. In the first part of the paper, are presented the place and role of technical textiles in the EU economy, and the impact of technical textiles on the environment is

presented in the second part. In the final part of this paper, are presented various solutions for reducing the environmental impact of technical textiles at different stages of their life cycle.

## THE PLACE AND ROLE OF TECHNICAL TEXTILES IN THE EU ECONOMY

The technical textile industry is generally considered to be a fast-growing value-added industry, where Europe has a strong market position and significant know-how potential. For example: about 60 percent of the value added of the German textile industry relates to technical textiles [6]. However, it is extremely fragmented and has several European SMEs that are experts in a particular product or market niche (such as ballistic protection) or technological niche (e.g., non-crimp fabric manufacturing).
In the EU27, industrial and technical textiles production represents 17% of the total production in the textile and clothing industry and it accounts for a growing share (29%) of total textile production (figure 1). The technical textiles subsector is one of the most dynamic, accounting for an increasing share of EU textile output [1]. Applications across a variety of industries, including healthcare, automotive, construction, agriculture, sportswear, etc., are driving up demand for technical textiles.

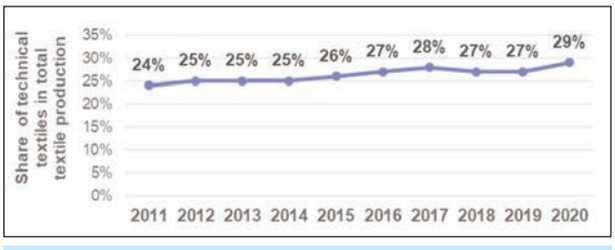


Fig. 1. Share of technical textiles in total textile production, in the EU 27 [1]

The technical textiles industry is still growing in the EU-27, where Germany is the market leader in Europe. In 2018, the largest production volumes of technical textiles were made in Germany (32,000 tons), Italy (18,000 tons) and the UK (15 000 tons). Together they made 47% of the total production of technical textiles from European countries.
The Netherlands, Spain, Belgium, France, Czech Republic, Sweden, Poland, Hungary and Romania are in the following positions, with a total production share of 43% [7].
Production of technical textiles in the European Union has fluctuated by about 140K tons over the last ten years. This sector was also affected by the COVID-19 pandemic, resulting in a significant decline in production in 2020. According to the Eurostat database, this decrease was EUR 977.1 million, in a single year [8] (figure 2).
Technical textiles also play an important role in the EU exports. In 2021, EU exports of technical textiles accounted for 14% of the total EU exports of products in the textiles and clothing industry and ranked third

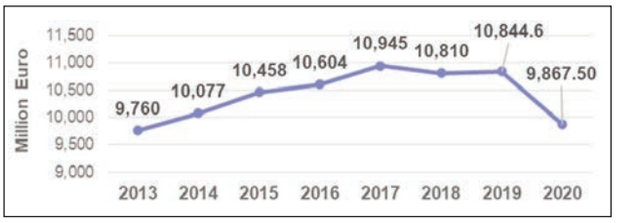


Fig. 2. Evolution of the production value of the technical and industrial textiles, in the EU27 [8]

in the top EU exports of textile and clothing products [1].
It is anticipated that the global market for technical textiles will continue to expand. The development of the technical textiles industry is presented with new prospects by the expansion of the automotive, healthcare, construction, packaging, and other industries. Another rapidly growing segment of the technical textile industry is medical textiles [7].

## THE IMPACT OF TECHNICAL TEXTILES ON THE ENVIRONMENT

As it is known, textiles are essential to human existence, both for the production of apparel items and owing to the growth of various fields of use, including the automobile, construction, computer, and agricultural industries [9]. The issues associated with the scarcity of raw materials and environmental harm are exacerbated by the rise in textile demand. The entire process of producing textile items creates several forms of pollution in the air, water, and soil, as well as noise and visual pollution and contributes significantly to global warming [10, 11].
Most of the processes carried out in textile factories generate air emissions. Air pollution produced during the production processes has significant health concerns that lead to occupational illnesses, such as tuberculosis, byssinosis and asthma [12, 13]. After effluent quality, air emissions have been identified as the textile industry's second-biggest environmental issue. Air emissions include dust, oil mists, formaldehyde, acids, hydrocarbons, softeners and other volatile compounds, odours, boiler exhausts etc [14]. In the case of technical textiles, air pollution occurs both during their production processes during their use, and after their useful life [15].
Water pollution manifests itself in different forms throughout the life cycle of textiles. In various stages of textile production, such as dyeing and printing, the industry employs more than 8000 chemicals [16]. Pesticides removed from cotton, flax and hemp, as well as other compounds (lactic acid, alcohols, peptides and wax) during their processing also contribute to a high level of contamination. For example: the cultivation of cotton uses about 11% of the world's pesticides [17]. Different kinds of acids, alkalis, oils, detergents, dyes, $SO_2$, $H_2O_2$, and others, are used in the degreasing, carbonizing, carding, washing, bleaching, and dyeing of wool, all of which have a severe impact on the water quality [18]. The textile industry also employs a wide range of dyes, chemicals,

and other materials for various forms of finishes applied to textile products to get various features, and attributes, or to give the fabrics the necessary qualities. The negative effects suffered by water are shown in the pH and colour changes, the presence of dissolved particles or in suspension, pesticides, peptides, lactic acid, phenolites, chlorides, oils and fats, detergents, dyes, etc. [19, 20]. Because of all of this, wastewater is produced. The removal of contaminants from the raw materials themselves and the leftover chemical reagents employed for processing both contribute to the increase in pollution load [21]. The wastewater from wet processing contains toxic substances, such as mutagens, carcinogens, and teratogens, if they are not appropriately treated before discharge, which can seriously harm the environment by contaminating wastewater and exhaust fumes [22]. Loss of lubricants or spinning oil from equipment can result in the unintentional release of hazardous materials. Such contaminants have harmful impacts on aquatic organisms or the development of new species, including algae that reduce water's oxygen content and harm aquatic life. Additionally, aquatic species can occasionally survive after ingesting such dangerous toxins, which they then pass on to humans by way of the food chain [23].

Soil pollution occurs through the use of pesticides, the seeping of polluted water into the soil, and the huge amount of textile waste that reaches landfills. Fibres or chemicals degrade under the influence of air, water, or sunshine, and they can turn in the process into hazardous agents [24, 25]. Several harmful degradation products made from nylon, polyester, or other polymeric materials that have been dumped in water streams and end up in landfills serve as examples of the issue [26].

Twisting, spinning, and weaving operations, for example, can cause noise pollution. Systems of transportation or other equipment used in the textile industry for loading, transporting, or handling may also produce unpleasant, loud noise [27]. Exposure to noise pollution, especially overexposure, is the most significant risk associated with the textile business. Depending on the length of exposure, the intensity and frequency of the noise, as well as individual sensitivity, hearing thresholds can be temporarily or, in the worst circumstances, permanently reduced [28]. Extended exposure to noise pollution has many other negative effects, such as agitation, persistent fatigue, disorientation, migraines, vertigo, hypertension, cardio-arrhythmia, and neurological and psychological diseases [29].

Between 1.22 and 2.93 billion tons of $CO_2$ are released annually by the textile sector. According to some estimations, the life cycle of textiles (including laundering) is responsible for 6.7% of all global greenhouse gas emissions [30].

At the same time, considerable volumes of textile waste are created [31]. Statistics show that in a single year, in 2020, 1,950,000 tons of textile waste were generated at the EU level [32].

Although manufacturing and using technical textiles have multiple negative effects on the environment, they are often used to reduce the impact on the environment generated by other industries. Technical textiles are widely used to reduce air pollution, being used as filters in various fields. Due to the possibility of creating high-tightness fabrics, these can reduce or even stop the passing through of polluting substances, flue gases, also, dust particles, without preventing the air from passing through [33]. As filters, technical textiles are successfully used to filter used water. They can also be used to separate the oil/water emulsions [34]. Furthermore, they are successfully used to prevent water and soil pollution when they are used as lining materials for landfill sites or when used in agriculture to prevent the dispersion of pesticides or other types of chemical substances used for various crops [5].

There have been identified five types of filtrations which can be achieved using technical textiles, namely: solid-gas filtration, solid-fluid filtration, solid-solid filtration, fluid-fluid filtration and gas-gas filtration. To achieve all these types of filters, technical textiles must observe certain standards and fulfil several requirements in connection with the fibres they are made of, the type and structure of materials, modality of assembly-all these being essential to the performances of filtering materials [35].

Technical textiles are also used to reduce noise pollution, by applying sound absorbent materials [36].

## SOLUTIONS TO REDUCE THE ENVIRONMENTAL PRESSURE EXERTED BY TECHNICAL TEXTILES

The reduction of the environmental impact of technical textiles should be considered throughout their life cycle and after their exit from use. Specialized literature presents several solutions in this regard, solutions that are presented in the following.

### Choice of materials

When creating technical textile goods, the first decision to be taken relates to the components of yarns and fabrics. As different fibres are made from various resources, they all have varied effects on the environment and the climate. Significant environmental effects are also caused by the dyeing agents utilized [37–39]. Treatments that are applied to technical fabrics in this situation also show the environmental effect. They entail adding chemicals to a yarn or fabric to give it a range of qualities, such as water-repellentness, flame-retardantness, antistatic or antibacterial properties, and antifungal capabilities.

Different fibre types will require various approaches to advancing circularity and sustainability. The largest strain on the land and water resources is seen while producing natural fibres like cotton, as cotton production makes extensive use of fertilizers and pesticides, runoff might contaminate surface and groundwater [40, 41]. Sustainable cotton production would entail using water and agrochemicals more effectively, switching to less harmful pesticides, and adopting

soil-conserving agricultural practices including composting, crop rotation, and decreased tillage [42]. One of the disadvantages of organic farming is that it can decrease yields, resulting in increased land use [43].
Synthetic fibres, like polyester, have an adverse effect on the environment due to their high energy consumption and reliance on fossil fuels for raw materials. Acrylic and nylon fibres are two other synthetic fibres with significant energy requirements [44].
The utilization of recycled fibres is suggested as a way to minimize energy and resource usage. The drawback of this solution is that the recycling procedures shorten the lifespan of the fibres, reducing the possibility of reuse [45].
Currently, a sizable quantity of yarns is created from a variety of fibres, which makes their recycling challenging. The suggested solution in this situation is to exclusively produce yarns using fibre combinations that can be recycled.
Chemicals used during textile production pose risks to the environment because they frequently leak out during usage and washing [46]. The proposed solutions refer to the reduction of chemicals used in the textile industry and the substitution of dangerous products with less dangerous products for the environment.
There is increasing talk of the use of natural dyes, and the use of pigments, and enzymes to reduce the use of chemicals, water, and energy consumption. To protect freshwater and seawater resources, Greenpeace launched the Detox campaign in 2011, focusing on having more environmentally friendly and toxic-free textiles. The list of substances to be removed increased to approximately 430 compounds [47].
Another solution is to reuse products because reused clothes have been washed many times, and have fewer chemicals in the fabric, which makes their use not only much more environmentally friendly, but also better for the consumer's wallet and their health [48]. Unfortunately, this solution has a very limited area of application in the case of technical textiles.

**Design stage**

The design stage is very important in the development of a circular value chain for technical textiles.
The decisions taken at this stage will have a considerable impact on the environmental and climatic effects of textile goods, as well as on their potential for circularity in later stages of the product's lifecycle. This stage is known by a variety of names in literature, including eco-design, design for the environment/design for sustainability, and sustainable product design.
Ecodesign is a design approach that takes into account a product's environmental impact from raw materials through manufacture and use to the end of its useful life. Ecodesign tries to enhance the product's visual appeal and functionality while simultaneously reducing the product's negative environmental impact [49].
Design for the environment or design for sustainability describes a change in product design, where the environmental impact (rather than only the economic impact) directs the direction of design decisions. Design for sustainability expands on ecodesign's work by taking economic and social problems into account, and its methodology incorporates both incremental and radical innovation [50, 51].
Sustainable product development and design look to minimise adverse sustainability impacts and maximise sustainable value throughout the life-cycle of the product [52]. Sustainable product design is a design theory and approach that emphasizes creating goods that contribute to social and economic well-being, have minimal negative effects on the environment, and can be made from renewable resources over the long term [53].
Design decisions have an impact on the different stages of the material and product life cycle. Because they make it easier to provide novel business models, allow reusing and recycling, and give chances to incorporate recycled materials or repurposed parts into new products, they are important key drivers in the development of more circular goods [54].
The lifetime, durability, and reparability of textiles are improved by the careful selection of materials at the design stage. The product's capacity to last longer and its ease of repair are both influenced by the materials utilized. Several fundamental design concepts, such as technical specifications for colourfastness and fabric resilience, as well as practical requirements for textiles to be suitable for their intended use, and readily available repair kits and/or replacement components, boost the longevity and quality of textile goods [55].
A large variety of eco-design tools are available. This allows designers to integrate environmental considerations into product development processes. They provide information on potential environmental issues and help to choose between various aspects [56].
The most usable tools with quantitative measures are life cycle assessment (LCA), streamlined LCA, matrices, ecolabels, and footprints. There are other types of tools for improving the environment, such as qualitative guidelines and manuals. They can be more straightforward to use early in the process of developing a product [57]. Also, introducing sustainable and environmentally friendly materials is very important to change the behaviour of consumers. Interdisciplinarity (between designers, chemists, material designers, etc.) is necessary for eco-design in both vocational training and programs for industry professionals who are involved in lifelong learning [58].

**Sustainable production**

One of the important pathways is optimized resource use to lower pressures. Companies in the textile industry are concentrating on lowering and optimizing water and energy usage, air emissions, and water

pollution, by employing secure chemicals and a variety of biodegradable materials [55].
Industry modernization and automation are required to provide cleaner manufacturing processes, which need less labour and resources. Resource-efficient production is a key element in a sustainable textile system. Moving towards healthy and renewable materials and energy would reduce the environmental impact of the textile industry. Moreover, to address the negative social impacts of the textile industry, it is necessary to improve workers' wages and working conditions [58].
Eco-design guidelines have been established to maximize resource utilization throughout production. Reduced emissions, waste, and inputs like water, chemicals, and energy are a few of them. Another one is the production of fibres from renewable sources or recycled content. Design requirements that certify a minimum content of recycled materials could optimize the use of resources. The collection of materials for recycling and reuse may also be indirectly increased by design requirements [59].

**Sustainable textiles consumption**

Reducing the amount of textiles purchased is one option which is open to all customers. As a result, the textile system's effects on the environment and the climate may be reduced. If fewer things are purchased, production and distribution will also decline, mitigating the negative effects on the environment, the climate, and the generation of waste. This may be accomplished through shared use, longer use, and reuse of textiles [60, 61]. In the case of technical textiles, the first 2 solutions can be applied.
Reusing them is not feasible for several reasons [62]:
- Technical textiles typically enter their end-of-life position because they were damaged rather than because they are old-fashioned.
- Protective garments (such as uniforms) must be destroyed since they serve as identifying characteristics (such as in the military) and are inadequate for reuse.
- Technological textiles and nonwovens are often used in complex items like vehicles. For economic considerations, it is not justifiable to disassemble end-of-life items. Vehicles are frequently shredded, after which is impossible to recycle the fibre parts.
- Medicinal fabrics, which are frequently polluted, must be burned.
- In the case of technical textiles used in composite materials, due to the strong adhesion between the fibre and matrix, separation is challenging and not economically feasible. Only for expensive fibres, like carbon fibres, the separation would be economically feasible.

**Textile waste management**

The term "waste prevention" refers to actions conducted before a (textile) product becomes garbage [63]. There must be a differentiation between quantitative and qualitative prevention. The extension of textile items' useful lives is a component of quantitative prevention. Once these wastes are produced, they must be collected. Greater reuse and recycling of textile waste, as well as avoiding its incineration or landfilling, depend on better textile waste collection, sorting, and management [64].
Recycling is any method of recovering waste materials and using them to create new products, materials, or substances that can be used for the original or different purposes. Energy recovery and backfilling activities are not included. Many studies show that recycling has greater benefits for the environment than landfills and incineration [65, 66]. For instance, Dutch aWEARness calculated that recycled textiles can save 64%, 95%, and 73% more energy, water, and carbon dioxide than conventional, non-recycled textiles. Another study shows that recycling textiles has a far better potential for reducing GHG emissions and energy savings than incineration [67].
The literature in the field presents a multitude of fields and modalities to recycle textile waste. One of them is the construction field, where textile waste can be used for the thermal and soundproofing of buildings [68] or they can be integrated into brick manufacturing [69]. Cotton waste has proved to be a very good catalyst in treating wastewater and removing Bisfenol from the water [70]. Textile waste can be successfully used in the automobile industry for manufacturing the materials used for lining seats, roofs or carpets as well as in the furniture industry, manufacturing mattress covers, upholstery and also as stuffing material for various furniture items. In agriculture, textile waste can be used as a ground covering layer to prevent it from drying, increasing thus the crop output [71]. Textile waste can also be used in manufacturing paper or various types of toys [70].
The variety of conventional textile and technical textile types makes it very difficult to collect them separately. Statistics and data on the quantities of technical textiles that are collected separately are rarely available. This is compounded by the multitude of fields in which technical textiles are used, which require various collection systems and, subsequently, distinct recycling programs. Contrary to apparel, technical textiles are in use for a considerable amount of time and are not immediately recyclable [72].
Recycling technical textiles is more complicated, but not impossible, as shown by research in recent years.
The potential of recycling flame-resistant protective clothing is described in the European patent EP3260595. Enzymatic hydrolysis is used to break down technical textiles, and the residual fibres (typically, aromatic polyamides go through a fibre-tearing process to obtain individual fibres suitable for subsequent yarn creation) [73].
In the TEX2MAT project, a novel method was established that incorporates the enzymatic hydrolysis of cellulose, where cotton can be converted into glucose and polyester remains as the only polymer and is, therefore, accessible to a relatively easy recycling process [74].

The Dutch carpet manufacturer Desso was one of the first companies to re-use closed-loop products in the carpet industry. Non-harmful raw materials are re-used to produce carpet tiles. The modular carpet tiles permit smart maintenance since it is possible to change only the tiles which are visibly worn or torn. In this way, Desso prolongs the life span of tiles placed in "low-traffic" areas, before ultimately taking them in for remanufacturing [75].

## CONCLUSIONS

In the textile industry, technical textiles are a growingly significant market category. Because the production volume of technical textiles has seen an upward trend at the EU level in recent years, special attention must be paid to aspects related to their impact on the environment. In this sense, solutions must be implemented regarding the circular economy, preventing and reducing waste, but also finding viable ways to recycle it. The reduction of the environmental impact of technical textiles should be considered throughout their life cycle and after their exit from use. Viable solutions for clothing are only partially transferable to technical textiles. Specialized literature presents several solutions in this regard, starting with the choice of materials and finishing with waste management. Among these, the most effective are those related to the exclusive production of yarns using combinations of fibres that can be recycled and the reduction of chemicals used in the textile industry or the replacement of hazardous products with less hazardous products for the environment. Developing a circular value chain for technical textiles from the design phase, maximizing the use of resources during production, and reducing emissions, waste and water, chemical and energy consumption are other solutions whose effectiveness has already been proven. Recently, new solutions, such as the use of highly specific enzymes for the decomposition of polymers and fibre-mixed materials, are currently being tested for possible industrial application on a large scale.

## ACKNOWLEDGEMENTS

The CircuTex project is funded by the Erasmus+ programme of the European Union under project reference number 2021-1-ES01-KA220-HED-000032075.
The European Commission's support for the production of this publication does not constitute an endorsement of the contents which reflects the views only of the authors, and the Commission cannot be held responsible for any use which may be made of the information contained therein.

## REFERENCES

[1] Euratex, *Facts & Key Figures 2022, of the European Textile and Clothing Industry*, Brussels, 2022, Available at: https://euratex.eu/wp-content/uploads/EURATEX_FactsKey_Figures_2022rev-1.pdf [Accessed on March 15, 2023]

[2] European Commission, *Textiles and clothing in the EU*, Available at: https://ec.europa.eu/growth/sectors/fashion/textiles-and-clothing-industries/textiles-and-clothing-eu_en [Accessed on April 23, 2023]

[3] European Union, *Opinion of the European Economic and Social Committee on 'Growth Driver Technical Textiles'*, Official Journal of the European Union: C 198/14, Brussels, 2013, Available at: https://eur-lex.europa.eu/LexUriServ/LexUriServ.do?uri=OJ:C:2013:198:0014:0025:en:PDF [Accessed on April 29, 2023]

[4] McCarthy, B.J., *An overview of the technical textiles sector*, In: Handbook of technical textiles, Woodhead Publishing, 2016, 1–20

[5] Aldalbahi, A., El-Naggar, M.E., El-Newehy, M.H., Rahaman, M., Hatshan, M.R., Khattab. T.A., *Effects of technical textiles and synthetic nanofibers on environmental pollution*, In: Polymers, 2021, 13, 1, 155

[6] Fromhold-Eisebith, M., Marschall, P., Peters, R., Thomes, P., *Torn between digitized future and context dependent past–How implementing 'Industry 4.0'production technologies could transform the German textile industry*, In: Technological Forecasting and Social Change, 2021, 166, 120620

[7] Izsak, K., Shauchuk, P., *Technological trends in the textiles industry*, 2020, Available at: https://ati.ec.europa.eu/sites/default/files/2021-01/Technological%20trends%20in%20the%20textiles%20industry.pdf [Accessed on May 3, 2023]

[8] Eurostat, *Annual detailed enterprise statistics for industry (NACE Rev. 2, B-E)*, Available at: https://ec.europa.eu/eurostat/databrowser/view/SBS_NA_IND_R2__custom_6477633/default/table?lang=en [Accessed on April 7, 2023]

[9] Tripa, S., Indrie, L., Zlatev, Z., Tripa, F., *Customized clothes–a sustainable solution for textile waste generated by the clothing industry*, In: Industria Textila, 2022, 73, 3, 275-281, http://doi.org/10.35530/IT.073.03.202112

[10] Goyal, A., Nayak, R., *Sustainability in yarn manufacturing*, In: Sustainable Technologies for Fashion and Textiles, Woodhead Publishing, 2020, 33–55

[11] Zhang, S., Xu, C., Xie, R., Yu, H., Sun, M., Li, F., *Environmental assessment of fabric wet processing from gate-to-gate per-spective: Comparative study of weaving and materials*, In: Science of The Total Environment, 2023, 857, 159495

[12] Desore, A., Narula, S.A., *An overview on corporate response towards sustainability issues in textile industry*, In: Environment, Development and Sustainability, 2018, 20, 1439–1459

[13] Khan, M., Muhmood, K., Noureen, S., Mahmood, H.Z., Amir-ud-Din, R., *Epidemiology of respiratory diseases and associated factors among female textile workers in Pakistan*, In: International Journal of Occupational Safety and Ergonomics, 2022, 28, 1, 184–198

[14] Meenaxi, T., Sudha, B., *Air pollution in textile industry*, In: Asian Journal of Environmental Science, 2013, 8, 1, 64–66
[15] Indrie, L., Tripa, S., Diaz-Garcia, P., Mikucioniene, D., Belda-Anaya, R., *A European perspective on circular economy for fibrous composites and technical textiles*, In: Annals of the University of Oradea, Fascicle of Textiles, Leatherwork, 2023, 24, 2, 51–56
[16] Kant, R., *Textile dyeing industry an environmental hazard*, In: Natural Science, 2012, 4, 22–26, http://doi.org/10.4236/ns.2012.41004
[17] Palm, D., *Improved waste management of textiles, Project 9 Environmentally improved recycling*, IVL Swedish Environmental Research Institute Ltd., Gothenburg, Sweden, 2011, Available at: https://www.ivl.se/download/18.34244ba71728fcb3f3f7b9/1591704633006/B1976.pdf [Accessed on April 7, 2023]
[18] Allafi, F.A., Hossain, M.S., Shaah, M., Lalung, J., Ab Kadir, M.O., Ahmad, M.I., *A review on characterization of sheep wool impurities and existing techniques of cleaning: industrial and environmental challenges*, In: Journal of Natural Fibers, 2022, 19, 14, 8669–8687
[19] Kulkaria, B.V., *Sequential coagulation studies for primary treatment of textile process effluent instead of acid neutralization*, In: Journal of the Industrial Pollution Control, 2007, 23, 123–130
[20] Heuer, M., Becker-Leifhold, C., *Eco-friendly and Fair: Fast Fashion and Consumer Behaviour*, 1st Edition, Routledge, 2018
[21] Correia, V.M., Stephenson, T., Judd, S.J., *Characterisation of textile wastewaters – a review*, In: Environmental technology, 1994, 15, 10, 917–929
[22] Gregory, P., *Toxicology of Textile Dyes*, In: Environmental Aspects of Textile Dyeing, Woodhead Publishing, 2007, 44–73
[23] Chowdhary, P., Bharagava, R.N., Mishra, S., Khan, N., *Role of industries in water scarcity and its adverse effects on environment and human health*, In: Environmental Concerns and Sustainable Development: Volume 1: Air, Water and Energy Resources, 2020, 235–256
[24] Singha, K., Pandit, P., Maity, S., Sharma, S.R., *Harmful environmental effects for textile chemical dyeing practice,* In: Green Chemistry for Sustainable Textiles, Woodhead Publishing, 2021, 153–164
[25] Al-Tohamy, R., Ali, S.S., Li, F., Okasha, K.M., Mahmoud, Y.A.G., Elsamahy, T., Sun, J., *A critical review on the treatment of dye-containing wastewater: Ecotoxicological and health concerns of textile dyes and possible remediation approaches for environmental safety*, In: Ecotoxicology and Environmental Safety, 2022, 231, 113160
[26] Sahoo, S.K., Dash, A.K., *Recycled fibres from polyester and nylon waste*. In: Sustainable Fibres for Fashion and Textile Manufacturing, Woodhead Publishing, 2023, 309–332
[27] Chabuk, A, Hammood, Z.A., Abed, S.A., Kadhim, M.M., Hashim, K., Al-Ansari, N., Laue, J., *Noise Level in Textile Industries: Case Study Al-Hillah Textile Factory-Company for Textile Industries, Al-Hillah-Babylon-Iraq*, In: IOP Conference Series: Earth and Environmental Science, IOP Publishing, 2021, 790, 1, 012048
[28] Roozbahani, M.M., Nassiri, P., Shalkouhi, P.J., *Risk assessment of workers exposed to noise pollution in a textile plant*, In: International Journal of Environmental Science & Technology, 2009, 6, 591–596
[29] Van Kempen, E.E., Kruize, H., Boshuizen, H.C., Ameling, C.B., Staatsen, B.A., Hollander, A.E., *The association between noise exposure and blood pressure and ischemic heart disease: a meta-analysis*, In: Environmental Health Perspectives, 2002, 110, 3, 307–317
[30] Trent, S., *Clothes and climate: Is cotton best?*, 2020, Available at: https://ejfoundation.org/news-media/clothes-and-climate-is-cotton-best [Accessed on March 3, 2023]
[31] Tripa, S., Indrie, L., *Households textile waste management in the context of a circular economy in Romania*, In: Environmental Engineering and Management Journal, 2021, 20, 1, 81–87
[32] Eurostat, *Generation of waste by waste category, hazardousness and NACE Rev. 2 activity*, Available at: https://ec.europa.eu/eurostat/databrowser/view/ENV_WASGEN__custom_5673879/default/table?lang=en [Accessed on March 19, 2023]
[33] Sakpal, P.P., Landage, S.M., Wasif, A.I., *Application of nonwovens for water filtration*, In: International Journal of Advanced Research in Management and Social Sciences, 2013, 2, 28–47
[34] Seddighi, M., Hejazi, S.M., *Water–oil separation performance of technical textiles used for marine pollution disasters*, In: Marine Pollution Bulletin, 2015, 96, 1–2, 286–293
[35] Tarafder, N., *Importance of Technical Textiles as Filtration Media-A Review*, In: Journal of Industrial Mechanics, 2019, 4, 1, 1–10
[36] Danihelová, A., Němec, M., Gergeľ, T., Gejdoš, M., Gordanová, J., Sčensný, P., *Usage of recycled technical textiles as thermal insulation and an acoustic absorber*, In: Sustainability, 2019, 11, 10, 2968
[37] Uddin, F., *Environmental hazard in textile dyeing wastewater from local textile industry*, In: Cellulose, 2021, 28, 17, 10715–10739
[38] Khattab, T.A., Abdelrahman, M.S., Rehan, M., *Textile dyeing industry: environmental impacts and remediation*, In: Environmental Science and Pollution Research, 2020, 27, 3803–3818
[39] Chequer, F.D., De Oliveira, G.R., Ferraz, E.A., Cardoso, J.C., Zanoni, M.B., de Oliveira, D.P., *Textile dyes: dyeing process and environmental impact*, In: Eco-friendly Textile Dyeing and Finishing, 2013, 6, 6, 151–176
[40] Mollaee, M., Mobli, A., Mutti, N.K., Manalil, S., Chauhan, B.S., *Challenges and opportunities in cotton production*, In: Cotton Production, 2019, 371–390

[41] Chapagain, A.K., Hoekstra, A.Y., Savenije, H.H., Gautam, R., *The water footprint of cotton consumption: An assessment of the impact of worldwide consumption of cotton products on the water resources in the cotton producing countries*, In: Ecological Economics, 2006, 60, 1, 186–203
[42] Goyal, A., Parashar, M., *Organic cotton and BCI-certified cotton fibres,* In: Sustainable Fibres for Fashion and Textile Manufacturing, Woodhead Publishing, 2023, 51–74
[43] Riar, A., Mandloi, L.S., Sendhil, R., Poswal, R.S., Messmer, M.M., Bhullar, G.S., *Technical efficiencies and yield variability are comparable across organic and conventional farms*, In: Sustainability, 2020, 12, 10, 4271
[44] Yacout, D.M., Abd El-Kawi, M.A., Hassouna, M.S., *Cradle to gate environmental impact assessment of acrylic fiber manufacturing*, In: The International Journal of Life Cycle Assessment, 2016, 21, 326–336
[45] Moazzem, S., Wang, L., Daver, F., Crossin, E., *Environmental impact of discarded apparel landfilling and recycling*, In: Resources, Conservation and Recycling, 2021, 166, 105338
[46] Roy Choudhury, A.K., *Environmental impacts of the textile industry and its assessment through life cycle assessment*, InȘ Roadmap to Sustainable Textiles and Clothing: Environmental and Social Aspects of Textiles and Clothing Supply Chain, 2014, 1–39
[47] Guenza, F., *DETOX: from threat for brands to opportunity for labs and manufacturers*, 2017, Available at: https://projects2014-2020.interregeurope.eu/fileadmin/user_upload/tx_tevprojects/library/5.RESET%20GP%20Detox_01.pdf [Accessed on March 27, 2023]
[48] Manshoven, S., Christis, M., Vercalsteren, A., Arnold, M., Nicolau, M., Lafond, E., Coscieme, L., *Textiles and the environment in a circular economy*, In: Eur Top Cent Waste Mater a Green Econ, 2019, 1–60
[49] Cicconi, P., *Eco-design and Eco-materials: An interactive and collaborative approach*, In: Sustainable Materials and Technologies, 2020, 23, e00135
[50] Calamari, S., *Design for the environment: An exploratory study on the processes that guide the design of interior textile products*, Doctoral dissertation, Colorado State University, 2014
[51] Clark, G., Kosoris, J., Hong, L.N., Crul, M., *Design for sustainability: current trends in sustainable product design and development*, In: Sustainability, 2009, 1(3), 409–424
[52] Tischner, U., Charter, M., *Sustainable product design*, In: Sustainable Solutions, Routledge, 2017, 118–138
[53] Ahmad, S., Wong, K.Y., Tseng, M.L., Wong, W.P., *Sustainable product design and development: A review of tools, applications and research prospects*, In: Resources, Conservation and Recycling, 2018, 132, 49–61
[54] Le Blevennec, K., Jepsen, D., Rödig, L., Vanderreydt, I., Wirth, O., *For Better Not Worse: Applying Ecodesign Principles to Plastics in the Circular Economy*, In: ECOS, VITO and ÖKOPOL, Belgium, Brussels, 2018
[55] EEA, *Textiles and the environment: the role of design in Europe's circular economy*, EEA Briefing No 2/2022: European Environment Agency, 2022, Available online: https://www.eea.europa.eu/publications/textiles-and-the-environment-the (accessed on 17 May 2023)
[56] Salo, H.H., Suikkanen, J., Nissinen, A., *Eco-innovation motivations and ecodesign tool implementation in companies in the Nordic textile and information technology sectors*, In: Business Strategy and the Environment, 2020, 29.6, 2654–2667
[57] Bovea, M.D., Pérez-Belis, V., *A taxonomy of ecodesign tools for integrating environmental requirements into the product design process*, In: Journal of Cleaner Production, 2012, 20(1), 61–71
[58] Vercalsteren, A., Nicolau, M., Lafond, E., *Textiles and the environment in a circular economy*, Eionet Report-ETC/WMGE, 2019, 6
[59] Pappas, E., *Latest trend keeps clothes out of landfill, Horizon – The EU Research and Innovation Magazine*, 2021, Available at: https://ec.europa.eu/research-and-innovation/en/horizon-magazine/latest-trend-keeps-clothes-out-landfill [Accessed on May 19, 2023]
[60] Dahlbo, H., Aalto, K., Eskelinen, H., Salmenperä, H., *Increasing textile circulation – Consequences and requirements*, In: Sustainable Production and Consumption, 2017, 9, 44–57
[61] Levänen, J., Uusitalo, V., Härri, A., Kareinen, E., Linnanen, L., *Innovative recycling or extended use? Comparing the global warming potential of different ownership and end-of-life scenarios for textiles*, In: Environmental Research Letters, 2021, 16, 5, 054069
[62] *The importance of recycling for the areas of application of technical textiles* (TU Wien), TRENDBOOK Technical Textiles 2018/2019, Available at: https://www.textiletechnology.net/technical-textiles/trendreports/TRENDBOOK-Technical-Textiles-20182019-The-importance-of-recycling-for-the-areas-of-application-of-technical-textiles-TU-Wien-12387 [Accessed on May 22, 2023]
[63] Pradhan, A., Samal, S., Panda, B., Acharya, B., *Waste Prevention: Its Impact and Analysis. In IoT-Based Smart Waste Management for Environmental Sustainability*, In: CRC Press, 2022, 19–36
[64] Sandin, G., Peters, G.M., *Environmental impact of textile reuse and recycling – A review*, In: Journal of Cleaner Production, 2018, 184, 353–365
[65] Juanga-Labayen, J.P., Labayen, I.V., Yuan, Q., *A review on textile recycling practices and challenges*, In: Textiles, 2022, 2, 1, 174–188
[66] Bukhari, M.A., Carrasco-Gallego, R., Ponce-Cueto, E., *Developing a national programme for textiles and clothing recovery*, In: Waste Management & Research, 2018, 36, 4, 321–331
[67] Zamani, B., Svanström, M., Peters, G., Rydberg, T., *A carbon footprint of textile recycling: A case study in Sweden*, In: Journal of Industrial Ecology, 2015, 19, 676–687

[68] Ahmad, S.S., Mulyadi, I.M.M., Ibrahim, N., Othman, A.R., *The application of recycled textile and innovative spatial design strategies for a recycling centre exhibition space*, In: Procedia-Social and Behavioral Sciences, 2016, 234, 525–535

[69] Briga-Sa, A., Nascimento, D., Teixeira, N., Pinto, J., Caldeira, F., Varum, H., Paiva, A., *Textile waste as an alternative thermal insulation building material solution*, In: Construction and Building Materials, 2013, 38, 155–160

[70] Shirvanimoghaddam, K., Motamed, B., Ramakrishna, S., Naebe, M., *Death by waste: Fashion and textile circular economy case*, In: Science of the Total Environment, 2020, 718, 137317

[71] Agarwal, M.S., *Application of textile in the agriculture*, In: International Journal of Advance Research in Science and Engineering, 2013, 2, 9–18

[72] Harmsen, P., Scheffer, M., Bos, H., *Textiles for circular fashion: The logic behind recycling options*, In: Sustainability, 2021, 13, 17, 9714

[73] Müller, B., Herrero Acero, E., Gübitz, G.M., *Process for production flame-resistant synthetic fibers from textile waste, flame-resistant synthetic fibers and their use*, US2019/0323169A1, 24.10.2019, Available at: https://worldwide.espacenet.com/patent/search/family/056263464/publication/US2019323169A1?q=pn%3DUS2019323169A1 [accessed on May 23, 2023]

[74] Piribauer, B., Jenull-Halver, U., Quartinello, F., Ipsmiller, W., Laminger, T., Koch, D., Bartl, A., *Tex2mat–Next Level Textile Recycling with Biocatalysts*, In: Detritus Multidiscip. J. Waste Resour. Residues, 2020, 13, 78–86

[75] Guldmann, E., *Best practice examples of circular business models*, Published by: The Danish Environmental Protection Agency, Copenhagen, Denmark, 2016

**Authors:**

SIMONA TRIPA[1], LILIANA INDRIE[1], PABLO DÍAZ GARCÍA[2], DAIVA MIKUCIONIENE[3]

[1]Department of Textiles, Leather and Industrial Management, Faculty of Energy Engineering and Industrial Management, University of Oradea, 4 Barbu Stefanescu Delavrancea Street, 410058 Oradea, Romania

[2]Deparment of Textile and Paper Engineering, Universitat Politècnica de València, Plaza Ferrándiz y Carbonell, 03801 Alcoy, Spain

[3]Department of Production Engineering, Faculty of Mechanical Engineering Engineering and Design, Kaunas University of Technology, Studentu str. 56, 51424 Kaunas, Lithuania

**Corresponding author:**

SIMONA TRIPA
e-mail: tripasimona@yahoo.com

# Electromagnetic shielding effectiveness of needle-punched composite nonwoven fabrics with stainless steel fibres

DOI: 10.35530/IT.075.01.202346

ALI BEYİT
MUSTAFA SABRI ÖZEN
ERHAN SANCAK

**ABSTRACT – REZUMAT**

**Electromagnetic shielding effectiveness of needle-punched composite nonwoven fabrics with stainless steel fibres**

*In the study, electromagnetic shielding efficiency (EMSE) absorption and reflectivity properties of fabric produced from staple stainless-steel fibres and recycled staple polyester fibres by carding and needling technologies were investigated. The bi-component core/sheath polyester fibres at a fixed ratio of 20% in producing all nonwoven fabrics were used. The staple stainless-steel fibres and recycled staple polyester fibres were blended at 13 different ratios such as 1%, 2.5%, 5%, 7.5%, 10%, 12.5%, 15%, 17.5%, 20%, 22.5%, 25%, 27.5%, 30%. The fibre webs were formed at wool type carding machine and then the folded webs were bonded mechanically with needle punching machines. Half of the produced nonwoven composite fabrics were bonded by thermal bonding technology with oven and calender machines. As the conductive fibres were costly, the study aimed to obtain optimum shielding effectiveness with the usage of minimum conductive fibres. Electromagnetic shielding properties, absorption and reflection characteristics of needle-punched nonwoven fabrics with calendered or un-calendered were performed by coaxial transmission line method according to ASTM-D4935-10 in the frequency range of 15 MHz to 3000 MHz. It is a known fact that electromagnetic shielding effectiveness increases with the increase in the amount of conductive fibre. It was found that nonwoven fabric produced with a usage of 17.5% stainless steel fibre has at least 90% electromagnetic shielding percentage in general use with 15 dB at a frequency of 1800 MHz. Increased stainless steel fibre content in nonwoven fabrics resulted in decreased nonwoven fabric thickness and tensile strength. Such a nonwoven composite material with electromagnetic shielding property could be used for construction and building applications.*

***Keywords:*** *electromagnetic shielding (EM) effectiveness, electromagnetic radiation, stainless steel fibre, recycled polyester fibre, needle punching, nonwoven fabric, bi-component core/sheath binder fibres, thermal bonding technology*

**Eficienţa ecranării electromagnetice a neţesutelor compozite intreţesute cu fibre de oţel inoxidabil**

*În cadrul studiului, au fost investigate proprietăţile de absorbţie şi reflectivitate ale eficienţei ecranării electromagnetice (EMSE) ale materialului textil produs din fibre scurte de oţel inoxidabil şi fibre scurte de poliester reciclat, prin tehnologii de cardare şi interţesere. Au fost utilizate fibre de poliester bicomponente miez/manta la un raport fix de 20% în producţia tuturor neţesutelor. Fibrele scurte de oţel inoxidabil şi fibrele scurte de poliester reciclat au fost amestecate în 13 rapoarte diferite, cum ar fi 1%, 2,5%, 5%, 7,5%, 10%, 12,5%, 15%, 17,5%, 20%, 22,5%, 25%, 27,5%, 30%. Vălurile de fibre au fost formate la o maşină de cardare de tip lână şi apoi vălurile pliate au fost consolidate mecanic cu maşini de interţesere. Jumătate dintre neţesutele compozite produse au fost consolidate prin tehnologia de lipire termică cu etuve şi calandre. Deoarece fibrele conductoare erau foarte scumpe, scopul studiului a fost de a obţine o eficienţă optimă de ecranare cu utilizarea unui minimum de fibre conductoare. Proprietăţile de ecranare electromagnetică, caracteristicile de absorbţie şi reflexie ale neţesutelor interţesute, calandrate sau necalandrate, au fost realizate prin metoda liniei de transmisie coaxiale conform ASTM-D4935-10 în intervalul de frecvenţă de la 15 MHz la 3000 MHz. Este un fapt cunoscut că eficienţa ecranării electromagnetice creşte odată cu creşterea cantităţii de fibre conductoare. S-a descoperit că neţesutul produs cu utilizarea a 17,5% fibre de oţel inoxidabil are cel puţin 90% procent de ecranare electromagnetică în utilizare generală cu 15 dB la frecvenţa de 1800 MHz. Conţinutul crescut de fibre de oţel inoxidabil în neţesute a dus la scăderea grosimii materialului neţesut şi a rezistenţei la tracţiune. Un astfel de material compozit neţesut cu proprietăţi de ecranare electromagnetică ar putea fi utilizat pentru aplicaţii în construcţii.*

***Cuvinte-cheie****: eficienţa ecranării electromagnetice (EM), radiaţii electromagnetice, fibră de oţel inoxidabil, fibră de poliester reciclat, interţesere, neţesut, fibre de legătură bicomponente miez/manta, tehnologie de consolidare termică*

## INTRODUCTION

Today, humanity is faced with a very serious danger that is invisible, intangible, and odourless. The danger is determined as electromagnetic radiation caused by electromagnetic waves. Most of the people in the world are seriously unaware of the electromagnetic radiation danger [1]. The level of electromagnetic radiation (EM) with extensive usage of electrical and electronic appliances in addition to the rapid development of wireless communication has been increasing day by day. Electromagnetic pollution caused by electromagnetic radiation is a form of energy propagated through free space or material medium in the

form of electromagnetic waves and is a very serious danger to human health and life on Earth.
Electromagnetic fields (EMFs) are defined as packets of energy that have no mass [2]. Electromagnetic fields in the universe occur naturally and artificially. Magnetic fields and lightning in the earth are the natural electromagnetic fields. All electronic devices, base stations and electric power transmission lines are artificial/man-made electromagnetic fields [3]. Electromagnetic radiation is generally classified into non-ionizing, which is known as not having enough energy to break chemical bonds and believed as harmless to humans and ionizing radiation, which is potentially harmful to cells and DNA chains [4]. The human body is very exposed to electromagnetic waves in non-ionizing radiation categories at various frequencies and wavelengths during daily life [1].
The International Agency for Research on Cancer (IARC) classify radiofrequency electromagnetic fields as possibly carcinogenic to humans. However, there is no study showing scientific evidence between electromagnetic radiation and cancer. The effect of exposure to electromagnetic fields (EMF) on the body and cells depends on the electromagnetic field frequency and its strength [1]. The strength of an EMF decreases with increasing distance from the source. In addition to that, EMF pass through the body at low frequency, while at radio frequencies the fields are partially absorbed and penetrate only a short depth into the tissue. The structural changes in the frontal cortex, brain stem and cerebellum of the Wistar albino rats' heads exposed to microwave irradiation for 1 hour per day for two months [5].
Various studies have been conducted in previous literature regarding the harmful impact of electromagnetic radiation on living organisms. It was found that electromagnetic radiation causes structural changes in the frontal cortex, brain stem and cerebellum of the rats. The authors said that this deterioration can cause disease including loss of these areas' function and cancer development. The non-ionizing electromagnetic radiations emitted from cell phones, laptops, Bluetooth, microwave, or wireless networks might have detrimental effects on female fertility [4]. It was said that non-ionizing radiations can have destructive effects on the ovary and uterus, affecting several reproduction parameters in females. The low-frequency electromagnetic fields generated by car electronics, physiotherapy equipment and LCD monitors may be a cause of oxidative stress in the human body and may lead to free radical diseases [6]. The scientific evidence about hazards causing electromagnetic fields is increasingly strong and in vivo and in vitro scientific experimental studies demonstrate adverse effects on male and female reproduction of the mobile phone frequencies [4]. There is some evidence for elevations in breast cancer risk among women who wear their mobile phones in their bra [7]. There is a parallelism in time between increased use of mobile phones, increased exposure coming from wi-fi, smart meters, other wireless devices and male hyperfertility in addition to sperm abnormalities in semen [8]. Long-term exposure to electromagnetic radiation emitted from electronic devices and wireless communication can cause many health risks such as depression, headaches, insomnia, nervousness and even cancer [9]. Electromagnetic radiation causes serious health problems for humans and other living creatures according to the above scientific studies. Due to these reasons, today, electromagnetic shielding materials have great attention.
As conductive textile materials are so expensive, it is important to use them at specific rates. Textile clothes and building materials with high-performance electromagnetic shielding properties should be produced to remove the adverse effects of electromagnetic waves. Today, textile clothes such as jackets, shirts, pants, and coats having EM shielding properties are necessary to manufacture. Indeed, building materials with EM insulation effectiveness in addition to sound and heat insulation properties are needed. All textile clothes must be produced with electromagnetic shielding effectiveness properties for human health. The negative effects of electromagnetic radiation can be reduced by using conductive textile materials such as conductive fibre or yarn. Stainless steel fibre produced by Bekaert/Belgium, silver-coated polyamide fibres manufactured by R-Stat/France, carbon-coated polyester fibres by Shakespeare/UK and carbon fibres are some of the conductive fibres.
Considering these effects, the needle-punched composite nonwoven fabrics were designed and manufactured with carding, needle-punching technologies and machines from staple recycled polyester fibres, bi-component sheath/core type low melting binder fibre and staple stainless-steel fibres. Half of the needle-punched nonwoven fabrics were bonded with oven and calender cylinders by using thermal bonding technology. As a result, two different needle-punched composite nonwoven fabrics with calendered and uncalendared were obtained. The tensile strength and thickness properties of nonwoven composite fabrics were measured. The electromagnetic shielding effectiveness, absorption, and reflection properties of calendered and uncalendared needle-punched nonwoven composite fabrics were tested, compared, and evaluated. As the conductive staple stainless steel fibres are very expensive, the amount of conductive stainless steel fibres for optimum shielding effectiveness in general use and professional use was explored.

## EXPERIMENTAL STUDY

### Material and method

The Bekaert Bekinox® VS 12/060/2000 type stainless steel fibres were obtained from Bekaert Company in Belgium. Bekaert Bekinox® VS metal fibre is a stretch-broken sliver of very fine stainless-steel fibres. The diameter of the fibre with 100% Bekinox® was around 12 μm. The fineness is 9.1 dtex (8.2 denier). The specific weight is 8.03 g/cm$^3$.
The specific electrical resistance of the fibres is 0.90 Ω·mm$^2$/m. The tensile strength and average

elongation percentage of the fibre is 17 cN and 1% respectively.

### Production of nonwoven fabrics

The needle-punched nonwoven fabrics were manufactured in three stages. In the first stage, the webs were produced at the laboratory-type carding machine and then the carded webs were needle punched at the laboratory-type needling machine with a meter working width. In the last stage, the needle-punched fabrics are bonded by thermal method in the oven.

The nonwoven fabrics were manufactured through carding followed by needle punching machines. Half of the nonwoven composite fabrics were thermally bonded with a calender cylinder and oven. The carding process was carried out by a laboratory-type Mesdan carding machine. The sheath/core bi-component binder fibres were used at a 20% blending ratio for all nonwoven fabrics. The stainless-steel fibres were mixed with recycled polyester fibres at weight ratios of 1%, 2.5%, 5%, 7.5%, 10%, 12.5%, 15%, 17.5%, 20%, 25%, 30%. The webs were produced at carding machines as two passages. The carded webs were bonded at pre and main needle punching machines. Half of the nonwoven fabrics were thermally bonded with calender cylinders and air-through bonding technologies in the oven. Two different nonwoven fabric sets produced as needle-punched and thermally bonded have been completed. The calendered and non-calendered nonwoven fabric samples and their properties are shown in figures 1 and 2 and table 1, respectively.

### Measurement of electromagnetic shielding effectiveness

All measurements were repeated three times on different areas of the fabric, and the average values of the measurements were then given. A coaxial transmission line method specified in ASTM D4935-10 was used to test the EMSE of the nonwoven fabrics. The specimen was prepared with a standard test size of various thicknesses. The outer ring of the specimen was 133 mm in diameter. Two specimens were

Table 1

PHYSICAL PROPERTIES OF CALENDERED AND NON-CALENDERED NONWOVEN FABRICS

| Sample codes | Areal density ($g/m^2$) | Thickness (mm) | Fibres composition of nonwoven fabrics (%) | |
|---|---|---|---|---|
| | | | Bi-component (PES) | Stainless Steel |
| Non-calendered reference | 332.68 | 4.795 | 100 | 0 |
| Non-calendered 1% SS | 349.25 | 5.010 | 99 | 1 |
| Non-calendered 2.5% SS | 332.68 | 4.685 | 97.5 | 2.5 |
| Non-calendered 5% SS | 412.91 | 5.150 | 95 | 5 |
| Non-calendered 7.5% SS | 379.54 | 5.235 | 92.5 | 7.5 |
| Non-calendered 10% SS | 405.82 | 4.980 | 90 | 10 |
| Non-calendered 12.5% SS | 388.22 | 4.870 | 88.5 | 12.5 |
| Non-calendered 15% SS | 402.28 | 4.605 | 85 | 15 |
| Non-calendered 17.5% SS | 386.28 | 4.435 | 82.5 | 17.5 |
| Non-calendered 20% SS | 384.34 | 4.630 | 80 | 20 |
| Non-calendered 22.5% SS | 395.54 | 4.345 | 77.5 | 22.5 |
| Non-calendered 25% SS | 401.37 | 4.180 | 75 | 25 |
| Non-calendered 27.5% SS | 413.02 | 3.885 | 72.5 | 27.5 |
| Non-calendered 30% SS | 395.65 | 3.905 | 70 | 30 |
| Calendered reference | 407.08 | 4.545 | 100 | 0 |
| Calendered 1% SS | 405.02 | 4.595 | 99 | 1 |
| Calendered 2.5% SS | 358.62 | 4.095 | 97.5 | 2.5 |
| Calendered 5% SS | 443.77 | 4.380 | 95 | 5 |
| Calendered 7.5% SS | 461.25 | 4.395 | 92.5 | 7.5 |
| Calendered 10% SS | 469.25 | 4.150 | 90 | 10 |
| Calendered 12.5% SS | 479.77 | 4.320 | 88.5 | 12.5 |
| Calendered 15% SS | 457.37 | 4.065 | 85 | 15 |
| Calendered 17.5% SS | 476.00 | 3.965 | 82.5 | 17.5 |
| Calendered 20% SS | 441.48 | 4.035 | 80 | 20 |
| Calendered 22.5% SS | 432.91 | 4.145 | 77.5 | 22.5 |
| Calendered 25% SS | 488.34 | 3.725 | 75 | 25 |
| Calendered 27.5% SS | 465.94 | 3.400 | 72.5 | 27.5 |
| Calendered 30% SS | 447.65 | 3.540 | 70 | 30 |

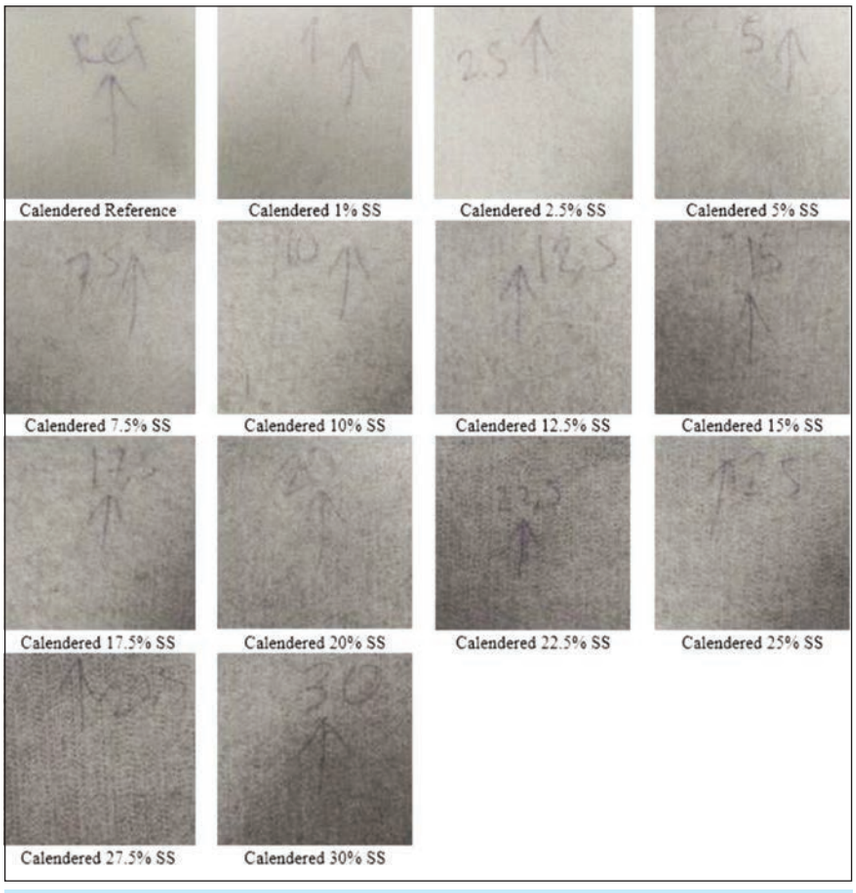


Fig. 1. Calendered nonwoven fabric samples (taken at x10 magnification)

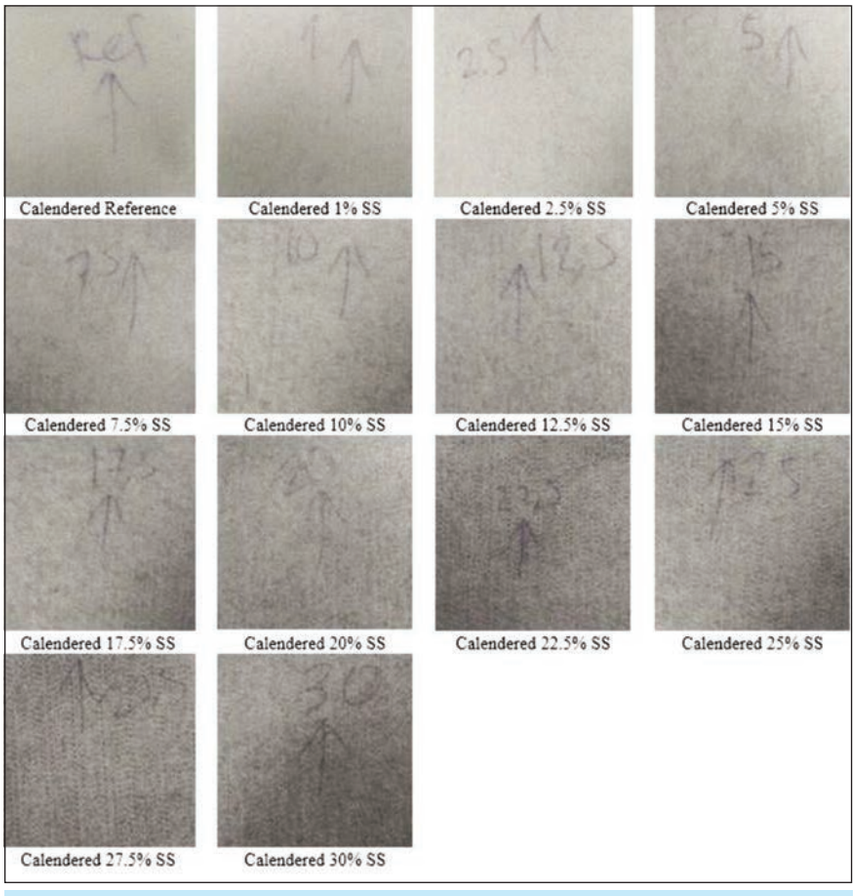


Fig. 2. Non-calendered nonwoven fabric samples (taken at x10 magnification)

required to be produced for the test, one for reference and another for load testing.

Various researchers have described the detailed set-up and testing procedure using a plane-wave electromagnetic field in the frequency range of between 0.1 and 3 GHz [25]. A network analyser (Rohde Schwarz, ZVL) to generate and receive the EM signals and a shielding effectiveness test fixture (Electro-Metrics, Inc., EM-2107A) were used to measure the EMSE, which was measured in decibels (dB) in this investigation. Where P1 (watts) received power with the fabric present, and P2 (watts) received power without the fabric present. The input power used was 0 dB, corresponding to 1 W [10, 26].

This standard determined the shielding effectiveness of the fabric using the insertion-loss method. The technique involved irradiating a flat, thin sample of the base material with an EM wave over the frequency range of interest, utilizing a coaxial transmission line with an interrupted inner conductor and a flanged outer conductor. A reference measurement for the empty cell was required for the shielding effectiveness assessment (figure 3, *b*). The reference sample was placed between the flanges in the middle of the cell, covering only the flanges and the inner conductors. A load measurement was performed on a solid disk shape, which had a diameter the same as that of the flange (figure 3, *c*). The reference and the load measurement were performed on the same material. The shielding effectiveness was determined from equation 1, which is the ratio of the incident field to that which passes through the material. The total shielding effectiveness ($SE_T$) that includes contributions due to reflection and absorption can be expressed as:

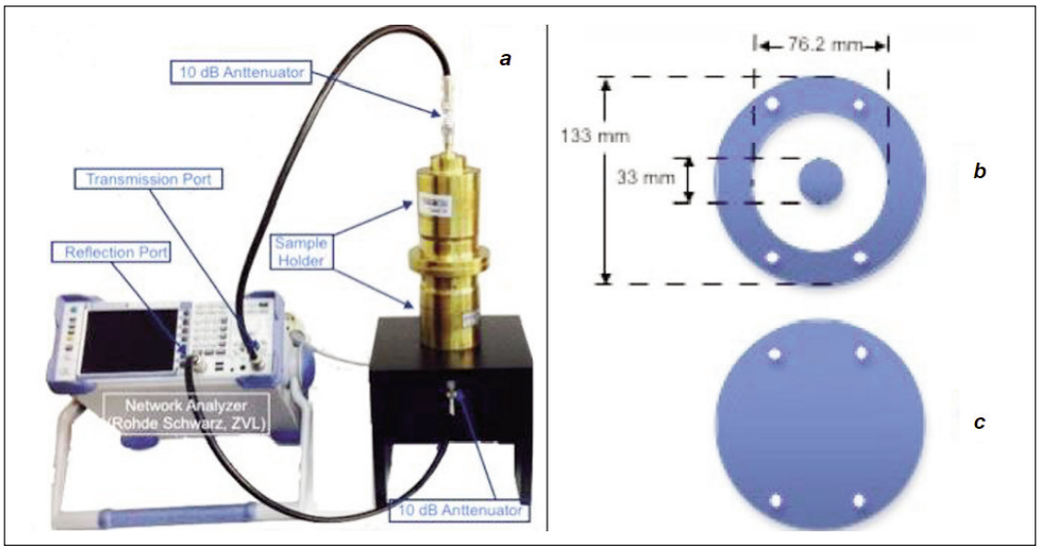


Fig. 3. Graphical representation of: *a* – set up of the Electromagnetic Shielding Effectiveness testing apparatus; *b* and *c* – specimen for reference and load respectively

$$SE_T(\text{dB}) = 10\log_{10}(P_T/P_I) = 20\log_{10}(E_T/E_I) = \\ = \log_{10}(H_T/20H_I) = \quad (1)$$

where $P_I$ ($E_I$ or $H_I$) and $P_T$ ($E_T$ or $H_T$) are the power (electric or magnetic field intensity) of the incident and transmitted EM waves, respectively. The scattering parameters $S_{11}$ ($S_{22}$) and $S_{12}$ ($S_{21}$) of VNA are related to reflectance ($R$) and transmittance ($T$), respectively. Therefore, attenuations due to reflection ($SE_R$) and absorption ($SE_A$) can be conveniently expressed as [11]:

$$T = |E_T/E_I|^2 = |S_{12}|^2 \ (=|S_{21}|^2), \\ R = |E_R/E_I|^2 = |S_{11}|^2 \ (=|S_{22}|^2) \quad (2)$$

$$A = (1 - R - T),\ A_{eff} = (1 - R - T)/(1 - R) \quad (3)$$

$$SE_R(\text{dB}) = 10\log_{10}(1 - R) \quad (4)$$

$$SE_A(\text{dB}) = 10\log_{10}(1 - A_{eff}) = \\ = 10\log_{10}[T/(1 - R)] \quad (5)$$

## RESULTS AND DISCUSSION

### Electromagnetic shielding efficiency

The shielding performances of the nonwoven fabrics are measured in non-calendered and calendered nonwoven. The electromagnetic shielding effectiveness (EMSE) performance of non-calendered and calendered nonwoven fabrics with conductive fibres (Stainless-Steel) measured between 0.1 and 3 GHz frequency range are presented in figures 4 and 5, respectively. It can be observed that the EM shielding properties of all non-calendered and calendered nonwoven fabrics have similar behaviours in figure 4 and figure 5, respectively. The shielding effectiveness of non-calendered and calendered nonwoven fabrics reveals that as frequency increases, EMSE values show a tendency to decrease between 0.1 and 0.3 GHz frequency range, then a tendency to rise between 0.3 and 3 GHz frequency range slightly in figures 4 and 5, respectively. As expected, The EMSE values increase with the increasing amount of conductive fibres in non-calendered and calendered nonwoven fabrics, as seen in figures 4 and 5, respectively. In this context, the frequency increases with decreasing of the wavelength [13–16]. Therefore, with an increase of conductive fibres, the amount of conductive materials increases (per unit area), and this increase in conductivity values leads to a higher EMSE. It is seen that non-calendered and calendered nonwoven fabrics containing 13 different ratios of conductive fibres are divided into 3 groups in terms of their Electromagnetic Shielding efficiency perfor-

Table 2

| PERFORMANCE SPECIFICATION OF EM SHIELDING TEXTILES IN GENERAL AND PROFESSIONAL USE [12] | | | |
|---|---|---|---|
| **Percentage of electromagnetic shielding (ES)** | **Shielding effectiveness (SE) in general use** | **Shielding effectiveness (SE) in professional use** | **Grade** |
| SE > 99.9% | SE > 30 dB | SE > 60 dB | 5 Excellent |
| 99.9% ≥ SE > 99% | 30 dB ≥ SE > 20 dB | 60 dB ≥ SE > 50 dB | 4 Very Good |
| 99% ≥ SE > 90% | 20 dB ≥ SE > 10 dB | 50 dB ≥ SE > 40 dB | 3 Good |
| 90% ≥ SE > 80% | 10 dB ≥ SE > 7 dB | 40 dB ≥ SE > 30 dB | 2 Moderate |
| 80% ≥ SE > 70% | 7 dB ≥ SE > 5 dB | 30 dB ≥ SE > 20 dB | 1 Fair |

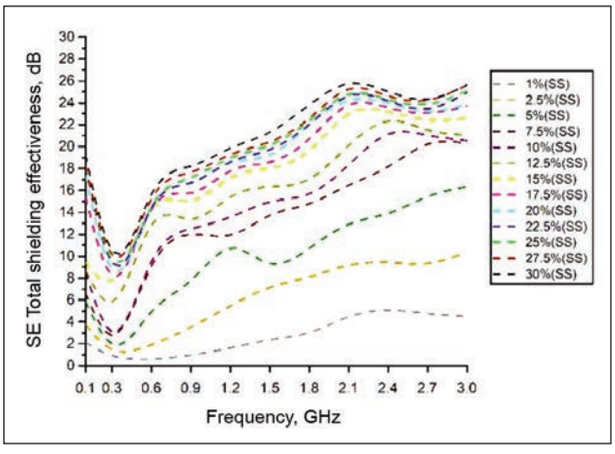


Fig. 4. Electromagnetic shielding effectiveness (EMSE) non-calendered nonwoven fabrics

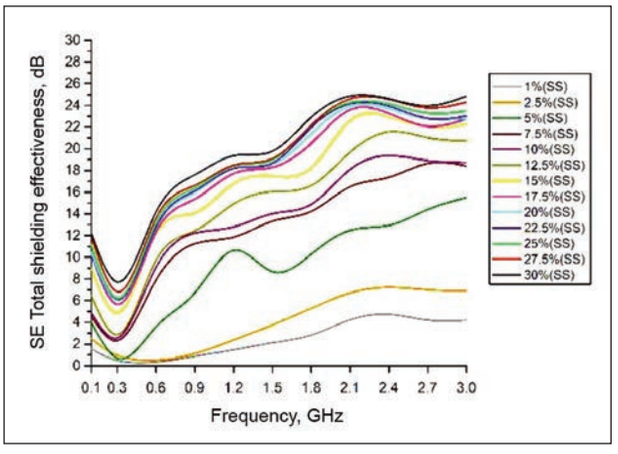


Fig. 5. Electromagnetic shielding effectiveness (EMSE) calendered nonwoven fabrics

mances. The electromagnetic shielding efficiencies of 2–3 dB increase with the increase of conductive stainless-steel fibres in the non-calendered and calendered nonwoven fabrics group containing 1%, 2.5%, and 5% conductive stainless-steel fibres. The electromagnetic shielding efficiencies of 1–2 dB increase with the increase of conductive stainless-steel fibres in the non-calendered and calendered nonwoven fabrics group containing 7.5%, 10%, and 12.5% conductive stainless-steel fibres. Conductivity is an effective parameter on the electromagnetic shielding effectiveness [17–21]. The electromagnetic shielding efficiencies of 0–1 dB increase with the increase of conductive stainless-steel fibres in the non-calendered and calendered nonwoven fabrics group containing 15%, 17.5%, 20%, 22.5%, 25%, 27.5% and 30% conductive stainless-steel fibres. It is observed that EMSE values increase with increasing amounts of conductive stainless-steel fibres. It is seen that the optimum level of electromagnetic shielding efficiency performance is obtained in non-calendered and calendered nonwoven fabrics containing 15% conductive stainless-steel fibres.

### Absorption and reflection results

The reflection and absorption behaviour of the nonwoven fabrics are shown in figure 6. It can be observed that the reflection values observed across the measurement range showed an opposite trend to the absorption values, with the absorption values increasing and reflection values decreasing with an increase in the frequency. The absorption values are consistently higher than reflectance values for non-calendered and calendered nonwoven fabrics with 1%, 2.5%, 5%, and 7.5% conductive stainless-steel fibres between 0.1 and 0.3 GHz frequency range. This behaviour of fabrics with conductive composite fibres is related to the properties of the materials. For instance, stainless-steel fibres are defined as more absorbent materials rather than being reflective in terms of the attenuation of electromagnetic waves especially increasing frequencies [22–25, 27]. As can be seen, the reflectance values decrease when the absorption values increase. The absorption values of non-calendered and calendered nonwoven fabrics with 1%, 2.5%, 5%, and 7.5% conductive stainless-steel fibres decrease gradually with increases of frequency between 0.3 and 1.8 GHz frequency range. In between the 1.8 and 3 GHz frequency ranges, the reflection values decrease progressively with a rise in frequency. Moreover, as compared to each other non-calendered and calendered nonwoven fabrics with 1%, 2.5%, 5%, and 7.5% conductive stainless-steel fibres consistently showed 1–2 dB higher EMSE values across the between 0.1 and 3 GHz frequency range. This difference became more significant at higher frequency values which is between 1.8 and 3 GHz frequency range where the difference reached nearly 2 dB. Besides, the calendered nonwoven fabrics display lower EMSE values than non-calendered nonwoven fabrics between 0.1 and 3 GHz frequency range.

The reflection and absorption behaviour of the nonwoven fabrics are shown in figure 7. It can be observed that the reflection values observed across the measurement range showed an opposite trend to the absorption values, with the absorption values increasing and reflection values decreasing with an increase in the frequency. The absorption values are consistently higher than reflectance values for non-calendered and calendered nonwoven fabrics with 10%, 12.5%, 15%, and 17.5% conductive stainless-steel fibres between 0.1 and 0.3 GHz frequency range. This behaviour of fabrics with conductive composite fibres is related to the properties of the materials. As can be seen, the reflectance values decrease when the absorption values increase. The absorption values of non-calendered and calendered nonwoven fabrics with 10%, 12.5%, 15%, and 17.5% conductive stainless-steel fibres decrease gradually with increases of frequency between 0.3 and 1.8 GHz frequency range. In between the 1.8 and 3 GHz frequency ranges, the reflection values decrease progressively with a rise in frequency. Moreover, as compared to each other non-calendered and calendered nonwoven fabrics with 10%, 12.5%, 15%, and

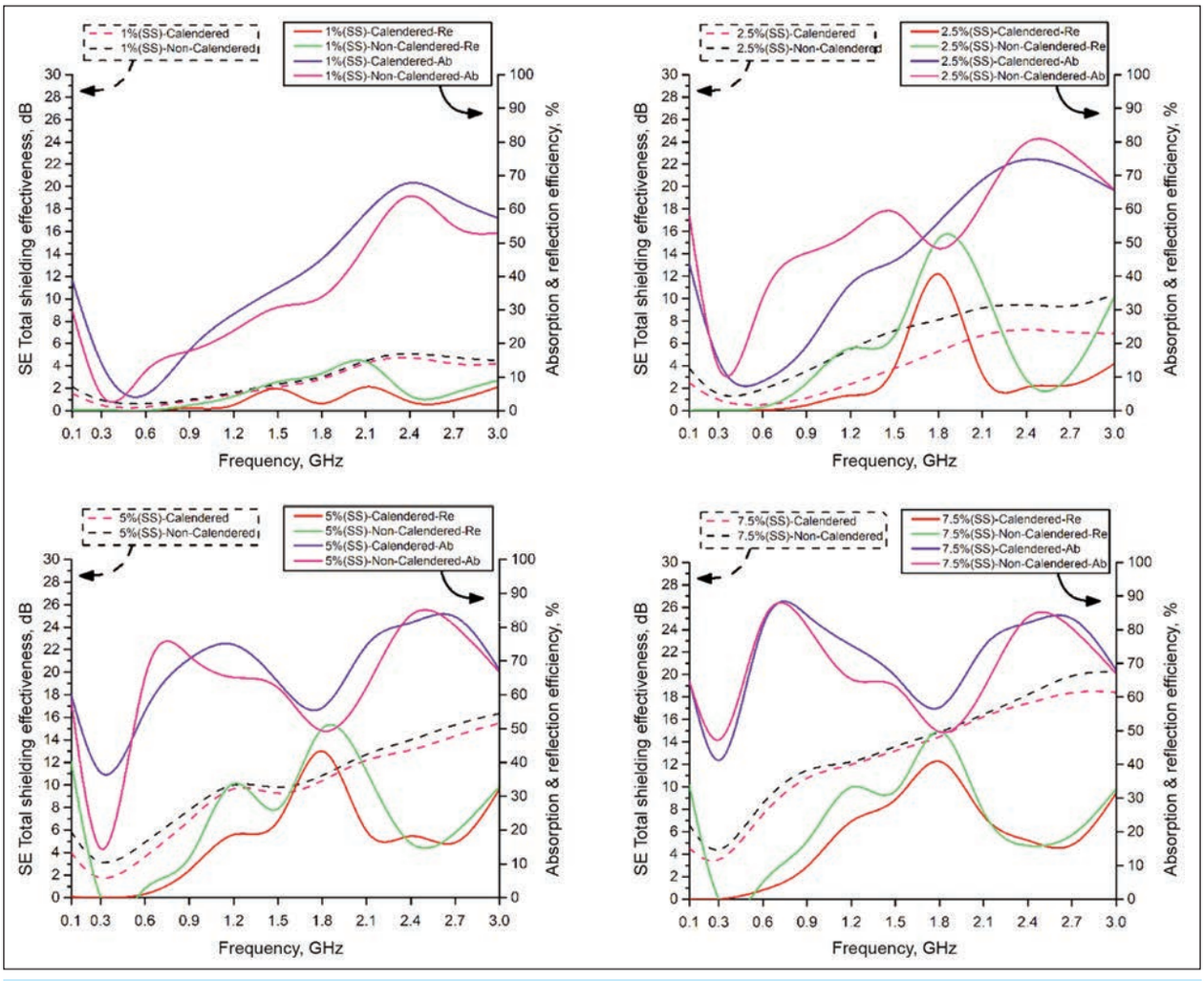


Fig. 6. Absorption and reflection results of calendered and non-calendered nonwoven fabrics with 1%, 2.5%, 5%, and 7.5% conductive stainless-steel fibres

17.5% conductive stainless-steel fibres consistently showed 1–2 dB higher EMSE values across the between 0.1 and 3 GHz frequency range. This difference became more significant at higher frequency values which is between 1.8 and 3 GHz frequency range where the difference reached nearly 2 dB. Besides, the calendered nonwoven fabrics display lower EMSE values than non-calendered nonwoven fabrics between 0.1 and 3 GHz frequency range.

The reflection and absorption behaviour of the nonwoven fabrics are shown in figure 8. It can be observed that the reflection values observed across the measurement range showed an opposite trend to the absorption values, with the absorption values increasing and reflection values decreasing with an increase in the frequency. The absorption values are consistently higher than reflectance values for non-calendered and calendered nonwoven fabrics with 20%, 22.5%, 25%, and 27.5% conductive stainless-steel fibres between 0.1 and 0.3 GHz frequency range. This behaviour of fabrics with conductive composite fibres is related to the properties of the materials. As can be seen, the reflectance values decrease when the absorption values increase. The absorption values of non-calendered and calendered nonwoven fabrics with 20%, 22.5%, 25%, and 27.5% conductive stainless-steel fibres decrease gradually with increases of frequency between 0.3 and 1.8 GHz frequency range. In between the 1.8 and 3 GHz frequency ranges, the reflection values decrease progressively with a rise in frequency. Moreover, as compared to each other non-calendered and calendered nonwoven fabrics with 20%, 22.5%, 25%, and 27.5% conductive stainless-steel fibres consistently showed 1–2 dB higher EMSE values across the between 0.1 and 3 GHz frequency range. This difference became more significant at higher frequency values which is between 1.8 and 3 GHz frequency range where the difference reached nearly 2 dB. Besides, the calendered nonwoven fabrics display lower EMSE values than non-calendered nonwoven fabrics between 0.1 and 3 GHz frequency range.

The reflection and absorption behaviour of the nonwoven fabrics are shown in figure 9. It can be observed that the reflection values observed across the measurement range showed an opposite trend to the absorption values, with the absorption values increasing and reflection values decreasing with an increase in the frequency. The absorption values are

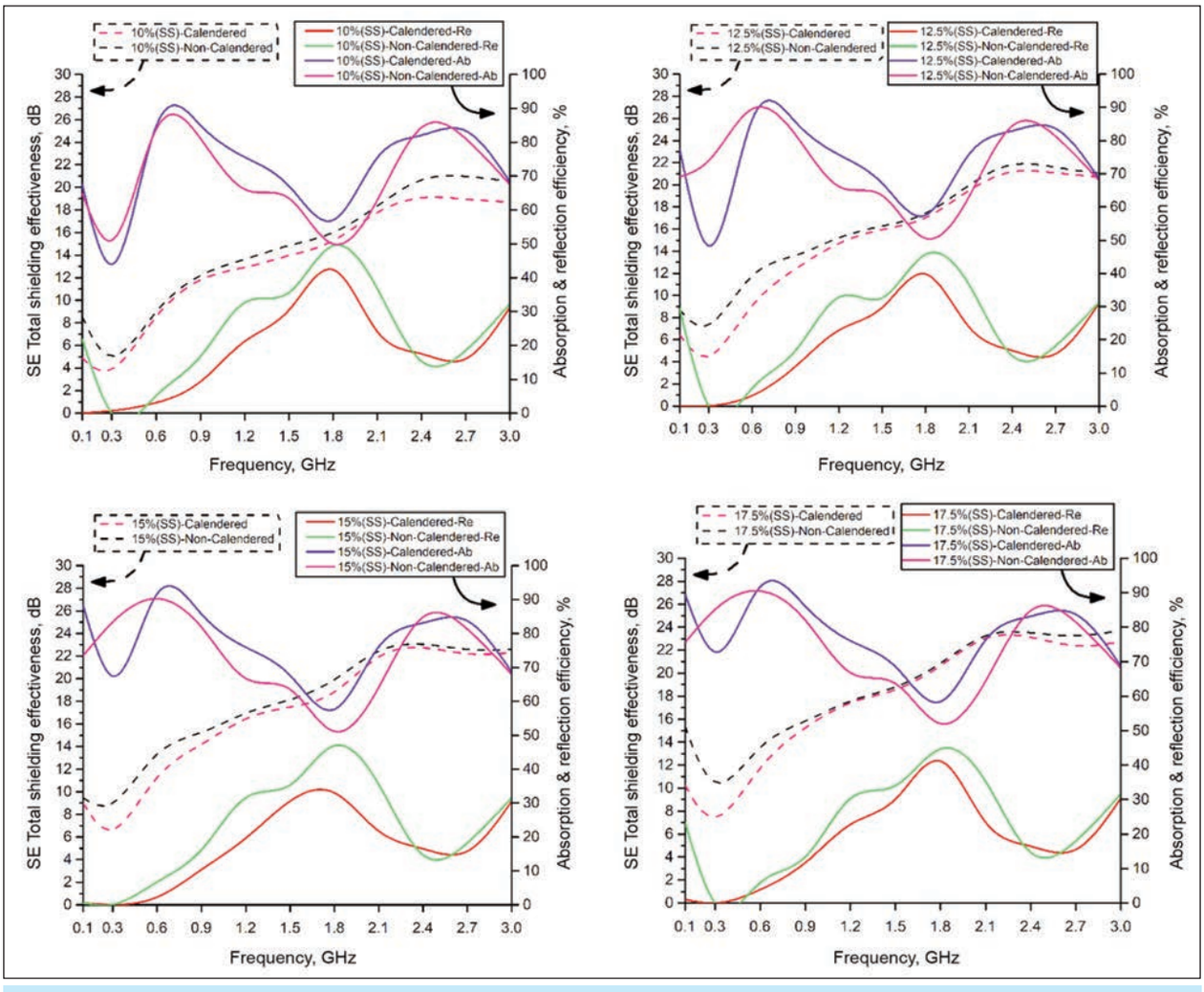


Fig. 7. Absorption and Reflection results of calendered and non-calendered nonwoven fabrics with 10%, 12.5%, 15%, and 17.5% conductive stainless-steel fibres

consistently higher than reflectance values for non-calendered and calendered nonwoven fabrics with 30% conductive stainless-steel fibres between 0.1 and 0.3 GHz frequency range. This behaviour of fabrics with conductive composite fibres is related to the properties of the materials. As can be seen, the reflectance values decrease when the absorption values increase. The absorption values of non-calendered and calendered nonwoven fabrics with 30% conductive stainless-steel fibres decrease gradually with increases of frequency between 0.3 and 1.8 GHz frequency range. In between the 1.8 and 3 GHz frequency ranges, the reflection values decrease progressively with a rise in frequency. Moreover, as compared to each other non-calendered and calendered nonwoven fabrics with 30% conductive stainless-steel fibres consistently showed 1–2 dB higher EMSE values across the between 0.1 and 3 GHz frequency range. This difference became more significant at higher frequency values which is between 1.8 and 3 GHz frequency range where the difference reached nearly 2 dB. Besides, the calendered nonwoven fabrics display lower EMSE values than non-calendered nonwoven fabrics between 0.1 and 3 GHz frequency range.

## CONCLUSIONS

In this study, the needle-punched nonwoven composite fabrics with EMI shielding properties were manufactured through a production process consisting of carding, cross lapper, needle punching machine and oven by blending stainless steel fibres, recycled polyester fibres and sheath/core bi-component binder fibres at different ratios. Increased stainless steel fibre content also resulted in higher EMI shielding effectiveness. The main objective of this study is to compare the properties of electromagnetic shielding effectiveness (EMSE) of non-calendered and calendered nonwoven fabrics. The non-calendered nonwoven fabrics have higher EMSE values than the calendered nonwoven fabrics. The highest electromagnetic shielding found in this work was 26 dB for non-calendered and calendered nonwoven fabrics containing a 15% 1.8–2.4 GHz frequency range. The optimum level of electromagnetic shielding efficiency performance is obtained in non-calendered and calendered nonwoven fabrics containing 15% conductive stainless-steel fibres. For higher shielding values, the percentage of stainless steel should be increased. EMSE values were evaluated,

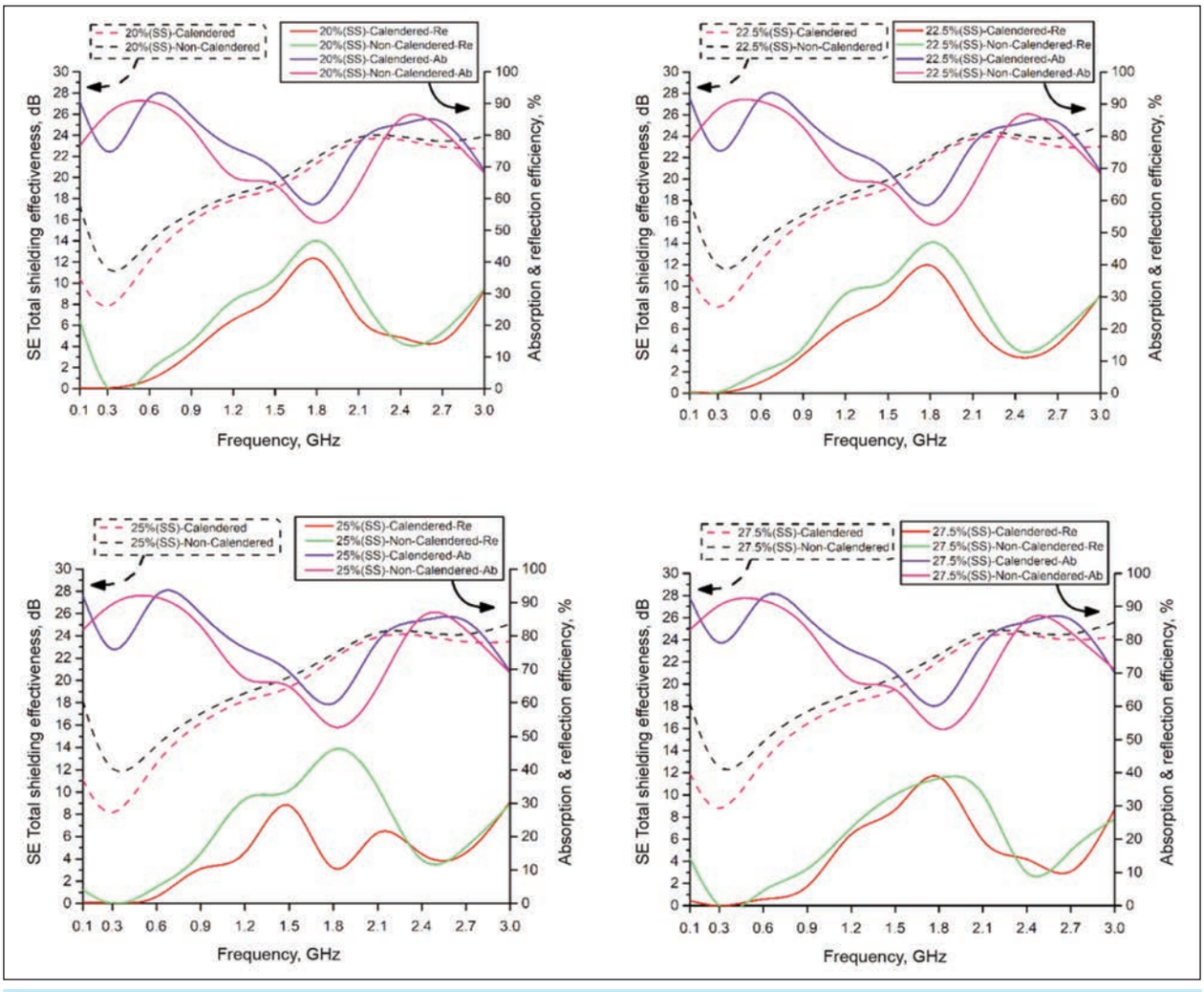


Fig. 8. Absorption and reflection results of calendered and non-calendered nonwoven fabrics with 20%, 22.5%, 25%, and 27.5% conductive stainless-steel fibres

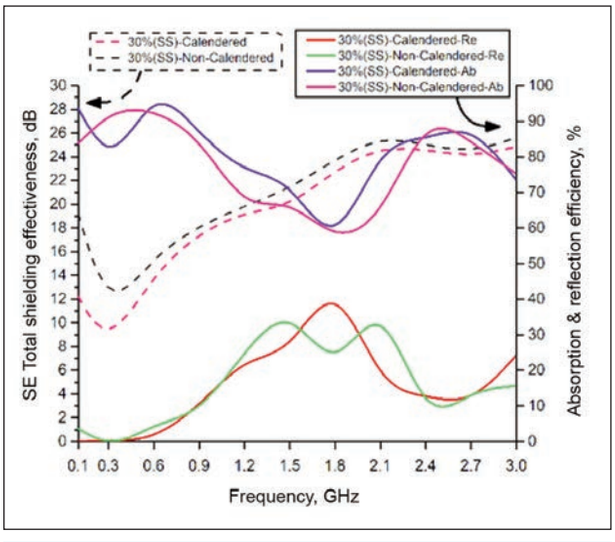


Fig. 9. Absorption and reflection results of calendered and non-calendered nonwoven fabrics with 30% conductive stainless-steel fibres

as shown in table 2, it was observed that non-calendered and calendered nonwoven fabrics containing 15%, 17.5%, 20%, 22.5%, 25%, 27.5% and 30% conductive stainless-steel fibres shield around 90 % and 99 % of electromagnetic waves between 0.1–0.6 GHz and 0.6–3 GHz frequency range, respectively. The non-calendered and calendered nonwoven fabrics containing 7.5%, 10% and 12.5%, conductive stainless-steel fibres shield around 80 % and 90 % of electromagnetic waves between 0.1–0.6 GHz and 0.6–3 GHz frequency range, respectively. The non-calendered and calendered nonwoven fabrics containing 1%, 2.5% and 5%, conductive stainless-steel fibres shield around 70 % and 80 % of electromagnetic waves between 0.1–0.6 GHz and 0.6–3 GHz frequency range, respectively. Concurrently, this suggests that these fabrics containing 1%, 2.5%, %5, 7.5%, 10%, 12.5% and 15% conductive stainless-steel fibres are highly suitable for most of the class-II (general) applications. The developed high EMSE non-calendered and calendered nonwoven fabrics containing 17.5%, 20%, 22.5%, 25%, 27.5% and 30% stainless steel fibres have potential applications in defence applications such as military tents, military secret rooms, protective covers, missile cover and building as an EMI shielding material.


## ACKNOWLEDGEMENTS

The study was produced from Ali BEYİT's Doctorate thesis.

## REFERENCES


[1] Rifai A.B, Hakami M.A., *Health hazards of electromagnetic radiation*, In: Journal of Biosciences and Medicines, 2014, 2, 1–12

[2] Belpomme, D., Hardell, L., Belyaev, I., Burgio, E., Carpenter, D.O., *Thermal and non-thermal health effects of low-intensity non-ionizing radiation: Environmental Pollution*, 2018, 242, 643–658

[3] Barnes, F.S, *Greenebaum B. Bioengineering and biophysical aspects of electromagnetic fields*, 3rd edition, Taylor&Francis Group, Boca Raton, Florida, USA, 2006

[4] Jangis, P., Rai, U., Shyam, R., Singh, R., *The role of non-ionizing electromagnetic radiation on female fertility: A Review*, In: International Journal of Environmental Health Research, 2022, https//doi.org/10.1080/09603123.2022.2030676

[5] Eser, O., Songur, A., Aktaş, C., Karavelioğlu, E., Çağlar, V., Aylak, F., Ozgüner, F., Kanter, M., *The effect of electromagnetic radiation on the rat brain*, In: Turkish Neurosurgery, 2013, 23, 6, 707–715

[6] Lewicka, M., Henrykowska, G.A., Pacholski, K., Szczesny, A., Dziedziczak-Buzynska, M., Buczynski, A., *The impact of electromagnetic radiation of different parameters on planet oxygen metabolism-in vitro studies,* In: Advances in Clinical and Experimental Studies, 2015, 24, 1, 31–35

[7] West, J.G., Kopoor, N.S., Liao, S.Y., Chen, J.W., Bailey, L., Nagourney, R.A., *Multifocal breast cancer in young women with prolonged contact between their breast and their cellular phone,* In: Case Report in Medicine, Hindawi Publishing Corporation, 2013, https://doi.org/10.1155//2013/354682

[8] Rolland, M., Le Moal, J., Wagner, V., Royere, D., De Mouzon, J., *Decline in semen concentration and morphology in a sample of 26609 men close to general population between 1989 and 2005 in Europe*, In: Human Reproduction, 2013, 28, 270–462

[9] Pakdel, E., Wang, J., Kashi, S., Sun, L., Wang, X., *Advances in photocatalytic self-cleaning superhydrophobic and electromagnetic interference shielding textile treatments,* In: Advances in Colloid and Interface Science, 2020, 277, 102116

[10] Ozen, M.S., Sancak, E., Usta, I., Beyit, A., Akalin, M., *Investigation of electromagnetic shielding properties of needle-punched nonwoven fabrics with stainless steel and polyester fiber*, In: Text. Res. J., 2013, 83, 8, 849–858

[11] Saini, P., Choudhary, V., Vijayan, N., Kotnala, R.K., *Improved Electromagnetic Interference Shielding Response of Poly(aniline)-Coated Fabrics Containing Dielectric and Magnetic Nanoparticles*, In: J. Phys. Chem. C., 2012, 116, 24, 13403–13412

[12] FTTS-FA-003: Test Method of Specified Requirements of Electromagnetic Shielding Textiles, Committee for Conformity Assessment on Accreditation and Certification of Functional and Technical Textiles: Taiwan, 2005, 1–4

[13] Kim, M.S., Kim, H.K., Byun, S.W., Jeong, S.H., Hong, Y.K., Joo, J.S., Song, K.T., Kim, J.K., Lee, C.J., Lee, J.Y., *PET fabric/Polypyrrole composite with high electrical conductivity for EMI shielding*, In: Syn. Metals, 2002, 126, 233–239

[14] Ortlek, H.G., Gunesoglu, C., Okyay, G., Turkoglu, Y., *Investigation of electromagnetic shielding and comfort properties of single jersey fabrics knitted from hybrid yarns containing metal wire*, In: Tekstil ve Konfeksiyon, 2012, 22, 90–101

[15] Perumalraj, R., Dasaradan, B.S., Anbarasu, R., Arokiaraj, P., Harish, S.L., *Electromagnetic shielding effectiveness of copper core-woven fabrics*, In: J. of the Textile Ins., 2009, 100, 512–524

[16] Cheng, K.B., *Electromagnetic shielding effectiveness of the twill copper woven fabrics*, In: J. of Rein. Plastics and Compos., 2006, 25, 699–709

[17] Roh, J.S., Chi, Y.S., Kang, T.J., Nam, S.W., *Electromagnetic shielding effectiveness of multifunctional metal composite fabrics*, In: Textile Research Journal, 2008, 78, 825–835

[18] Kim, T., Chung, D.D.L., *Mats and fabrics for electromagnetic interference shielding*, In: J. of Mat. Eng. and Perf., 2006, 15, 295–298

[19] Chung, D.D.L., *Electromagnetic interference shielding effectiveness of carbon materials*, In: Carbon, 2001, 39, 279–285

[20] Palamutcu, S., Ozbek, A., Karpuz, C., Dag, N., *Electrically conductive textile surfaces and their electromagnetic shielding efficiency measurement*, In: Tekstil ve Konfeksiyon, 2010, 3, 199–207

[21] Cheng, K.B., Cheng, T.W., Lee, K.C., Ueng, T.H., Hsing, W.H., *Effects of yarn constitutions and fabric specifications on electrical properties of hybrid woven fabrics*, In: Composites Part A: Applied Sci. and Manuf., 2003, 34, 971–978

[22] Kang, G.H., Kim, S.H., *Electromagnetic wave shielding effectiveness based on carbon microcoil-polyurethane composites*, In: J. of Nanomat., 2014, 1–6

[23] Rea, S., Linton, D., Orr, E., Connell, J., *Electromagnetic shielding properties of carbon fibre composites in avionic systems*, In: Microwave Review, 2005, 29–32

[24] Wu, Y., Zhous, S., Xu, Z., Yu, W., *Effect of carbon fiber buckling waved arrangement on the absorption of electromagnetic wave*, In: Asia Pacific Conf. on Env. Sci. and Tech. Adv. in Bio. Eng., 2012

[25] Li, K., Wang, C., Li, H., Jiao, G., Wei, J., *Study on the electromagnetic interference of CFRC composites by reflectivity*, In: J. Mat. Sci. Tech., 2008, 24, 2265–2271

[26] Erdem, R., *Evaluation of electromagnetic shielding effectiveness of multi-axial fabrics and their reinforced PES composites,* In: Bull Mater Sci, 2016, 39, 963–970

[27] Erdem, R., Ilhan, M., Sancak, E., *Analysis of EMSE and mechanical properties of sputter coated electrospun nanofibers*, In: Applied Surface Science, 2016, 380, 326–330

[28] Yilmaz, A.C., Ozen, M.S., Sancak, E., Erdem, R., Erdem, O., Soin, N., *Analyses of the mechanical, electrical and electromagnetic shielding properties of thermoplastic composites doped with conductive nanofillers,* In: Journal of Composite Materials, 2018, 52, 11, 1423–1432

**Authors:**

ALI BEYİT, MUSTAFA SABRI ÖZEN, ERHAN SANCAK

Marmara University, Technology Faculty, Department of Textile Engineering, Istanbul, Türkiye
e-mail: alibeyit@marmara.edu.tr, mustafaozen@marmara.edu.tr

**Corresponding author:**

ERHAN SANCAK
e-mail: esancak@marmara.edu.tr

# Professional skateboarding trousers design: according to the three-dimensional kinematic analysis for varied skateboarding manoeuvres

DOI: 10.35530/IT.075.01.202388

XIAO WEI JIN ZHOU

## ABSTRACT – REZUMAT

**Professional skateboarding trousers design: according to the three-dimensional kinematic analysis for varied skateboarding manoeuvres**

*The popularity of skateboarding has caused an expansion of enthusiasts worldwide. Moreover, skateboarding is becoming increasingly professional at an international level. Professional skateboarding trousers are regarded as critical equipment and their design research should not be overlooked. This research aims to use motion capture to measure the angular changes characteristics of critical lower limb joints in skaters during sports activities, measure the length of the knee joint during actions, and establish a formula that describes the change characteristics between the angle and the length. The formula would allow for a data reference when designing the elasticity at the knee joints of skateboarding trousers. Thus, the initial step in this research methodology was to use a Vicon motion capture system to test and analyse the kinematic characteristics of seven skaters in the squat, jump, ollie, pop shove it, heel flip, kickflip, and 180° ollie. Based on the kinematic characteristics, the dynamic movements were broken down into static postures at 0°, 45°, 90°, 112.5°, and 135°. The body surface drawing method was then employed to measure changes in the knee joint body surface dimensions of the subjects. Next, the experimental data were analysed to explore the relationship between angle and length changes. Finally, the design was developed based on the data. Analysis and processing of the experimental data yielded the following conclusions: (1) The most significant knee joint change characteristics during skateboarding was the angle change observed during an ollie. (2) Knee joint skin stretch deformation is most evident in the anterior mid-leg line y2. (3) The relationship between kinematics and the structural design of skateboarding trousers was derived from the experimental data. Specifically, the equation for the relationship between angle change and length change is given by y2 = 0.0442x + 23.906. (4) The results show that the extreme range of skin stretching in the anterior midline is between –0.7 and 6.3 cm. Therefore, the loose design of the knee part of professional skateboarding trousers should not exceed 6.3 cm. This research approach can offer an effective design solution for professional skateboard trousers and can also be applied to other types of trousers.*

***Keywords:*** *kinematic, 3D motion capture, skin deformation, skateboarding pants, sports*

**Designul pantalonilor de skateboarding profesionist: conform analizei cinematice tridimensionale pentru manevre variate de skateboarding**

*Popularitatea skateboarding-ului a provocat o expansiune a entuziaștilor din întreaga lume. Mai mult, skateboarding-ul devine un sport din ce în ce mai profesionist la nivel internațional. Pantalonii de skateboarding profesionist sunt priviți ca echipamente deosebit de importante, iar cercetarea designului acestora nu trebuie trecută cu vederea. Acest studiu își propune să utilizeze captura de mișcare pentru a măsura caracteristicile modificărilor unghiulare ale articulațiilor critice ale membrelor inferioare la patinatori în timpul activităților sportive, să măsoare lungimea articulației genunchiului în timpul acțiunilor și să stabilească o formulă care descrie caracteristicile schimbării dintre unghi și lungime. Formula ar permite o referință de date atunci când se proiectează elasticitatea la articulațiile genunchilor la pantalonii de skateboarding. Astfel, pasul inițial în această metodologie de cercetare a fost utilizarea unui sistem de captare a mișcării Vicon pentru a testa și analiza caracteristicile cinematice ale unui număr de șapte patinatori în poziţiile ghemuit, săritură, ollie, pop shove it, heel flip, kickflip și ollie la 180°. Pe baza caracteristicilor cinematice, mișcările dinamice au fost împărțite în posturi statice la 0°, 45°, 90°, 112,5° și 135°. Metoda de desenare a suprafeței corporale a fost apoi utilizată pentru a măsura modificările dimensiunilor suprafeței articulației genunchiului la subiecți. Apoi, datele experimentale au fost analizate pentru a explora relația dintre modificările de unghi și lungime. În cele din urmă, designul a fost dezvoltat pe baza datelor obținute. Analiza și prelucrarea datelor experimentale au condus la următoarele concluzii: (1) Cea mai semnificativă caracteristică de modificare a articulației genunchiului în timpul skateboardingului a fost modificarea unghiului observată în timpul unui ollie. (2) Deformarea întinderii pielii articulației genunchiului este cea mai evidentă în linia mediană anterioară a piciorului y2.(3) Relația dintre cinematică și designul structural al pantalonilor de skateboarding a fost derivată din datele experimentale. Mai exact, ecuația pentru relația dintre modificarea unghiului și modificarea lungimii este dată de y2 = 0,0442x + 23,906. (4) Rezultatele arată că intervalul extrem de întindere a pielii în linia mediană anterioară este între –0,7 și 6,3 cm. Prin urmare, designul liber al părții genunchiului pantalonilor de skateboarding nu trebuie să depășească 6,3 cm. Această abordare a cercetării poate oferi o soluție eficientă de design pentru pantalonii de skateboarding profesionist și poate fi aplicată și altor tipuri de pantaloni.*

***Cuvinte-cheie****: cinematică, captură de mișcare 3D, deformare a pielii, pantaloni de skateboarding, sport*

## INTRODUCTION

Skateboarding originated in the United States in the 1960s as a form of evolution of surfing but with greater freedom and flexibility. As skateboarding becomes more prevalent, the scale of its community of enthusiasts around the world continues to grow. On 4 February 2022, the International Olympic Committee announced that skateboarding would be included in the 2024 Paris Olympics and that it had become a permanent Olympic sport as of the 2028 Los Angeles Olympics. Since the professional and competitive development of skateboarding, sports companies and researchers alike have made professional equipment designed for the sport a new priority. Despite the athletic nature of skateboarding coupled with sporadic motions and non-standard equipment, quantitative analysis of its kinematics remains inadequate. Kristin et al., [1] referred to skateboarding injuries and suggested that research could include more standardized data collection, as well as a greater focus on kinetic analyses of this sport, and encouraging interdisciplinary research. Jeremy et al. [2] described the dynamics of skateboarding aerial landings and showed that there was no systematic understanding of the biomechanical factors responsible for injurious skateboarding at the stage before their study; Bryant et al. [3] investigated ground reaction forces, stride kinematics, and metabolic costs of skateboarding on a running motion apparatus, and the energetics of skateboarding compared to other forms of motion, however similar studies of the kinematic characteristics of skateboarding manoeuvres were less from most published research; Skateboarding have the characteristics of diversity and flexibility, Luana et al. [4] analysed the three-dimensional kinematics of skateboard ollie movements and compared the ollie movements in static and dynamic manoeuvrability. Their findings supported skateboarders to obtain higher scores in competitions

Although there were few reported cases of professional design for skateboarding trousers, examples from other sports provide beneficial insights. Jeehye et al. [5] showed that the size of the key areas in the climbing position is an important basis for determining the comfort of climbing trousers. Weirong et al. [6] chose five representative yoga poses on eight female participants selected for standard standing and yoga poses, measured the lower limbs of the participants through 3D scanning technology, analysed the skin deformation of female limbs under yoga, and established a digital design model of weft knitted seamless yoga trousers based on the skin deformation, and the results of the study can provide a basis for the structural and stylistic yoga trouser. Wenfang et al. [7] developed novel work trousers based on deformation rates that create folded structures in regions that can stretch and shorten after human movement, which can effectively improve the mobility and comfort of the wearer's limbs; meanwhile, according to human testing, these novel trousers significantly increased the range of motion in hip flexion, improved the ease of movement and comfort in the knees and limbs, and reduced the feeling of stress in these areas. A professional analysis of kinematics will provide data to support the design of skateboarding trousers

This research aimed to assess the angular changes of the ankle, knee, and hip joints in skaters' lower limbs during skateboarding. Additionally, it aimed to establish a correlation between the changes in skin surface and angular motion. Finally, this study intended to develop professional skateboarding pants.

## METHODS

### Subjects

Seven subjects were selected as young skaters with more than 2 years of skateboarding experience. A male-to-female ratio of 6:1, an average age of 19 years, an average height of 169.5 cm, an average weight of 54.1 kg, and an average boarding experience of 4.4 years, were obtained. Data were collected on knee, hip and ankle joint movement characteristics during skateboarding in 7 subjects who were required to perform standing, squatting, and jumping as well as two basic manoeuvres of an ollie, pop shoves and one of the movements of heel flip, kickflip or 180° ollie. The above subjects participated in two experiments, the motion capture and the skin stretching trails.

### Marking for kinesiological

To safeguard the accuracy of motion capture, doors and windows were closed before the experiment, and all reflective objects in the experimental environment were removed or shaded. Calibrated the Vicon Nexus system with a T-shaped calibration stand. Basic information such as the subject's height, body mass, lower limb length, knee width, and ankle width were measured and entered.

Subjects were labelled with reflective dots and then marked with 16 marker balls of 14 mm diameter. Marker points located on the left and right (anterior superior iliac spine, posterior superior iliac spine, lateral thigh, lateral epicondyle of the knee, lateral calf, tip of the lateral ankle, second metatarsal, heel) are shown in figure 1.

### Kinesiology testing process

Subjects performed standing, squatting and skateboarding manoeuvres at their usual walking speed in the test area. Formal testing began after acclimatizing to the experimental environment and meeting the experimental requirements. The Vicon Motion Capture System will record the trajectory of all marker balls as they are walked. Seven subjects were then asked to perform manoeuvres as required. The motion capture is summarized in table 1, with each manoeuvre being captured three times.

### Kinematic data processing

All seven subjects completed five of the squat, jump, ollie, pop shove it, and heel flip or kickflip or 180° ollie.

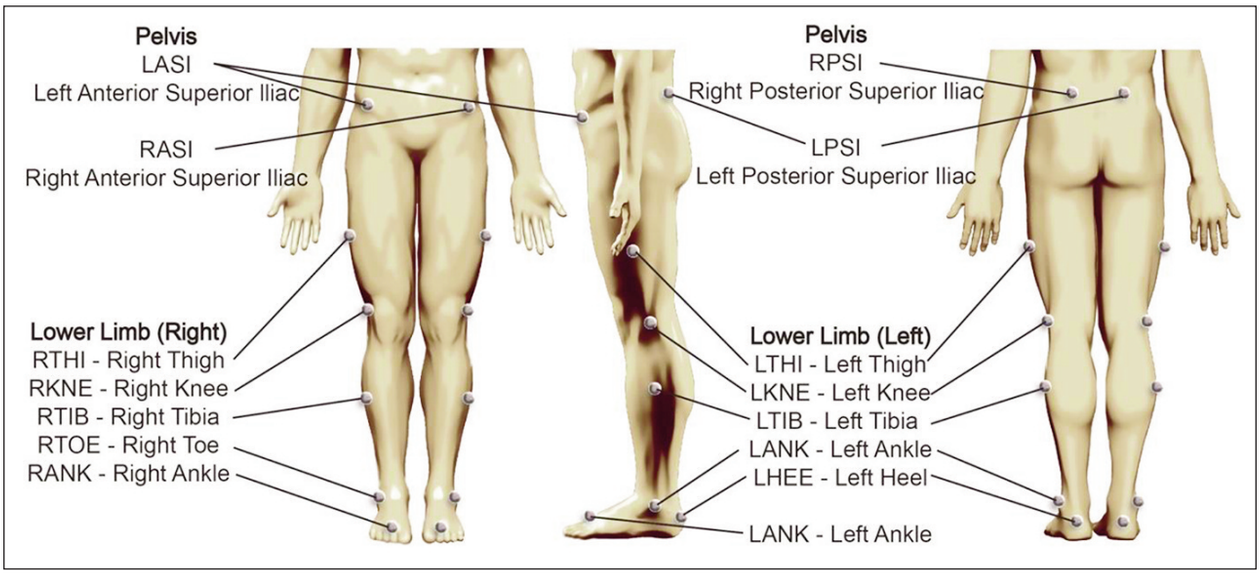


Fig. 1. *Reflective point marker before the experiment*

Table 1

| MOTION CAPTURE SUMMARY TABLE | |
|---|---|
| **Motion** | **Figure** |
| Ollie | 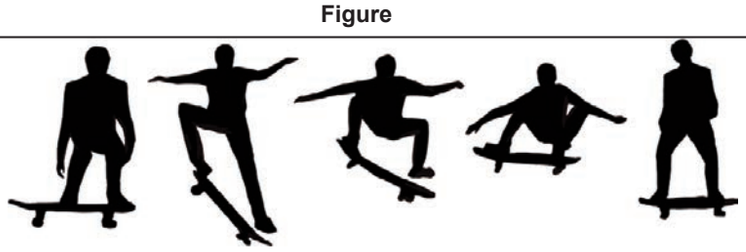 |
| Pop shove it |  |
| Heel flip | 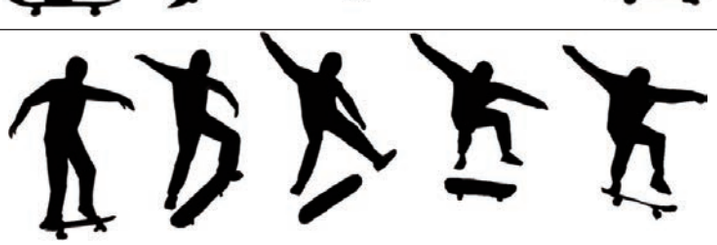 |
| Kickflip | 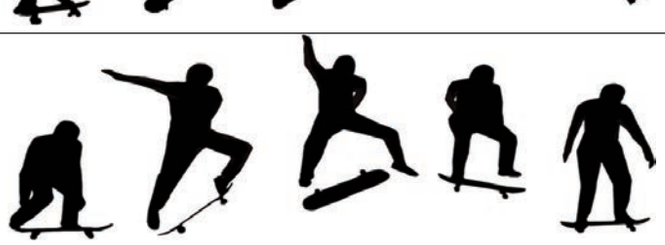 |
| 180°ollie |  |

Specifically, they all finished the squat, jump, ollie, and pop shove it, two of the subjects completed the heel flip, three of them completed the kickflip, and one completed the 180° ollie. The Plug-in Gait lower body model was applied to output the angular data of seven subjects performing skateboarding manoeuvres, which was used to analyse the angular range of motion of the ankle, knee and hip joints in the X-axis. (Dorsiflexion and plantar flexion joint movements of the ankle, flexion and extension joint movements of the knee and hip joints, all joints in coordinates around the X-axis in the left and right directions of the spatial origin). Further, maximum, minimum, mean and standard deviation, with a range of angular movement between the maximum and minimum values, were considered

### Skin stretching test

According to the skateboarding movement characterization, the dynamic movements were separated into five static movements for easy data measurement. The squat angles were 180°, 135°, 90°, 67.5°, and 45° as shown below (figures 2, *b* and *c*).

The subjects' lower limbs were wearing sports shorts with bare knees, and according to the human body surface characteristics, reference lines were drawn on the subjects' leg body surface with a marker pen before the measurement. It is clearly shown from figure 2, *a*, that the four longitudinal auxiliary lines targeting the knee joint kinematic characteristics were, in order, the medial suture line y1, anterior mid-leg line y2, lateral suture line y3, and posterior mid-leg line y4.

During the measurement, the static data were first measured, who stood on the ground with their hands naturally hanging down on both sides of the body and their feet 20 cm apart, keeping the symmetry of the left and right sides with the midline of the body as the standard. To reduce the error when measuring, the soft ruler should be close to the skin surface, the skin should not deform, the elasticity should be kept consistent, and the line of sight should be kept straight when reading the data. When measuring the data, the longitudinal data were measured in order from left to right and recorded in time, and the length data of each line segment of the dynamic decomposition squatting angle (0°, 45°, 90°, 112.5°, 135°) of the gliding movement were measured in order. Observe the data of y1, y2, y3, and y4 at different angles longitudinally, and measure and record the data to derive the range of variation.

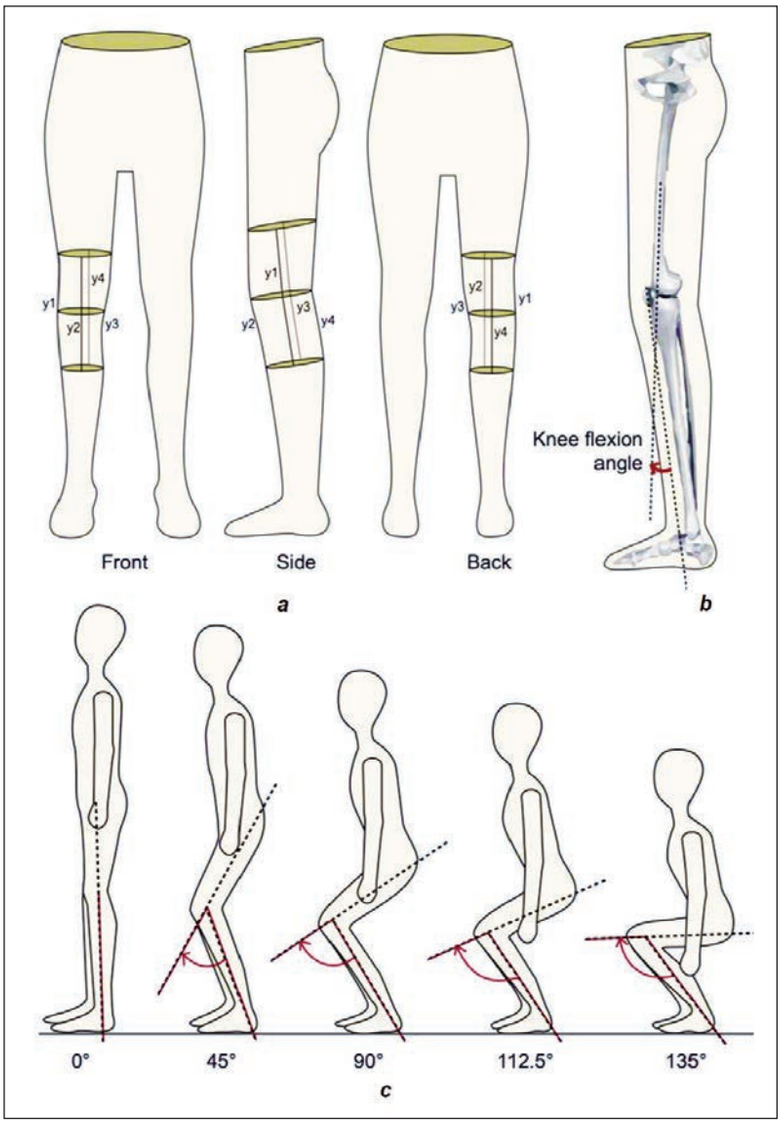


Fig. 2. Graphical representation of: *a* and *b* – The breakdown angle of the dynamic squat movement; *c* – schematic diagram of lower extremity data measurement

## RESULTS

### Data results

*Motion capture experimental data*

The extreme, range, and mean values of the sagittal plane angles of the hip, knee, and ankle joints for different skateboarding motions are shown in table 2.

To ensure stability during movement, the sagittal planes of the ankle, knee and hip joints all produced varying degrees of angular change during the different skateboarding manoeuvres described above. The angular movements of the knee are greater than the angular range of motion values of the hip and the ankle during the same movement. Therefore, it was easy to conclude that the knee has the most pronounced changes in the X-axis, which is the joint part with the greatest change in sagittal plane angle in skateboarding.

Furthermore, the following findings were obtained:

- The angular range values in the X-axis of the hip, knee, and ankle joints were all maximal during the ollie movement in all seven tested manoeuvres.

Table 2

| HIP, KNEE, AND ANKLE SAGITTAL CORONAL AXIS (X-AXIS) ANGLE EXTREMES, RANGES, AND MEANS | | | | | | | |
|---|---|---|---|---|---|---|---|
| **Joint data** | **squat** | **Jump** | **ollie** | **Heel flip** | **Kickflip** | **Pop shove it** | **180ollie** |
| Hip max | 113.2 | 119.2 | 140.0 | 104.9 | 121.6 | 117.7 | 112.9 |
| Hip min | –7.0 | –7.6 | –76.0 | 6.3 | –6.9 | –8.6 | 1.2 |
| Hip range | 120.1 | 126.8 | 216.0 | 98.5 | 128.5 | 126.3 | 111.7 |
| Hip mean | 53.1 | 55.8 | 32.0 | 55.6 | 57.3 | 54.5 | 57.0 |
| Keen max | 141.1 | 142.0 | 228.9 | 134.4 | 108.7 | 56.2 | 132.8 |
| Keen min | –14.9 | –21.6 | –13.5 | 5.0 | –16.1 | 136.1 | –3.9 |
| Keen rang | 156.0 | 163.6 | 242.4 | 129.4 | 124.8 | 95.3 | 136.7 |
| Keen mean | 63.1 | 60.2 | 107.7 | 69.7 | 46.3 | 18.7 | 64.5 |
| Ankle max | 45.5 | 52.4 | 99.6 | 66.2 | 90.0 | 111.8 | 32.1 |
| Ankle min | –149.8 | –137.3 | –157.6 | –28.6 | –69.1 | –71.6 | –46.2 |
| Ankle rang | 195.3 | 189.6 | 257.3 | 94.9 | 159.1 | 183.4 | 78.3 |
| Ankle mean | –52.2 | –42.5 | –29.0 | 18.8 | 10.5 | 20.1 | –7.1 |

- The ordering of the hip X-axis angular range values with both ends data removed was kickflip, jump, pop shove it, squat, 180ollie, and the movement with the smallest angular range was the heel flip.
- The ordering of the knee X-axis angular range values with both ends data removed was jump, squat, 180ollie, heel flip, kickflip, and the movement with the smallest angular range was pop shove it.
- The ordering of the ankle X-axis angular range values with both ends data removed was squat, jump, pop shove it, kickflip, heelflip, and the movement with the smallest angular range was the 180° ollie.

*Results of body skin stretching*

The length of the skin stretches produced at the knee joint varies depending on the angle of the static squat. In the case of 180° at the knee joint, the tester is in a static standing position, so the value of the skin stretch is the length at the other angles minus the length at 180°.

The graph below shows a scatter plot of the relationship between the mean change in angle length during skin stretching derived from the fit.

## DISCUSSION

By investigating the characteristics of skateboarding movements, 0°, 45°, 90°, 112.5° and 135°, and the skin stretch data for the above five static angles were summarized. According to the formula between the skin stretch and squatting angle, the minimum value

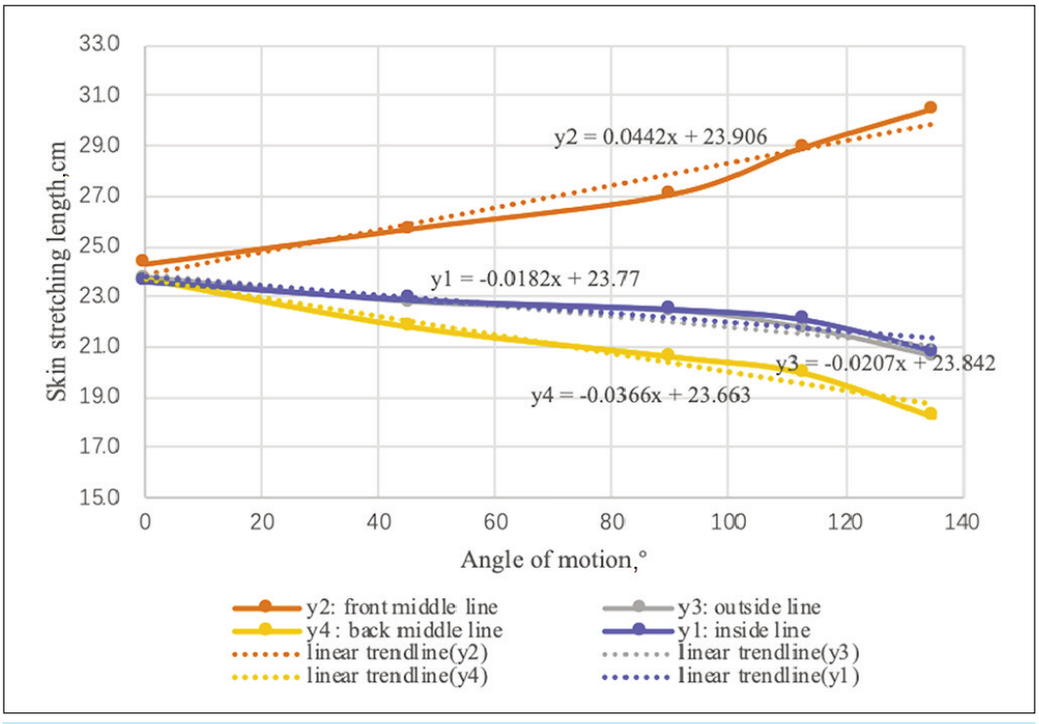


Fig. 3. Scatterplot of angle-length mean relationship

of the knee joint in the coronal axis during skateboarding was –21.6° and the mean of the minimum value was 7.6°; the maximum value of the angle was 136.1° and the mean of the maximum value of the angle was 25.4°. The corresponding range of the extreme value of the front midline y2: was 22.9 to 29.9 cm, the average range of the extreme value: was 24.2 to 25.0 cm, the stretch range of the skin of the front midline y2, which was the extreme range of the looseness of the skateboarding trousers: –0.7 to 6.3 cm, and the average stretch range of the extreme value: 0.6 to 1.4 cm. The above reference ranges can provide data reference for the design of the knee joints of the skateboarding trousers.

Besides, it is worth noting that the most common skateboarding trousers on the market come in a loose, straight fit (figure 4, *a*) on the top of the left side of the picture, which has the disadvantage of not being able to provide both fit and comfort when skateboarding. The same problem occurs with the regular fitted trousers (figure 4, *a*) at the bottom of the figure. Therefore, we divided the trousers into three types: tight (figure 4, *b*), fitted (figure 4, *c*) and slim (figure 4, *d*), as shown in the picture, and designed them with loose volume in the knee area of each of these three types of trousers. In addition, a detail worth paying attention to was that these three different levels of looseness of the trousers were designed to have different lengths of loose fit in the knee area, with the length of the loose fit decreasing from tight to slim (figure 4, *e*).

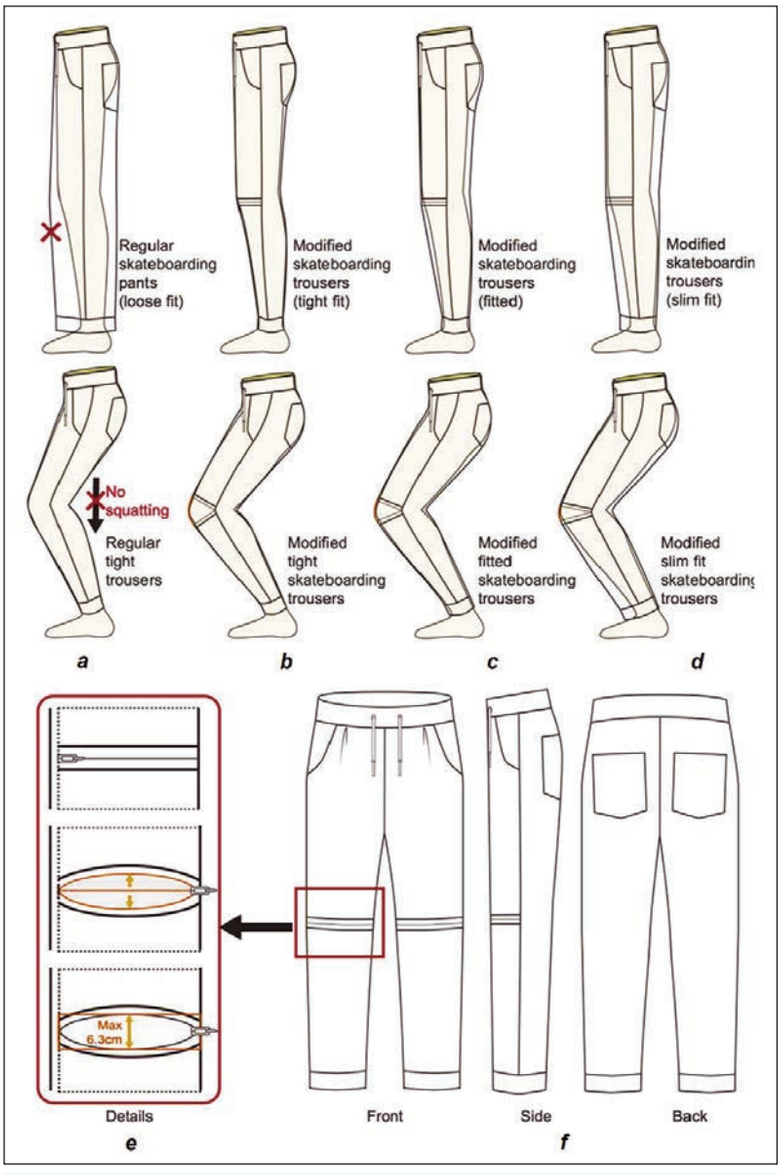


Fig. 4. Professional skateboard pants design: *a* – loose, straight fit; *b* – tight; *c* – fitted; *d* – slim; *e* – details; *f* – pant design

Based on the above data, it is concluded to design a professional skateboarding trouser as shown in figure 4, *f*. This professional sport trouser is a slim straight trouser skateboarding trouser in terms of style. Firstly, the waist is designed as an easily adjustable drawstring design. Secondly, it is designed with patch pockets at the hips as well as at the knees to thicken the wear-resistant design, and flap design at the trouser legs. Finally, the most important feature is that the knee loft is designed with an aesthetic zip-type invisible stitching design. As shown in figure 4, *e*, the maximum knee loft at the front midline is 6.3 cm, which is within the range of all the movements involved in the experiment.

Weirong et. al. [6] analysed the effect of different posture poses on the skin deformation of the lower limbs, and they pointed out that the change of the anterior midline of the knee was most obvious when the knee was bent. Meanwhile, Jeehye et.al. [5] analysed consumer needs through the functional design of sport-climbing trousers and pointed out that the flexible movement of the knee joint was one of the most important elements in the sport of rock climbing and the use of a three-dimensional design at the knee joints could enhance the wearing sensation of the trousers in the knee area. Based on our knowledge of skateboarding, it could be extended to sports such as yoga and rock climbing, which rely on the movement of the knee joints. Therefore, designing the looseness for the knee joint of skateboarding trousers would greatly enhance the amount of space in the knee joint and finally achieve a more comfortable sporting experience.

There were limitations of this study. The participants we recruited were non-professional skaters, and there was a lack of standardized movement. Meanwhile, we did not test the trouser's real performances. In future research, we will research movement charac-

terization for professional skaters. In addition, we will also use the research methodology in this paper to further produce real professional skateboarding trousers for functional testing.

## CONCLUSIONS

In summary, we have presented a new methodology for designing trousers. By analysing the kinematics of skateboarding, we have identified that the most significant change in knee joint action occurs. We then used the relationship equation between angle and skin stretch to determine the range of knee motion required for skateboarding. Finally, we determined the looseness design based on the collected range of motion data. We hypothesized that wearing this style of trousers would increase comfort while skateboarding. Additionally, this design methodology can be applied to the research of other activities such as yoga, rock climbing, and cycling, all requiring tight-fitting trousers.


## ACKNOWLEDGEMENT

Supported by Sichuan Science and Technology Program: 2021YJ0143.


## REFERENCES


[1] Shuman, K.M., Meyers, M.C., *Skateboarding injuries: An updated review. The Physician and Sports Medicine,* 2015, 43, 317–323, https://doi.org/10.1080/00913847.2015.1050953

[2] Determan, J.J., Frederick, E.C., Cox, J.S., Nevitt, M.N., *High impact forces in skateboarding landings affected by landing outcome*, In: Footwear Science, 2010, 2, 159–170, https://doi.org/10.1080/19424280.2010.525534

[3] Pham, B.T., *The biomechanics and energetics of skateboarding*, University of Colorado at Boulder

[4] Bianchini Wood, L., Oliveira, A., Santos, K., Rodacki, A., Lara, J., *3D Kinematic Analysis of the Ollie Maneuver on the Skateboard*, In: Apunts, 2020, 87–91, https://doi.org/10.5672/apunts.2014-0983.es.(2020/3).141.10

[5] Park, J., Chun, J., *Consumer's demands on functional design for sports climbing pants and product developments,* In: The Research Journal of the Costume Culture, 2017, 25, 391–404, https://doi.org/10.7741/RJCC.2017.25.3.391

[6] Wang, W., Cong, H., Dong, Z., Gao, Z., *Digital design model for weft-knitted seamless yoga pants based on skin deformation*, In: Journal of Engineered Fibers and Fabrics, 2021, 16, 155892502199050, https://doi.org/10.1177/1558925021990503

[7] Song, W., Ye, Y., Huiming, H., Chai, L., Chen, Z., *Improving ergonomic performance of work pants for delivery personnel based on skin deformation measurement*, In: Journal of Engineered Fibers and Fabrics, 2022, 17, 155892502211385, https://doi.org/10.1177/15589250221138546



**Authors:**

XIAO WEI, JIN ZHOU

Sichuan University, College of Biomass Science and Engineering, National Engineering Laboratory for Clean Technology of Leather Manufacture, Section of Chengdu No. 24 Southern Yihuan, 610065, Chengdu, China

**Corresponding author:**

JIN ZHOU

e-mail: zj_scu@scu.edu.cn

# Textile material-based grid structure for EM attenuation

DOI: 10.35530/IT.075.01.2022142

RALUCA MARIA AILENI DOINA TOMA

**ABSTRACT – REZUMAT**

**Textile material-based grid structure for EM attenuation**

*This paper presents several aspects concerning materials with potential applications for electromagnetic shields. For this objective, grid structures coated by ultrasound treatments in conductive polymeric dispersions were designed to obtain appropriate models for electromagnetic attenuation. To anticipate the potential use of these samples in EM shields, the samples were analysed to observe the values for electrical resistance.*

***Keywords:*** *textile, electromagnetic attenuation, resistance, conductive, EM shields*

**Material textil pe bază de structură tip reţea pentru atenuare EM**

*Această lucrare prezintă câteva aspecte privind materialele cu aplicaţii potenţiale pentru ecranare electromagnetică. Pentru realizarea acestui obiectiv, structurile tip reţea au fost tratate prin ultrasonare utilizând dispersii polimerice conductive concepute pentru a obţine modelele adecvate pentru atenuare electromagnetică. Pentru a anticipa potenţialul de utilizare a acestor probe în cadrul ecranelor EM, probele au fost analizate pentru a observa valorile rezistenței electrice.*

***Cuvinte-cheie****: textil, atenuare electromagnetică, rezistenţă, conductiv, ecran EM*

## INTRODUCTION

All electrical and electronic equipment are sources of electromagnetic disturbances so that they can cause problems for other electrical/electronic devices. Electrical interference can also affect them, which means they are receivers. In general, shielding systems are expensive and increase the weight of the equipment [1].

Electromagnetic inferences/disturbances and pulses affecting aircraft, medical equipment, navigational instruments and signalling systems are classified as health and safety hazards [1–3].

Familiar sources for electromagnetic pulses are radio, TV, radar equipment, power lines, electronic circuits, light intensity control devices, electric arc welding machines, electric motors, storms with electrical discharges and enormous solar flares, and weapons with electromagnetic pulses. The principal receivers (potential victims) are radio and TV receivers, home devices, computers, and phones. In general, sources and receivers have no problem as long as they are not connected, and by eliminating the coupling, protection against electromagnetic fields can be obtained [1–3].

The primary way to transmit the electromagnetic pulses can be obtained through [1]:

- Transmitted coupling path – electromagnetic disturbance travels through cables and pipes. The coupling can be inductive magnetic or capacitive electrical coupling [1–3].
- Radiated coupling path – the electromagnetic disturbance travels through the air as waves. Its energy is absorbed and generates a current flow in the receiving cable/pipe or the electronic equipment [1–3].

Electromagnetic protection can be achieved by electromagnetic attenuation through reflection. The electromagnetic wave represents the incident electromagnetic field that propagates in the direction of the screen, undergoes a reflection in contact with the screen and repeated internal reflections inside the screen, and part of the wave is also sent into the screened space. At low frequencies, magnetic materials can channel magnetic fields in a specific area of space [1, 2, 4–7].

Electromagnetic protection can be achieved by electromagnetic attenuation through absorption [1, 2].

At the incidence of an electromagnetic wave with a surface separating two media with different electrical properties – the first being free space and the second – the screen (textile surface with conductive or magnetic properties), the two components, the electric field and the magnetic field, transmitted to the screen, undergo changes that can be appreciated by comparing the surface impedances *Zs* of the two media [1–3].

$$Zs = E / H \quad (1)$$

where *H* is the magnetic field intensity and *E* is the electric field intensity.

For EM shielding, materials based on polymer matrices containing carbon, copper (Cu), nickel (Ni), aluminium (Al), iron, and carbon nanotubes (CNTs) as well as conductive polymers (e.g., PEDOT PSS –

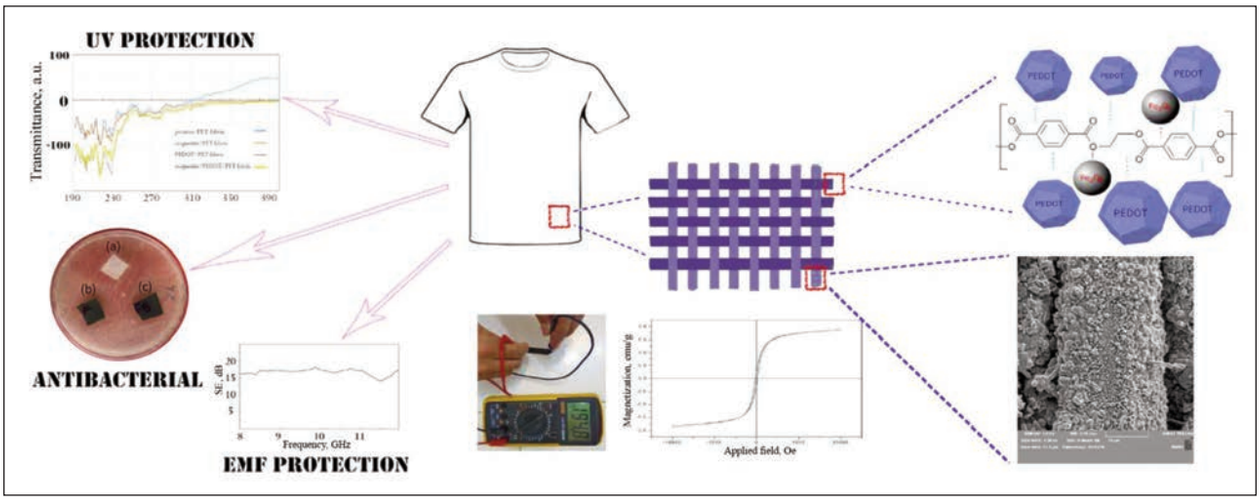


Fig. 1. Multifunctional fabric for electromagnetic shielding [11]

figure 1) are used. Other metals, such as platinum (Pt), gold (Au) and silver (Ag), are not recommended for this purpose because they are costly [7–9].

By incorporating conductive and magnetic textile materials, multifunctional, flexible and wearable substrates can be created. Some research has shown the use of magnetic nanoparticles with the PEDOT PSS polymer to create a superconductive fabric [3, 9–11].

## EXPERIMENTAL PART

During the research, 15 fabric samples with electroconductive properties were made based on ultrasound technology. A 100% cotton fabric (BBC) with the following characteristics was used to make the experimental samples:

- mass per surface unit 129.38 g/m$^2$;
- thickness 0.824 mm;
- density in the direction of the warp 60 threads/10 cm;
- density in the weft direction 70 threads/10 cm;
- elongation at break in the warp direction 6.13%;
- elongation at break in the weft direction 8.65%;
- water vapour permeability 31.3%;
- air permeability 3298 l/m$^2$/sec at a pressure of 100 Pa.

For the realization of the 15 experimental samples of fabrics, (A1 – A15) functionalized by treatment in dispersions based on microparticles of nickel (Ni), copper with a particle size smaller than 63 μm, or graphite, the technology of cleaning and deposition by ultrasound was used for 60–100 minutes.

Polyvinyl alcohol (PVA), polyvinylpyrrolidone (PVP), polyethylene glycol (PEG), gelatin, citric acid and metal microparticles of Cu and Ni, respectively graphite, were used to obtain electroconductive properties.

The samples were treated by ultrasound for 60–100 minutes in dispersions based on polymer matrices (PVA, PEG, PVP) and microparticles of Cu, Ni and graphite, followed by drying at a temperature of 170–180°C for 8–10 minutes (table 1).

Table 1 shows that only samples A5 and A6 have specific characteristics of conductive materials that can be used for electromagnetic shielding.

Table 2 shows the images obtained by electron microscopy (magnitude 60x) of fabrics A0 (without ultrasound treatment) and fabrics A1 – A15 functionalized by ultrasound in dispersions based on polymers (PVA, PEG, PVP) and microparticles of Cu, Ni or graphite.

## RESULTS AND DISCUSSION

In previous research to evaluate the attenuation of electromagnetic shields, the following specific equipment was used (from the INCDIE ICPE-CA endowment): coaxial cell model TEM 2000; oscilloscope Tektronix model MDO 3102; power amplifier Model SMX5; and signal generator type E8257D. The measurements were performed in the frequency range of 0.1 MHz – 1 GHz.

Analysing the experimental samples obtained for electromagnetic shielding, we observed that 2 representative samples (A5, A6) obtained by ultrasound present relevant characteristics for electromagnetic shielding such as electrical conductivity, and can lead to values of electromagnetic efficiency between 17 dB and 22.9 dB for low or high frequencies.

## CONCLUSIONS

In conclusion, by analysing experimental models A1 – A15, the following can be concluded:

- Experimental models A1 – A4 and A13 – A15 present values of surface electric resistance specific to antistatic materials and are not recommended for use in electromagnetic shielding systems because they do not shield electromagnetic radiation;
- The experimental models A7 – A12 present values specific to semiconductor materials that cannot conduct electric current and are not recommended for electromagnetic shielding;
- The experimental models A5 – A6 based on graphite microparticles can be used for electromagnetic shielding systems because they are conductive.

Table 1

EXPERIMENTAL SAMPLES FUNCTIONALIZED IN DISPERSIONS BASED ON POLYMER MATRICES CONTAINING MICROPARTICLES OF CU, NI OR GRAPHITE

| No. | PVA | PVP | PEG | Citric acid | $H_2O$ | Gelatin | Ni | Cu | Grafit | Al | Rs* (Ω) | Electroconductive property |
|---|---|---|---|---|---|---|---|---|---|---|---|---|
| A1 | x | x | | | x | | | x | | | $10^9$ | Antistatic |
| A2 | | x | x | | x | | | x | | | $10^8$ | Antistatic |
| A3 | x | x | | | x | | x | | | | $10^9$ | Antistatic |
| A4 | | x | x | | x | | x | | | | $10^8$ | Antistatic |
| A5 | x | x | | | x | | | | x | | $10^4$ | Conductive |
| A6 | | x | x | | x | | | | x | | $10^3$ | Conductive |
| A7 | | x | x | | x | x | x | | | | $10^6$ | Semiconductor |
| A8 | | | x | | x | x | x | | | | $10^7$ | Semiconductor |
| A9 | | | x | | x | x | | | x | | $10^7$ | Semiconductor |
| A10 | | x | x | | x | x | | | x | | $10^7$ | Semiconductor |
| A11 | | | x | | x | x | | x | | | $10^7$ | Semiconductor |
| A12 | | x | x | | x | x | | x | | | $10^7$ | Semiconductor |
| A13 | | x | x | x | x | x | | x | | | $10^9$ | Antistatic |
| A14 | | | x | x | x | x | | x | | | $10^9$ | Antistatic |
| A15 | | x | x | x | x | x | | x | | | $10^9$ | Antistatic |

Note: * Rs – surface electrical resistance.

Table 2

ANALYSIS OF THE SURFACE TOPOGRAPHY OF SAMPLES A0 – A15 BY DIGITAL ELECTRON MICROSCOPY WITH MAGNITUDE 60X

| A0 | A1 | A2 | A3 |
|---|---|---|---|
| 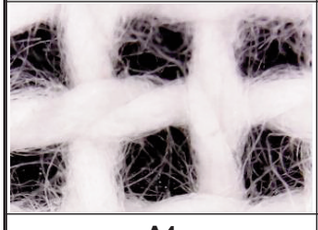 |  | 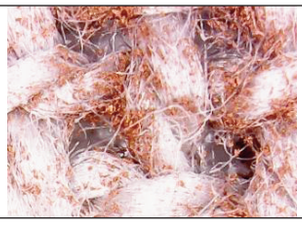 |  |
| **A4** | **A5** | **A6** | **A7** |
| 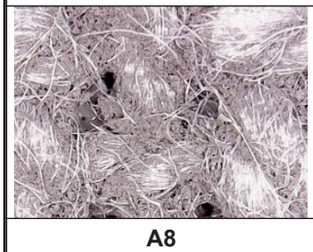 | 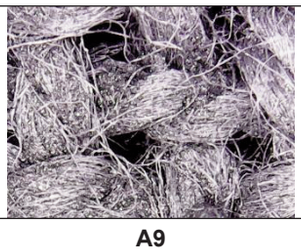 | 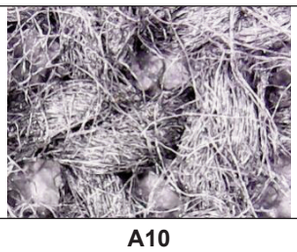 | 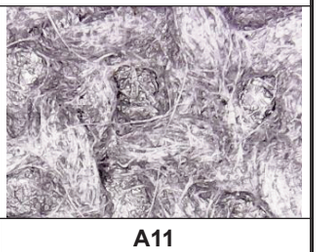 |
| **A8** | **A9** | **A10** | **A11** |
| 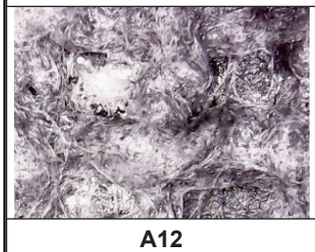 | 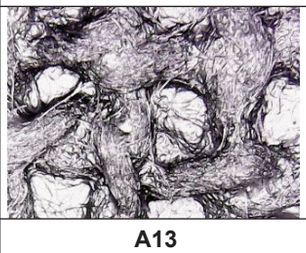 |  | 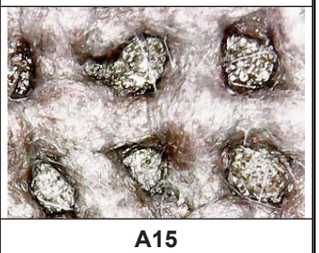 |
| **A12** | **A13** | **A14** | **A15** |
|  |  |  |  |

## ACKNOWLEDGEMENTS

The research presented in this paper was prepared in the INCDTP laboratories. Funds support this work from MCID, National Project “Electroconductive composite textile materials based on 3D polymer matrices for sensor systems for monitoring and attenuation of electromagnetic waves (3D ELECTROTEX)”, Grant Agreement PN 19 17 01 01.

## REFERENCES

[1] *Seals for electromagnetic shielding*, Available at: www.roxtec.com/ro/produse/tehnologii-inovatoare/emc-compatibilitate-electromagnetica [Accessed on September 2022]

[2] Salceanu, A., *Fundamente teoretice de compatibilitate electromagnetică*, Curs

[3] Stet, D., *Compatibilitate electromagnetica*, Note de curs

[4] Cătuţeanu, V., Iancu, O., *Materiale şi componente electronice*, E.D.P., 1972

[5] Ignea, A., *Introducere în compatibilitatea electromagnetică*, Editura de Vest, Timisoara, 1998

[6] Ignea, A., *Compatitilitate electromagnetică*, Editura de Vest, Timisoara, 2007

[7] Ignea, A., Mârza, E., De Sabata, A., *Antene si propagare*, Editura de Vest, Timisoara, 2002

[8] Sora, C., *Bazele electrotehnicii*, Editura Facla, Timisoara, 1983

[9] Nicolae, G., Ogruian N., P., Aciu, L., Mailat, A., *Sisteme de masura si metode pentru determinarea atenuarii campului electromagnetic in nanomateriale*

[10] Iosif, F.D., Costea, M.A., *Ecrane electromagnetice multistrat pentru aparatura electronica*, In: Electrotehnica, Electronica, Automatica, 2014, 62, 3, 96

[11] Sedighi, A., Montazer, M. and Mazinani, S., *Fabrication of electrically conductive superparamagnetic fabric with microwave attenuation, antibacterial properties and UV protection using PEDOT/magnetite nanoparticles*, In: Materials & Design, 2018, 160, 34-47

**Authors:**

RALUCA MARIA AILENI, DOINA TOMA

National Research & Development Institute for Textiles and Leather,
Lucretiu Patrascanu 16, 030508 Bucharest, Romania

**Corresponding author:**

RALUCA MARIA AILENI
e-mail: raluca.aileni@incdtp.ro

# A knitted smart sneaker system based on piezoresistive strain sensing for stride counting

DOI: 10.35530/IT.075.01.20232

HAN JIANLIN
RAJI RAFIU KING
CHEN YUAN
WANG WEIJUN

**ABSTRACT – REZUMAT**

**A knitted smart sneaker system based on piezoresistive strain sensing for stride counting**

*Currently, smart shoes are not as common as other wearable devices such as fitness trackers or smartwatches. However, with the continuous improvement in sensor and IOT technologies, it is expected that shoes with smart capabilities will catch up with the other popular wearables. The emergence of 3D knitting and its subsequent application in footwear manufacture has revolutionized the shoe manufacturing process. The use of knitwear allows for shoe parts such as the upper or the sole (insole, Strobel sole, midsole and/or outer sole) to be tailored with specific areas having different characteristics and providing different functions with low production effort. This study presents the design and manufacture of a knitted smart sneaker for cadence mensuration. The specified part of the sneaker is knitted with silver-plated polyester yarn to serve as a strain sensor. During the weight-bearing and release phases of the foot, while walking, this strain sensor is stressed and relaxed by this oscillatory phenomenon thus allowing footstep data to be measured. Stride estimate tests were carried out and the results established that strides taken by a user can accurately be correlated to the readings of the system. This study is the first to develop a smart shoe-sensing system where the sensor is inherently embedded within the shoe upper.*

***Keywords:*** *step counting, smart wear, knitting technology, strain sensor, textiles*

**Un sistem inteligent de încălțăminte sport tricotată bazat pe senzorul piezorezistiv al deformării pentru numărarea pașilor**

*În prezent, pantofii inteligenți nu sunt la fel de obișnuiți ca alte dispozitive portabile, cum ar fi trackerele de fitness sau ceasurile inteligente. Cu toate acestea, odată cu îmbunătățirea continuă a tehnologiilor senzorilor și IOT, este de așteptat ca pantofii cu capacități inteligente să ajungă din urmă celelalte dispozitive purtabile populare. Apariția tricotării 3D și aplicarea sa ulterioară în fabricarea de încălțăminte a revoluționat procesul de fabricare a pantofilor. Utilizarea tricotajelor permite ca părți ale încălțămintei, cum ar fi căptușeala sau talpa (brant, talpă Strobel, talpă intermediară și/sau talpă exterioară) să fie realizate cu zone specifice, având caracteristici diferite și oferind diferite funcții cu un efort de producție redus. Acest studiu prezintă proiectarea și fabricarea de încălțăminte sport inteligentă tricotată pentru măsurarea cadenței. Partea specificată a încălțămintei sport este tricotată cu fire de poliester acoperite cu argint pentru a servi drept senzor de tensiune. În timpul fazelor de susținere a greutății și de eliberare a piciorului în timpul mersului, acest senzor de tensiune este stresat și relaxat de acest fenomen oscilator, permițând astfel măsurarea datelor de pas. Au fost efectuate teste de estimare a pasului și rezultatele au stabilit că pașii făcuți de un utilizator pot fi corelați cu precizie la citirile sistemului. Acest studiu este primul care a dezvoltat un sistem inteligent de detectare a încălțămintei inteligente, în care senzorul este încorporat în mod inerent în căptușeală.*

***Cuvinte-cheie:*** *numărarea pașilor, încălţăminte inteligentă, tehnologie de tricotare, senzor de tensiune, textile*

## INTRODUCTION

According to anthropological evidence, the wearing of footwear began approximately 40,000 years ago [1]. From simple open-toe sandals in the early years, footwear has since evolved into more complex items of fashion. Footwear has been classified into different many categories. These include but are not limited to classes based on gender – ladies' and men's, occasion of wear – casual ladies' shoes, casual men's shoes, and type of activity – running shoes, etc. [2]. Other classifications include the type of material used such as leather shoes, and canvas shoes as well as age-based classes – children's shoes and adult shoes. There also exist sports shoe classes, such as a running shoe, basketball shoes, soccer shoes, American football shoes, baseball shoes tennis shoes etc. The terms sneakers/kicks/flats/trainers are also used to describe a certain category of shoes primarily designed for sports or other forms of physical exercise, but which are now also widely used for everyday casual wear. Conventionally, a shoe describes an item of footwear intended to protect and comfort the human foot. Shoes are also used as an item of decoration and fashion.

Generally, shoe manufacturing requires footwear uppers to be manufactured with multiple separate components, requiring multiple individual sub-assemblies and seams. The emergence of 3D knitting and

its subsequent application in footwear manufacture has however revolutionized the shoe manufacturing process. Flat-knitted shaped uppers refer to the upper which are produced by flat knitting machines [3]. A knitted shoe upper is advantageously devoid of any sewn seams and does not require any manual post process in terms of cutting or sewing to create the dimensional shape [4].

The developments in knitting technology allow products such as a shoe upper or a sole of a shoe, such as an insole, Strobel sole, midsole and/or outer sole to be embedded with different characteristics at specified areas to provide different functions with low production effort [5]. The embeddable properties may include bending, stretching, air and water permeability, thermal conductivity, thermal capacity, moisture absorption, static friction, abrasion resistance, hardness, thickness etc.

With the improvement in living standards, people have a higher demand for the comfort of sportswear, such as lightweight, functional and other decorative effects [6]. The shoe upper plays a wrapping and supporting role for the foot in the process of walking and sports. It not only helps to keep warm while also providing a guarantee of safety and stability [7].

Designing functionally adequate footwear requires an understanding of the dynamic biomechanical behaviour of the foot during locomotion [8]. Footwear manufacture using flat-knitted shaped uppers presents opportunities for the use of materials with excellent properties and also with a high degree of formability. Knitting is carried out with dyed yarns thereby requiring no dying of finished product and thus delivering plentiful colours and pattern structure variability. It also provides effective ways to minimize production complexities and times, cut back on environmental pollution [9] and improve product integrity have attracted massive research attention.

With the development of IOT technology, conventional articles are all equipped with smart functionalities, from chairs [10], beds [11], and caps [12] to underwear [13]. However smart shoes tend to lag in terms of volume and popularity among these smart device craze. Many smart shoe researches directed at physical activity monitoring however exist in the literature [14]. Nonetheless most if not all are based on insole sensing systems [15, 16]. Therefore to the best of our knowledge, this is the first smart shoe walking cadence monitoring system that is integral to the shoe itself rather than the insole or footwear attachments.

The main functionality of this proposed smart sneaker is stride counting. Even though similar functionalities have been referred to as step counting, the use of the term step counting is a misnomer as only one foot was engaged in the tests conducted. The measurement of step or stride counting is important for so many reasons. It has been scientifically proven that humans routinely alter their walking paces to adapt to functional goals and meet physical demands [17]. Studies have also hinted that damage to the central nervous system oftentimes results in irregular modulation of the pace of locomotion and increased risk of falls [17].

According to a study by [18], individuals who took 12,000 steps a day possess a 65% lower risk of dying compared to individuals who only took 4,000. Higher step counts were also linked with decreased rates of death from cardiovascular disease [19] and cancer [20]. These benefits were consistent across age, sex, and race groups. There is thus overwhelming evidence supporting the need for tracking steps taken as a means of goal setting and encouraging more people to take more steps considering its immense health benefits.

## EXPERIMENTAL

### Materials and methods

The STOLL CMS530 E7.2 computerized flat knitting machine was selected to produce the flat-knitted shaped uppers. Materials used for the sneaker upper include silver-plated yarns purchased from Qingdao Hengtong X-Silver Speciality Textile Company; nylon DTY and covered elastic yarn from Zhejiang Jinqi New Material Tech. Co., Ltd.; and connecting cables purchased online from Tmall.com (figure 1).


Fig. 1. Photos of: *a* – smart sneaker with connection cable; *b* – signal acquisition and processing unit

### Smart sneaker cadence system

The test interface is presented in figure 2; it is enabled with a panel to enter the type of test and signal display range and the electrical resistance of the sensor. There is also a start button, a pause/resume button and a replay button.

The software has the capability of automatically detecting the peak change in resistance over time, information which corresponds to a single step and is automatically recorded and saved in an Excel format strip-chart for further analysis. The smart sneaker connects to a signal processing unit (KTC electro-box) described in our previous studies [21, 22].

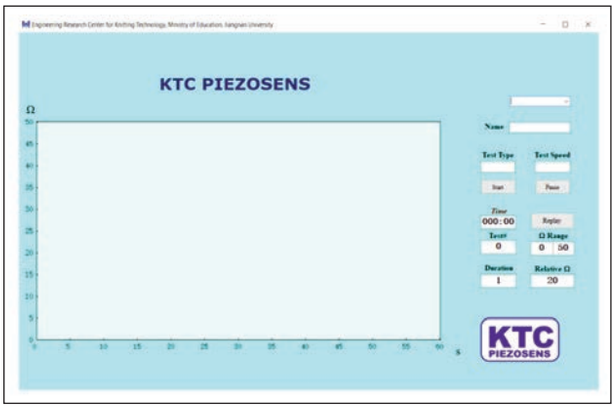


Fig. 2. Stride counting display interface

The system works such that deformation of the loop structures within the textile fabric (shoe upper) causes a change in resistance of the conductive section and is sensed by the basic circuitry in the electro-box. The indexes measured include steps per minute which is the number of steps taken per minute while walking corresponds to peaks shown in the interface.

### User trials – stride counting experiments

Stride count trials were carried out and compared with a wrist-worn fitness tracker. Three main walking activities were used namely normal walking, and walking up and down seven-tier stairs. With regards to normal walking activity step accumulation within an epoch of one minute was measured. With the stair climbing and descending, the counting was done when the volunteer reached the summit and the foot of the stairs respectively.

Stairs climbing has been associated with several health benefits [23] including boosting cardiovascular health by improving blood circulation and enhancing good cholesterol levels in the body. Likewise, stair climbing has the possibility of allowing the individual to attain their fitness goals without the need for any major equipment or special training.

## RESULTS AND DISCUSSIONS

The human foot acts in concert with the rest of the body during standing and movement. It provides man with his most effective physical contact with the environment and is especially responsible for the successful regulation of initial and final contact of the body with the ground.

Muscles, tendons, and ligaments run along the surfaces of the feet, allowing for the complex movements needed for motion and balance. During movement, the extensor digitorum brevis works in unison with other muscles to raise the toes off the ground when walking [24].

The human walking cycle can be partitioned into two main phases viz stance phase which occupies about 65% and swing phases – about 35–40% [25]. The stance phase (weight-bearing phase) is used to describe the period where the foot under consideration is in contact with the ground [26] while the swing phase in turn describes the period when the foot leaves the ground [27].

During the weight-bearing phase of ambulation, the sensor is stressed as the midfoot is flattened (instep girth expansion) [28] and therefore a change in resistance occurs. The swing phase which follows releases the stress on the sensor and so this recurrent action is used in computing the cadence of the user. From the wear tests carried out, it can be seen that the sneaker can satisfactorily estimate step counts over time.

The results of the three walking activities are shown in table 1. Within a time of 60 seconds and covering a distance of 43 meters, 28 strides were recorded during normal walking. Walking tests on seven-tier stairs were also carried out and within a time of 8 seconds, an average of 5 strides were recorded. The same values of 5 strides were recorded during the descent activity too.

The terms step counts or step accumulated per minute and cadence have been widely used interchangeably across literature over time. Both Dall et al. [29] and Stansfield et al. [30] however hint that this practice cannot be accurate. “True cadence” is the rate of stepping during the period of stepping. “Step accumulation” is the number of steps within an epoch of time (e.g. 1 minute) [29]. In the context of this manuscript, stride counts or stride accumulated per minute is most appropriate since only one foot was engaged in the tests conducted.

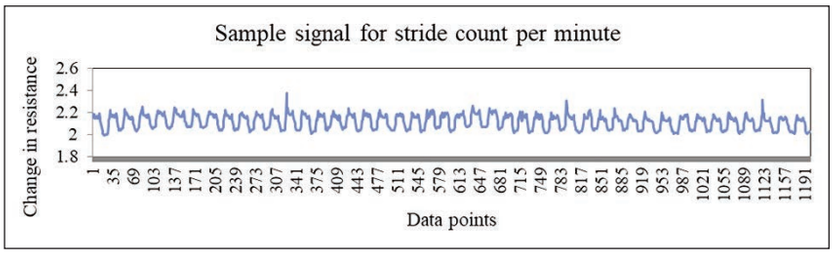


Fig. 3. Determination of strides from a sample walking data

Table 1

| STRIDE COUNTING ACTIVITIES AND RESULTS | | | | |
|---|---|---|---|---|
| **Walking activity** | **Number of steps** | | **Distance (m)** | **Time (s)** |
| | **AVG** | **SD** | | |
| Normal walking | 28 | 2.08 | 43 | 60 |
| Walking down stairs | 5 | 0.6 | 7 tier stairs | 8.0 |
| Walking up stairs | 5 | 0.6 | 7 tier stairs | 8.0 |

This is corroborated when an attempt was made to compare the step-counting results with the commercially available wristband activity tracker. Within the same walking activities over the same periods, the commercial tracker recorded what it describes as average step counts of 88 steps for normal walking and 8 steps for climbing and descending stairs respectively compared to our device's 28 and 5, 5 respectively. This has discouraged any attempt to compare the device's output with other devices as information on computation algorithms and mechanisms of the other devices are dissimilar and or not known.

### Sensing unit Repeatability / Stability / Durability / Aging

Sensor durability describes the capacity of flexible strain sensors to sustain steady electrical functionality and mechanical connection under long-term dynamic cyclic elongation cycles [31]. This property can also be referred to as stability in the short term, while it is described as ageing in the long term. Cronbach's alpha coefficient was thus applied to estimate these properties. By using four test results conducted within three weeks in the computation, high reliability was realized with normal walking accounting for $\alpha = 0.87$, $\alpha = 0.92$ for walking down the stairs and $\alpha = 0.88$ for stair climbing respectively.

## CONCLUSIONS

The study presented for the first time a shoe-based step counting system, where the sensor is inherently embedded in the shoe upper. The sneaker can measure stride count or stride accumulation per minute when tested using some walking activities.

The use of the term step counting is a misnomer as only one foot was engaged in the tests conducted. The authors therefore found no strong basis to compare the stride outcomes with wrist-worn or related activity trackers as there are disparities in mechanisms and the algorithms for these devices are also unknown.

## REFERENCES


[1] Trinkaus, E., Shang, H, *Anatomical evidence for the antiquity of human footwear: Tianyuan and Sunghir,* In: Journal of Archaeological Science, 2008, 35, 7, 1928–1933, https://doi.org/10.1016/j.jas.2007.12.002

[2] Nácher, B., Alemany, S., González, J., Alcántara, E., García-Hernández, J., Heras, S., Juan, A., *A Footwear Fit Classification Model Based on Anthropometric Data*, In: Proceedings of the 8th Annual Digital Human Modelling for Design and Engineering Symposium, 4–6th July 2006, Lyon; 2327 https://doi.org/10.4271/2006-01-2356

[3] Lu, Z., Jiang, G., Cong, H., Yang, X., *The Development of the Flat-Knitted Shaped Uppers based on Ergonomics,* In: Autex Research Journal, 2016, 16, 2, 67–74, https://doi.org/10.1515/aut-2015-0029

[4] Huffa, B., Huffa, C.M., *System and method for knitting shoe uppers*, U.P. Organization, Editor Huffa, Bruce (Encino, CA, US), Huffa, Concetta Maria (Encino, CA, US), USA, 2019, 1–2

[5] Stefan, T., Carl, A., James, C., *Knitted shoe upper*, USPTO, U.P. Organization, Editor adidas AG (Herzogenaurach, DE): United States of America, 2021, https://doi.org/US 20140310984 A1

[6] Özdil, N., et al., *Recent Developments in Textile Materials and Products Used for Activewear and Sportswear,* In: Tekstil Teknolojileri Elektronik Dergisi, 2014, 8, 3, 68–83

[7] Nishiwaki, T., *Requirement Properties and Materials Used in Sport Shoes*, In: Sen-i Gakkaishi, 2009, 65, https://doi.org/10.2115/fiber.65.P_150

[8] Price, C., Schmeltzpfenning, T., Nester, C.J., Brauner, T., *Chapter 3 - Foot and footwear biomechanics and gait*, Handbook of Footwear Design and Manufacture (Second Edition), A. Luximon, Editor Woodhead Publishing, 2021, 79–103, https://doi.org/10.1016/B978-0-12-821606-4.00013-2

[9] Tsai, W.-H., Jhong, S.-Y., *Production decision model with carbon tax for the knitted footwear industry under activity-based costing*, In: Journal of Cleaner Production, 2019, 207, 1150–1162, https://doi.org/10.1016/j.jclepro.2018.09.104

[10] Bujnowski, A., Kaczmarek, M., Wtorek, J., Osinski, K., Nieke, C., Birrer. E., *Respiratory signals derived from capacitive electrocardiogram on the smart chair*, In: 2020 13th International Conference on Human System Interaction (HSI), IEEE, 2020

[11] Hart, A., Tallevi, K., Wickland, D., Kearney, R.E., Cafazzo. J.A., *A contact-free respiration monitor for smart bed and ambulatory monitoring applications*, In: 2010 Annual International Conference of the IEEE Engineering in Medicine and Biology, IEEE, 2010

[12] Madanian, S., Airehrour, D., Kumar, N., Cherrington, M., *Smart cap for visually impaired in disaster situations*, In: Proceedings of the ISCRAM Asia Pacific, K.S.a.D. Bunker Editor, Wellington, New Zealand, 2018, 1–9

[13] Pacelli, M., Caldani, L., Paradiso. R., *Performances evaluation of piezoresistive fabric sensors as function of yarn structure*, In: 35th Annual International Conference of the IEEE EMBS, Osaka, Japan, IEEE Engineering in Medicine and Biology Society, 2013, https://doi.org/10.1109/EMBC.2013.6611044

[14] Drăgulinescu, A., Drăgulinescu, A.-M., Zincă, G., Bucur, D., Feieș, V., Neagu, D.-M., *Smart socks and in-shoe systems: state-of-the-art for two popular technologies for foot motion analysis, sports, and medical applications*, In: Sensors, 2020, 20, 15, 4316

[15] Wang, C., Kim, Y., Min, S.D., *Soft-Material-Based Smart Insoles for a Gait Monitoring System*, In: Materials, 2018, 11, 12, 2435

[16] Mohd Noor, A., *An Instrumented Insole System for Gait Monitoring and Analysis,* In: International Journal of Online Engineering (iJOE), 2014, 10, 30, https://doi.org/10.3991/ijoe.v10i6.3971

[17] Evans, E., Dass, M., Muter, W.M., Tuthill, C., Tan, A.Q., Trumbower, R.D., *A Wearable Mixed Reality Platform to Augment Overground Walking: A Feasibility Study*, In: Front Hum Neurosci., 2022, 16, 868074, https://doi.org/10.3389/fnhum.2022.868074

[18] Saint-Maurice, P.F., Troiano, R.P., Bassett, Jr., D.R., Graubard, B.I., Carlson, S.A., Shiroma, E.J., Fulton, J.E., Matthews, C.E., *Association of Daily Step Count and Step Intensity with Mortality Among US Adults*, In: Jama, 2020, 323, 12, 1151–1160, https://doi.org/10.1001/jama.2020.1382

[19] Nozoe, M., Mase, K., Takashima, S., Matsushita, K., Kouyama, Y., Hashizume, H., Kawasaki, Y., Uchiyama, Y., Yamamoto, N., Fukuda, Y., Domen, K., *Measurements of chest wall volume variation during tidal breathing in the supine and lateral positions in healthy subjects,* In: Respiratory Physiology & Neurobiology, 2014, 193, Supplement C, 38–42, https://doi.org/10.1016/j.resp.2013.12.016

[20] Koprowska, J., Ziaja, J., Janukiewicz, J., *Plasma metallization textiles as shields for electromagnetic fields*, In: International Symposium on Electromagnetic Compatibility, 2008

[21] Raji, R.K., Miao, X., Wan, A., Niu, L., Li, Y., Boakye, A., *Knitted piezoresistive smart chest band and its application for respiration patterns assessment,* In: Journal of Engineered Fibers and Fabrics, 2019, 14, 1–14, https://doi.org/10.1177/1558925019868474

[22] Raji, R.K., Miao, X. Wan, A., Niu, L., Li, Y., Boakye, A., *Design and Fabrication of Smart Bandeau Bra for Breathing Pattern Measurement*, In: Future Technologies Conference, 2019, K. Arai, Editor, Springer International Publishing: San Francisco, 2020, 40–48, https://doi.org/10.1007/978-3-030-32523-7_3

[23] Sendić, G., *Extensor digitorum brevis muscle*, In: Anatomy Histology, A. Rad Editor, Germany, 2022

[24] Brunelli, A., *Postmus PE. 26 – Preoperative Functional Evaluation of the Surgical Candidate,* In: Pass, H.I., Ball, D., Scagliotti, G.V., editors, IASLC Thoracic Oncology (Second Edition), Philadelphia: Elsevier, 2018, 265-73.e3

[25] Senthilkumar, M., et al., *Elastane fabrics – A tool for stretch applications in sports,* In: Indian Journal of Fibre and Textile Research, 2011, 36, 3, 300–307

[26] De Groote, A., Paiva, M., Verbandt, Y., *Mathematical assessment of qualitative diagnostic calibration for respiratory inductive plethysmography*, In: Journal of Applied Physiology, 2001, 90, 3, 1025-1030

[27] Webster, J.B., Darter, B.J., *4 – Principles of Normal and Pathologic Gait*, In: Atlas of Orthoses and Assistive Devices (Fifth Edition), J.B. Webster and D.P. Murphy, Editors, Elsevier: Philadelphia, 2019, 49-62.e1

[28] Zhang, L., Yick, K.-l., Li, P.-l., Yip, J., Ng, S.-p., *Foot deformation analysis with different load-bearing conditions to enhance diabetic footwear designs,* In: Plos one, 2022, 17, 3, e0264233

[29] Dall, P.M., et al., *Step accumulation per minute epoch is not the same as cadence for free-living adults,* In: Med Sci Sports Exerc., 2013, 45, 10, 1995–2001

[30] Stansfield, B., et al., *True cadence and step accumulation are not equivalent: the effect of intermittent claudication on free-living cadence,* In: Gait Posture, 2015, 41, 2, 414–419, https://doi.org/10.1016/j.gaitpost.2014.11.002

[31] Li, M., Pei, Y., Cao, Y., Chen, S., Guo, X., *Flexible strain sensors: from devices to array integration,* In: Flexible and Printed Electronics, 2021, 6, 4, 043002

[32] Raji, R.K., Miao, X., Zhang, S., Li, Y., Wan, A., *Influence of Rib Structure and Elastic Yarn Type Variations on Textile Piezoresistive Strain Sensor Characteristics,* In: Fibers & Textiles in Eastern Europe, 2018, 26, 5, 24–31

**Authors:**

HAN JIANLIN[1], RAJI RAFIU KING[1], CHEN YUAN[1], WANG WEIJUN[2]

[1]Guangdong Provincial Key Laboratory of Electronic Functional Materials and Devices, Huizhou University, Huizhou City, 516001, Guangdong Province, China
e-mail: 525586813@qq.com

[2]Department of Clothing Engineering, Hebei Vocational University of Technology & Engineering, Xingtai, 054035, Hebei Province, China
e-mail: 448099547@qq.com

**Corresponding author:**

RAJI RAFIU KING
e-mail: mrkingraji@outlook.com

# Testing and characterization of high-temperature degradation performance of para-aramid fibres

DOI: 10.35530/IT.075.01.2023115

CHUNYAN ZHU
YANPING LIN
XIANGAI ZHANG
CHEN YANG

**ABSTRACT – REZUMAT**

**Testing and characterization of high-temperature degradation performance of para-aramid fibres**

*Para-aramid fibres possess excellent properties, including high modulus, high strength, and high-temperature resistance, making them highly practical and cost-effective reinforcement materials. To further analyse the usage performance of para-aramid fibres under extreme conditions and explore their degradation behaviour and mechanisms at high temperatures, this paper investigates para-aramid fibres through high-temperature annealing. Various tests, including thermogravimetric analysis, infrared spectroscopy, X-ray diffraction, Ubbelohde viscometry, and universal material testing, were employed to analyse changes in the thermal degradation temperature, molecular structure, and mechanical properties of para-aramid fibres. Tests have shown that after high-temperature treatment of para-aramid fibres, different protruding particles and pits appear on the surface of the fibres, and the molecular structure gradually undergoes cleavage and cross-linking. This results in varying degrees of increase in the crystallinity, intrinsic viscosity, and apparent grain size of crystal planes in different directions of the para-aramid fibres with rising temperatures. On the other hand, the degree of orientation, the rate of the second type of lattice distortion, thermal performance, and mechanical properties show a declining trend. The thermal degradation conforms to the kinetics of a second-order reaction.*

***Keywords:*** *microscopic morphology, viscosity, activation energy, mechanical properties, mechanism, molecular structure, para-aramid, thermal degradation*

**Testarea și caracterizarea performanței de degradare la temperatură înaltă a fibrelor para-aramidice**

*Fibrele para-aramidice posedă proprietăți excelente, inclusiv modul înalt, rezistență ridicată și rezistență la temperatură ridicată, făcându-le materiale de armare extrem de practice și rentabile. Pentru a analiza în continuare performanța de utilizare a fibrelor para-aramidice în condiții extreme și pentru a explora comportamentul și mecanismele de degradare ale acestora la temperaturi ridicate, această lucrare investighează fibrele para-aramidice prin tratament la temperatură înaltă. Diverse teste, inclusiv analiza termogravimetrică, spectroscopie în infraroșu, difracția de raze X, vâscozimetria Ubbelohde și testarea universală a materialelor, au fost utilizate pentru a analiza modificările temperaturii de degradare termică, structurii moleculare și proprietăților mecanice ale fibrelor para-aramidice. Testele au arătat că, după tratamentul la temperatură înaltă a fibrelor para-aramidice, pe suprafața fibrelor apar diferite particule proeminente și orificii, iar structura moleculară suferă treptat scindare și reticulare. Acest lucru are ca rezultat grade diferite de creștere a cristalinității, a vâscozității intrinseci și a mărimii aparente a granulelor planurilor cristalografice în diferite direcții ale fibrelor para-aramidice odată cu creșterea temperaturii. Pe de altă parte, gradul de orientare, rata celui de-al doilea tip de distorsiune a rețelei, performanța termică și proprietățile mecanice arată o tendință de scădere. Degradarea termică se conformează cineticii unei reacții de ordinul doi.*

***Cuvinte-cheie:*** *morfologie microscopică, viscozitate, energie de activare, proprietăți mecanice, mecanism, structura moleculară, para-aramidic, degradare termică*

## INTRODUCTION

This experimental study focuses on para-aramid fibres produced by Shengma Corporation in Pingdingshan, China. The research investigates the molecular structure, thermal, and mechanical property changes of these fibres after baking at temperatures of 20°C, 200°C, 350°C, and 500°C for 50 minutes. The study aims to analyse the influence of high-temperature treatment on the physicochemical degradation performance of para-aramid fibres and explore the high-temperature degradation mechanisms of these fibres. As widely recognized, the chemical name of para-aramid fibre is “Poly-p-phenylene terephthalamide”, abbreviated as PPTA. Its chemical structure consists of para-linked benzene amide units, with the benzene rings and amide bonds forming an π-conjugated structure. The macromolecular configuration is characterized by an axially extended chain, a cross-linked network, and a high degree of internal rotation. The regular molecular arrangement, along with high crystallinity and orientation, imparts para-aramid fibres with high strength, high modulus, acid and alkali resistance, and high-temperature resistance [1–3]. These fibres find extensive applications in advanced fields such as

industrial reinforcement, papermaking, aerospace, and defence industries [4–6].

In recent years, with the expansion of para-aramid fibre applications and their increased use across various industries, research on the performance of para-aramid fibres has become increasingly profound. Given that para-aramid fibres are predominantly used in high-temperature environments, studying their thermal degradation behaviour has become imperative. In 1977, Brown et al. used DTA, TG, and TMA techniques to evaluate the high-temperature resistance of Kevlar® fibres. Tests showed that the degree of oxidation reaction in Kevlar® fibres was more severe than their high-temperature resistance [7]. In 1982, Brown and Power used pyrolysis/gas chromatography-mass spectrometry to test the thermal degradation of Kevlar® fibres in the 300–700°C range analysed the degradation products at each temperature range and explained the thermal degradation mechanism [8, 9]. In the same year, Power studied the thermal degradation of aromatic polyamide Kevlar® fibres in air and vacuum using electron spin resonance spectroscopy. The results showed that the presence of oxygen reduced the stability of Kevlar® fibres, causing the aromatic NH and amide NH-CO bonds in Kevlar® fibres to break in the initial stage of thermal degradation. Subsequent stages of thermal degradation confirmed that the participation of oxygen led to an increase in the free radical g-factor, with oxygen acting as a substituent functional group, integrating into the aromatic polyamide, and leading to the detachment of oxygen-containing structural units in the course of homolytic reactions, thus completing thermo-oxidative degradation [10]. In 1982, YP Khanna and others tested the thermal stability, thermal form stability, and thermal transition properties of substituted and unsubstituted aromatic polyamides. The results showed that the exothermic temperature range of polyamides was concentrated between 630–700°C, and although substituents reduced the thermal stability of Kevlar® fibres, they improved their thermo-oxidative stability [11]. In 1984, Wu tested the solubility, intrinsic viscosity, modulus, and strength of para-aramid fibres after heat treatment, concluding that the degradation of para-aramid fibres was due to branching and crosslinking between molecules in the fibres [12]. In 1989, Hindeleh et al. studied the effect of thermal ageing and degradation on the microstructure of Kevlar® fibres. Tests showed that the crystallinity of Kevlar® fibres decreased with temperature, being 75.5% at 350°C and 51% at 500°C. The microcrystalline size remained constant before 250°C and then decreased. TGA tests showed that mass loss intensified with increasing dimensions, with about 1% loss at 350°C, 3.9% at 450°C, and 20.4% at 657°C [13].

In 1994, Zhang tested the physicochemical property changes of para-aramid fibres during pyrolysis. The fibres were heated to 300–710 °C in flowing nitrogen and static air and maintained for 10–30 seconds.

Tests showed that the skin-core structure, mechanical properties, and degree of crystal structure damage in para-aramid fibres all intensified with increasing temperature, and the damage to para-aramid fibres in high-temperature oxygen was greater than in a nitrogen atmosphere [14]. In 2000, Yue et al. analysed the effect of 2–8 hours of heat treatment at 100–300°C on the mechanical properties of Kevlar® yarns. Tests showed that the tensile stress and strength of Kevlar® yarns decreased with increasing temperature, while research by Iyer et al. indicated that the duration of heating at a constant temperature had little effect on the tensile strain and strength of para-aramid fibres [15, 16]. In 2004, James et al. used TG and SCS techniques to test the compressive properties of heat-treated Kevlar® fibres, characterizing the relationship between hydrogen bond breakage, crosslinking, and fibre compressibility, and used Fourier-transform infrared spectroscopy to describe the crosslinking of the cortex and hydrogen bond breakage in the core of para-aramid fibres at 400°C, 440°C, and 470°C [17]. In 2008, Xinwei et al. used TGA-DTA/MS to test the thermal degradation of para-aramid fibres under different atmospheric conditions. The results showed that the thermal degradation of para-aramid fibres in argon was endothermic, while in air it was exothermic [18]. In 2010, Renqin et al. tested the thermal degradation of Kevlar® fibres in an inert atmosphere and at different heating rates, concluding that the activation energy of thermal decomposition of Kevlar® fibres was 210.93 KJ/mol, and the reaction order of thermal decomposition kinetics was first-order [19]. In 2014, Fang-Long et al. conducted thermogravimetric analysis and differential thermal analysis of polysulfone aramid fibres in nitrogen and air atmospheres, showing that at a heating rate of 10 K/min, the initial degradation temperature was 375°C in nitrogen and 410°C in air. When the temperature reached 800°C, the fibres lost all their mass in the air. The differential thermogravimetric curve showed two distinct exothermic peaks, leading to the conclusion that the degradation of polysulfone aramid occurred in a two-step process [20]. In 2019, Naveen et al. used hand lay-up and hot-pressing methods to make composites of different ratios using Kevlar 29 (K) and Cocos nucifera sheath (CNS) as materials. Tests showed that when the ratio of Kevlar 29 (K) and Cocos nucifera sheath (CNS) was 75/25, the composite had better rigidity, thermal stability, and renewability [21]. However, current research on heat treatment of para-aramid fibres is extensive, but the process of changes in the surface functional groups of para-aramid fibres after heat treatment is not clear, and the specific process of increased oxygen content on the fibre surface after heat treatment is also not clear. Therefore, investigating the thermal oxidation behaviour of para-aramid fibres, characterizing changes in their surface groups during heat treatment, and understanding the conditions of thermal oxidation treatment are of paramount importance.

Through this study, we can further delve into the impact of molecular structural changes in para-aramid fibres under different temperature conditions

on their thermal and mechanical properties. This research provides valuable insights into the high-temperature degradation mechanisms of para-aramid fibres and offers a reference for their further development and utilization.

## EXPERIMENTAL SECTION

### Materials and instruments

Materials: Para-aramid fibres (linear density: 70 tex/187f), supplied by Shennong Company, Pingdingshan, China; Potassium bromide (analytical grade), purchased from Hongyan Chemical Reagent Factory, Tianjin, China.

Instruments: SU3500 Scanning Electron Microscope (Hitachi High-Tech, Shanghai, China); Universal Material Testing Machine (INSTRON 5590), manufactured by Instron Corporation, USA; Thermogravimetric Analyzer (TG/DTG-DSC, TG209F3), supplied by NETZSCH Scientific Instruments Trading (Shanghai) Co., Ltd.; Electronic Analytical Balance (FA3004), provided by Shanghai Yanfeng Electronic Technology Co., Ltd.; Constant Temperature and Humidity Test Chamber (KSD-TH-80L), manufactured by Dongguan Keiside Testing Instrument Co., Ltd.; Tabletop Forced Air Drying Oven (DHG-9035A), manufactured by Wuhan Lihui Environmental Detection Equipment Co., Ltd.; High-Temperature Muffle Furnace (YB-1700A), supplied by Luoyang Bolaimante Test Electric Furnace Co., Ltd.; Ubbelohde Viscometer (1833), manufactured by Qianbo Teaching Instruments Co., Ltd., Tianchang, China; Fourier Transform Infrared Spectrometer (FT-IR, Nicolet iS10), distributed by YuNuo Industry (Shanghai) Co., Ltd.; X-ray Diffractometer (XRD, XRD-7000S), provided by Shimadzu (China) Management Co., Ltd.

### Sample preparation

*Sample treatment*

Para-aramid fibre samples were placed in a muffle furnace and heated for 50 minutes at temperatures of 20°C, 200°C, 350°C, and 500°C.

*Performance testing and characterization*

Characteristic viscosity testing

A certain amount of para-aramid fibre, both before and after high-temperature treatment, was placed in a forced air drying oven at 110°C for 5 hours. After removal, it was dissolved in a concentrated sulfuric acid solution with a mass fraction of 98%, resulting in a concentration of 0.05 g/dl for para-aramid sulfuric acid solution. The relative viscosity of the dissolved sulfuric acid solution was measured using a Ubbelohde viscometer, and the characteristic viscosity of para-aramid fibres before and after high-temperature treatment was calculated following reference [3].

FT-IR Testing

Para-aramid fibres, both before and after high-temperature treatment, were crushed into powder and then mixed with potassium bromide before being pressed into sample pellets. The FT-IR spectra were recorded at a resolution of 4 $cm^{-1}$ in the range of 4000 to 400 $cm^{-1}$, with 36 scans per sample. FT-IR testing was conducted to analyse the structure of para-aramid fibres.

Crystalline structural property testing

XRD testing was performed to investigate the crystalline structural properties of para-aramid fibre samples. Using Cu target, Kα radiation with a wavelength of 0.1541 nm, voltage of 40 kV, and current of 40 mA, diffraction scans of the meridian and equatorial lines of para-aramid samples were conducted in transmission mode. The orientation diffraction scan was carried out at 2θ = 22.8° corresponding to the 200 crystal plane of para-aramid samples, with a scanning angle range from 5 to 45 degrees. The measured diffraction curve parameters were corrected for factors such as absorption, angle factors, polarization, and scattering, following reference [22], and used for the calculation of crystalline structural parameters. Data obtained from the tests were subjected to peak fitting using the Gauss+Lor Area function and analysed based on equation 1 following reference [23] to calculate the crystallinity of para-aramid fibre samples.

$$X_d = \left[1 - \frac{S_a}{S_a + S_{cr}}\right] \times 100\% \quad (1)$$

In the equations below, $X_d$ represents the crystallinity of para-aramid fibre samples. $S_a$ denotes the area of the amorphous diffraction peak (corresponding to 2θ = 21°) in para-aramid fibre samples. $S_{cr}$ refers to the area of the crystalline diffraction peaks (corresponding to the peaks at 110, 200, and 002) in para-aramid fibre samples.

For the meridional (002) diffraction scan of para-aramid fibre samples, Gaussian functions were selected for peak fitting. The apparent grain size of para-aramid fibre samples was calculated according to Scherer's formula (equation 2) [24].

Simultaneously, peak fitting was performed for the diffraction peaks at 002, 004, and 006 crystallographic planes, and based on equations 2 and 3 references, the second-class lattice distortion parameters for para-aramid fibre samples were calculated.

$$L = \frac{k\lambda}{\beta \cos\theta} \quad (2)$$

$$G = \sqrt{\frac{d}{360\lambda}} \times \sqrt{\frac{\Delta(\beta\cos\theta)}{\Delta h^2}} \quad (3)$$

In the equations below, $L$ is the apparent grain size of para-aramid fibre samples, $\theta$ – the Bragg angle (°), $\beta$ – the half-width of the diffraction peak (calculated in radians and then substituted into the formula), $\lambda$ – the wavelength of the incident beam in the diffractometer ($\lambda$ = 0.154 nm), k – the Scherrer constant (k = 0.89) and $d$ – the crystal cell parameter along the fibre axis direction ($d$ = 1.29 nm).

TG/DTG-DSC testing

Para-aramid fibre samples underwent TG/DTG-DSC curve testing, with nitrogen gas flowing at a rate of 60–70 mL/min to create a protective atmosphere. The heating rate was set to 20°C/min.

Mechanical property testing

Referring to the American material standard ASTM D885-2010A, the para-aramid long filaments were twisted to 60 twists/meter. A constant temperature and humidity test chamber was set to the standard environment (20°C, 65% relative humidity) for humidity conditioning for 24 hours. Then, using a universal material testing machine with a clamp length of 250 mm and a stretching speed of 120 mm/min, the breaking strength and elongation at the break of the para-aramid long filament samples were tested (for each temperature point, 30 sets of degradation samples were tested).

## RESULTS AND DISCUSSION

### Microscopic morphological analysis

Scanning electron microscope (SEM) images of para-aramid fibre's microscopic morphology are shown in figure 1. From the SEM images, it can be observed that before reaching 350°C, the surface of para-aramid fibres is smooth and clean, with relatively high reflectivity. After treatment at 500°C, the surface of para-aramid fibres exhibits granular protrusions and a minimal number of pits. This indicates that the fibre surface undergoes oxidation to varying degrees due to the influence of high-temperature treatment. It can be seen that after heat treatment, the surface friction coefficient of para-aramid fibres increases, which can effectively enhance the binding force of the fibres, making it easier to use para-aramid fibres in the weaving of special garments such as firefighting suits and bulletproof vests. Additionally, the increase in the specific surface area of para-aramid fibres improves their dyeability to a certain extent.

### Thermal property analysis

The thermal property test curves for para-aramid fibres are shown in figure 2. Observing the trends of the four DSC-TG curves in figure 2, it can be seen that the overall heating process can be divided into three stages. The first stage occurs between room temperature and 150°C, where the mass loss is primarily due to the evaporation of free water, bound water, and molecular crystalline water within the fibres. This stage is characterized by an endothermic peak, corroborating the absorption of moisture evaporation. The second stage, occurring between 200°C and 500°C, exhibits a slight decrease in fibre mass, indicating that the temperatures within this range are insufficient to cause significant degradation of the para-aramid fibre's internal molecular chains. Combining the results from table 1, which includes characteristic viscosity and dissolution characteristics of para-aramid fibre samples, it can be observed that the characteristic viscosity of para-aramid fibres remains relatively stable up to 200°C, with minor changes as the processing temperature increases. At 350°C, partial solubility is observed, resulting in a decrease in characteristic viscosity. This is mainly due to the initial reduction in characteristic viscosity resulting from the thermal oxidative degradation of

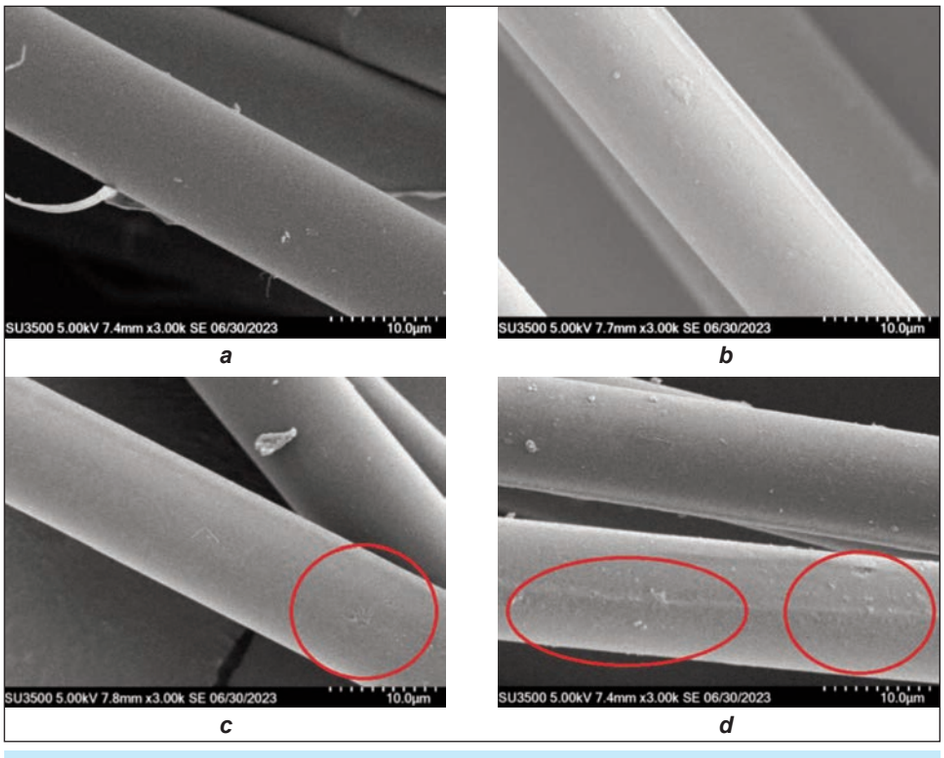


Fig. 1. Scanning electron microscope images of para-aramid fibre's microscopic morphology: *a* – 20°C; *b* – 200°C; *c* – 350°C; *d* – 500°C

molecular chain segments in para-aramid fibres. The appearance of partial solubility and insolubility at this point is attributed to the cross-linking reactions occurring in the molecular chain segments of para-aramid fibres. According to Downing and Newell [17], at temperatures below 350°C, thermal-oxidative degradation and molecular cross-linking reactions have a minimal impact on the characteristic viscosity of para-aramid fibres. However, when the temperature surpasses 350°C, para-aramid fibres exhibit varying degrees of thermal oxidative degradation and molecular cross-linking reactions. With increasing temperature, the proportion of cross-linking reactions becomes more prominent.

Referring to the DSC-TG curves for the second stage (200–500°C), it can be observed that, while para-aramid fibres undergo thermal oxidative degradation and molecular cross-linking within their internal molecular chains, the magnitude of these effects is relatively small. This indicates that a significant amount of fibre molecular chain segments remain intact and unlinked, thus preserving the fibre's properties. This will be further confirmed in subsequent sections through infrared spectroscopy and mechanical property testing. The third stage, occurring above 500°C, exhibits a substantial reduction in mass for para-aramid fibres, accompanied by a significant endothermic peak. During this stage, extensive chain fragmentation and cross-linking reactions occur within the para-aramid fibre's molecular chain segments, ultimately leading to carbonization.

Based on the DSC-TG curves, the rate of mass loss ($\alpha$) for para-aramid fibre samples at any time $t$ can be determined. By substituting this rate into the Arrhenius equation, the thermal degradation kinetic equation (equation 4) for para-aramid fibre samples can be obtained:

$$\frac{d\alpha}{dt} = A\,e^{-E/RT} f(\alpha) = A\,e^{-E/RT}(1-\alpha)^n \qquad (4)$$

In the equations below, $E$ is the activation energy of para-aramid fibre samples, $A$ – the frequency factor, $R$ – the gas constant, $T$ – the absolute temperature, and $n$ – the reaction order.

In the DSC-TG experiments, the heating rate (experiment parameter setting) $\beta = dT/dt$ can be substituted into equation 4, simplifying it into equation 5:

$$\frac{d\alpha}{dt} = \frac{A}{\beta} e^{-E/RT} f(\alpha) = \frac{A}{\beta} e^{-E/RT}(1-\alpha)^n \qquad (5)$$

By integrating both sides of equation 5, when $n \neq 1$, equation 6 can be derived:

$$\ln\left[\frac{1-(1-\alpha)^n}{T^2(1-n)}\right] = \ln\left[\frac{AR}{\beta E}\left(1-\frac{2RT}{E}\right)\right] - \frac{E}{ER} \qquad (6)$$

When $n = 1$, formula 7 can be obtained:

$$\ln\left[\frac{-(1-\alpha)^n}{T^2}\right] = \ln\left[\frac{AR}{\beta E}\left(1-\frac{2RT}{E}\right)\right] - \frac{E}{ER} \qquad (7)$$

For typical reaction temperature ranges and activation energies, $RT/E$ is much smaller than 1. In other words, $(1-2RT/E)$ can be approximated as 1. By selecting an appropriate reaction order $n$ that satisfies the reaction kinetics, a linear approximation can be obtained by plotting $1/T$ on the left side. If it matches the reaction order, an approximate straight line can be drawn. The slope of this line corresponds to $-E/R$. The intercept on the vertical axis represents $\ln(AR/\beta E)$. Using this information, the activation energy $E$ can be calculated, as shown in table 1. The calculated activation energy values for para-aramid fibre samples align with the reported range of 42.0 to 57.8 kJ/mol in the literature [25, 26]. Within this range, an $n$ value of 2 is determined, indicating that the thermal degradation of para-aramid fibres follows second-order reaction kinetics.

Further observation of the TG curves in the four DSC-TG plots shows that the weight of the para-aramid fibres treated at high temperatures decreases at 1100°C compared to 20°C, to varying degrees. This is due to the thermal oxygen degradation and molecular crosslinking reactions exhibited by the para-aramid fibres after high-temperature treatment. With the increase in temperature, there is a transition from thermal oxygen degradation of molecular chain segments to molecular crosslinking reactions, leading to a declining trend in the orientation degree of the molecular structure, showing a disorientation trend. The non-crystalline regions are further opened up (this part is verified in the subsequent molecular structure section), exacerbating the thermal loss of fibre mass.

## Molecular structure analysis

The curves related to molecular structure analysis are shown in figure 3. The infrared spectroscopy curve of para-aramid fibre samples is presented in figure 3, *a*). According to reference [27], the thermal decomposition of para-aramid fibre occurs through uninitiated decomposition, with the main molecular chain segments undergoing decomposition on the main chain. This involves the C-O bonds and C-N bonds of the amide groups, as well as C (aromatic

Table 1

TEST RESULTS FOR CHARACTERISTIC VISCOSITY, DISSOLUTION CHARACTERISTICS, AND ACTIVATION ENERGY OF PARA-ARAMID FIBRE SAMPLES

| Test parameters | Temperature (°C) | | | |
|---|---|---|---|---|
| | 20 | 200 | 350 | 500 |
| Inherent viscosity (dl·g$^{-1}$) | 7.189 | 7.211 | Slightly insoluble | Partially insoluble |
| Activation energy, $E$ (kJ·mol$^{-1}$) | 49.42 | 49.13 | 48.94 | 48.55 |

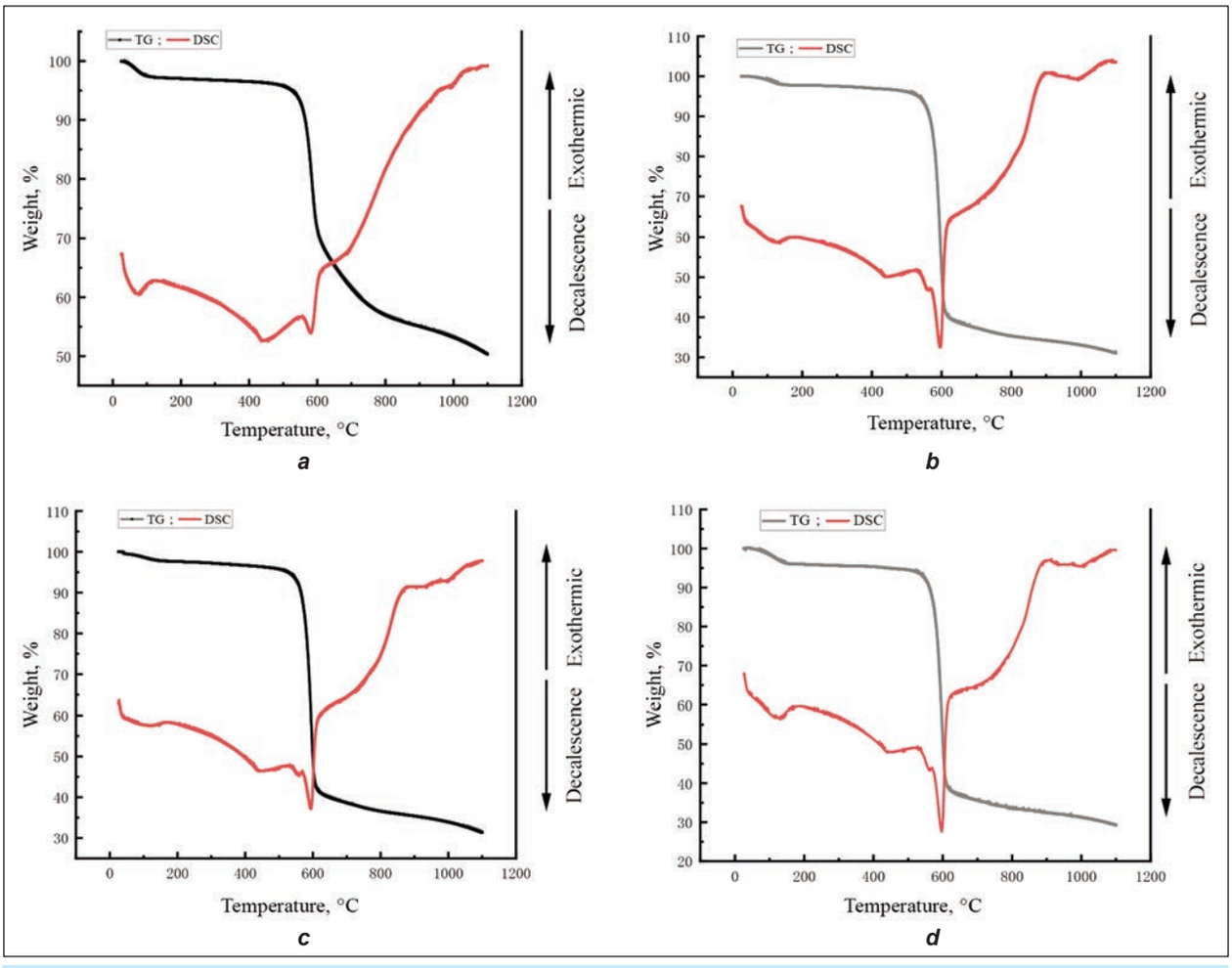


Fig. 2. Thermal properties testing curve of para-aramid fibre: *a* – 20°C; *b* – 200°C; *c* – 350°C; *d* – 500°C

ring) -C (carboxyl), C (aromatic ring) -N. At 20°C, within the range of 3325–3025 $cm^{-1}$ corresponding to the aromatic groups, there is no significant change in absorption peaks. However, the infrared spectroscopy curves at 200°C, 350°C, and 500°C exhibit slight variations in absorption peaks, indicating a slight fragmentation of the aromatic groups due to the electronic shift of N-H and the weakening of hydrogen bonds upon temperature treatment.

The characteristic peaks, such as the amide I band at 1640 $cm^{-1}$, the amide II band at 1540 $cm^{-1}$, the amide III bands at 1260 $cm^{-1}$, 650 $cm^{-1}$, and 520 $cm^{-1}$, and the amide V band at 720 $cm^{-1}$, remain in approximately the same positions after high-temperature treatment of the para-aramid fibre, with a slightly increased intensity. This suggests that although there is some degree of fragmentation and cross-linking within the molecular chain segments of the para-aramid fibre under these conditions, the extent of these changes is relatively small. At 1050 $cm^{-1}$, there is an absorption peak corresponding to the fragmentation of C-N bonds in the amide groups, indicating that the molecular chain segments in the para-aramid fibre samples have undergone significant fragmentation and cross-linking, consistent with the analysis of decomposition temperatures in the DSC-TG curves mentioned earlier.

Combining the results of molecular structure parameter tests of para-aramid fibre samples in table 2, it can be seen that below 350°C, the crystallinity of para-aramid remains stable. As the temperature further increases, the crystallinity of the fibres shows an increasing trend. This is because, at a certain temperature, the amorphous regions inside the fibres undergo cleavage first, thereby reducing the proportion of amorphous regions and increasing the crystallinity of the fibres.

The orientation degree and the second-class lattice distortion rate of para-aramid fibre both exhibit a continuous decreasing trend. The decrease in orientation degree is primarily due to the unravelling of amorphous molecular chains, which inevitably results in a decrease in fibre mechanical properties, as will be verified in the subsequent mechanical performance testing. The decrease in the second-class lattice distortion rate with increasing temperature is attributed to the microcrystalline structure of the para-aramid fibre, which exhibits long-range disorder and short-range order, causing incomplete alignment and stacking of adjacent molecular chains. The apparent grain size of the 110, 200, and 002 crystal planes in para-aramid fibre increases to varying degrees with

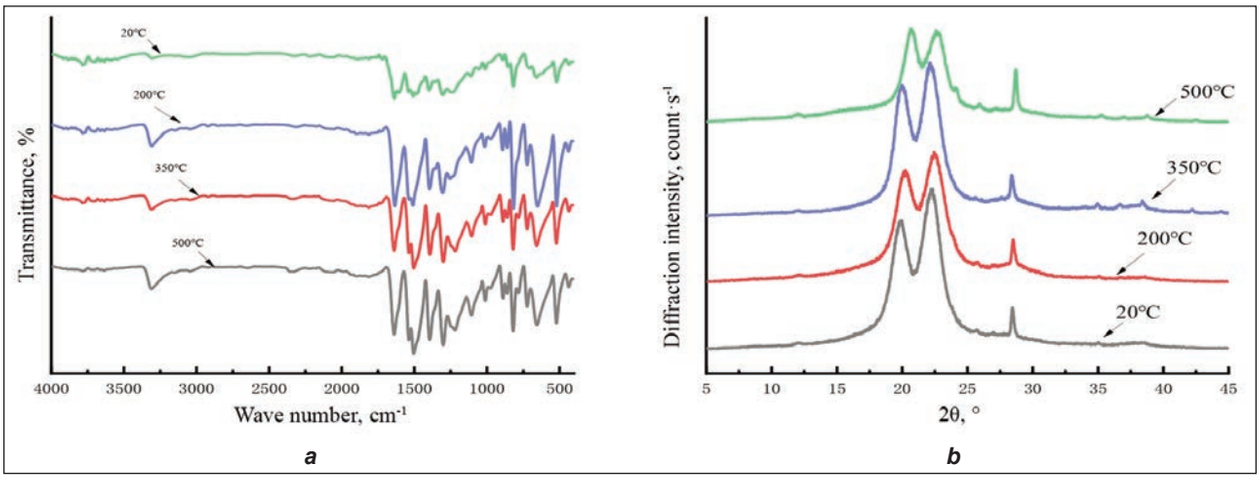


Fig. 3. Molecular structure-related test curves: *a* – infrared spectroscopy curve; *b* – X-ray diffraction curve

Table 2

CALCULATED RESULTS OF MOLECULAR STRUCTURE PARAMETERS FOR PARA-ARAMID FIBRE SAMPLES

| Temperature (°C) | Crystallinity (%) | Orientation degree (%) | Second-class lattice distortion rate (%) | The apparent grain size of crystal planes | | |
|---|---|---|---|---|---|---|
| | | | | 110 crystal plane (nm) | 200 crystal plane (nm) | 002 crystal plane (nm) |
| 20 | 75.51 | 90.58 | 2.18 | 4.73 | 4.22 | 52.55 |
| 200 | 75.39 | 90.16 | 2.14 | 5.49 | 4.47 | 54.26 |
| 350 | 75.17 | 90.05 | 2.07 | 6.77 | 4.82 | 56.33 |
| 500 | 79.14 | 88.79 | 1.93 | 8.18 | 5.16 | 57.82 |

increasing temperature, with the increase in grain size for the 110 and 200 crystal planes being greater than that for the 002 crystal plane. This is because the arrangement of molecular chains in para-aramid fibre is distributed along the fibre axis, with some constraints on the amorphous molecular chains. The amorphous molecular chains distributed perpendicular to the fibre axis can merge laterally through conformational alignment, leading to significant growth.

The decrease in the second-class lattice distortion rate and the increase in apparent grain size of the 110, 200, and 002 crystal planes with increasing temperature indicate structural changes in para-aramid fibre to ensure the stability of the molecular structure during the process of structural decomposition, confirming the analysis of thermal properties and molecular structural changes mentioned earlier.

### Mechanical performance analysis

The mechanical performance test curves are shown in figure 4. From the curves in the figure, it can be observed that the tensile strength of para-aramid fibres remains relatively stable until 200°C. However, beyond 200°C, the tensile strength of the fibres rapidly decreases, and the elongation at break increases significantly. This observation is consistent with the thermal and molecular structural analyses discussed above. Based on the previous analysis, it can be inferred that at temperatures below 200°C, the molecular structure of para-aramid fibres remains relatively stable. However, when the temperature exceeds 200°C, the molecular structure within the amorphous region of the fibres gradually undergoes cleavage and non-crystalline molecular chain disorientation, increasing the number of weak points for fibre fracture. Additionally, the crystallite size increases while the degree of orientation decreases, reducing the interfacial area of para-aramid fibres treated at high temperatures. This leads to a decreased alignment between the molecular arrangement direction and the fibre axial direction, causing a decrease in the strength of the fibres. Conversely, the elongation at break exhibits an increasing trend. From this

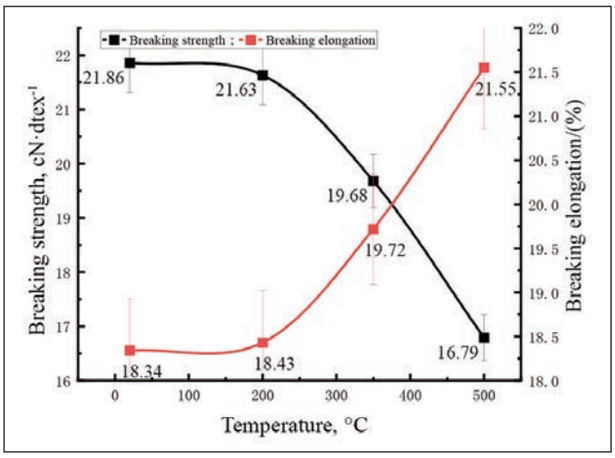


Fig. 4. Mechanical performance test curves

perspective, it can be concluded that in the design and production of para-aramid fibres, reducing the size of fibre crystallites and increasing fibre orientation can improve the mechanical properties of the fibres and reduce their degradation under high-temperature conditions.

## CONCLUSION

Through the study of the thermal degradation properties and mechanisms of para-aramid fibres, it was found that after high-temperature treatment, different protruding particles and pits appear on the surface of the fibres, and the molecular structure gradually undergoes cleavage and cross-linking. This leads to varying degrees of increase in the crystallinity, intrinsic viscosity, and the apparent grain size of crystal planes in different directions of the para-aramid fibres as the temperature rises. On the other hand, the degree of orientation, the rate of the second type of lattice distortion, thermal performance, and mechanical properties show a declining trend. The thermal degradation conforms to the kinetics of a second-order reaction. The conclusions drawn from this study can provide a reference for the design and production of crystallite size and orientation of para-aramid fibres. It can also provide theoretical support for the design temperatures of firefighting suits, heat-resistant gloves, as well as vehicle and aircraft tyre cord threads, among others. It should be noted that the experiments in this study were limited to temperatures below 500°C, and an analysis of the thermal degradation mechanisms of para-aramid fibres at higher temperatures was not conducted. The study also focused on para-aramid fibres and did not investigate the high-temperature resistance of finished products made from para-aramid fibres. In the future, research will be conducted on the thermal degradation performance of fabrics made from para-aramid fibres, to reduce the thermal degradation of para-aramid fibre products and extend their service life from a fabric perspective.

## ACKNOWLEDGEMENTS

This paper was financially supported by the Science and Technology Research Project of the Jiangxi Provincial Education Department (GJJ2202802; GJJ202417).

## REFERENCES

[1] Rebouillat, S., Peng, J.C.M., Donnet, J.B., *Surface structure of Kevlar® fibre studied by atomic force microscopy and inverse gas chromatography*, In: Polymer, 1999, 40, 26, 7341–7350, http://doi.org/10.1016/S0032-3861(99)00040-3

[2] Morgan, R.J., Pruneda, C.O., Steele, W.J., *The relationship between the physical structure and the microscopic deformation and failure processes of poly (p-phenylene terephthalamide) fibres*, In: Journal of Polymer Science: Polymer Physics Edition, 1983, 21, 9, 1757–1783, http://doi.org/10.1002/pol.1983.180210913

[3] Kunugi, T., Watanabe, H., Hashimoto, M., *Dynamic mechanical properties of poly (p-phenyleneterephthalamide) fibre*, In: Journal of Applied Polymer Science, 1979, 24, 4, 1039–1051, http://doi.org/10.1002/app.1979.070240417

[4] Li, J., Tian, W., Yan, H., He, L., Tuo, X., *Preparation and performance of aramid nanofibre membrane for separator of lithium ion battery*, In: Journal of Applied Polymer Science, 2016, 133, 30, http://doi.org/10.1002/app.43623

[5] Cao, K., Siepermann, C.P., Yang, M., Waas, A.M., Kotov, N.A., Thouless, M.D., Arruda, E.M., *Reactive aramid nanostructures as high-performance polymeric building blocks for advanced composites*, In: Advanced Functional Materials, 2013, 23, 16, 2072–2080, http://doi.org/10.1002/adfm.201202466

[6] Park, B., Lee, W., Lee, E., Min, S.H., Kim, B.S., *Highly tunable interfacial adhesion of glass fibre by hybrid multilayers of graphene oxide and aramid nanofibre*, In: ACS Applied Materials & Interfaces, 2015, 7, 5, 3329–3334, http://doi.org/10.1021/am5082364

[7] Brown, J.R., Ennis, B.C., *Thermal analysis of Nomex and Kevlar fibres*, In: Textile Research Journal, 1977, 47, 1, 62–66, http://doi.org/10.1177/004051757704700113

[8] Brown, J.R., Power, A.J., *Thermal degradation of aramids – Part I: Pyrolysis/gas chromatography/mass spectrometry of poly(1,3-phenylene isophthalamide) and poly(1, 4-phenylene terephthalamide)*, In: Polymer Degradation and Stability, 1982, 4, 5, 379–392, http://doi.org/10.1016/0141-3910(82)90044-1

[9] Brown, J.R., Power, A.J., *Thermal degradation of aramids – Part II: Pyrolysis/gas chromatography/mass spectrometry of some model compounds of poly(1,3-phenylene isophthalamide) and poly(1,4-phenylene terephthalamide)*, In: Polymer Degradation and Stability, 1982,4, 6, 479–489, http://doi.org/10.1016/0141-3910(82)90018-0

[10] Brown, J.R., Hodgeman, D.K.C., *An e.s.r. study of the thermal degradation of Kevlar 49 aramid*, In: Polymer, 1982, 23, 3, 365–368, http://doi.org/10.1016/0032-3861(82)90336-6

[11] Khanna, Y.P., Pearce, E.M., *Aromatic polyamides. V. substituent effect on thermal properties*, In: Journal of Applied Polymer Science, 1982, 27, 6, 2053–2064, http://doi.org/10.1002/app.1982.070270618

[12] Wu, Z.Q., Zhao, Z.Q., Ye, Z.W., Qian B.J., *The Effects of Heat-Treatment on the Macro-Molecular Structure of the PPTA Fibre by GPC-[η] Method*, In: Journal of Textile Research, 1984, 5, 5, 261–266, http://doi.org/10.13475/j.fzxb.1984.05.001

[13] Hindeleh, A.M., Abdo, S.M., *Effects of annealing on the crystallinity and microparacrystallite size of Kevlar 49 fibre*, In: Polymer, 1989, 30, 2, 218–224, http://doi.org/10.1016/0032-3861(89)90108-0

[14] Zhang, Q., Liang, Y., Warner, S.B., *Partial carbonizationof aramid fibres,* In: Journal of Polymer Science Part B: Polymer Physics, 1994, 32, 13, 2207–2220, http://doi.org/10.1002/polb.1994.090321308

[15] Yue, C.Y., Sui, G.X., Looi, H.C., *Effects of heat treatment on the mechanical properties of Kevlar-29 fibre,* In: Composites science and technology, 2000, 60, 3, 421–427, http://doi.org/10.1016/S0266-3538(99)00137-2

[16] Iyer, V.R., Vijayan, K., *Effect of thermal spikes on the structural characteristics of Kevlar fibres,* In: Journal of Materials Science, 2000, 35, 22, 5731–5739, http://doi.org/10.1023/A:1004870827838

[17] Downing, J.W., Newell, J.A., *Characterization of structural changes in thermally enhanced Kevlar-29 fibre,* In: Journal of Applied Polymer Science, 2004, 91, 1, 417–424, http://doi.org/10.1002/APP.13021

[18] Wang, X.W., Hu, Z.M., Liu, Z.F., *Thermal Degradation Process of PBO Fibre,* In: Journal of East China University of Science and Technology, 2008, 34, 2, 235–241, http://doi.org/10.14135/j.cnki.1006-3080.2008.02.012

[19] Cai, R.Q., Peng, T., Wang, F.D., Ye, G.D., Xu, J.J., *Comparison of thermal decomposition behaivor of aramid fibres II and III,* In: China Synthetic Fibre Industry, 2010, 33, 4, 14–17, http://doi.org/10.3969/j.issn.1001-0041.2010.04.005

[20] Zhu, F.L., Feng, Q.Q., Xin, Q., Zhou, Y., *Thermal degradation process of polysulfone aramid fibre,* In: Thermal Science, 2014, 18, 5, 1637–1641, http://doi.org/10.2298/TSCI1405637Z

[21] Naveen, J., Jawaid, M., Zainudin, E.S., Sultan, M.T.H., Yahaya, R., Abdul Majid, M.S., *Thermal degradation and viscoelastic properties of Kevlar/ Cocos nucifera sheath reinforced epoxy hybrid composites,* In: Composite Structures, 2019, 219, 194–202, http://doi.org/10.1016/j.compstruct.2019.03.079

[22] Rao, Y., Waddon, A.J., Farris, R.J., *Structure–property relation in poly (p-phenylene terephthalamide) (PPTA) fibres*, In: Polymer, 2001, 42, 13, 5937–5946, http://doi.org/10.1016/S0032-3861(00)00905-8

[23] Ahtee, M., *An X-ray diffraction method for determination of crystallinity in wood pulp*, In: Pap Puu-Pap Tim, 1983, 65, 475–480, http://doi.org/10.1080/02773818308085176

[24] Bohn, A., Fink, H.P., Ganster, J., Pinnow, M., *X-ray texture investigations of bacterial cellulose*, In: Macromolecular Chemistry and Physics, 2000, 201, 15, 1913–1921, http://doi.org/10.1002/1521-3935(20001001)201:15<1913::AID-MACP1913>3.0.CO;2-U

[25] Auerbach, I., *Kinetics for the tensile strength degradation of nylon and kevlar yarns*, In: Journal of Applied Polymer Science, 1989, 37, 8, 2213–2227, http://doi.org/10.1002/app.1989.070370813

[26] Hall III, W.R., Knoff, W.F., *Heat aged tensile strength retention of poly (p-phenylene terephthalamide) sewing thread*, In: Journal of Engineered Fibres and Fabrics, 2008, 3, 4, 155892500800300403, http://doi.org/10.1177/155892500800300403

[27] Castro-Muñiz, A., Martínez-Alonso, A., Tascón, J.M., *Porosity development in chars from thermal decomposition of poly (p-phenylene terephthalamide)*, In: Polymer Degradation And Stability, 2009, 94, 10, 1890–1894, http://doi.org/10.1016/j.polymdegradstab.2009.06.017

**Authors:**

CHUNYAN ZHU[1], YANPING LIN[1], XIANGAI ZHANG[2], CHEN YANG[1,3]

[1]Jiangxi Institute of Fashion Technology, Jiangxi Centre for Modern Apparel Engineering and Technology,
No. 108, Lidu Middle Avenue, Xiangtang Economic Development Zone, 330201, Nanchang City, China
ORCID: 0000-0002-4399-7619, e-mail: tree_0206@hotmail.com

[2]Guangdong Technology College, Institute of Arts and Design,
No.3 Qifu Street Gaoyao District, 526100, Zhaoqing City, China
ORCID: 0009-0007-3773-3792, e-mail: 782131548@qq.com

[3]Hainan Normal University, Institute of Fine Arts,
No. 99 Longkun South Road, 571158, Haikou City, China

**Corresponding authors:**

YANPING LIN
ORCID: 0009-0005-7851-2924, e-mail: 42579825@qq.com

CHEN YANG
ORCID: 0000-0003-1593-7739, e-mail: comradeyang@qq.com

# Geometric developments in functional clothing

DOI: 10.35530/IT.075.01.2022154

MANUELA AVADANEI
MALINA ROSCA
ANA-DIANA VATRA
LAURA CHIRILA

**ABSTRACT – REZUMAT**

**Geometric developments in functional clothing**

*This study presents a geometric development of functional clothing (for pregnant women). In the beginning, we discuss the main changes women's bodies undergo during pregnancy and the requirements of an adequate wardrobe. Using specific design tools (Gemini CAD – a Lectra Company), we develop a geometric network for designing made-to-measure maternity clothes (case study – blouse). From this network, three specific blocks have been developed in accordance with the body changes. The estimated increments of the second and third pregnancy trimesters have been expressed as correspondent angles and used to design the adequate shape of the blouse patterns (front and back). We have also evaluated the blouse patterns when dressed on the corresponding avatars for each trimester via 3D simulations.*

***Keywords:*** *functional clothing, geometric development, network, blocks*

**Dezvoltări geometrice în îmbrăcămintea funcţională**

*Această lucrare prezintă o dezvoltare geometrică a îmbrăcămintei funcționale (pentru femeile însărcinate). În partea introductivă sunt discutate aspecte teoretice referitoare la principalele schimbări pe care le suferă corpul femeilor în timpul perioadei de sarcină și cerințele unei garderobe adecvate pentru această perioadă. În lucrare, se elaborează o rețea geometrică necesară proiectării personalizate a produselor vestimentare pentru femei însărcinate, în funcție de trimestrul de sarcină (studiu de caz – bluză), utilizând instrumente avansate de proiectare CAD (Gemini CAD – o companie Lectra). Pe baza acestei rețele, în funcție de modificările corporale specifice fiecărui trimestru de sarcină, au fost dezvoltate trei blocuri, câte unul pentru fiecare trimestru. Creșterile corporale aferente trimestrului doi și trei de sarcină au fost exprimate sub forma unor unghiuri corespunzătoare și au fost utilizate pentru a proiecta forma adecvată a elementelor principale de produs ale blocurilor (față și spate – bluză). Validarea formei elementelor de produs ale blocurilor personalizate s-a realizat prin simulare 3D; prototipurie virtuale ale blocurilor au fost îmbrăcate și analizate pe avatarurile corespunzătoare pentru fiecare trimestru de sarcină.*

***Cuvinte-cheie:*** *îmbrăcăminte funcțională, dezvoltare geometrică, rețea personalizată, blocuri*

## INTRODUCTION

Clothes are designed and manufactured to fulfil the customers' needs: comfort, protection, aesthetics and others according to the product's destination and utilisation. Functional clothes represent a category designed to meet special user needs for particular situations: protection (from high or low temperatures, rain, snow, wind, UV light, fire, skin contact with dangerous substances, radioactivity, etc.), health functions (ensure good blood for better blood circulation, monitoring heart rate, blood oxygenation or body temperature), athletic function (improves performance, lowers fatigue), aesthetic function (shaping the body for a better aspect), complex functions (multifunctional performance, protection, support, comfort), special needs support (for infants, people with disabilities, elderly, pregnant women) [1].

The shape and structure of functional clothes (the number of pieces/models, the geometry of the outline contour of each piece) are influenced by their destination. The materials and manufacturing technology of these items contribute to their performance and functionality. In the design process of this type of clothes, it is necessary to consider ergonomic requirements such as the degrees of freedom, momenta of forces in human joints, forces, posture, proportions, conformation, etc.) [2–5].

Clothes for pregnant women have to be designed according to the specific needs and requirements of this period, especially by taking into account the physical modifications from one pregnancy trimester to another. Nowadays, the market for this type of product offers items with the following details to ensure wearing comfort: large volume (pleats, folds and creases), adjustable straps and flexible and variable closure solutions (buttons, staples, elasticated bands) manufactured for typical bodies. The existing range of this type of clothing is not adapted to the diversity of women's body shapes; some of the items produced do not sell because they do not fit any customer (these items become waste). This situation can be changed through a win-win solution for manufacturers and customers: designing and manufacturing ready-to-wear or made-to-measure clothes. The

CAD producers have developed specific modules for the geometric development of the shapes of the garment pieces (made-to-measure module) where the designer has the possibility to decide on the shape of the garment pieces by taking into account the peculiarities of the body shape and model details. In this paper, the authors propose the development of a personalised geometric network for a blouse that can be adapted to the specific changes in the body for each trimester of pregnancy [6]. This network is used to develop three blocks for each trimester of pregnancy. The outlines of the main elements of the blouse (front, back and sleeve) are drawn in the designed network and automatically linked to the value of the initial data, and the body changes from one trimester of pregnancy to the next.

## GENERAL INFORMATION

### General information about body changes

Pregnancy is an important event in every woman's life, with physical, hormonal and emotional changes. Significant lifestyle changes must be made to ensure the child's normal and healthy development. The mother's state of health, age and social, professional, and physical activities influence the evolution of her body shape during pregnancy. During this period, the body silhouette, posture, size and weight change differently depending on the trimester of pregnancy: in the first trimester (1–12 weeks) the body does not undergo any physical changes (this period is a transition to the new stage: mood swings, strong sense of smell, nausea and vomiting, etc.), in the second trimester (13–28 weeks) important changes in shape and weight take place (the abdomen grows because the fetus/baby is growing), while in the third trimester (29–40 weeks) the body weight, posture and shape are completely different (the mother's body has to strike a new balance between its weight and the baby) (figure 1) [7].

Pregnancy clothes must be comfortable and beautiful but perfectly adapted to the pregnancy trimester. The future mother must be able to work and be involved in different social activities, so she has to find proper and diversified clothes. While she can wear clothes from her already existing wardrobe during the first trimester, in the 2nd and 3rd trimesters she must wear suitably sized products. The first noticeable physical changes occur around the fourth month (second trimester). These changes require special care in developing maternity clothing in terms of comfort, fit and size.

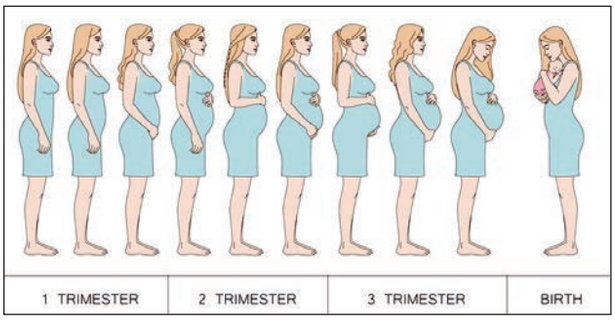


Fig. 1. Stages of pregnancy [8]

Medical studies have shown that women gain about 10–16.5 kg during pregnancy depending on their age and BMI [9].

Most women notice an increase of 20 to 26 centimetres around the waist. The expansion of the abdomen varies depending on the position of the foetus. Some pregnant women carry their baby low, and others high. Sometimes, the abdomen appears to be pushed forward or hidden in the body. The breasts also increase in size, with a peak of 5–8 cm in terms of average circumference. The waist circumference may increase by up to 37 cm, and the hip and high hip circumference (10 cm below the waist) may increase by up to 36 cm [10]. The body depth increases differently at the main levels: the bust level (chest depth) increases by around 1%, the abdominal level increases by 4%, the hip level increases by 1%, and the upper thigh level increases by 7% (concerning the values before pregnancy) [11].

During pregnancy, the spine is temporarily curved to keep the body in equilibrium (balanced). This changes the posture, with the body tilted backwards. The change in posture, the centre of gravity, and weight cause discomfort: lower back pain, pelvic girdle pain, fatigue and general malaise [12, 13].

Besides physical transformations, pregnancy brings noticeable psychological changes: emotional fluctuations between a happy/normal state and a fearful/agitated one. Society, friends and family must provide emotional support to pregnant women because their emotional state has a significant influence on the development process of the fetus.

### Clothes for the pregnancy period

Clothing plays an essential role in reaching and maintaining self-confidence. Clothes must be comfortable, beautiful, of good quality, varied (model and category) and affordable. Due to physical changes, clothes that fit in the second trimester will be inappropriate in the 9th month (in the first trimester, women can wear usual clothes as the size and shape of the body do not change). On the other hand, the women's preferences may vary: some prefer styles and product categories that emphasise the shape of the belly (because they are proud of their baby bump), while others prefer oversized clothes (for more comfort). During this period, women are very sensitive to contact with clothing surfaces; for this reason, they look for apparel made from materials with natural fibres.

The maternity clothing market represents a small part of the general one. This type of clothes (blouses, sundresses, overalls, cardigans, dresses, T-shirts) can mainly be bought in specialised shops and department stores, where the range is not as varied and profitable as in other shops (figure 2).

For ergonomic and functional reasons, clothing for pregnancy is designed with support on the shoulders.

Fig. 2. Examples of clothes for pregnant women (2nd and 3rd trimester) [12]

The styles have accessible fastening solutions (buttons, staples) with or without straps (with adjustable length), usually with a cross-section above the waist (yoke) and pleats/folds or creases on the component(s) below the yoke (figure 2).

The nine months of pregnancy are an important part of a woman's life. During this time, she wants to wear different garments that are fashionable, ergonomic, comfortable and fit her body shape perfectly. The size of the garments worn during this period must be the same as before the pregnancy because the garments must be well-balanced on the body (to ensure psychological comfort).

## GEOMETRICAL DEVELOPMENTS IN FUNCTIONAL CLOTHING

The fit of functional clothing is considered successful when the needs of the wearer are harmonised with the required functionality of the garment. There are two essential aspects–comfort and appearance. Comfort is perceived by the customer when wearing the garment, and appearance refers to the look, style and fashion. The fit is determined by the interaction of various factors: the shape and biomechanics of the human body, the textile materials (the interaction with the body shape and the ones between them) and the details of the model [13–15].

Lectra, Gemini – a Lectra company –, Assyst, Optitex and Clo3D are often used to develop the shape of the model patterns and to obtain a virtual 3D prototype. In a 3D environment, the designer checks (validates) the methodology used to obtain the shapes of the pieces of the pattern and analyses the position and appearance of the garment model dressed on a virtual avatar (this consists of checking the balance of the model and its fitting degree). In other words, even if these products are considered functional, they must also fit into fashion trends and be manufactured on demand (as personalised or made-to-measure items) or in minimal series (according to the market requests). Suppose the manufacturer has the possibility to communicate with the customer, to determine her preferences or needs, and to evaluate/measure some key body dimensions (using non-invasive measurement technology-scanning apps). In that case, they can use all the data to develop the shape of the desired items in a particular way (the designers will have the possibility to obtain the 3D model prototype and check its appearance when dressed in the client's avatar). Suppose the manufacturer cannot obtain specific data on the customer's preferences and body dimensions. In that case, they developed the new model using standardised information on body measurements [16] and the results of previous marketing studies applied on the market (among the customers) to identify which category and number of products should be manufactured.

Based on all the aspects of the specificities of pregnancy already discussed and analysed in the previous sections of this article, a solution for the geometric development of made-to-measure maternity clothing (case study – blouse) using specific tools of the Pattern Design module (Gemini CAD-a Lectra Company) can be found by going through the following steps:

a) Deciding which key data is needed to design a customised network;
b) Determining the structure of the mathematical relations needed to develop the personalised network (design methodology);
c) Designing the 3 basic blocks about the particularities of each pregnancy trimester;
d) Extracting the shape of the main elements. Creating the virtual 3D prototype and analysing it;
e) Altering the size and shape of the main elements (if necessary). Validating the design solution.

The Pattern Design module (from Gemini CAD-a Lectra Company) has specific functions/tools and instruments that enable the designer to interactively obtain the shape of the main elements, as their size and shape are determined by selected initial data via various mathematical relations [17, 18].

a) Deciding which key data is needed to design a customised network;

The necessary data for designing the blouse network can be classified into the following categories: values of the body dimensions, values of product dimensions, values of allowances (constructive allowance for the bust level); and lengths of different contour lines, which have been measured on the main pieces (front and back) (figure 3)

b) Determining the structure of the mathematical relations needed to develop the personalised network (design methodology);
c) Designing the 3 basic blocks in relation to the particularities of each pregnancy trimester;
d) Extracting the shape of the main elements (front, back and sleeve).

The personalised network is designed using various mathematical relationships (case study blouse) and specific tools from Gemini CAD's Made-to-Measure module (figures 4 and 5).

The shape of the blouse elements (first block) is drawn in this network.

The necessary steps in obtaining the shape of the main elements consist of: connecting the points in the geometric layer by drawing straight lines (Draw tool);

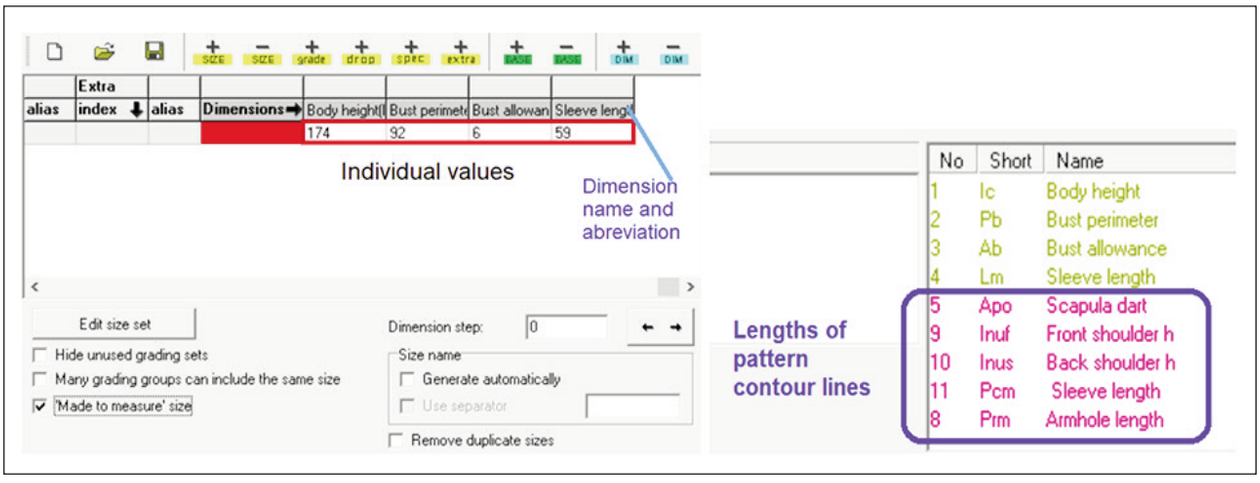


Fig. 3. Key data for designing the blouse network

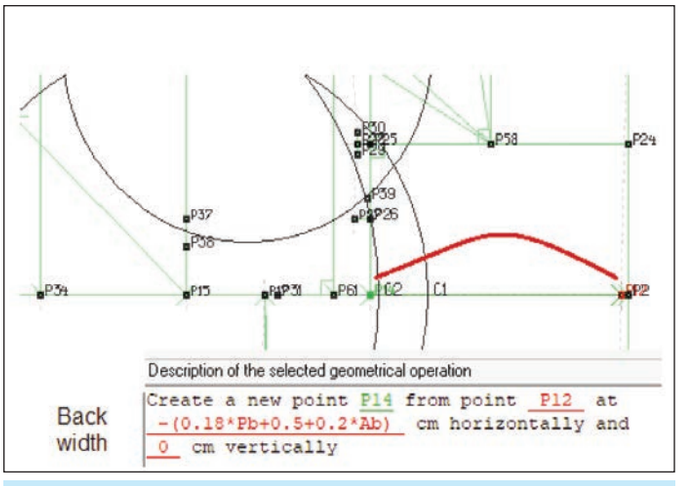


Fig. 4. Back width

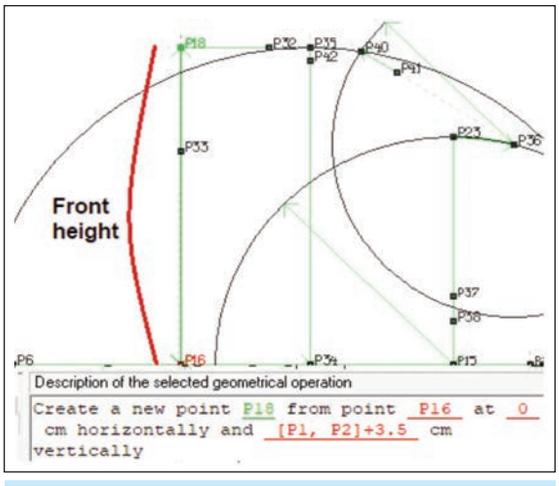


Fig. 5. Front height

converting the straight lines into curves and modelling their shape (neckline, armhole and hem) by using the Shape tool; moving the pieces from the geometric layer (Piece Tool) (figure 6). When the pieces are moved, the connection with the geometric layer is not destroyed (if a value of the initial data is changed, the shapes of all the pieces are automatically redrawn).

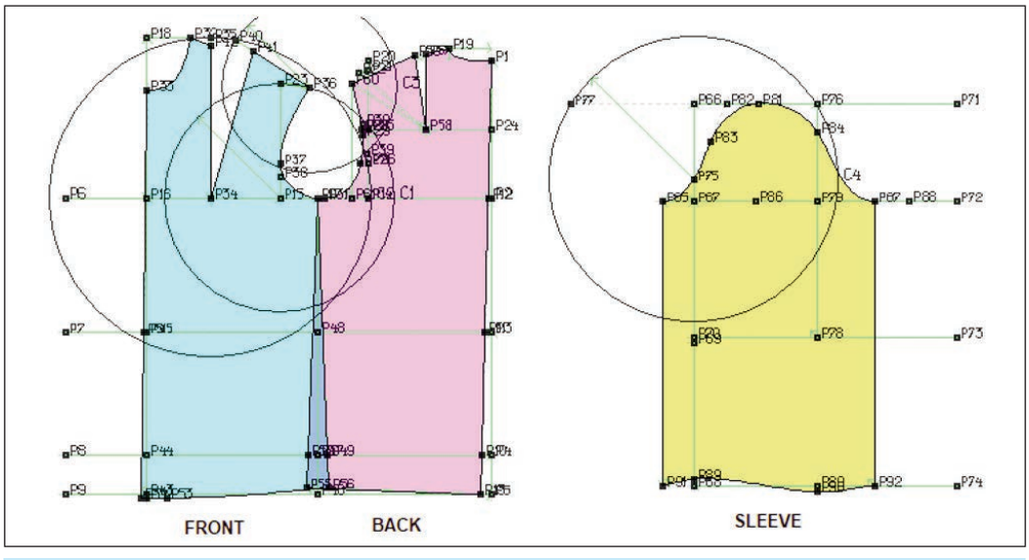


Fig. 6. The blouse patterns (front, back and sleeve – for ½ of the product). First block

The next two blocks are designed by using the previous one as a starting point. Based on the previous information about how the shape of the body varies, the following steps are going to be necessary:

- the width of the front piece will have to be changed. For the second block, one will have to use 40% of the body increment (waistline). For the third block, 60% of the body increment will have to be used;
- the front pattern will have to be divided into 2 pieces (by drawing a vertical line through the bust point). The lateral part is then going to be slanted by a specific angle (the value is in sexagesimal degrees, taking values between 0° and 360°). The value of the angle is determined by considering the increment at the waist level and the length of the vertical line used to divide the front pattern;
- the back will also have to be divided by a vertical line drawn from the vertex of the scapula dart. The lateral part is also going to be slanted by an angle (the value is in sexagesimal degrees). Its value is determined by considering the increment at the bust level (partial) and the vertical line length used to divide the front pattern.

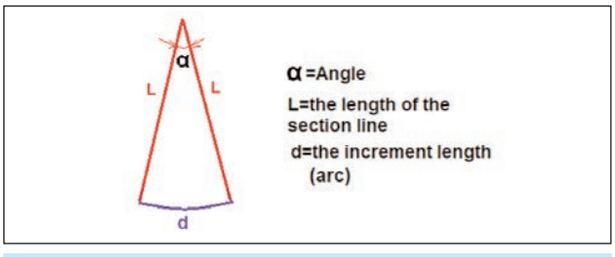


Fig. 7. Details for determining the value of the α angle

The general formula used to determine the value of the angle is (the terms are explained in figure 7):

$$\alpha = \frac{180 \cdot d}{\pi \cdot L} \quad (1)$$

Based on the information already described, the corresponding angle of the increment on the waist (front piece) and bust (back piece) has been determined for the 2nd and 3rd trimesters of pregnancy. For the front element, only the increment on the waist level was necessary, because in the 2nd and 3rd trimesters, the body undergoes major changes at the waist level, more significant than at the bust (the front piece has to cover the new shape of the body).

Fig. 9. The virtual prototype

The new pieces have been imported into CLO [19] to obtain the 3D virtual prototype that is going to be tested on the corresponding avatar (2nd trimester).

By analysing the appearance of the virtual prototype; we can reach the following conclusions:

– the widths of the elements (front, back and sleeve) are well-dimensioned;
– the product is well-balanced;
– the position of the front hemline must be changed (lower).

In the design scenario for the front element, the position of the hemline has to be changed. To do this, one has to evaluate the height of the front middle point and the one of the back middle point. The difference between these heights is then used to change the level of the front hemline.

The shapes of the main elements (front, back and sleeve) for the third trimester are obtained by applying the same procedure.

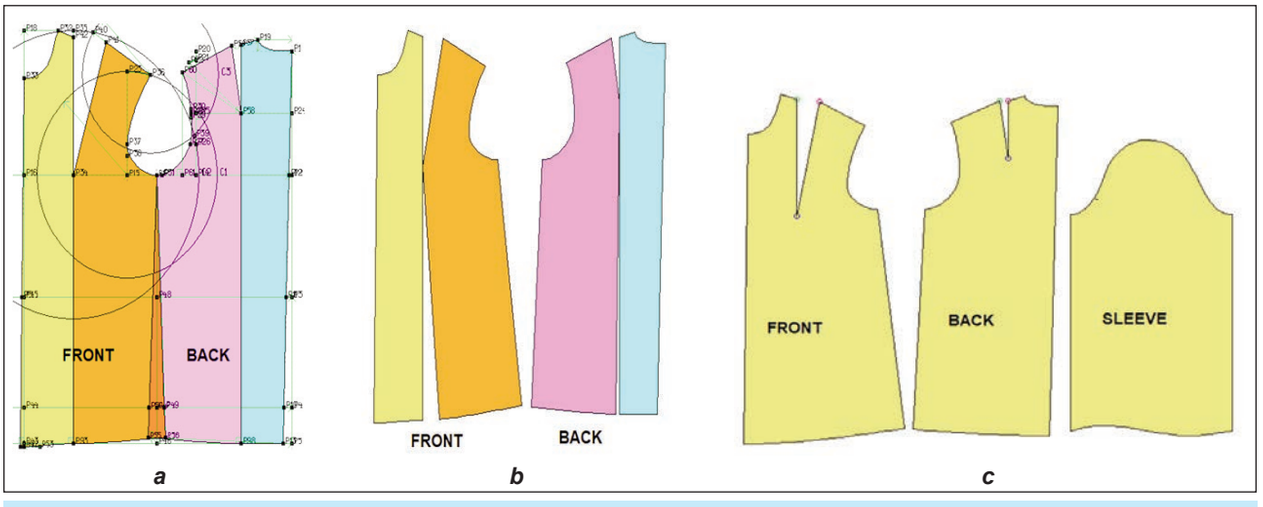


Fig. 8. The block patterns for the 2nd trimester: *a* – draw the section lines; *b* – rotate lateral pieces; *c* – final patterns (1/2 product)


Fig. 10. Alteration of the front hemline position

## CONCLUSIONS

The digital development of this type of product involves the following steps: designing the 2D shape of the components, creating the virtual 3D prototype (selection of materials) and evaluating the appearance of the corresponding avatar. A geometric development of the size and shape of the garment pieces, based on the peculiarities of the body changes, may fulfil the customer's needs.

The geometric development of the blouse patterns concerning a network involves describing the dependence of the shape of the garment pieces on the changes of the body (increments) and model details by using mathematical relations. The proposed design solution allows:

- interactive changes in the network size, determined by alterations of the initial data (values or structure) or the structure of the mathematical relations. The shapes of the blouse components (front, back and sleeve) are automatically redrawn because they are determined by the geometric network;
- the possibility of considering the body changes (increments) during pregnancy in adapting the shape of the front and back patterns (the 2nd and 3rd trimesters). These have been used to calculate the values of the corresponding angles "αi" (for the front and back patterns), for the 2nd and 3rd trimesters (40% for the 2nd trimester and 60% for the 3rd trimester);
- if, during the simulation phase for the front element, some tension forces occur within its surface, the mathematical relationship used to dimension its width will have to be readjusted so that it takes into account the increment in breast circumference from the 2nd to the 3rd trimester, with the same coefficient used for the bust circumference;
- the network can be personalised for different body postures and conformations or other clothes with support on shoulders;
- the shape of the main elements can be easily changed/modelled according to the customer's demands (fashion on demand).

As for further developments, the proposed solution can be used to develop geometric networks for garments with support at the waist (trousers) or models with different cut lines (e.g. raglan cut) (e.g. raglan cut).

## ACKNOWLEDGEMENTS

The authors acknowledge the Gemini Company – a Lectra Company, for its technical support and collaboration with the Faculty of Industrial Design and Business Management.

## REFERENCES

[1] Deepti, G., *Functional clothing – Definition and classification,* In: Indian Journal of Fibre & Textile Research, 2011, 36, 321–326, Online ISSN: 0975-1025, Print ISSN: 0971-0426

[2] Broadhead, R., Craeye, L., Callewaert, C., *The Future of Functional Clothing for an Improved Skin and Textile Microbiome Relationship*, In: Microorganisms, 2021, 9, 6, 1192, https://doi.org/10.3390/microorganisms9061192

[3] Avadanei, M., Olaru, S., Ionescu, I., Ursache, M., Ciobanu, L., Alexa, L., Luca, A., Olmos, M., Aslanidis, T., Belakova, D., Silva, C., *ICT new tools for a sustainable textile and clothing industry*, In: Industria Textila, 2020, 71, 5, 504–512, http://doi.org/10.35530/IT.071.05.1811

[4] Olaru, S., Mocenco, A., Teodorescu, M., Niculescu, C., Salistean, A., *Shape categories for the Romanian female population and specific clothing recommendations*, Industria Textila, 2011, 62, 3, 155–160

[5] Chen, J.-Z., Guo, Z.-Y., Li, T., Du, L., Zou, F.-Y., *An undamaged pattern generation method from 3D scanned garment sample based on finite element approach*, In: Industria Textila, 2023, 74, 1, 35–41, http://doi.org/10.35530/IT.074.01.202185

[6] MyungHee, S., *A Pattern Adaptation for Body Changes during Pregnancy: A Single Case Study,* Master Thesis, University of Minnesota, November 2009

[7] Rn, N.G., *Pregnancy trimesters: Everything you need to know. Medical and health information,* 2018, Available at: https://www.medicalnewstoday.com/articles/323742 [Accessed on November 20, 2022]

[8] *Stages of pregnancy*, Available at: https://www.freepik.com [Accessed on November 20, 2022]

[9] *Weight gain in pregnancy*. (n.d.). Pregnancy, Birth and Baby, Available at: https://www.pregnancybirthbaby.org.au/weight-gain-in-pregnancy [Accessed on November 17, 2022]

[10] Cieśla, K., Frydrych, I., Krzywinski, S., Kyosev, Y., *Development workflow for virtual design of clothing for pregnant women*, In: Communications in Development and Assembling of Textile Products, 2020, 1, 2, 148–159, https://doi.org/ 10.25367/cdatp.2020.1

[11] Faust, M.E., *Designing for Pregnant Women,* In: Proc. of the 4th International Conference on 3D Body Scanning Technologies, Long Beach CA, USA, 19–20 November 2013

[12] *Maternity clothes*, Available at: https://www.freepik.com/free-photos-vectors/maternity-clothes/ [Accessed on November 20, 2022]

[13] Boorady, L.M., *Functional clothing – Principles of fit,* In: Indian Journal of Fibre & Textile Research, 2011, 36, 344–347, Online ISSN: 0975-1025, Print ISSN: 0971-0426

[14] Olaru, S., Filipescu, E., Niculescu, C., *Morphological indicators for characterization of women thorax and basin shape, for garment design in customised*, Industria Textila, 2011, 62, 6, 289–295

[15] Rosca, M., Vatra, A.-D., Avadanei, M., *The digital transformation of garment product development*, In: Industria Textila, 2023, 74, 1, 98–106, http://doi.org/10.35530/IT.074.01.2022148

[16] ASTM D7197-13, *Standard table of body measurements for misses maternity sizes two to twenty-two (2-22)*, ASTM International, https://doi.org/10.1520/D7197-13

[17] Filipescu, E., Avădanei, M., *Structura şi proiectarea confecţiilor textile. Îndrumar laborator*, Ed. Performantica, Iaşi, 2007, ISBN 978-973-730-412-4

[18] Gemini – a Lectra company, Available at: https://www.geminicad.com [Accessed on November, 2022]

[19] Clo3D, Available at: https://www.clo3D.com [Accessed on November, 2022]

**Authors:**

MANUELA AVADANEI[1], MALINA ROSCA[1], ANA-DIANA VATRA[1], LAURA CHIRILA[2]

[1]"Gheorghe Asachi" Technical University of Iasi, Faculty of Industrial Design and Business Management, 29 Blvd D. Mangeron, 700050, Iasi, Romania

[2]National Research & Development Institute for Textiles and Leather, Lucretiu Patrascanu 16, 030508 Bucharest, Romania
e-mail: laura.chirila@incdtp.ro

**Corresponding author:**

MANUELA AVADANEI
e-mail: mavad@tex.tuiasi.ro,
manuela-lacramioara.avadanei@academic.tuiasi.ro

# Effects of MWCNT and Sodium Dodecyl Sulfate (SDS) contents on the electrical conductivity and sensor properties of thermoplastic polyurethane nanosurfaces

DOI: 10.35530/IT.075.01.2023105

RUSEN INAN
ISMAIL USTA
YESIM MUGE SAHIN

**ABSTRACT – REZUMAT**

**Effects of MWCNT and Sodium Dodecyl Sulfate (SDS) contents on the electrical conductivity and sensor properties of thermoplastic polyurethane nanosurfaces**

*Recently, strain sensors have significant areas of usage with their strain, stretching and wearable features for various applications such as personal health monitoring, joint movement detection, robotics, etc. To achieve this, various studies are conducted to optimize the production of MWCNT-based nanocomposites. In the present study, a total of 12 solutions were formulated by introducing Multi-Walled Carbon Nanotubes (MWCNT) and Sodium Dodecyl Sulfate (SDS) at different concentrations and ratios into the Thermoplastic Polyurethane (TPU) solution, and then nanocomposite surfaces were produced from these solutions through an electrospinning process. These samples were subjected to resistance changes due to elongation, gauge factor changes due to elongation to evaluate the sensor property and cycle tests to evaluate the sustainability of the sensor feature. According to the results, the best sensor properties were obtained in the samples with SDS added at a rate of 1/20 (MWCNT:SDS) for 0.3 MWCNT and 0.5 MWCNT; on the other hand 1/26 weight ratio of MWCNT:SDS for 0.7 MWCNT.*

***Keywords:*** *smart textiles, wearable sensors, MWCNT, SDS, electrospinning*

**Influența conținutului de MWCNT și de dodecil sulfat de sodiu (SDS) asupra conductivității electrice și proprietăților senzoriale ale nanosuprafețelor din poliuretan termoplastic**

*Recent, senzorii de deformare au început să aibă domenii semnificative de utilizare pe baza caracteristicilor lor de deformare, întindere și purtare pentru diverse aplicații, cum ar fi monitorizarea sănătății personale, detectarea mișcării articulațiilor, robotică etc. În scopul de a realiza aceste funcții, sunt efectuate diverse studii pentru a optimiza producția de nanocompozite pe bază de MWCNT. În studiul de față, a fost sintetizat un total de 12 soluții prin introducerea de nanotuburi de carbon cu pereți multipli (MWCNT) și dodecil sulfat de sodiu (SDS) la diferite concentrații și rapoarte în soluția de poliuretan termoplastic (TPU), iar apoi suprafețele nanocompozite au fost produse din aceste soluții printr-un proces de electrofilare. Aceste probe au fost supuse modificărilor de rezistență din cauza alungirii, ale factorului de etalonare datorat alungirii pentru a evalua proprietățile senzoriale și testelor ciclice în vederea evaluării sustenabilității proprietăţilor senzoriale. Conform rezultatelor, cele mai bune proprietăți senzoriale au fost obținute în probele cu SDS adăugat la un raport de flotă de 1/20 al MWCNT:SDS pentru 0,3 MWCNT și 0,5 MWCNT; pe de altă parte, raportul de flotă de 1/26 al MWCNT:SDS pentru 0,7 MWCNT.*

***Cuvinte-cheie****: textile inteligente, senzori purtabili, MWCNT, SDS, electrofilare*

## INTRODUCTION

With the evolution of wearable electronics technology, the anticipated characteristics of textile products have transformed; in the contemporary context, textiles are expected to not only offer warmth and comfort but also to provide a sense of ease and additional functionalities, such as the detection of human movement, information processing, and energy storage [1, 2]. Textile materials present advantages over other materials, such as hardness and strength, but they can also be easily integrated into a wide range of end-use requirements and have softness and flexibility that allow for different uses [3, 4]. Products with electrical conductivity, called smart or electronic textiles, can be obtained by combining textile structures and electronic elements. E-textiles are an outstanding technology capturing significant attention for their ability to incorporate attributes such as antennas, mobile memory elements and wearable sensors into established textile products [5]. With their ability to strain, stretch and be wearable, strain sensors are a remarkable sub-branch of the wearable electronics field and can be applied in the fields of health imaging, joint movement detection, robotics and wearable electronics thanks to these properties [6–9]. Interest in smart textile applications, such as stretchable batteries and wearable sensors increases day by day. The high precision, robustness, and expansive operational scope of strain sensors are important in meeting the requisites of real-world applications [10, 11]. However, commercially available strain sensors lack these characteristics. Carbon black, metallic

nanoparticles, carbon nanotubes, nanocables, and graphene stands can be used for fabricating strain sensors with the desired characteristics. Carbon nanotubes stand out among these materials for their ability to provide high conductivity even at very low concentration levels [12–14]. Using their electrical conductivity, high strength and good mechanical properties, carbon nanotubes are known for their high potential for use in the production of flexible strain sensors [9, 15].

During the literature review, many investigations on strain sensor production have been documented.

In the study conducted by Şanli, a structure is produced by placing the KNT/TPU mat with an electrospun structure between two PDMS mats. KNTs within KNT (-COOH functionalized)/TPU samples are prepared by utilizing three distinct dispersion methods: magnetic stirring, ultrasonic bathing, and sonication. By detailed microscopic examination of the samples, electromechanical properties, piezoresistive properties and the KNT/TPU strain sensor mechanism in the electrospun sandwich structure are examined [14].

In their study, He et al. obtained the MWCNT/TPU structure with high flexibility and good efficiency by the process of wet spinning. In this structure, TPU serves as the flexible matrix material while MWCNT provides the sensor properties. Then, an assessment encompassing structural, mechanical, electrical, and strain detection features of the material is conducted. The optimal conductivity value at 28 MPa and 565% elongation is achieved as 6.77 Siemens/cm [7].

In their study, Nankali et al. obtained PDMS/MWCNT-based strain sensors by utilising the vacuum filtration technique and investigating the electrical characteristics of the structure. The electrical characteristics of CNT samples at varying rates of concentration are examined. As revealed by the measurements, the electrical resistance is observed to be within the range of 12.5 KΩ to 22.8 MΩ. Piezoresistive films within the CNT concentration range of 1.4–2.9 mg/mm$^2$ exhibit pronounced resistance drops, establishing this interval as the filtration threshold region. According to SEM images, the nanocomposite layer thicknesses of the strain sensors in this region are observed to be between 790 nanometers and 1210 nanometers. Then, the percolation curve is determined by using the curve fitting method on the experimental data. The percolation threshold is detected to be 1.992 mg/mm$^2$. Finally, to determine the minimum gauge factor of the sensors in the percolation zone, a flexible strain sensor is selected at the upper limit of this zone and the piezoresistive properties of the sample obtained are examined [16].

In their study, Wang et al. prepare a fibre-shaped strain sensor using TPU MWCNT and the cost-effective wet-spun method. The prepared sensor achieves 320% strain in uniaxial (---sided) strain tests. In addition, high precision (22.2 gauge factor at 160% strain, 97.1 gauge factor at 160% – 320% strain) and fast response time (<200 ms) are achieved [8].

In their study, Kumar et al. prepare a robust, stretchable and high-sensitivity MWCNT-reinforced TPU nanocomposite for piezoresistive strain/detection. The distribution of MWCNT within the TPU matrix provides a low leaching threshold (0.1% by weight) and superior electrical conductivity. MWCNT/TPU nanocomposites have shown different sensitivity and strain ranges depending on MWCNT concentrations. For TPU nanocomposites loaded with MWCNT of 0.3%, 0.5% and 1% by weight, a near-linear piezoresistive response is achieved at 15%, 35% and 45% strain, as well as 22, 8.3 and 7.0 gauge factor values [17].

In their study, Wang et al. obtain nanofiber films using the electrospinning method with 10%, 12.5% and 15% MWCNT TPU. TPU functions as the matrix framework while MWCNT operates as the conductive framework. An analogous trend is observed wherein elevating the quantity of MWCNT results in a reduction of thermal weight loss within the fibre film. Electrical conductivity improves, and thermal and sensing properties suggest a change. When all performance values are taken into consideration, it is observed that MWCNT/TPU nanofiber film containing 12.5% MWCNT obtains the best values for human movement and pressure sensing [15].

In the study conducted by Şanli et al., the effect of electrospinning parameters on the morphological and electromechanical properties of MWCNT/TPU nanofibers is examined. They observe that electrospinning parameters as well as MWCNT concentrations influence the morphological, electromechanical and sensor properties of MWCNT/TPU nanofiber membranes. They suggest that when the collector speed decreases and the collector distance increases, particularly during extended electrospinning periods, the resulting fibre structures exhibit a higher degree of uniform distribution, and this phenomenon has a beneficial impact on conductivity and strain sensitivity [18].

## MATERIAL AND METHODS

### Materials and chemicals

MWCNTs with COOH Function with more than 92% purity and outer diameter of 8–15 nm were purchased from Nanografi Nano Technology. Thermoplastic polyurethane (TPU) (Ellastolan 1185A10) was supplied from Biesterfeld GmbH (Istanbul, Türkiye) in granular form, N, N-Dimethylformamide (DMF) and Tetrahydrofuran (THF) from Progen Kimya and Sodium Dodecyl Sulfate (SDS) from Merck.

### Nanocomposite production by electrospinning method

In the sample preparation stage which is schematized in figure 1, it was first dried in the oven at 60°C for 1 h to blow the moisture off the TPU granules. Then, a TPU solution with a concentration of 10% by weight was prepared. When this solution was prepared, TPU granules weighing 1 g were dissolved in 10 ml of DMF: THF solvent system. During the

preparation of this solvent system, the mass proportion of DMF to THF was established as 2:3. The mixture underwent homogenization via magnetic stirring for 2 hours under ambient conditions. Secondly, a solution was created by introducing MWCNT in weights of 0.3%, 0.5%, and 0.7% into 30 ml of DMF, along with (MWCNT:SDS) weight ratios of 1/0, 1/20, 1/23, and 1/26 about the weight of MWCNTs. A sonication process of 90 minutes was applied to the solution, ensuring the harmonious dispersion of MWCNTs and SDS. The mixture of these two solutions in a 1:1 ratio was followed by a 30-minute sonication to attain a stable composite mixture. Then, 10 ml of this solution was drawn into a syringe and nanocomposites were produced via the electrospinning technique. In the electrospinning method in nanocomposite production, the voltage applied was 32 kV, the feed rate was 1.6 ml/h, the ambient temperature was 21±2°C, and the collector rotation speed was 280 rpm.

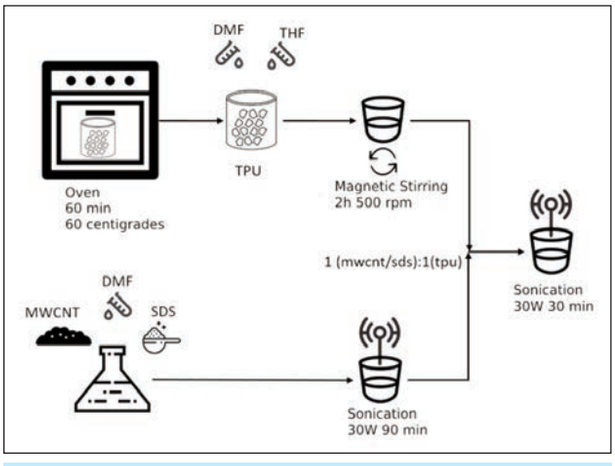


Fig. 1. Nanocomposite production

### Characterization techniques

SEM analyses of nanocomposite structures derived from solutions, featuring distinct MWCNT and SDS ratios, were conducted using the Fei Quanta 450 model FEG SEM ESEM instrument. Viscosity measurements of the solution systems were performed by utilizing the Lamy Rheology RM 100 Plus Viscometer. The solution's conductivity was measured by using the WTW Profile Cond 3110 Conductivity Meter equipment. Alterations in resistance within the nanocomposite structures were measured employing the Keithley 2450 Sourcemeter and the Instron 4411 instruments. During measurements, nanocomposite surfaces measuring 3 cm × 1 cm were sectioned and evaluated using the Instron instrument. During this measurement, probes of the Keithley resistance measurement instrument were attached to the sample from the top and bottom, and resistance changes under voltage were measured for 30 minutes. Additionally, regarding the endurance of the sensor behaviour exhibited by these nanocomposite surfaces, resistance variations were identified through 100 repetitions under identical test conditions.

## RESULTS AND DISCUSSION

The results of microscopic tests, electromechanical analyses of nanocomposite structures obtained from MWCNT at different concentrations and SDS used at different rates are shown and interpreted.

### Morphological properties

The morphological properties of samples were examined by scanning electron microscope (SEM) and the results showed excessive bead formation and agglomeration on the samples' surface which were prepared with a 1/0 (MWCNT:SDS) (figure 2, *a, e, i*). Figure 2, *b, f, j* indicates that SDS addition is eliminated agglomeration. Also, bead formation is strongly inhibited in the presence of SDS (figure 2, *b, c, d, f, g, h, j, k, l*). Therefore, these results show that SDS addition improved the distribution uniformity of MWCNTs in TPU and prevented agglomeration and bead formation. According to resistivity measurements, it was found that there was no resistivity change in the samples with agglomeration (figure 2, *a, e, i*).
The SEM images of the samples with the best sensor characteristics shown in the measurements are given in figure 2.

### Electromechanical properties

Electromechanical examination of the samples obtained by the addition of different MWCNT and varying rates of SDS is performed.
The resistance change is observed when the load is applied to the strain sensor. To make sense of this change, a gauge factor calculation is made. The gauge factor is calculated by the following formulas 1 and 2.

$$GF = \frac{\Delta R/R_0}{\varepsilon} \quad (1)$$

$$\left(\frac{\Delta R}{R_0}\right) = \frac{R_t - R_0}{R_0} \quad (2)$$

$\Delta R/R_0$ is calculated by the formula above. Here, $\Delta R$ represents the change in resistance, $R_0$ represents the sensor resistance when no load is applied, and $R_t$ represents the resistance shown by the sensor under load. ε represents the amount of strain applied. Electromechanical examinations of the samples obtained by adding different MWCNTs and varying amounts of SDS were carried out (figure 3). Correlation and regression analyses of the values obtained in these examinations were performed and the statistical validity of the results was analysed.
Figure 3, *a* shows the elongation-gauge factor graph of the sample with 0, 1/20, 1/23 and 1/26 MWCNT/SDS ratios with a concentration of 0.3 MWCNT, The resistance changes under a tensile stress of the samples obtained by adding 0.3 MWCNT and varying amounts of SDS are given in figure 3, *a*. When figure 3, *a* is examined, the sample with 1/20 ratio of MWCNT:SDS showed up to 2% elongation, this change in resistance against elongation was evident that this nanocomposite can be applicable as a strain sensor. Therefore, it can be seen that the sample

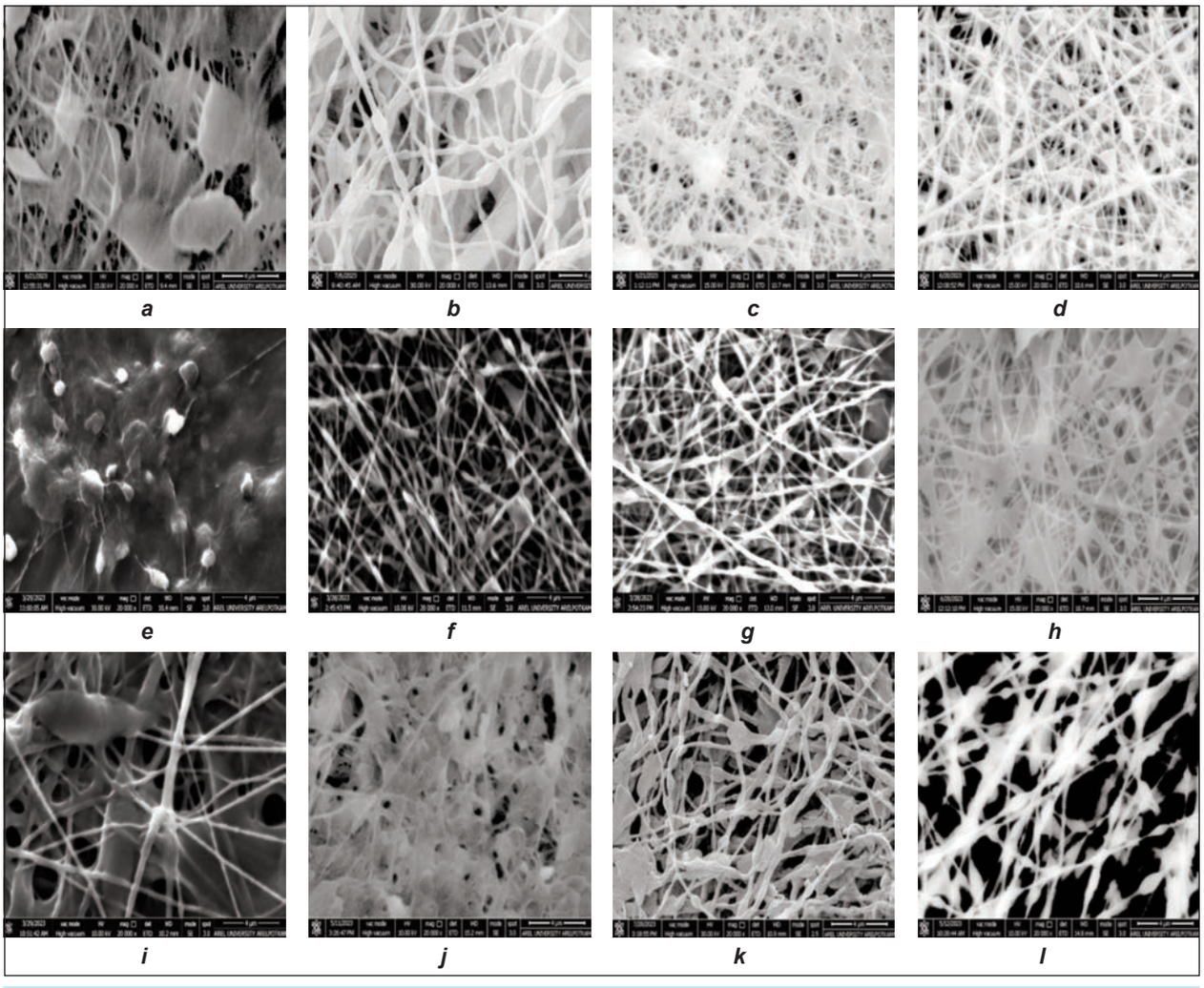


Fig. 2. SEM images: *a* – MWCNT 0.3 SDS 0; *b* – MWCNT 0.3 SDS 20; *c* – MWCNT 0.3 SDS 23; *d* – MWCNT 0.3 SDS 26; *e* – MWCNT 0.5 SDS 0; *f* – MWCNT 0.5 SDS 20; *g* – MWCNT 0.5 SDS 23; *h* – MWCNT 0.5 SDS 26; *i* – MWCNT 0.7 SDS 0; *j* – MWCNT 0.7 SDS 20; *k* – MWCNT 0.7 SDS 23; *l* – MWCNT 0.7 SDS 26

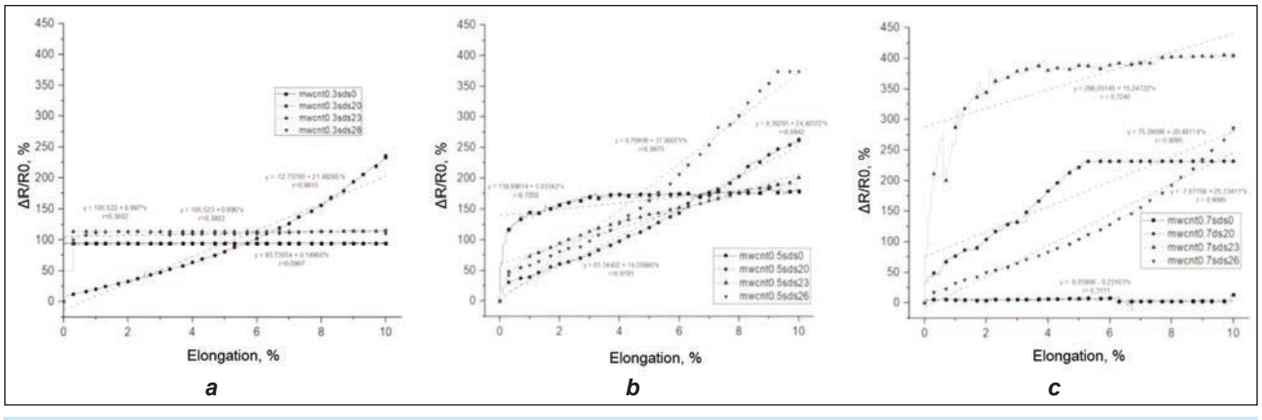


Fig. 3. Graphical representation of: *a* – ΔR/R0 change at MWCNT 0.3 constant value at 1/20, 1/23 and 1/26 MWCNT:SDS ratios; *b* – ΔR/R0 change at MWCNT 0.5 constant value at 1/20, 1/23 and 1/26 MWCNT:SDS ratios; *c* – ΔR/R0 change at MWCNT 0.7 constant value at 1/20, 1/23 and 1/26 MWCNT:SDS ratios

created by adding 1/20 SDS showed the best resistance change among the samples with 0.3 MWCNT added. It is considered that the increase in resistance of this sample largely depends on the increase of elongation, as can be seen from the correlation coefficient ($r = 0.98$), so it can be used as a tension sensor. It was statistically observed that the increase in resistance in response to the increase in stress did not occur in other samples. Therefore, these samples do not have sensor features.

The resistance changes under the tension test of the samples obtained by adding 0.5 MWCNT and varying

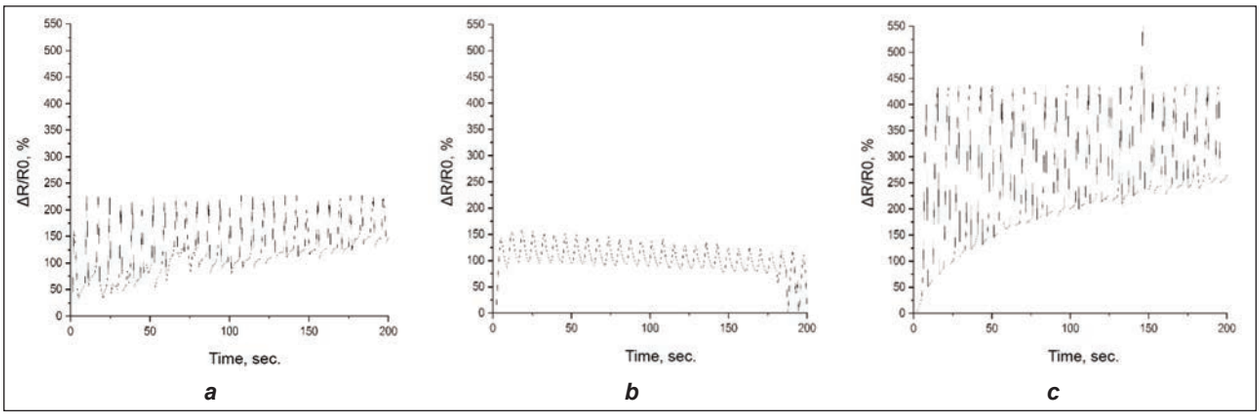


Fig. 4. Strain Cycle Tests performed to samples: *a* – MWCNT 0.3 and MWCNT:SDS 1/20; *b* – MWCNT 0.5 with MWCNT:SDS 1/2; *c* – MWCNT 0.7 with MWCNT:SDS 1/26

amounts of SDS are given in figure 3, *b*. When figure 3, *b* is examined, the sample obtained by adding 1/0 MWCNT:SDS shows a resistance change behaviour up to 2% elongation, but at an elongation value above 2%, it does not show sensor behaviour due to no resistance change. Sensor behaviour was observed in the samples obtained by adding MWCNT:SDS at the rate of 1/20, 1/23 and 1/26, the increase in resistance in the samples was due to the increase in elongation and this increase was statistically significant for all three samples ($r = 0.99$ for 1/20, $r = 0.98$ for 1/23, $r = 0.99$ for 1/26) was found to be significant.

The resistance changes under the tension test of the samples obtained by adding 0.7 MWCNT and varying amounts of SDS are given in figure 3, *c*. When figure 3, *c* is examined, it is seen that there is a change in resistance to extension stress in all of the samples, except for the sample obtained by adding 1/0 MWCNT:SDS. An increase in resistance was observed in response to a 5% increase in elongation in samples created by adding 1/20 and 1/23 MWCNT:SDS. Although sensor behaviour was observed up to 5% elongation value, no resistance change occurred at higher elongation values. Although the correlation coefficients for these samples were significant ($r = 0.91$ for 1/20, $r = 0.72$ for 1/23), no sensor behaviour was observed. As can be seen from the correlation coefficient ($r = 0.91$), the sample created by adding 1/26 MWCNT:SDS shows sensor properties as it is observed that there is a stable resistance change against the increase in elongation.

To reveal the continuity of the sensor behaviour of the resulting nanocomposites, these samples are tested with 100 cycles for 400 seconds to understand their characteristics of resistance against strain. The resistance changes that occurred as a result of the applied cycle tests are observed and presented graphically. In these graphs, MWCNT 0.3 MWCNT:SDS 1/20, MWCNT 0.5 MWCNT:SDS 1/20, and MWCNT 0.7 MWCNT:SDS 1/26 examples that best express sensor behaviour are evaluated.

Figure 4, *a* shows the graph of the strain-cycle test performed at a concentration of 0.3 MWCNT, figure 4, *b* 0.5 MWCNT and a ratio of 1/20 SDS, and figure 4, *c* 0.7 MWCNT and a ratio of 1/26 SDS as well. For all 3 measurements, it is determined that the resistance change continues at the end of each cycle. The fact that resistance values obtained in the cycle tests are same at the peak of the curves, is an evidence of a stable sensor behavior under strain for the samples. At the same time, it was determined that the resistance change decreased over time at the lower peak of the durational cycle test performed.

## CONCLUSION

In this study, nanocomposites with different MWCNT concentrations and different SDS ratios were produced. Morphological and electromechanical examinations of these samples were performed and the following results were obtained.

Electrospinning could not be performed healthily for samples without SDS participation. Particularly, with the increase in the MWCNT ratio, MWCNTs could not be distributed homogeneously, causing blockages and disruptions in the electrospinning process. Furthermore, it has been detected that in response to the increase in MWCNT concentration, difficulties occur in the electrospinning process.

To avoid aggregation, the introduction of SDS additives was implemented and this enabled sample production. When the scanning electron microscope (SEM) images of the samples without any SDS addition are examined; it is observed that there is excessive pilling and agglomeration (clumps) on the obtained surfaces and it is observed that these clumps decrease as the SDS rate increases. Thus, it is understood that the SDS ratio ensures the uniformity of the distribution of MWCNTs within the TPU and prevents agglomeration. Accordingly, it is seen that there is no resistance change for the samples where agglomeration is present when the voltage is applied to the samples.

When the resistance changes of the samples to elongation are examined; best sensor properties were obtained for 0.3, 0.5 MWCNT at 1/20 MWCNT:SDS and for 0.7 MWCNT at 1/26 MWCNT:SDS ratios.

When the gauge factor behaviour indicating the sensor characteristic of the samples is examined, similar

results are obtained. It is understood that the samples prepared at MWCNT:SDS ratio of 1/20 for MWCNT 0.3 and MWCNT 0.5 concentration as well as MWCNT:SDS 1/26 for MWCNT 0.7 concentration presents the best sensor behavior. For other samples, it is evaluated that the gauge factor value varies in a narrow range and this change will adversely affect the sensor characteristics. In this content, the evaluation emphasizes the significance of the alteration in the linear direction between resistance values resulting from voltage increments, which present more significance for the manifestation of sensor behaviour. On the other hand, challenges encountered during sample production processes and the prevailing production conditions are believed to exert an influence on the sensor attributes exhibited by the samples.

Under the strain applied for the sustainability of the sensor characteristics, the following samples are found to display the best sensor characteristics in the resistance change loop test: the ones obtained with SDS 1/20 ratio at 0.3 concentration, with SDS 1/20 ratio at MWCNT 0.5 concentration and with SDS 1/26 ratio at MWCNT 0.7 concentration. Under an applied strain to investigate the sustainability of the sensor characteristics, the following samples are found to display the best sensor properties in the resistance change loop test: the ones obtained with 1/20 MWCNT:SDS ratio for MWCNT 0.3 and MWCNT 0.5 as well as 1/26 MWCNT:SDS ratio for MWCNT 0.7. It is seen that the divergence in resistance values among the chosen samples exhibits a partial decline as a response to the increase in time during the cycle test. Thus, it is thought that the MWCNTs in the TPU cannot be distributed completely homogeneously and this affects the resistance values of the samples. As a result, it has been demonstrated that samples with voltage sensor characteristics are produced in the study. Among these samples, samples with very good voltage sensor characteristics as well as samples with little or no voltage sensor characteristics are obtained. Here, it is evaluated that the MWCNT ratio and SDS ratio play a critical role together and electrospinning parameters are also effective.


## ACKNOWLEDGMENT

This research is supported by Istanbul Arel University, Project No. 2019/ST07.


## REFERENCES


[1] Erol, A.D., Çetiner, S., *Giyilebilir Elektronik/Akıllı Tekstiller ve Uygulamaları*, Kahramanmaraş Sütçü İmam Üniversitesi Mühendislik Bilimleri Dergisi, 2017

[2] Kayacan, O., Bulgun, E.Y., *Akıllı Tekstiller ve elektriği ileten tekstil esaslı malzemeler*, In: Tekstil ve Mühendis, 2005, 29–34

[3] Choi, C.M., Kwon, S.-N., Na, S.-I., *Conductive PEDOT: PSS-coated poly-paraphenylene terephtalamide thread for highly durable electronic textiles*, In: Journal of Industrial and Engineering Chemistry, 2017, 155–161

[4] He, Z., Byun, J.-H., Zhou, G., Park, B.-J., Kim, T.-H., Lee, S.-B., Yi, J.-W., Um M.-K., Chou, T.-W., *Effect of MWCNT content on the mechanical and strain–sensing performance of Thermoplastic Polyurethane composite fibers*, In: Carbon, 2019, 701-708

[5] Wang, X., Sun, H., Yue, X., Yu, Y., Zheng, G., Dai, K., *A highly strechable carbon nanotubes/thermoplastic polyurethane fiber-shaped strain sensor with porous structure for human motion monitoring*, In: Composites Science and Technology, 2018, 126–132

[6] Zhan, P., Zhai, W., Wei, W., Ding, P., Zheng, G., Dai, K., Liu, C., *Stretchable strain sensor with high sensivity,large workable range and excellent breathability for wearable electronic skins*, In: Composite Science and Technology, 2022

[7] Sanli, A., Yildiz, K., Uzun, M., *Experimental study of the impact of electrospinning parameters on the electromechanical proporties of strain sensitive electrospun multiwalled carbon nanotubes/thermoplastic polyurethane nanofibers*, In: Advanced Composite Materials, 2022, 335–350

[8] Wang, X., Xue, R., Li, M., Guo, X., Liu, B., Xu, W., Wang, Z., Liu, Y., Wang, G., *Strain and stress sensing proporties of the MWCNT/TPU nanofiber film*, In: Surfaces and Interfaces, 2022

[9] Şanlı, A., *Farklı Dispersiyon Tekniklerinin Elektroeğirilmiş Karbon Nanotüp/Termoplastik Ploiüretan Nanokompozitlerin Elektromekanik Özelliklerine Etkisinin Deneysel İncelenmesi*, In: Düzce Üniversitesi Bilim ve Teknoloji Dergisi, 2022, 2039–2051

[10] Nankali, M., Nouri, N., Malek, N.G., Shahrezaei, M.S., *Electrical proporties of strechable and skin-mountable PDMS/MWCNT hybrid composite films for flexible strain sensors*, In: Journal of Composite Materials, 2019, 3047–3060

[11] Kumar, S., Gupta, T.K., Varadarajan, K.M., *Strong,Strechable and ultrasensitive MWCNT/TPU nanocomposites for piezoresistive strain sensing*, In: Composites Part B, 2019

[12] Erol, A.D., *Akıllı Tekstillere yönelik basınç sensör özelliği gösteren kumaş tasarımı ve geliştirilmesi*, 2018

[13] Erol, A.D., Çetiner, S., *Elektronik Tekstillere Yönelik Akıllı Kumaş Sensörleri*, In: Tekstil ve Mühendis, 2017

[14] Zheng, Y., Li, Y., Dai, K., Liu, M., Zhou, K., Zheng, G., Liu, C., Shen, C., *Conductive thermoplastic polyurethane composites with tunable piezoresistivity by modulating the filler dimensionality for flexible strain sensors*, In: Composites:Part A, 2017, 41–49

[15] ur Rehman, M.H., Nazar, R., Yasin, S., Ramzan, N., Habib, M.S., *Development of PANI-TPU/MWCNTs based nanocomposites for piezoresistive strain sensing applications*, In: Materials Letters, 2022, 1–4

[16] Hu, Q., Nag, A., Zhang, L., Wang, K., *Reduced graphene oxide-based composites for werable strain-sensing applications*, In: Sensors and Actuators: A Physical, 2022
[17] Wang, Y., Li, W., Zhou, Y., Jiang, L., Ma, J., Chen, S., Jerrams, S., Zhou, F., *Fabrication of high-performance wearable strain sensors by using CNTs-coated electrospun polyurethane nanofibers*, In: Polymers&biopolymers, 2020, 12592–12606
[18] Zheng, Y., Li, Y., Dai, K., Liu, M., Zhou, K., Zheng, G., Liu, C., Shen, C., *Conductive thermoplastic polyurethane composites with tunable piezoresistivity by modulating the filler dimensionality for flexible strain sensors*, In: Composites:Part A, 2017, 41–49
[19] Sui, G., Liu, D., Liu, Y., Ji, W., Zhang, Q., Fu, Q., *The dispersion of CNT in TPU matrix with different preparation methods: solution mixing vs melt mixing*, In: Polymer, 2019
[20] Khodke, M., Chavan, U., Joshi, S., Shinde, S., *Experimental studies on carbon nanotube strain sensors*, In: Materials Today: Proceedings, 2023

**Authors:**

RUSEN INAN[1], ISMAIL USTA[2], YESIM MUGE SAHIN[3,4]

[1]Istanbul Arel University, Vocational School, Fashion Design,
34537, Istanbul, Türkiye

[2]Marmara University, Faculty of Technology, Department of Textile Engineering,
34854, Istanbul, Türkiye
e-mail: iusta@marmara.edu.tr

[3]Istanbul Arel University, Faculty of Engineering and Architecture, Department of Biomedical Engineering,
34537, Istanbul, Türkiye
e-mail: ymugesahin@arel.edu.tr

[4]Polymer Technologies and Composite Application and Research Center (ArelPOTKAM)
Istanbul Arel University, Istanbul, Türkiye

**Corresponding author:**

RUSEN INAN

e-mail: rusenparlak@arel.edu.tr